Abstract

COLINA, CORAY MARIÚ. Thermodynamics and Phase Equilibria of Carbon Dioxide/Polymer Systems. (Under the direction of Keith E. Gubbins)

A theoretical approach, the SAFT (Statistical Associating Fluid Theory) equation of state, is adapted and extended to understand the thermodynamics and phase equilibria of systems containing carbon dioxide (CO_2), CO_2-philic and CO_2-phobic compounds, including both small molecules (such as *n*-alkanes and *n*-perfluoroalkanes) and macromolecules (homopolymers, polymer blends and copolymers), to provide rapid *reliable predictions* for a wide range of systems of interest.

Most prior research has concentrated on developing SAFT equations suitable for phase equilibrium calculations (vapor-liquid and liquid-liquid). In the present work we demonstrate that the SAFT equations are particularly useful not only in pressure-temperature-volume-composition phase equilibrium problems but, also for more difficult aspects of the behavior of mixtures such as derivative properties (e.g., Joule-Thomson inversion curves) and formation of aggregates. To accomplish this goal, we studied the strengths and limitations that different thermodynamic models present not only for pure CO_2, but also for its mixtures with small molecules and macromolecules. The research is divided in three major areas: a) a fundamental investigation of the thermophysical properties of pure carbon dioxide, using predictions from both molecular simulations and equations of state; b) a detailed study of the phase equilibria of binary and ternary mixtures of CO_2, *n*-perfluoroalkanes and *n*-alkanes as a representation of small CO_2-philic and partially CO_2-phobic compounds; and c) a study of phase equilibria in binary and ternary mixtures of CO_2, CO_2-philic and CO_2-phobic polymers. The ability of the SAFT approach to perform such predictions relies on its more rigorous foundation, since it is practically the only approach that has been able to describe both small molecules and macromolecules.

THERMODYNAMICS AND PHASE EQUILIBRIA OF CARBON DIOXIDE/POLYMER SYSTEMS

by

CORAY MARIU COLINA

A dissertation submitted to the Graduate Faculty of
North Carolina State University
in partial fulfillment of the
requirements for the Degree of
Doctor of Philosophy

CHEMICAL ENGINEERING

Raleigh

2004

APPROVED BY:

Keith E. Gubbins — **Keith E. Gubbins, Chair**

Carol K. Hall — **Carol K. Hall**

Richard J. Spontak — **Richard J. Spontak**

Keith P. Johnston — **Keith P. Johnston**

A Jhon

Por tu gran amor, apoyo,

paciencia y compresión

Biography

Coray M. Colina was born in Caracas, Venezuela, to her parents Consuelo Gamero de Colina and César Colina. She was raised in Caracas, along with her two younger brothers David and Ricardo. Coray attended Universidad Simón Bolívar at Caracas to study Chemical Engineering, graduating in 1993. In 1994 she finished her Master in Chemical Engineering (honor mention) at the same university. While a graduate student, Coray was a teaching/research assistant in thermodynamics, her passion. She carried out her research project on developing new cubic equations of state equivalent to the Lee-Kesler equation, under the supervision of Prof. Claudio Olivera-Fuentes. On August 26, 1995 she married Jhon A. Castaño (Jhon is the correct spelling of his name!) in Caracas.

Coray joined the faculty at the Thermodynamics and Transport Phenomena Department at Simón Bolívar University, immediately after she finished her master studies. She has taught several courses such as thermodynamics, process engineering and transport phenomena laboratories since 1995. She started as an Assistant Professor (tenured in 1997) and later was promoted to Senior Assistant Professor (in 2000). During that time she was also pursuing research mainly in thermodynamics, as a member of the Applied Thermodynamics for Process Design (TADiP) Group.

In 2000 she stayed at North Carolina State University (NCSU) as a visiting scientist in Profs. Keith E. Gubbins and Carol K. Hall's groups, working on predicting phase behavior of CO_2-based systems. In 2001 she began her Ph.D. studies in the Department of Chemical Engineering at NCSU. She joined Prof. Gubbins' research group, where she carried out the work presented in this dissertation. Coray defended her dissertation on August 6, 2004. She then joined Prof. Lee Pedersen's research group at the University of North Carolina at Chapel Hill to pursue postdoctoral research in molecular biochemistry.

Acknoledgements

I am very grateful to Keith Gubbins for giving me the opportunity not only of working with him, his group and collaborators but for sharing his knowledge, and moreover his friendship. He gave me the flexibility that a student of my experience could need, making conversations with him very enjoyable, as well as challenging me everyday to do my best. I will always regard you as a mentor and a friend. Gracias Keith!

To my committee members Profs. Carol K. Hall, Richard J. Spontak and Keith P. Johnston. For their time, dedication and sincere support. Each of you made possible this work. I truly appreciate your help over all these years (and the years to come ;)).

To our collaborators: Valery Bondar, Amparo Galindo, Zhang Ling, Martin Lisal, Richard Spontak, Carol Hall, Claudio Olivera-Fuentes, J. Ilja Siepmann, Flor Siperstein and Teri Walker; as well as Gubbins' group members specially Francisco Hung, Erik Santiso, Alberto Striolo and Henry Bock. Due to your expertise, collaboration and patience a big fraction of this work was possible.

This work has been supported by the STC Program of the National Science Foundation.

To my everyday friends Henry Bock, John Brennan, Naresh Chennamsetty, Benoit Coasne, Francisco Hung, Martin Lisal, Claudio Olivera-Fuentes, Ravi Radhakrishnan, Erik Santiso, Flor Siperstein, Silvia Siquier, Alberto Striolo, Heath Turner and Teri Walker, for making possible to enjoy ☺ and argue ;) Everyday…

And last but not least to my family, in Raleigh and Venezuela. Sin su amor y apoyo nada sería posible….. Gracias Jhon, Jorge, mamá, papá, David, Ricardo, Maribel, Valeria, Daniel, Rodrigo and Carlos.

Table of Contents

List of Tables

List of Figures

Chapter 1

Introduction

The aim of this research program is to adapt and extend a theoretical approach, the SAFT (Statistical Associating Fluid Theory) equation of state, to understand the thermodynamics and phase equilibria of systems containing carbon dioxide (CO_2), and CO_2-philic and CO_2-phobic compounds including both small molecules (*n*-alkanes, *n*-perfluoroalkanes, *etc*) and macromolecules (homopolymers, polymer blends and copolymers) in order to provide rapid *reliable predictions* for a wide range of systems of interest to the scientific community in general.

Carbon dioxide properties have been studied in academia and in industry in a continuous manner since the 1950's; however in the last decade the studies have increased in an exponential fashion. This is principally due to the widely extended use of CO_2 in commercial plants, as well as potential use as sustainable fluid for the protection of the environment, at least compared to many common organic solvents. Several independent studies[1-4] have explored the utility of CO_2 over the last two decades, where it has been used as solvent, co-solvent, plasticizer, penetrant and foaming agent. Practical considerations motivating the use of CO_2 in these areas include: (*i*) it has tunable solvent properties at easily accessible conditions (its critical conditions are 304.13 K and 7.37 MPa); and (*ii*) it can be readily separated from multicomponent systems by simple depressurization rather than by energy-intensive thermal evaporation. From a thermodynamic point of view, CO_2 is the best reference of a molecule with a strong quadrupole. Several multiparametric equations of state are available for this fluid, the most popular being the equation due to Span and Wagner[5]. Due to the important role that CO_2 plays (and will play) in the chemical industry, among others, it is imperative to study the strengths and limitations of different thermodynamic models for representing pure CO_2, as well as its mixtures with different fluids, including macromolecules such as polymers.

The study of small-molecules/solvent or macromolecules/solvent systems would be greatly facilitated if it were possible to simulate different process scenarios with an accurate equation of state. Models or correlations developed for this purpose should be able to predict the changes in phase behavior, as a function of solvent quality or as a function of the solute (e.g. polymer) architecture with a minimum number of fitted parameters[3]. Most conventional engineering equations of state (EOS) are variations of the van der Waals equation. They are based on the idea of a hard-sphere reference term to represent the repulsive interactions, and a mean-field term to account for the dispersion and any other long-range forces. Commonly used EOS (e.g. cubics) involve improvements to either the treatment of the hard-sphere contribution or the mean-field terms. Such models may be very convenient to reasonably fit phase equilibrium data for simple, nearly spherical molecules such as low-molecular-mass hydrocarbons, simple inorganics such as nitrogen and carbon monoxide, etc., but a better predictive capability can be expected with a more fundamental equation such the Statistical Associating Fluid Theory (SAFT)[6-9] or, in the polymer area, the Sanchez-Lacombe (SL)[10] equation of state. These two equations are widely used by the thermodynamics community, and they are representative examples of the lattice-gas and perturbation models[3].

Both the SL and SAFT equations are based in statistical mechanics. The SL equation is a lattice-gas expression, and accounts for dispersion and repulsive interactions. Chain formation for short chains can be considered, but association is not accounted for. The SAFT equation is based on a resummed perturbation series due to Wertheim[11-15], and accounts in a realistic way for association between molecules, in addition to dispersion and repulsive interactions. Moreover, SAFT can account for chain effects, including polymer molecules. Furthermore, SAFT can be used to calculate the phase behavior not only of mixtures of "small molecules" but also of mixtures comprised of components that exhibit wide disparities in molecular size, such as solvent-polymer mixtures. The ability of the SAFT approach to perform such predictions relies on its more rigorous foundation, since it is, practically, the only approach that has been able to migrate from "small molecules" to macromolecules.

1.1 SAFT Model

In SAFT[6-9], molecules are modeled as chains of covalently bonded spheres. Homologous series, such as *n*-alkanes and polymers, can be modeled as chains of identical spheres, where the number of spheres in the chain is proportional to the molecular weight. In SAFT, the residual Helmholtz energy, a^{res}, is of the form

$$a^{res} = a^{seg} + a^{chain} + a^{assoc} \tag{1.1}$$

where a^{seg} is the part of the Helmholtz energy due to segment-segment interactions (interactions between monomer units in different molecules, usually modeled as hard sphere, Lennard-Jones or square-well interactions), a^{chain} is the additional Helmholtz energy due to chain formation, and a^{assoc} represents the contribution due to association, e.g. hydrogen bonding, between different molecules.

A detailed discussion of the mathematical form of the SAFT equation can be found elsewhere[9,16] and is not provided here. However in each chapter a brief description of the SAFT model used is given. Several reviews[16-18] of equations of state that include comparisons of some of the SAFT models are available. For mixtures, the dispersion part of the segment Helmholtz energy is the only part that requires the use of mixing rules; the composition dependence is built into the chain and association terms by statistical thermodynamics.

Over the past decade, a number of studies (see, e.g. refs. 16-18) have already demonstrated that the SAFT framework provides a state-of-the-art thermodynamic description of complex multicomponent mixtures. A review of the papers published in the past 14 years (since SAFT appeared) reveals more than 270 articles dealing directly with the SAFT approach and its applications, and more than 1000 cross-references. In this section, we will focus only on the four most used versions of the SAFT approach, based on their reference term: SAFT-HR

(hard sphere), Soft-SAFT (Lennard-Jones), SAFT-VR (square-well) and PC-SAFT (chain of hard spheres). A detailed description of the models is given in the following chapters.

1.1.1 The Huang-Radosz SAFT EOS

The most widely used version of SAFT is the implementation of Huang and Radosz[9] (SAFT-HR), who fitted the potential parameters to the experimental vapor pressure and saturated liquid density data of more than 100 real fluids. For the segment term, they use the sum of a hard-sphere part, given by the Carnahan-Starling equation[19], and a dispersion part, given by the BACK equation of Chen and Kreglewski[20]. The SAFT-HR EOS for pure fluids can be written in terms of the compressibility factor as

$$Z = 1 + Z^{seg} + Z^{chain} + Z^{assoc} \tag{1.2}$$

where

$$Z^{seg} = m\left[\frac{4\eta - 2\eta^2}{(1-\eta)^3} + \sum_i \sum_j jD_{ij}\left(\frac{u}{kT}\right)^i \left(\frac{\eta}{\tau}\right)^j\right] \tag{1.3}$$

$$Z^{chain} = (1-m)\frac{\frac{5}{2}\eta - \eta^2}{(1-\eta)\left(1-\frac{1}{2}\eta\right)} \tag{1.4}$$

$$Z^{assoc} = \left[1 + N_{AV}\sum_B \rho X^B \Delta^{AB}\right]^{-1} \tag{1.5}$$

with the auxiliary definitions

$$\eta = \tau m \frac{v^0}{v}, \quad v^0 = v^{00}\left[1 - C\exp\left(-\frac{3u^0}{kT}\right)\right]^3, \quad \frac{u}{k} = \frac{u^0}{k}\left[1 + \frac{e}{kT}\right] \tag{1.6}$$

In these equations, $\tau = 0.74048$, $C = 0.12$ and $e/k = 10$ except for a few small molecules (e/k = 0 for argon; 1 for methane, ammonia and water; 3 for nitrogen; 4.2 for carbon monoxide; 18 for chlorine; 38 for CS_2; 40 for carbon dioxide and 88 for SO_2).

Parameters for pure components

The first step in the application of the SAFT equation of state to multicomponent mixtures, or in fact any equation of state, is to determine the pure component parameters. There are five pure-component parameters in the equation. The first parameter is the number of hard spheres m that forms a molecule, and this is treated as an adjustable parameter. The second parameter is the volume of a mole of these spheres when they are closely packed, v^{00}; this variable sets their size. The third pure-component parameter is the segment energy u^0, which determines segment-segment interactions. In addition to these three parameters for nonassociating molecules, the equation has two association parameters, ε^{AA} and κ^{AA}. The parameter ε^{AA} characterizes the association energy and the parameter κ^{AA} characterizes the association volume for association site A. These parameters are normally determined by fitting experimental data for vapor pressure and liquid molar volume data, but it is known that the resulting prediction around the critical point is not very good.[1,3] This is also the case for all analytic (mean field) equations of state.

In order to provide a better description of the critical region, the crossover formalism[21] has been attempted by several groups within the SAFT approach[22-28]. Unfortunately, this formalism cannot be applied to mixtures in a straightforward way, and in fact its application to even pure fluids is intricate enough to avoid its use for practical applications. As an alternative, the pure-component parameters of the SAFT equation can be rescaled to the critical point of each pure fluid, and then used to predict the mixture behavior. We should note here that, although the critical region is more accurately represented with the scaled

parameters, this is always at the expense of accuracy at lower temperatures. In particular, the saturated liquid densities are underpredicted with these parameters. On the other hand, pressure-temperature-compositions are well predicted and in numerous cases (such as CO_2/polymer systems), these are the main variables of interest.

Supercritical carbon dioxide

Due to its structural symmetry, CO_2 does not have a dipole moment, but it does have a substantial quadrupole moment that operates over a much shorter distance than dipolar interactions. Despite this, it is normally assumed that CO_2 exhibits dispersive attractions only, which means that just three parameters (m, v^{00}, u^0) need to be determined with the SAFT-HR EOS. Takishima *et al.*[29] re-determined pure CO_2 parameters by regressing saturated vapor pressures, saturated liquid densities and the critical properties. With these parameters the resulting SAFT prediction for critical properties were T_c=306.3 K, P_c = 7.88 MPa and ρ_c=10.7 mol/l (471.014 kg/m^3). These are close to the experimental values[13] (T_c = 304.128 ± 0.015 K, P_c= 7.3773 ± 0.0030 MPa, ρ_c=467.6 ± 0.6 kg/m^3).

Polymer parameters

Since high molecular weight polymers have no detectable vapor pressure and thermally degrade before exhibiting a critical point, EOS parameters for polymers are generally determined using measured data for pure liquid molar volumes. Unfortunately, with SAFT-HR, it is known that a regression of polymer parameters from this type of data generally leads to incorrect phase equilibrium calculations[1,3]. A number of sustainable component parameters can be determined from a fitting of such restricted data.

In their original work[9], Huang and Radosz proposed v^{00} = 12 ml/mol and u^0/k = 210 K for polymers, and estimated the segment number parameter from the *n*-alkane corollary:

$$\boldsymbol{m} = 0.05096\, \boldsymbol{M_n} \qquad (1.7)$$

where M_n stands for the number average polymer molecular weight*. This number average molecular weight is the sum of all the molecular weights of the individual molecules present in a sample divided by their total number, that is $M_n = \sum N_i M_i / \sum N_i$. This approach should be reasonable for predicting the phase behavior of polyolefin-supercritical solvents systems because it is based on the values of an infinite molecular weight alkane[3].

An alternative approach to obtain the polymer parameters is to regress a pure component parameter for the polymer from binary phase equilibrium data[3,29,30]. The polymer-supercritical fluid solvent cloud-point curve could be used to obtain a value for u^o/k. A third alternative based on a combination of these two approaches, was proposed by Lora *et al*.[30] They extended the group contribution approach of Huang and Radosz[9] for calculating m and v^{00} for acrylate polymers as a function of the values for a repeat unit, with m being corrected for the size of the polymer according to the number average molecular weight.

Even though the polymers are polydisperse in all of these approaches, the calculations are performed by taking a "monodisperse" molecular weight equal to M_n, because an enormous amount of work is required to model (and characterize) polydisperse polymers. However, it is possible to model the polymer as a mixture of pseudo-components, if the data for the molecular weight fractions of the polymer are available (see for example ref. 31).

Binary mixtures

The extension to binary and multicomponent mixtures is possible with the SAFT EOS since the three reference terms can be extended to mixtures based on rigorous statistical mechanics. Mixing rules are only required for the dispersion term in the SAFT EOS.

---

* In their original publication and in some later works, Radosz and co-workers used the weight average molecular weight ($M_w = \sum N_i M_i^2 / \sum N_i M_i$),however they were working with nearly monodisperse polymers in those cases.

Mixing rules

One of the more useful mixing rules is based on the van der Waals one-fluid theory, which is often referred to as the vdW1 mixing rule. There are only two parameters in the dispersion term that require mixing rules[32], *u/k* and *m*,

$$\frac{u}{kT} = \frac{\sum_i \sum_j x_i x_j m_i m_j \left[\frac{u_{ij}}{kT}\right] \left(v^o\right)_{ij}}{\sum_i \sum_j x_i x_j m_i m_j \left(v^o\right)_{ij}} \tag{1.8}$$

where

$$\left(v^o\right)_{ij} = \left[\frac{1}{2}\left[\left(v^o\right)_i^{1/3} + \left(v^o\right)_j^{1/3}\right]\right]^3 \tag{1.9}$$

$$u_{ij} = \left(1 - k_{ij}\right)\left(u_{ii} u_{jj}\right)^{1/2} \tag{1.10}$$

and

$$m = \sum_i \sum_j x_i x_j \left[\frac{1}{2}\left(m_i + m_j\right)\right] \tag{1.11}$$

An alternative mixing rule is the so-called "volume-fraction" mixing rule,

$$\frac{u}{kT} = \sum_i \sum_j f_i f_j \left[\frac{u_{ij}}{kT}\right] \tag{1.12}$$

where f_i is the volume fraction of component i

$$f_i = \frac{x_i m_i v_i^0}{\sum_j x_j m_j v_j^0} \tag{1.13}$$

This volume-fraction mixing rule, represents experimental data near critical conditions better than the vdW1 mixing rules[3,32], and so is to be preferred if the system under study has one of the components near its critical point.

Binary interaction parameter

The binary interaction parameter k_{ij} is a fitted, binary mixture parameter that corrects the mean-field energy contribution to SAFT. This parameter is usually determined by fitting SAFT to experimental data on mixture phase equilibrium, and is expected to lie between ± 0.15. A second mixture parameter, l_{ij}, could also be used, but the fit of the cloud curves is not expected to be significantly improved by this because the two parameters k_{ij} *and* l_{ij} have similar effects on the calculated fit[3]. It is essential to keep in mind that binary interaction parameters are used to "correct" a theory, in a way that real systems can be represented with higher accuracy. Larger values of these parameters would indicate that the model (or combining rule) used is not the most adequate to represent the system under investigation and modifications or different models should be utilized. We would like to stress that the present rule of thumb is valid for interaction parameters in any model, combining or mixing rule.

Copolymer parameters

In many copolymer-solvent studies, the copolymer properties are determined with mixing rules that combine parameters for the two homopolymers that comprise the copolymer. In one approach, the mixing rules used for these calculations are similar to the vdW1 mixing rule, except that they are applied to the two homopolymers that comprise the copolymer rather than to two components in the mixture.

Takishima *et al.*[29] suggested another approach in which simple averaging rules, dependent only upon the molecular weights of the blocks, were used to estimate the parameters. These rules are also physically realistic since they are based on the volume fractions of the different blocks,

$$v_{A-B}^{00} = \frac{\sum_i v_i^{00} m_i}{\sum_i m_i} \tag{1.14}$$

$$\left(u_{A-B}^{0}\right)^{1/2} = \sum_i f_i^0 \left(u_i^0\right)^{1/2} \tag{1.15}$$

$$f_i^0 = \frac{m_i v_i^{00}}{\sum_i v_i^{00} m_i} \tag{1.16}$$

$$\left(1 - k_{12(A-B)}\right)\left(u_{A-B}^{0}\right)^{1/2} = \sum_i f_i^0 \left(1 - k_{12(i)}\right)\left(u_i^0\right)^{1/2} \tag{1.17}$$

where the subscript *A-B* represents the copolymer formed by the polymer *A* and the polymer *B*, and the sum is over all components.

1.1.2 Soft-SAFT

The Soft-SAFT EOS[33,34] is a modification of the original SAFT equation proposed by Chapman[35] and Huang and Radosz[9], in which the reference term is a Lennard-Jones (LJ) fluid. As in the rest of the SAFT equations, the chain contribution is obtained based on Wertheim's first order perturbation theory[11-15]. The equation of Johnson *et al.*[36] is used for modeling the Lennard-Jones fluid.

Recently, Pàmies and Vega[37] have published predictions for the phase equilibria of pure and binary mixtures of heavy *n*-alkanes, using the Soft-SAFT EOS. They proposed a new set of transferable molecular parameters that provide a significant improvement over previous calculations[33], especially for the heavy members of the series. A correlation for the critical properties of heavy *n*-alkanes was also proposed. Comparisons of the Soft-SAFT EOS

predictions with available experimental and simulation data of pure and selected binary mixtures showed that the equation is able to capture the main features of the phase envelope in all cases, giving the same degree of accuracy as molecular simulation models[33,34]. Excellent quantitative agreement with experimental data for these mixtures was obtained by using two fitted binary interaction parameters, that were independent of the thermodynamic conditions.

1.1.3 SAFT-VR

Gil-Villegas *et al.*[38,39] recently proposed a version of SAFT with an attractive potential of variable range (SAFT-VR). Within the perturbation theory framework, they deduced analytical expressions for the contribution to the Helmholtz free energy for several potentials, such as the square well, Sutherland, Yukawa and Mie *m*-*n* potentials. The addition of a non-conformal range parameter allows for an accurate description of the bulk thermodynamics of systems ranging from small strongly associating or polar molecules such as water[38] and replacement refrigerants[39], to long-chain alkanes[40] and polyethylene[41].

1.1.4 PC-SAFT

The development of the Perturbed-Chain (PC) SAFT equation-of-state is described in detail by Gross and Sadowski[42]. PC-SAFT is a theoretical-based equation of state, which was proposed for the thermodynamic modeling of systems containing long-chain molecules such as polymers.

In the framework of PC-SAFT, molecules are assumed to be chains of freely jointed spherical segments. The compressibility factor Z of a non-associating molecule can be written as:

$$Z = Z^{hard\ chain} + Z^{dispersion} \tag{1.18}$$

where $Z^{hard\ chain}$ accounts for the repulsion of the chain-like molecule and is described using the hard-chain expression derived by Chapman *et al*.[6] In contrast to the SAFT equations of state presented previously, the PC-SAFT model accounts for the non-spherical shape of the molecules also in the dispersion term $Z^{dispersion}$. The perturbation theory of Barker and Henderson[43] was applied using a hard *chain* fluid as the reference system. The theory was tested against computer simulations[44] of square-well chains leading to a satisfactory prediction of the simulated behavior. Readjusting of the model constants for real substances led to the PC-SAFT equation of state[42].

In order to characterize the properties of copolymer systems, the perturbed-chain SAFT model is extended for heteronuclear hard-chain fluids using the approach suggested by Banaszak *et al.*[45], and Shukla and Chapman[46]. This extended PC-SAFT version is referred to as copolymer PC-SAFT, in which each segment in a chain can have different properties. In this model, the copolymer chains are built from segments of the homopolymers. As a result, the modeling of copolymer-solvent mixtures requires appropriate pure component parameters for the respective homopolymers and for the solvent.

1.1.5 Other SAFT equations

SAFT-like association terms have been incorporated into group-contribution, lattice, and cubic EOS, and into the UNIQUAC and UNIFAC models[16]. Additionally, attempts have been made to simplify the mathematical form of the equations, to provide algorithms for calculating phase equilibria using SAFT, and for solving the root-finding problem in an efficient way.

Some recent papers[16-18] compare the SAFT EOS and its extensions against other existing methods. In general, SAFT, with its more rigorous foundation, is found to be more reliable both for data fitting and prediction; this is particularly the case for associating fluids and chain molecules.

1.2 Final Comments

Most efforts in the past have concentrated on developing SAFT equations suitable for equilibrium calculations (vapor-liquid and liquid-liquid). The present work demonstrates that the SAFT equations are particularly useful not only in phase equilibrium problems but also for studying more difficult aspects of the behavior of mixtures such as derivative properties (e.g. Joule-Thomson inversion curves, isothermal compressibilities, speed of sound, etc.) and formation of aggregates. To accomplish this goal, we study the strengths and limitations that different thermodynamic models present not only for pure CO_2, but also for its mixtures with small molecules and macromolecules. We chose to evaluate three of the several versions available of the SAFT approach, based on their reference term: SAFT-HR[9] (hard sphere), Soft-SAFT[33] (Lennard-Jones) and SAFT-VR[38] (square-well). We divide the project in three major areas: a) a fundamental investigation, using predictions from both molecular simulations and equations of state, of the thermophysical properties of pure carbon dioxide; b) a detailed study of the phase equilibria of binary and ternary mixtures of CO_2, *n*-perfluoroalkanes and *n*-alkanes, as a representation of small CO_2-philic and partially CO_2-phobic compounds; and c) a study of phase equilibria of binary and ternary mixtures of CO_2, CO_2-philic and CO_2-phobic polymers.

The importance of carbon dioxide, especially in its supercritical state, is well known in a variety of fields, e.g. the oil industry (as a carrier gas for enhanced oil recovery) and "green chemistry", where research efforts are underway to identify sustainable processes and products using CO_2-related technology. In the majority of these processes carbon dioxide acts as a solvent, and subsequently the properties of the mixtures mainly depend on its contribution. Due to its relatively low critical point, CO_2 is normally used at supercritical conditions, that are close enough to its critical point to allow a fine adjustment of the properties of the mixture with a relatively moderate change in pressure and/or temperature. Consequently the first logical step of this project is to evaluate the predictive capabilities of the SAFT equations for pure carbon dioxide in its supercritical state.

In general, one of the most demanding tests that can be performed on a set of experimental (or simulation) data or on analytical equations of state at supercritical conditions is the evaluation of Joule Thomson inversion curves (JTIC). A literature search shows a controversy about the correct shape of the JTIC of CO_2. Knowledge of the correct shape of the JTIC is essential to our project due to its effects in the supercritical region. If the model is not able to reproduce the correct shape, it could be argued that the model would need modifications, e.g. to account for the CO_2 quadrupole in an explicit manner.

We present in chapter 2 the results of our Monte Carlo simulations in the isothermal-isobaric ensemble using two different approaches to obtain the JTIC for carbon dioxide[47]. Chacín *et al.*[48] observed an anomalous behavior of the CO_2 JTIC in the high temperature range when performing Monte Carlo simulations using a two-center Lennard-Jones plus point quadrupole moment (2CLJQ) potential. The simulated JTIC deviated from the expected quasi-parabolic shape, exhibiting a change of slope and curvature (a "hump"). Their results appeared to be consistent with the original experimental data of Price[49] and the predictions of the Pitzer and Sterner EOS[50] . We model carbon dioxide using the 2CLJQ moment potential. The agreement between the experimental data, Span-Wagner[5] equation of state and our simulations results indicates that the 2CLJQ potential represents an excellent balance between simplicity and accuracy in modeling carbon dioxide. Additionally, we calculate the JTIC using the BACKONE EOS[51] (which uses the same intermolecular potential as in our simulations) and it is show that such EOS performs very well in predicting the JTIC for carbon dioxide. The agreement between our simulations, recent experimental data, the state of the art multiparametric[5] equation of state for CO_2 and the BACKONE EOS is remarkable and we believe the anomalous behavior of the JTIC obtained by Chacín *et al.*[48] is due to the high uncertainty of their results in the high-temperature branch of the JTIC, rather than the 2CLJQ potential model. We also obtain[52] derivative properties (volume expasivity, isothermal compressibility, isobaric heat capacity, Joule-Thomson coefficients and speed of sound) at supercritical conditions and compare with the results obtained from the Span-Wagner equation[5] (which is essentially equivalent to high-precision experimental data). The results of this part of the project are presented in chapter 3.

In chapter 4 we predict[53] complete Joule-Thomson inversion curves for pure carbon dioxide and the *n*-alkanes series, including heavy *n*-alkanes up to octatetracontane (*n*-$C_{48}H_{98}$) with the Soft-SAFT equation. Comparisons with available experimental and correlation data for carbon dioxide and the lighter *n*-alkanes show good quantitative agreement.

In chapter 5 the phase behavior of mixtures containing carbon dioxide, *n*-alkanes and *n*-perfluoroalkanes is studied[54] using the statistical associating fluid theory for potentials of variable attractive range (SAFT-VR). A set of transferable mixture parameters is presented, which provide a good description of the mixture phase behavior, and offer insight into the higher solubility of *n*-perfluoroalkanes in carbon dioxide as compared to the solubility of *n*-alkanes. The previous work is extended[55] to ternary mixtures in Chapter 6, where we present, for the first time, predictions of vapor-liquid and vapor-liquid-liquid equilibria of binary and ternary systems of carbon dioxide/*n*-perfluoroalkane/*n*-alkane. We study the influence of temperature, pressure, composition and chain length on the phase diagram. The predicted phase diagrams are based on temperature-<u>in</u>dependent binary interaction parameters, and <u>no</u> ternary parameters are introduced. Comparisons against the scarce experimental and molecular simulation data available show that the predicted diagrams should provide a good representation of the phase equilibria.

In chapter 7 we evaluate[56] the SAFT-HR model for polymer/solvent mixtures as well as copolymer/solvent mixtures. We study the phase equilibria (*cloud curves*) of homopolymers (both associating and non-associating) as well as copolymers in CO_2. The possibility of formation of aggregates from copolymers with two associating points in the presence of carbon dioxide is evaluated.

We extend the study of phase equilibria to polymer blends in presence of CO_2 in chapter 8. We have modeled[57] the phase behavior of low-polydispersity PDMS/PEMS (poly(dimethylsiloxane)/poly(ethylmethylsiloxane)) in CO_2 systems using the SAFT-HR equation of state. The ability of the model to predict the phase behavior of the ternary PDMS/PEMS/CO_2 system is corroborated by comparing theoretical predictions with the

experimental data reported. In a complementary work[58], these experimental data was also analyzed by the Sanchez-Lacombe equation of state to ascertain the temperature dependence of an effective interaction parameter (χ) in terms of $A + B/T$, where A and B are both pressure-sensitive.

Finally in chapter 9 we present our conclusions and suggest future directions of this work.

1.3 References

[1] Beckman, E. J., *J. Supercrit. Fluid,* **28**, 121-191 (2004).
[2] Kendall, J. L., Canelas, D. A., Young, J. L. and J. M. DeSimone, *Chem. Rev.* **99**, 543-563 (1999).
[3] Kirby, C. F. and M. A. McHugh, *Chem. Rev.* **99**, 565-602 (1999).
[4] Tomasko, D. L., Li, H., Liu, D., Han, X., Wingert, M.J., Lee, L. J. and K. W. Koelling, *Ind. Eng. Chem. Res.* **42**, 6431-6456 (2003).
[5] Span, R. and W. Wagner, *J. Phys. Chem. Ref. Data*, **25** 1509-1596 (1996).
[6] Chapman, W. G., Jackson, G. and K. E. Gubbins, *Mol. Phys.* **65**, 1057 – 1079 (1988).
[7] Jackson, G., Chapman, W. G. and K. E. Gubbins, *Mol. Phys.* **65**, 1 – 31 (1988).
[8] Chapman, W. G., Gubbins, K. E., Jackson, G. and M. Radosz, *Ind. Eng. Chem. Res.* **29**, 1709-172 (1990).
[9] Huang, S.H, and M. Radosz, *Ind. Eng. Chem. Res*., **29**, 2284-2294 (1990).
[10] Sanchez, I. C. and Lacombe R.H., *Macromolecules*, **11**, 1145-1156 (1978).
[11] Wertheim, M. S., *J. Chem. Phys.* **85**, 2929-2936 (1986).
[12] Wertheim, M. S., *J. Stat. Phys*. **42**, 459-476 (1986).
[13] Wertheim, M. S., *J. Stat. Phys*. **42**, 477-492 (1986).
[14] Wertheim, M. S., *J. Stat. Phys*. **35**, 19-34 (1984).
[15] Wertheim, M. S., *J. Stat. Phys*. **35**, 35-47 (1984).
[16] Müller, E. A. and K. E. Gubbins, *Ind. Eng. Chem. Res.* **40**, 2193-2211 (2001).
[17] Müller, E. A. and K.E. Gubbins, in J.V.Sengers, R.F. Kayser, C.J. Peters and H. J. White, Jr. (Eds), *Equations of State for Fluids and Fluid Mixtures*. Experimental Thermodynamics, Volume 5, Elsevier, Amsterdam, 2000, pp 435-478.
[18] Wei, Y.S. and R. J. Sadus, *AIChE J.*, **46**, 169 –196 (2000).
[19] Carnahan, N.F. and K. E. Starling, *J. Chem. Phys.* **51**, 635 (1969).
[20] Chen, S. S. and A. Kreglewski, *Ber. Bunsen-Ges. Phys. Chem*., **81**, 1048-1052 (1977).

[21] Anisimov, M.A. and J.V. Sengers, in J.V.Sengers, R.F. Kayser, C.J. Peters and H. J. White, Jr. (Eds), *Equations of State for Fluids and Fluid Mixtures*. Experimental Thermodynamics, Volume 5, Elsevier, Amsterdam, 2000, pp 434.
[22] Kiselev, S. B. and J. F. Ely, *Ind. Eng. Chem. Res.*, **38**, 4993-5004 (1999)
[23] Kiselev, S.B. and J.F. Ely, *Fluid Phase Equilb*., **174**, 93-113 (2000).
[24] Kiselev, S.B., Ely, J. F., Adidharma, H. and M. Radosz, *Fluid Phase Equilb*., **183**, 53-64 (2001).
[25] Hu, Z-Q, Yang, J-C and Yi-G Li, *Fluid Phase Equilb*., **205**, 1-15 (2003).
[26] Hu, Z-Q, Yang, J-C and Yi-G Li, *Fluid Phase Equilb.,* **205**, 25-36 (2003).
[27] McCabe, C. and S. B. Kiselev, *Fluid Phase Equilb.,* **219**, 3-9 (2004).
[28] McCabe, C. and S. B. Kiselev, *Ind. Eng. Chem. Res.,* **43**, 2839-2851 (2004).
[29] Takishima, S., O'Neil, M.L. and K.P. Johnston, *Ind. Eng. Chem. Res.*, **36**, 2821-2833 (1997).
[30] Lora, M. Rindfleisch, F., and M. A. McHugh, *J. Appl. Poly. Sci*. **73**, 1979-1991 (1999)
[31] Behme, S., Sadowski, G. and W. Arlt, *Fluid Phase Equilb.,* **158-160**, 869-877 (1999).
[32] Huang, S.H, and M. Radosz, *Ind. Eng. Chem. Res*., **32**, 762 (1993).
[33] Blas, F. J. and L. F. Vega, *Ind. Eng. Chem. Res.* **37**, 660-674 (1998)
[34] Blas, F. J. and L. F. Vega, *J. Chem. Phys.* **109**, 7405-7413 (1998).
[35] Champan, W. J., *J. Chem. Phys.* **93**, 4299-4304 (1990).
[36] Johnson, J. K., Zollweg J.A. and K. E. Gubbins, *Mol. Phys.* **78**, 591-618 (1993).
[37] Pàmies, J.C., Vega, L.F. *Ind. Eng. Chem. Res*. **40**, 2532-2543 (2001).
[38] Gil-Villegas, A., Galindo, A., Whitehead, P.J., Mills, S.J., Jackson, G. and A. N. Burgess, *J. Chem. Phys.* **106**, 4168-4186 (1997).
[39] Galindo, A., Gil-Villegas, A., Jackson, G. and A.N. Burgess. *J. Phys. Chem*. B **103**, 10272-10281 (1999).
[40] McCabe, C. and G. Jackson. *Phys. Chem. Chem. Phys*. **1**, 2057-2064 (1999).
[41] McCabe, C., Galindo, A., Garcia-Lisbona, M. N. and G. Jackson. *Ind. Eng. Chem. Res*. **40**, 3835-3842 (2001).
[42] Gross, J. and Sadowski G., *Ind. Eng. Chem. Res.* **40**, 1244-1260 (2001).
[43] Barker, J. A. and Henderson D., *J. Chem. Phys.* **47**, 2856- (1967).
[44] Gross, J. and Sadowski G., *Fluid Phase Equilb.* **168**, 183-199 (2000).
[45] Banaszak M, Chen CK, Radosz M, *Macromolecules*, **29**, 6481-6486 (1996) .
[46] Shukla ,K. P, Chapman W. G., *Mol. Phys*. **91**, 1075-1081 (1997).
[47] Colina, C. M., Lísal, M., Siperstein, F. R. and K. E. Gubbins, *Fluid Phase Equilib*. **202**, 253-262 (2002).
[48] Chacín, A., Vázquez, J.M. and E.A. Müller. *Fluid Phase Equilib.* **165**, 147-155 (1999).
[49] Price, D. *Ind. Eng. Chem.* **1**, 83-86 (1956).
[50] Pitzer, K.S. and S.M. Sterner. *J. Chem. Phys.* **101**, 3111-3116 (1994).
[51] Möller, D. and J. Fischer. *Fluid Phase Equilib.* **100**, 35-61(1994).

[52] Colina, C. M., Olivera-Fuentes, C. G., Siperstein, F. R., Lísal, M. and K. E. Gubbins, *Molecular Simulation*, **29**, 405-412 (2003).
[53] Colina, C. M., Turrens, L. F., Gubbins, K. E., Olivera-Fuentes, C. and L. F. Vega, *Ind. Eng. Chem. Res.* **41**, 1069-1075 (2002).
[54] Colina, C. M., Galindo, A., Blas, F. J. and K. E. Gubbins, in press, *Fluid Phase Equilib.* (2004).
[55] Colina, C. M. and K. E. Gubbins, submitted to *J. Phys. Chem. B.* (2004).
[56] Colina, C. M., Hall, C. K. and K. E. Gubbins, *Fluid Phase Equilib.* **194-197**, 553-565 (2002).
[57] Colina, C. M., Walker, T. A., Spontak, R. J. and K. E. Gubbins, 6th International Symposium on Supercritical Fluids, CD-ROM, Document MP2.pdf, Versailles, France, (2003).
[58] Walker, T. A., Colina, C. M., Gubbins, K. E. and R. J. Spontak, Macromolecules, **37**, 2588-2595 (2004).

Chapter 2

Accurate CO_2 Joule-Thomson Inversion Curve by Molecular Simulations*

Coray M. Colina[1], Martin Lísal[2], Flor R. Siperstein[1] and Keith E. Gubbins[1]

[1]Chemical Engineering Department, North Carolina State University
Raleigh, NC 27695, USA
Phone: +1- 919 – 513-2051 ; Fax: +1 – 919- 513- 2470
[2] E. Hála Laboratory of Thermodynamics, Institute of Chemical Process Fundamentals, Academy of Sciences of the Czech Republic, Prague, Czech Republic

2.1 Abstract

We present simulation of the Joule-Thomson inversion curve (JTIC) for carbon dioxide using two different approaches based on Monte Carlo simulations in the isothermal-isobaric ensemble. We model carbon dioxide using a two-center Lennard-Jones plus point quadrupole moment (2CLJQ) potential. We show that a precision of four significant figures in ensemble averages of thermodynamic quantities of interest is needed to obtain accurately the JTIC. The agreement between the experimental data, Wagner equation of state (EOS) and our simulations results indicates that the 2CLJQ potential represents an excellent balance between simplicity and accuracy in modeling of carbon dioxide. Additionally, we calculate the JTIC using the BACKONE EOS (that uses the same intermolecular potential as in our simulations) and show that the BACKONE EOS performs very well in predicting the JTIC for carbon dioxide.

* *Fluid Phase Equilb.* **202**, 253-262 (2002)

2.2 Introduction

The Joule-Thomson inversion curve (JTIC) is the locus of states where fluid temperature is invariant upon isenthalpic expansion [see e.g. ref. 1 and 2]. Knowledge of the inversion curve is essential for the design and operation of throttling processes (such as refrigeration, production of petroleum fluids), as well as for the evaluation of equations of state (EOSs) and their prediction capabilities. Unfortunately, direct measurement of inversion points is difficult and unreliable.

Experimental JTICs are rarely obtained by direct measurement of inversion points, because this would demand extremely accurate temperature determinations. Instead, experimental pressure-volume-temperature (*PvT*) data are processed e.g. by fitting them with a high-precision multiparameter EOS, and the JTIC is then computed from thermodynamic relations [3]. Even so, the complete JTICs of many fluids cannot be established, because they extend into inaccessible regions of high temperatures and pressures. Hence, experimental data on the JTICs are too scarce to permit a rigorous test of the various predictions.

An alternative way to obtain the JTICs is from molecular simulations. JTICs are obtained from molecular simulations via calculation of either compressibility or thermal expansivity along isotherms [4, 5, 6]. It should be mentioned that calculations of JTICs in high-temperature regions require very long simulation in comparison with low-temperature regions to obtain results with sufficient accuracy, because temperature changes of isenthalps in the high-temperature regions are less sensitive to changes in pressure in comparison with low-temperature regions.

The JTIC of a Lennard-Jones (LJ) fluid has been obtained by different techniques. Heyes and Llaguno [7] were the first to attempt to calculate the LJ JTIC by molecular dynamics (MD), generating isenthalps in the isothermal-isobaric (NPT) ensemble. Their results show reliable values only at low temperatures and high scatter of results is presented near the peak of the curve (high pressure zone) as well as in the high temperature branch. Recently Kioupis and

Maginn [8] developed a new algorithm, which enables the direct simulation of isenthalpic pressure changes using MD. The determination of JTICs is a natural choice to test this technique. Kioupis *et al*. [9] computed the LJ JTIC using their proposed pressure-enthalpy driven molecular dynamics (PHD MD) method, and obtained very good agreement with previously published data.

Colina and Müller [4, 5] used NPT Monte Carlo (MC) simulation to obtain a series of isobars to predict the LJ JTIC. They simulated the inversion points in the same way as they are obtained experimentally, i.e. by looking for the location of an extremum in the compresibility factor along the isobars.

Escobedo and Chen [10] have recently reported results for the LJ JTIC using a novel integration scheme in conjunction with NPT MC simulations. Their results follow those of Colina and Müller [4, 5], but show an ever closer match when comparing them with prediction using the Johnson *et al*.'s EOS for LJ fluid [11].

Lagache *et al*. [6] proposed to use simultaneous determination of derivative properties from statistical fluctuations. They obtained the thermal expansivity, the residual heat capacity and the isothermal compressibility from an explicit isobaric-isothermal partition function. They found excellent agreement of these properties with experimental measurements for pure light hydrocarbons (methane, ethane and butane) in the vapor and liquid states. Furthermore, they showed that this method can be used to accurately determine the Joule-Thomson coefficient.

The determination of JTICs of real fluids by molecular simulations may help in understanding practical problems, such as the possibility of heating that occurs during expansion of high-temperature, high-pressure gas condensate due to the Joule-Thomson effect. The JTICs of real fluids such as carbon dioxide [12] and a series of alkanes up to heptane [6,10] have been calculated using molecular simulation. The importance of carbon dioxide, especially in the supercritical state, is broadly known in a variety of fields, e.g. the oil industry (as a carrier gas for enhanced oil recovery) and "green chemistry", where

research efforts are underway to identify sustainable processes and products using CO_2-related technology.

Chacín *et al*. [12] observed an anomalous behavior of the CO_2 JTIC in the high temperature range. The simulated JTIC deviated from the expected quasi-parabolic shape, exhibiting a change of slope and curvature (a "hump"). Their results appeared to be consistent with the original experimental data of Price [13] and the predictions of the Pitzer-Sterner EOS [14]. However, Colina and Olivera-Fuentes [15] have recently shown that the CO_2 JTIC obtained from the Pitzer-Sterner EOS is incorrect at high temperatures, due to physically erroneous prediction of the third virial coefficients.

In this work, we show that the anomalous behavior of the CO_2 JTIC obtained by Chacín *et al.* is not due to the potential model used (2CLJQ potential), but arises from high uncertainty in the high-temperature branch of the JTIC. The JTIC for carbon dioxide is calculated using the compressibility and thermal expansivity routes. Both routes appear to be equally accurate and efficient for calculating the JTIC when simulation averages are taken over 1.5 x 10^8 configurations. The 2CLJQ potential gives an accurate description of the JTIC even outside the range where the potential model was originally developed.

2.3 Joule-Thomson Inversion Curves (JTICs)

JTICs are usually represented in the pressure, *P,* and temperature, *T,* plane. The JTIC starts from a saturated liquid state at low temperature and pressure, passes through a pressure maximum at intermediate temperature, and goes to zero pressure at maximum temperature as the fluid approaches ideal gas behavior. The inversion criterion can be expressed as

$$\left(\frac{\partial T}{\partial P}\right)_h = 0 \qquad (2.1)$$

where h is the enthalpy. The inversion criterion given by eqn. (2.1) may be written in several alternative forms, e.g. for use with a pressure-explicit EOS $P = P(T, \rho)$, as

$$T\left(\frac{\partial P}{\partial T}\right)_{\rho} - \rho\left(\frac{\partial P}{\partial \rho}\right)_{T} = 0 \tag{2.2}$$

where ρ is the density, or for use with corresponding states models $Z = Z(T, P)$, as

$$\left(\frac{\partial Z}{\partial T}\right)_{P} = 0 \tag{2.3}$$

where $Z=P/(\rho RT)$ is the compressibilty factor and R is the universal gas constant. Alternatively, the inversion criterion can be expressed as a function of the thermal expansivity, α, as

$$(T\alpha - 1) = 0 \tag{2.4}$$

where

$$\alpha = \frac{1}{v}\left(\frac{\partial v}{\partial T}\right)_{P} \tag{2.5}$$

The compressibility and thermal expansivity routes use eq. (2.3) and (2.4), respectively, to determine JTICs.

2.4 Potential Model

We model carbon dioxide as a 2CLJQ fluid [16]. The 2CLJQ molecule is composed of two identical LJ sites a distance l apart and a point quadrupole Q placed in the geometric center of the molecule. The 2CLJQ potential $u_{2\mathrm{CLJQ}}$ can be written as

$$u_{2CLJQ}\left(r_{ij},\omega_i,\omega_j,l,Q^2\right)=u_{2CLJ}\left(r_{ij},\omega_i,\omega_j,l\right)+u_Q\left(r_{ij},\omega_i,\omega_j,Q^2\right) \tag{2.6}$$

where

$$u_{2CLJ}\left(r_{ij},\omega_i,\omega_j,l\right)=4\varepsilon\sum_{a=1}^{2}\sum_{b=1}^{2}\left[\left(\frac{\sigma}{r_{ab}}\right)^{12}-\left(\frac{\sigma}{r_{ab}}\right)^{6}\right] \tag{2.7}$$

and

$$u_Q\left(r_{ij},\omega_i,\omega_j,Q^2\right)=\frac{3}{4}\frac{Q^2}{4\pi\varepsilon_0\left|r_{ij}\right|^5}\left[1-5\left(c_i^2+c_j^2\right)-15c_i^2c_j^2+2\left(c-5c_ic_j\right)^2\right] \tag{2.8}$$

In eqns. (2.7) and (2.8), r_{ij} is the distance between the centers of molecules *i* and *j*, ω_i and ω_j are the orientations of molecules *i* and *j*, r_{ab} is the distance between the center of two LJ sites a and b of different molecules, ε is the LJ energy parameter, σ is the LJ size parameter, $c_i = \cos\theta_i$, cj = $\cos\theta_j$, and c = $\cos\theta_i\cos\theta_j + \sin\theta_i\sin\theta_j\cos\phi_{ij}$, where θ_i and θ_j are the polar angles of the molecular axis with respect to a line joining the molecular centers, ϕ_{ij} is the difference in the azimuthal angles and ε_0 is the permittivity of free space. We used potential parameters suggested by Möller *and* Fischer [16]: ε/k = 125.317 K, σ = 3.0354 Å, l/σ = 0.699 and $Q^2/(4\pi\varepsilon_0\varepsilon\sigma^5)$ = 3.0255.

2.5 Simulation Details

A total of *N* = 500 molecules was initially placed in a random configuration in a cubic simulation box. Periodic boundary conditions and minimum image conventions were applied. Simulations were organized in cycles. Each cycle consists of *N* attempts to displace or rotate a randomly chosen molecule and an attempt of volume change. Acceptance probabilities of displacement and volume changes were adjusted to be about 30%. Averages have been taken over $5\text{x}10^5$ cycles, after a stabilization period of at least $3\text{x}10^5$ cycles.

2.6 Results and Discussion

Two different approaches, the compressibility (Colina and Müller [4]) and thermal expansivity (Lagache *et al*. [6]) routes, were used to simulate the JTIC of CO_2. We restrict ourselves to methodologies that rely exclusively on MC simulations to determine the JTIC, and do not include Escobedo and Chen's technique that uses a combination of EOS and MC simulations for accurate determination of *PvT* properties. Simulations were performed in the entire range of temperatures and pressures where the JTIC is expected for carbon dioxide.

Colina and Müller [4, 5] suggested that to find an inversion curve point, a series of NPT simulations (generally from five to ten) need to be carried out in the vicinity of an expected inversion point. The compressibility factor $Z=P/\rho RT$ is calculated from densities obtained from NPT MC simulations. The derivative in Eq. (2.3) is calculated numerically from a collection of simulations at constant pressure.

Figure 2.1a shows the compressibility factor as a function of reduced temperature $T^* = Tk/\varepsilon$ for a typical isobar ($P^* = P\sigma^3/\varepsilon = 1.15$, $P = 73.24$ MPa). The low-temperature inversion point can be easily found from a well-pronounced minimum ($T^* = 3.13$, $T = 398.5$ K). On the other hand, the high-temperature inversion point corresponds to a maximum that is less obvious in this figure. Figure 2.1b shows only the high-temperature points with a more refined scale, where now the maximum is clearly observed ($T^* = 6.89$, $T = 877.3$ K). Even though the error bars are relatively bigger for the high temperature branch, the maximum is still clearly observed. It is important to note that precision of four significant figures in the compressibility factor is needed to have good statistics. Although this level of accuracy is not normally pursued in molecular simulations, nowadays it is possible to obtain it in a reasonable simulation time, and this opens the door to the possibility of using computer simulations as a convenient method to extrapolate experimental data to other conditions of difficult experimental access.

Figure 2.2 shows a typical Z vs. number of cycles plot for the determination of a point after equilibration have been reached. Due to the high precision that is needed for the determination of the JTIC, at least 3 x 10^5 cycles (1.5 x 10^8 configurations) have to be performed to have good statistics.

The JTIC of carbon dioxide was also calculated using the thermal expansivity method proposed by Lagache *et al.* [6], where the inversion condition given by Eq. (2.4) is obtained from fluctuations in the enthalpy h and volume v:

$$T\alpha - 1 = \frac{\langle vh \rangle - \langle v \rangle \langle h \rangle}{\langle v \rangle T} - 1 = 0 \tag{2.9}$$

Figure 2.3 shows, as an example, the $T^*\alpha - 1$ function for P^* = 1.15 for a complete range of temperatures (filled diamonds). For the determination of the JTIC, it is not necessary to generate all these points. In fact, for the determination of the inversion point, only the points near the inversion condition (usually four) were taken and correlated with a linear approximation [(Tα-1) = mT + b] to obtain the inversion temperatures at the pressure under study. From a linear approximation the low temperature inversion point was T^* =3.17 (T = 404.1 K) and the high temperature inversion point T^* = 6.90 (T = 879.0 K). These temperatures correspond to the values obtained as T_{inv}=-b/m from the different linear correlations. The error propagation in the inversion temperature is given by:

$$\sigma_{T_{inv}}^2 = \frac{b^2}{m^4}\sigma_m^2 + \frac{1}{m^2}\sigma_b^2 + \cdots \tag{2.10}$$

where σ_i is the standard deviation of i.

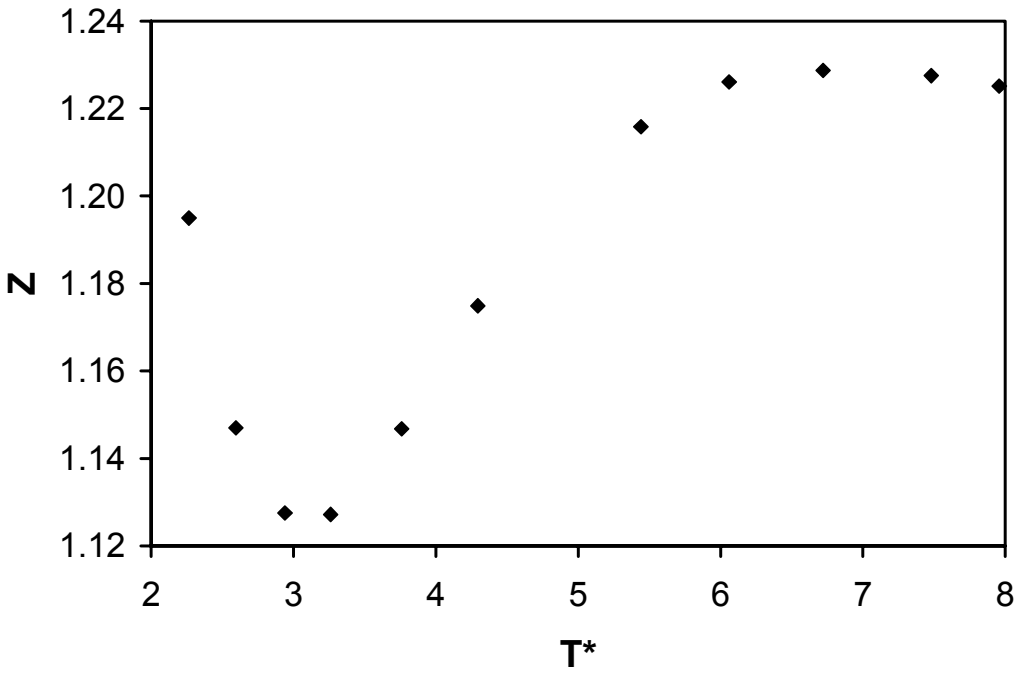

Figure 2.1 (a). Compressibility factor as a function of reduced temperature T^* for a typical isobar ($P^* = 1.15$).

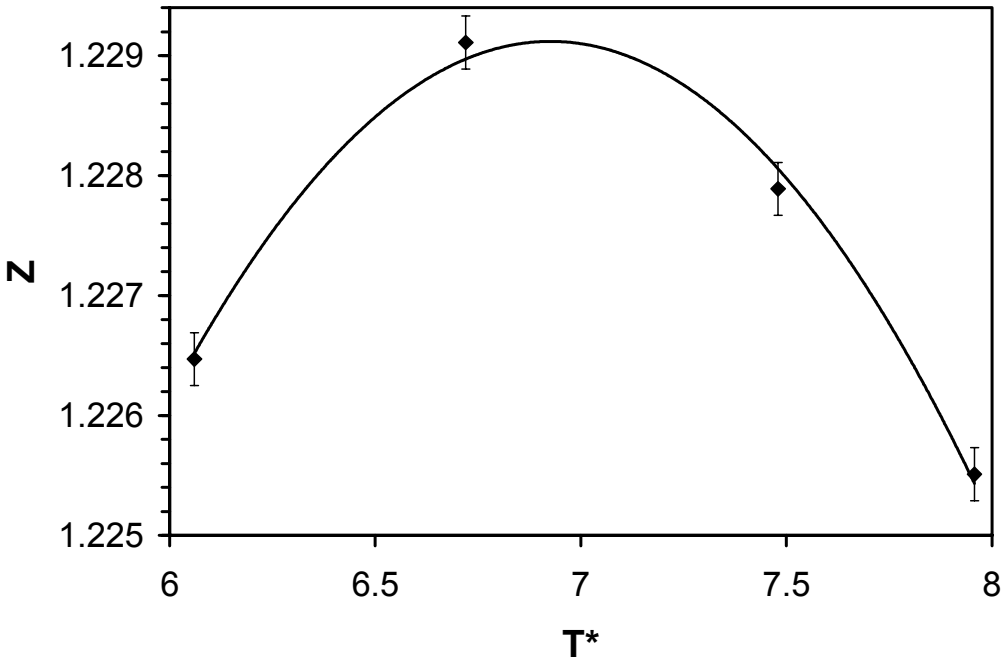

Figure 2.1 (b). High-temperature points at the same conditions as figure 2.1 (a).

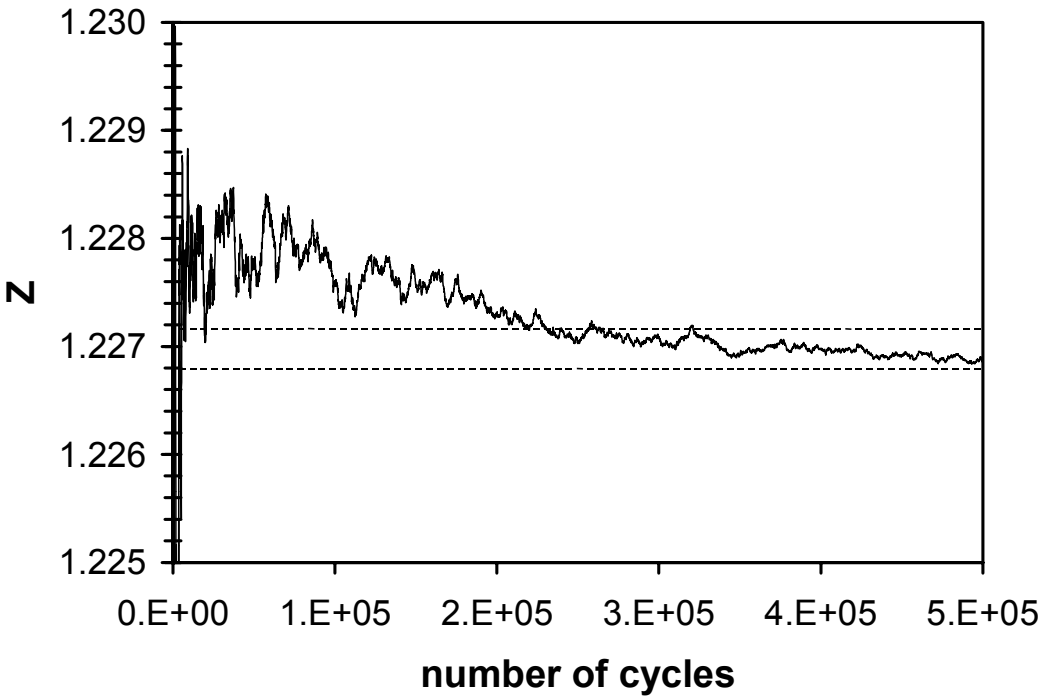

Figure 2.2. Compressibility factor versus number of cycles for a typical isobar.

Therefore, low values of m result in larger errors in the determination of the inversion point for equivalent scatter in the slope and intercept (σ_b, σ_m). To obtain an accurate JTIC in the whole temperature range, it is important to be extremely careful at high temperatures where changes in ($T\alpha$-1) are less sensitive than in the low-temperature range. This effect is more evident at low pressures, as is also shown in figure 2.3 (open circles).

The simulated JTIC of carbon dioxide, expressed in reduced units: $T_r = T^*/T_c^*$, $P_r = P^*/P_c^*$, is shown in Figure 2.4. The simulation results of this work using both approaches are compared with previously published simulations from Chacín *et al.* [12] and with our calculations using the BACKONE EOS [17, 18, 19]. This EOS was selected because it uses the same intermolecular potential as is used in this simulation. The agreement between our simulations and the BACKONE EOS is remarkable and we believe that the anomalous behavior of the JTIC obtained by Chacín *et al.* [12] is not due to the 2CLJQ potential model

but is due to the high uncertainty of Chacín *et al.*'s results in the high-temperature branch of the JTIC. The calculation of the JTIC is a "stringent" test for EOSs and the almost quantitative agreement between our simulations and the BACKONE EOS indicates its excellent performance for this 2CLJQ fluid at such extreme conditions.

Figure 2.5 shows the JTIC of carbon dioxide computed from the Span-Wagner EOS [20], experimental values interpolated from Vukalovich and Altunin's interpolation of data of Price, given in Perry's handbook [21]. Figure 2.5 shows very good agreement between the experimental data, Span-Wagner EOS and our simulations results. Such agreement indicates that the 2CLJQ potential represents an excellent balance between simplicity and accuracy in modeling thermodynamic properties of carbon dioxide in the supercritical region, outside the range of thermodynamic conditions where the 2CLJQ potential parameter were fitted.

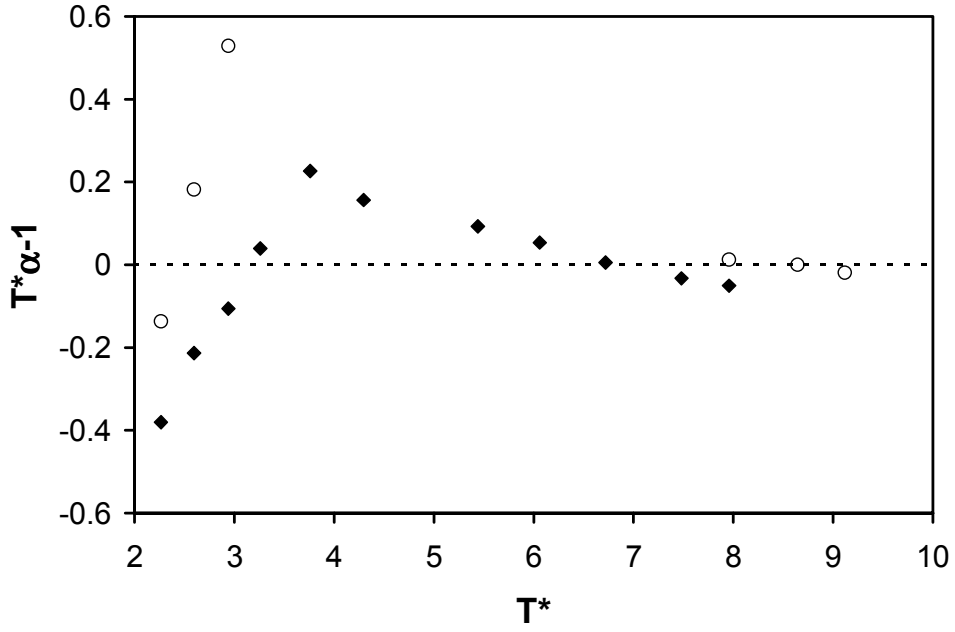

Figure 2.3. T*α –1 function versus T* at high and low pressure, (♦) P* = 1.15 (P = 73.24 MPa). (o) P* = 0.65 (P= 41.40 MPa).

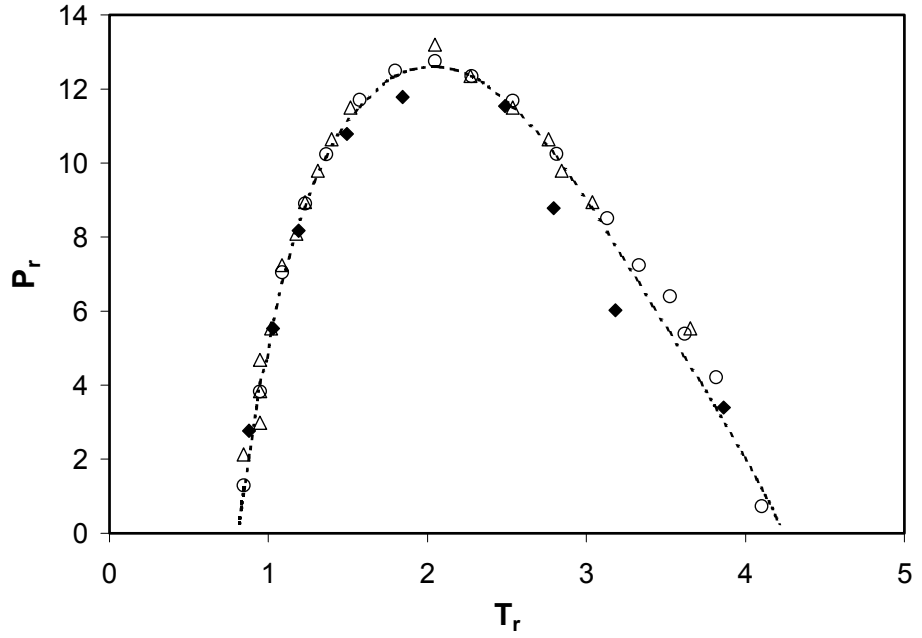

Figure 2.4. Joule-Thomson Inversion Curve for carbon dioxide modeled as the two-center Lennard-Jones plus point quadrupole fluid. (Δ) from compressiblity factor, (o) from T*α-1 function, (♦) previous simulation of Chacín *et al*. [12]. Dotted-dashed line, BACKONE EOS.

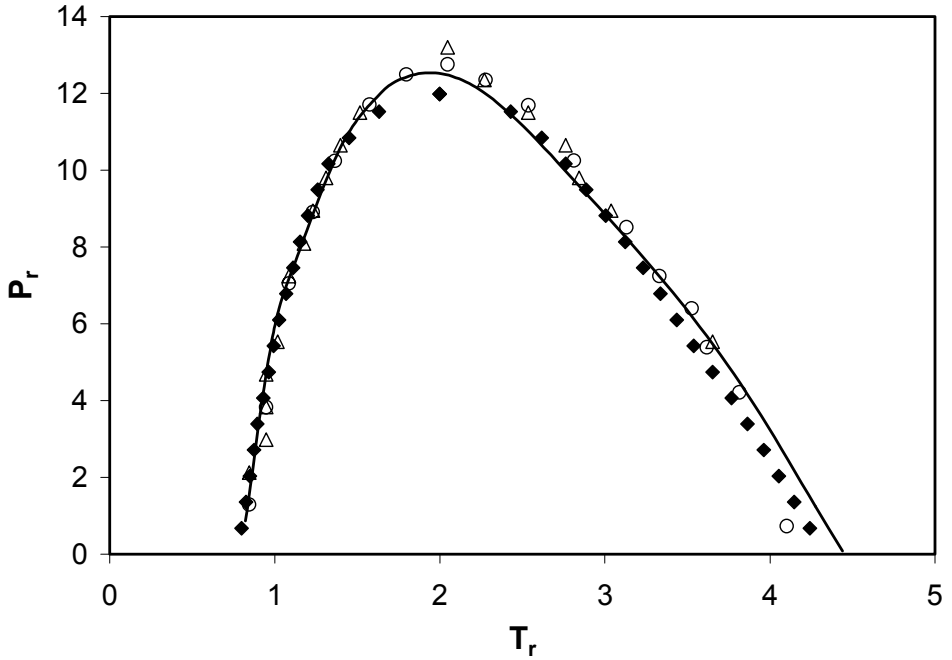

Figure 2.5. Joule-Thomson Inversion curve of carbon dioxide predicted by: the Span-Wagner EOS (continous line), (Δ) from compressiblity factor, (o) from T*α-1 function, (♦) Experimental data as reported in Perry's handbook [21].

2.7 Conclusions

In this work, two different approaches, the compressibility (Colina and Müller [4, 5]) and thermal expansivity (Lagache *et al*. [6]) routes, were used to simulate the JTIC of carbon dioxide. We showed that precision of four significant figures in the thermodynamic quantities of interest was needed in both methods, to obtain good statistics especially for the high-temperature branch of the JTIC.

Our results illustrate the predictive capabilities of molecular simulations. We have found quantitative agreement for JTIC with both experimental measurements [21] and equation of state predictions [20]. We have found excellent agreement, however, despite not including all properties in the optimization of the intermolecular potential.

Acknowledgments

We thank Edward Maginn for providing us a copy of references [8, 9] prior to publication. This material is based upon work supported in part by the STC Program of the National Science Foundation under Agreement No. CHE 9876674, and by the Grant Agency of the Czech Republic under Grant No. 203/02/0805.

2.8 References

[1] P.W. Atkins, Physical Chemistry, Sixth edition, Oxford University Press, USA, 1998.

[2] M.J. Moran and H.N. Shapiro, Fundamentals of Engineering Thermodynamics, second edition, Wiley, USA, 1992.

[3] C.M. Colina and C. Olivera-Fuentes, *Cryogenics* 38 (1998) 721-728.

[4] C. M. Colina and E.A. Müller. *Int. J. of Thermophys.*, 20, (1999) 229-235.

[5] C.M. Colina and E.A. Müller. *Mol. Simulat.*, 19 (1997) 237-246.

[6] M. Lagache, P. Ungerer, A. Boutin and A.H. Fuchs. *Phys. Chem. Chem. Phys*., 3 (2001) 4333-4339.

[7] D.M. Heyes and C.T. Llaguno. *Chem. Phys*., 168 (1992) 61-68.

[8] L.I. Kioupis and E. J. Maginn. *Fluid Phase Equilb*. 200 (2002) 75-92

[9] L.I. Kioupis, G. Arya and E. J. Maginn. *Fluid Phase Equilb*. 200 (2002) 93-110

[10] F.A. Escobedo. and Z. Chen, *Mol. Simulat.* 26 (2001) 395-416.

[11] J.K. Johnson, J.A. Zollweg and K.E. Gubbins. *Mol. Phys.* 78 (1993) 3 591-618.

[12] A. Chacín, J.M. Vázquez and E.A. Müller. *Fluid Phase Equilib.*, 165 (1999) 147-155.

[13] D. Price. *Ind. Eng. Chem.* 1 (1956) 83-86.

[14] K.S. Pitzer and S.M. Sterner. *J. Chem. Phys.* 101 (1994) 4, 3111-3116.

[15] C. M. Colina and C. Olivera-Fuentes. *Ind. Eng. Chem. Res*. 41 (2002) 5, 1064-1068.

[16] D. Möller and J. Fischer. *Fluid Phase Equilib.* 100 (1994) 35-61.

[17] A. Müller, J. Winkelmann and J. Fischer. *AIChE Journal*, 42 (1996) 4, 1116-1126.

[18] M.A. Mecke, J. Müller, J. Winkelmann and J. Fischer. *Int. J. Thermophys*. 18 (1997) 683-698; Erratum, *Int. J. Thermophys*. 19 (1998) 1495.

[19] B. Saager and J. Fischer. *Fluid Phase Equilib*. 72 (1992) 67-88.

[20] R. Span and W. Wagner *J. Phys. Chem. Ref. Data* 25 (1996) 6 1509-1596.

[21] R.H. Perry and D. W. Green, Perry's Chemical Engineers' Handbook, 7th ed.pp 2-134; McGraw-Hill: New York, 1997.

Chapter 3

Thermal Properties of Supercritical Carbon Dioxide by Monte Carlo Simulations*

C. M. Colina[1,2], C. G. Olivera-Fuentes[1], F.R. Siperstein[2], M. Lísal[3,4] and K.E. Gubbins[2]

[1]TADiP Group, Thermodynamics and Transport Phenomena Department, Simón Bolívar University, Apartado Postal 89000, Caracas 1080, Venezuela
[2]Chemical Engineering Department, North Carolina State University
Raleigh, NC 27695, USA
[3] E. Hála Laboratory of Thermodynamics, Institute of Chemical Process Fundamentals, Academy of Sciences of the Czech Republic, Prague, Czech Republic
[4]Department of Physics, J. E. Purkyne University, 400 96 Usti n. Lab., Czech Republic

3.1 Abstract

We present simulation results for the volume expansivity, isothermal compressibility, isobaric heat capacity, Joule-Thomson coefficient and speed of sound for carbon dioxide in the supercritical region, using the fluctuation method based on Monte Carlo simulations in the isothermal-isobaric ensemble. We model carbon dioxide as a quadrupolar two-center Lennard-Jones fluid with potential parameters reported in the literature, derived from vapor-liquid equilibria of CO_2.We compare simulation results with an equation of state for the two-center Lennard-Jones plus point quadrupole fluid and with a multiparametric equation of state adjusted to represent carbon dioxide experimental data. It is concluded that the VLE-based parameters used to model CO_2 as a quadrupolar two-center Lennard-Jones fluid (both simulations and equation of state) can be used with confidence for the prediction of thermodynamic properties, including those of industrial interest such as the speed of sound or Joule-Thomson coefficient, for CO_2 in the supercritical region, except in the extended critical region.

* *Molecular Simulation*, **29**, 405-412 (2003).

3.2 Introduction

Simulation methods that make use of force fields, parameterized on the basis of quantum mechanical calculations and/or experimental measurements, offer an immediate and practical alternative for the prediction of the properties of molecular fluids. The quality of a given force field model depends on its simplicity and transferability beyond the set of conditions that were used for the parameterization. Transferability may imply that the force field parameters for a given interaction site can be used in different molecules (e.g. the parameters used to describe a methyl group should be applicable in many organic molecules), or that the force field is transferable to different state points (e.g. pressure, temperature or composition) and to different properties (e.g. thermodynamic, structural or transport).

In general, for pure components, the transferability of a force field to different state points is tested against vapor-liquid equilibria (VLE), heats of vaporization, second virial coefficients and the prediction of mixture properties. Some work has focused on the evaluation of heat capacities from fluctuations in molecular simulations [1], since heat capacities are derivatives of the basic thermodynamic functions, and are usually not taken into account when obtaining model parameters from experimental data. In this work, we are interested in applying the two-center Lennard-Jones plus point quadrupole (2CLJQ) model for carbon dioxide (CO_2), with VLE-based parameters proposed by Möller and Fischer [2], to the computation of volumetric and thermal properties of CO_2 at supercritical conditions. The molecular simulation results are compared to an analytical equation of state (EOS), hereafter called the 2CLJQ EOS [3,4], and with the Span-Wagner [5] EOS. The 2CLJQ EOS is based on the Boublik-Nezbeda EOS and simulation results for two-center Lennard-Jones and 2CLJQ fluids. The Span-Wagner EOS is the current standard for CO_2 and it is accepted as essentially equivalent to experimental data.

There have been a number of potential models proposed for CO_2, obtained from correlation of VLE properties [2,6,7,8], liquid properties [9], crystal structures and lattice properties [10], or from combinations of experimental data for non-bonded interactions and *ab initio*

electrostatic potentials for charge distributions [11]. Several of these models have been used to study mixture properties [12,13,14,15], structural properties [16] and the pure component vapor-solid coexistence curve [17].

The 2CLJQ model for CO_2 offers an excellent balance between simplicity and accuracy for the description of pressure-volume-temperature (PVT) properties. The interaction parameters presented by Möller and Fischer [2] were optimized to describe VLE and the authors showed that good predictions for densities and enthalpies could be obtained using this potential in a temperature range between 230 and 570 K, and for pressures up to 400 MPa. Although the authors calculated thermodynamic derivatives such as the isothermal compressibility during the optimization process of the potential model, they did not present a comparison with experimental values.

In an earlier publication [18], we used the 2CLJQ model of Möller and Fischer [2] to calculate the Joule-Thomson inversion curve (JTIC) of CO_2. The JTIC was calculated from different thermodynamic properties (thermal expansivity and compressibility factor) and showed good agreement with experimental values. In this work, we present a comprehensive comparison between calculated values of several thermodynamic properties for CO_2 against experimental values as well as against results from the 2CLJQ EOS. We present simulation results for the isobaric heat capacity, volume expansivity, isothermal compressibility, and combinations of these quantities such as the speed of sound and the Joule-Thomson coefficient.

3.3 Thermodynamic Properties in the Isobaric-Isothermal Ensemble

The isobaric-isothermal ensemble partition function, Δ, of a molecular system with N particles at pressure P and temperature T is given by [19]:

$$\Delta(N,P,T) = \sum_{U}\sum_{V} \exp(-\beta U)\exp(-\beta PV)\Omega(N,V,U) \tag{3.1}$$

where Ω is the microcanonical partition function, $\beta = 1/(k_B T)$, k_B is Boltzmann's constant, V is the system volume and U is the system energy. The average of a property X in this ensemble can be expressed as:

$$\langle X \rangle = \frac{\sum_U \sum_V X\Omega(N,V,U)\exp[-\beta(U+PV)]}{\sum_U \sum_V \exp[-\beta(U+PV)]} \tag{3.2}$$

Temperature and pressure derivatives of X in the isobaric-isothermal ensemble can be expressed in terms of fluctuations [20,21]:

$$\left(\frac{\partial\langle X\rangle}{\partial\beta}\right)_P = \left\langle \left(\frac{\partial X}{\partial\beta}\right)_P \right\rangle = \left(\langle X\rangle\langle H\rangle - \langle XH\rangle\right) \tag{3.3}$$

$$\left(\frac{\partial\langle X\rangle}{\partial P}\right)_\beta = \left\langle \left(\frac{\partial X}{\partial P}\right)_\beta \right\rangle = \beta\left(\langle X\rangle\langle V\rangle - \langle XV\rangle\right) \tag{3.4}$$

where H is the system enthalpy. From the above equations, it is possible to derive expressions for the volume expansivity, β_P, the isothermal compressibility, κ, and the configurational isobaric heat capacity, C_P^{conf}:

$$\beta_P = \frac{1}{\langle V\rangle}\left(\frac{\partial\langle V\rangle}{\partial T}\right)_P = -\frac{k_B\beta^2}{\langle V\rangle}\left(\frac{\partial\langle V\rangle}{\partial\beta}\right)_P = -\frac{k_B\beta^2}{\langle V\rangle}\left(\langle V\rangle\langle H\rangle - \langle VH\rangle\right) \tag{3.5}$$

$$\kappa = -\frac{1}{\langle V\rangle}\left(\frac{\partial\langle V\rangle}{\partial P}\right)_\beta = -\frac{\beta}{\langle V\rangle}\left(\langle V\rangle^2 - \langle V^2\rangle\right) \tag{3.6}$$

$$C_p^{conf} = \left(\frac{\partial\langle H\rangle}{\partial T}\right)_P = \left(\frac{\partial\langle U\rangle}{\partial T}\right)_P + P\left(\frac{\partial\langle V\rangle}{\partial T}\right)_P - Nk_B = -k_B\beta^2\left(\frac{\partial\langle U\rangle}{\partial\beta}\right)_P - k_B\beta^2 P\left(\frac{\partial\langle V\rangle}{\partial\beta}\right)_P - Nk_B$$

$$C_p^{conf} = -k_B\beta^2\left[\langle U\rangle\langle H\rangle - \langle UH\rangle\right] - k_B\beta^2 P\left[\langle V\rangle\langle H\rangle - \langle VH\rangle\right] - Nk_B \tag{3.7}$$

where U is the configurational energy. The molar configurational isobaric heat capacity can be obtained as $c_P^{conf} = C_P^{conf}\left(N_A / N\right)$, where N_A is Avogadro's number. To obtain the total isobaric heat capacity it is necessary to add to the above expression the ideal gas heat capacity, C_P^{ideal}:

$$C_P = C_P^{ideal} + C_P^{conf} \tag{3.8}$$

The ideal gas heat capacity was calculated from the correlation given in ref. 5 which represents a data set that consider first order corrections to the rigid rotator, harmonic-oscillator model, with deviations less than ± 0.02%.

From these properties, it is possible to derive other thermodynamic properties of interest, such as the isochoric heat capacity, the Joule-Thomson coefficient and the speed of sound.

The isochoric heat capacity, C_v, can be calculated from thermodynamic relations as:

$$C_P - C_v = -T\frac{\left[\left(\dfrac{\partial\langle V\rangle}{\partial T}\right)_P\right]^2}{\left(\dfrac{\partial\langle V\rangle}{\partial P}\right)_T} = T\langle V\rangle\frac{\beta_P^2}{\kappa} \tag{3.9}$$

Finally, the Joule-Thomson coefficient, μ_{JT}, and speed of sound, u, can be expressed as:

$$\mu_{JT} = \left(\frac{\partial T}{\partial P}\right)_h = \frac{1}{C_P}\left[T\left(\frac{\partial\langle V\rangle}{\partial T}\right)_P - \langle V\rangle\right] = \frac{\langle V\rangle}{C_P}\left[T\beta_P - 1\right] \tag{3.10}$$

$$u^2 = -\frac{C_P}{C_v}\frac{\langle V\rangle^2}{\left(\frac{\partial\langle V\rangle}{\partial P}\right)_T}\frac{MN_A}{N} = \frac{C_P}{C_v}\frac{MN_A}{N}\frac{\langle V\rangle}{\kappa} \tag{3.11}$$

where M is the molecular weight. Expressions for other thermodynamic properties, such as the adiabatic expansivity or the Grüneisen parameter can be obtained from combinations of the relations in this section.

3.4 Potential Model

The model of Möller and Fischer for a 2CLJQ fluid [2] was used to describe CO_2. A molecule is composed of two identical Lennard-Jones sites a distance l apart plus a point quadrupole moment Q placed in the geometric center of the molecule. The full potential, u_{2CLJQ}, is written as:

$$u_{2CLJQ}\left(r_{ij},\omega_i,\omega_j,l,Q^2\right) = u_{2CLJ}\left(r_{ij},\omega_i,\omega_j,l\right) + u_Q\left(r_{ij},\omega_i,\omega_j,Q^2\right) \tag{3.12}$$

where

$$u_{2CLJ}\left(r_{ij},\omega_i,\omega_j,l\right) = 4\varepsilon\sum_{a=1}^{2}\sum_{b=1}^{2}\left[\left(\frac{\sigma}{r_{ab}}\right)^{12} - \left(\frac{\sigma}{r_{ab}}\right)^{6}\right] \tag{3.13}$$

and

$$u_Q\left(r_{ij},\omega_i,\omega_j,Q^2\right) = \frac{3}{4}\frac{Q^2}{4\pi\varepsilon_0\left|r_{ij}\right|^5}\left[1 - 5\left(c_i^2 + c_j^2\right) - 15c_i^2c_j^2 + 2\left(c - 5c_ic_j\right)^2\right] \tag{3.14}$$

In equation (3.13), r_{ab} is one of the four Lennard-Jones site-to-site distances (see Figure 3.1a) where a counts the two sites of molecule i, and b counts those of molecule j. The Lennard Jones parameters σ and ε represent the size of each site and the well depth of the potential energy, respectively.

The contribution to the potential energy due to the quadrupole-quadrupole interactions is given by equation (3.14), where r_{ij} is the center-to-center distance between two molecules, i and j (see Figure 3.1b). The vectors ω_i and ω_j represent the orientation of molecules i and j; θ_i and θ_j are the angles between the axis of the molecule and the center-to-center connection line, and ϕ_{ij} is the difference in azimuthal angles of molecules i and j. In this equation, ε_0 is the permittivity of free space.

We used potential parameters suggested by Möller and Fischer [2]: ε/k_B = 125.317 K, σ = 3.0354 Å, $L = l/\sigma$ = 0.699 and $Q^{*2} = Q^2/(4\pi\varepsilon_0\sigma^5)$ = 3.0255.

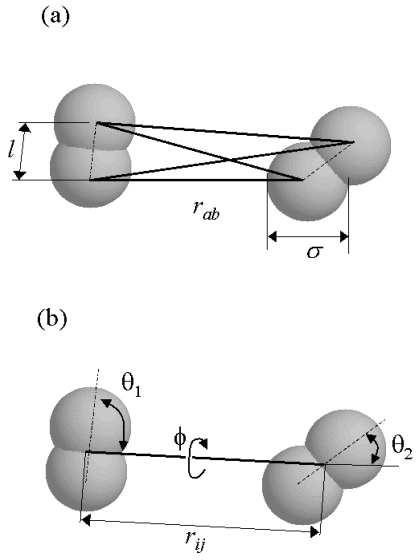

Figure 3.1. Representation of the 2CLJQ model. (a) Each molecule consists of two LJ centers of diameter σ separated by a distance l. Dispersion-repulsion interactions between the sites are calculated for all distances r_{ab}. (b) Point quadrupoles are located at the center of each 2CLJ molecule. Quadrupole-quadrupole interactions between two molecules depend on the orientation of the molecules (θ_1, θ_2, ϕ) and the distance r_{ij} between the two molecules.

3.5 Simulation Details

The fluctuation method based on Monte Carlo simulations in the isothermal-isobaric ensemble was used. Simulations containing 500, 864 and 1320 molecules, initially placed on a face-centered cubic lattice, were performed at low and high temperature, and it was verified that the results were independent on the size of the system. Therefore, the results in this work correspond to a total of N = 500 molecules. Periodic boundary conditions and minimum image conventions were applied. Simulations were organized in cycles. Each cycle consisted of N attempts to displace or rotate a randomly chosen molecule and an attempt of volume change. A variable spherical cut-off radius r_c, equal to half the box length was used (e.g. at 330.39 K and P= 2.5 MPa, $r_c = 15.5\sigma = 4.7$ nm, and at 330.39 K and P= 72.3 MPa, $r_c = 5.4\sigma = 1.6$ nm), and long-range corrections were recalculated after each volume change assuming an homogeneous density for $r>r_c$. Acceptance probabilities of displacement and volume changes were adjusted to be about 30%. Averages were taken over $5x10^5$ cycles, after a stabilization period of at least $3x10^5$ cycles.

3.6 Results for Volumetric Properties

Figure 3.2 shows the simulated densities as a function of pressure in comparison with the values predicted from the Span-Wagner EOS and the 2CLJQ EOS for eight isotherms, one of them (T = 288.37 K) corresponding to the sub-critical region. This figure shows an excellent agreement between the 2CLJQ EOS and our simulations results, except at the highest densities. Stoll et al. [22] carried out an extensive comparison of molecular simulation results of 30 individual 2CLJQ fluids, with different values of L and Q^{*2}, against the 2CLJQ EOS. It should be mentioned that the quadrupolar contribution of the 2CLJQ EOS is assumed to be L independent and was obtained for L = 0.505. They observed increasing deviations in the VLE predictions for fluids as L departs from 0.505; in particular, they found that the EOS systematically under-predicts the saturated liquid densities and the critical flatness of the phase envelope. Figure 3.2 shows that the 2CLJQ EOS for CO_2 (L = 0.699) does predict lower densities, especially on the liquid-like branch of the sub-critical isotherm studied (T =

288.37 K), but the agreement between simulation results and the 2CLJQ EOS improves in the supercritical region, especially at the higher temperatures and pressures.

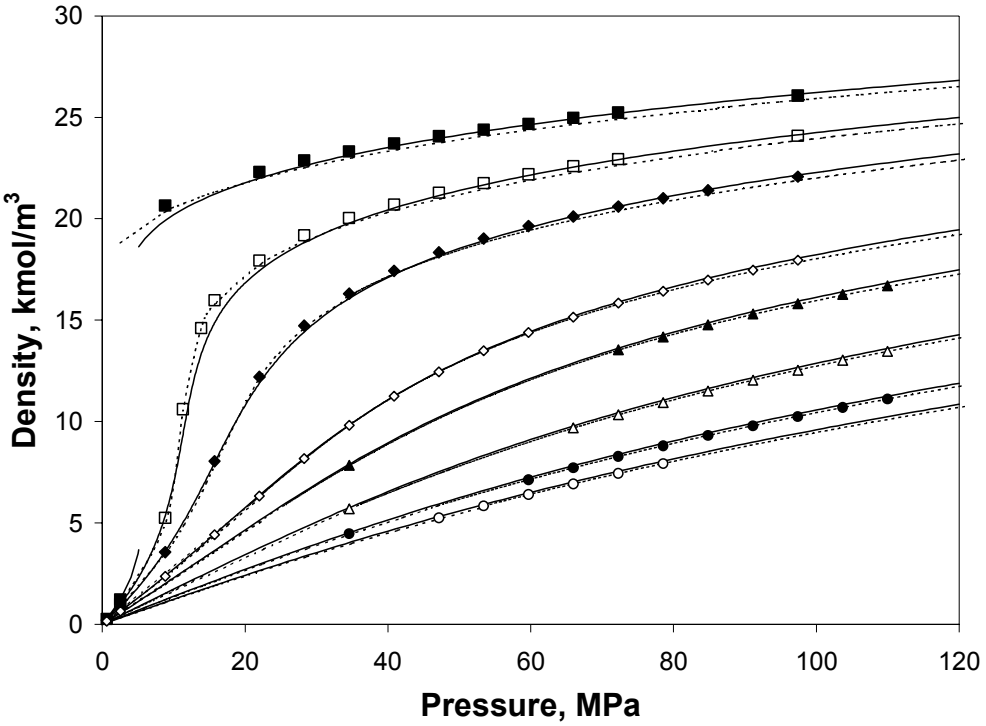

Figure 3.2. Density versus pressure diagram for carbon dioxide. Continuous lines predicted by the Span-Wagner EOS [5], dashed lines predicted by the 2CLJQ EOS [3,4], and symbols this work: (■) 288.37 K, (□) 330.39 K, (♦) 374.31 K, (◊) 478.71 K, (▲) 546.83 K, (Δ) 692.60 K, (●) 855.57 K and (○) 952.33 K.

In general, good agreement is also found between these results and the predictions of the Span and Wagner EOS, except in the extended critical region where deviations in densities up to 5% can be found. The extended critical region includes a temperature range of 20 K and a pressure range of 10 MPa around the critical point. Möller and Fischer obtained similar results from constant pressure-constant temperature molecular dynamics simulations in this region.

The volume expansivity (β_P) and the isothermal compressibility (κ) as functions of pressure are shown in figures 3.3 and 3.4 respectively. The discrepancies between the 2CLJQ model

(both simulations and EOS) and the Span-Wagner EOS are obvious in the extended critical region for both quantities. The volume expansivity is overpredicted by the 2CLJQ model by more than 90% at 330 K, as shown by comparison with the Span-Wagner EOS, and even at 288 and 374 K deviations up to 80 % can be found. However, these deviations are not surprising since it is known that these derivatives, as well as other properties such as heat capacities, diverge at the critical point, so that any discrepancies between the molecular model and the Span-Wagner EOS are bound to be greatly magnified in this region. In fact, it is known that the 2CLJQ model fails to reproduce the critical point of CO_2 exactly; from the correlations developed by Stoll et al. [22] for the 2CLJQ fluid, we expect for CO_2 a model-predicted critical temperature T_c = 307.83 K from simulations and T_c = 318.4 K from the 2CLJQ EOS, higher than the accepted experimental value T_c = 304.128 K which the Span-Wagner EOS is designed to reproduce. Thus, for instance, for CO_2 at 330.39 K the 2CLJQ model gives results that are more near-critical (reduced temperature $T_r = T^*/T_c^* = 1.07$) than in the actual case (T_r = 1.09). The corresponding "spikes" in the isotherms in figures 3.3 and 3.4 are therefore more pronounced for the 2CLJQ model than for the Span-Wagner EOS. A substantially closer agreement between both sets of data would be obtained by computing the isotherms from the reference EOS at the same *reduced* temperature as the simulations.

On the other hand, these differences become less significant at higher temperatures and pressures, away from the extended critical region. At pressures above 40 MPa the agreement between the Span-Wagner EOS and the 2CLJQ model is very good for all temperatures; for temperatures higher than 374 K the agreement is excellent in the entire range of pressures as can be seen in the insert of figure 3.3. A similar behavior for the isothermal compressibility is shown in figure 3.4 (and the insert therein).

Figure 3.5 illustrates the isobaric heat capacity obtained in this work as a function of density. We have chosen to plot these results (as well as those in the following figures) in terms of density for visual clarity, but the analysis from a C_p vs. P plot shows the same tendency. Deviations smaller than 3% are found between the 2CLJQ model and the Span-Wagner EOS except in the already mentioned extended critical region. Nevertheless, the deviations of C_p

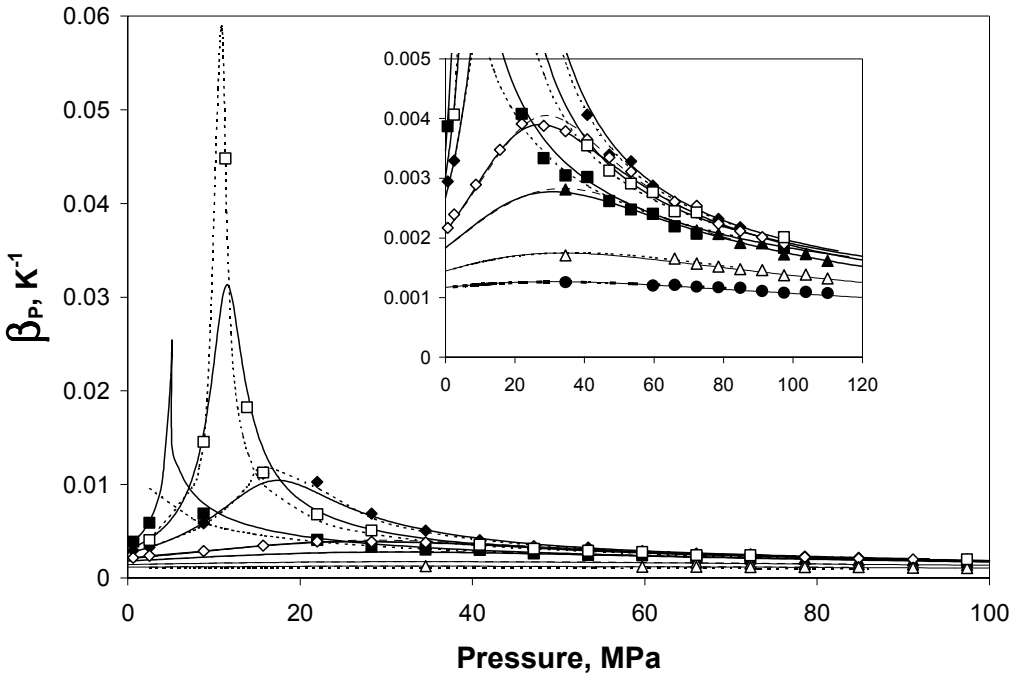

Figure 3.3. Volume expansivity (β_P) versus pressure. Legend as in figure 3.2.

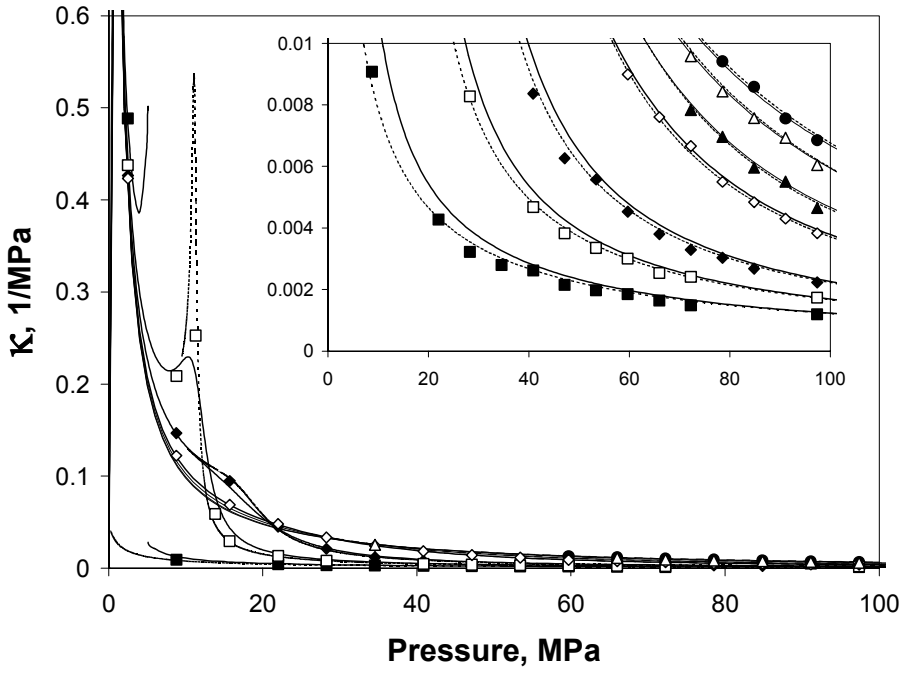

Figure 3.4. Isothermal compressibility (κ) as a function of pressure. Legend as in figure 3.2.

in the extended critical region are considerably smaller than those found for the isothermal compressibility (κ) and the volume expansivity (β_P). It is interesting to note that κ and β_P involve fluctuations in volume whereas C_p only involves fluctuation in energy and enthalpy.

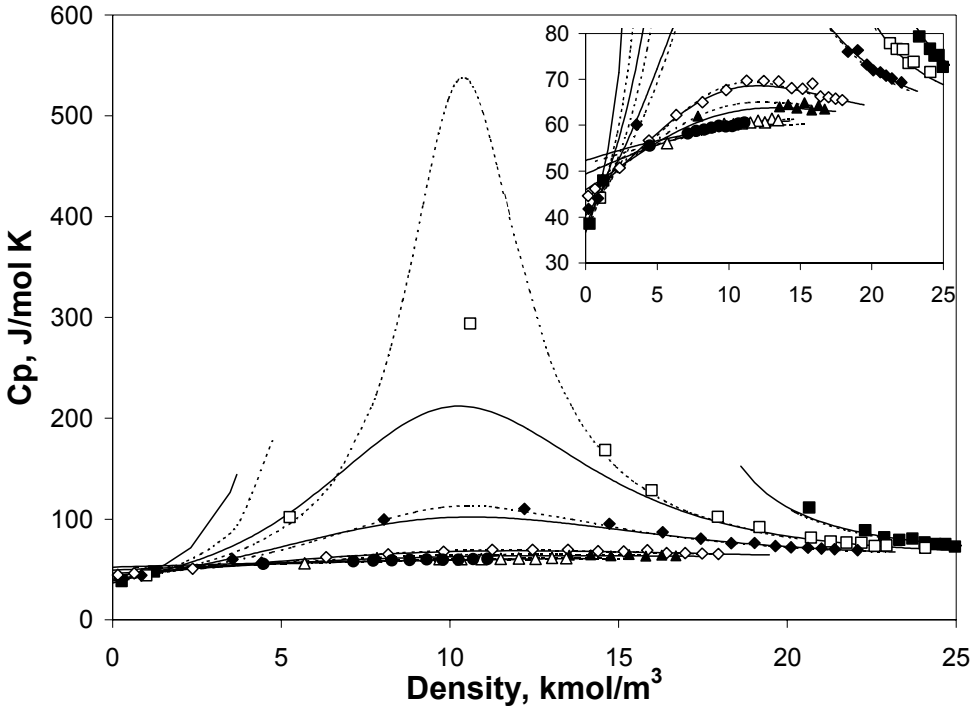

Figure 3.5. Isobaric heat capacity (C_P) as a function of density. Legend as in figure 3.2.

3.7 Results for Derived Properties

Joule-Thomson coefficients are plotted in figure 3.6 as a function of density. In this case, excellent agreement is found in the entire region of study except at very low densities. Lagache *et al.* [20] recently reported similar results for the low-density region in simulations of methane, ethane and butane with a united atom potential.

The insert in figure 3.6 shows the points obtained in the region where this coefficient changes in sign. The locus of states where the Joule-Thomson coefficient is equal to zero is called the Joule-Thomson inversion curve. The determination of this curve is considered one of the

most demanding tests that can be performed on any equation of state. In a previous work [18], we obtained the Joule-Thomson inversion curve for carbon dioxide, using the same 2CLJQ potential as in the present work. Very good agreement was obtained with both experimental data and molecular simulations, and the work helped to resolve an apparent anomaly in the Joule-Thomson inversion curve that had been reported in the literature.

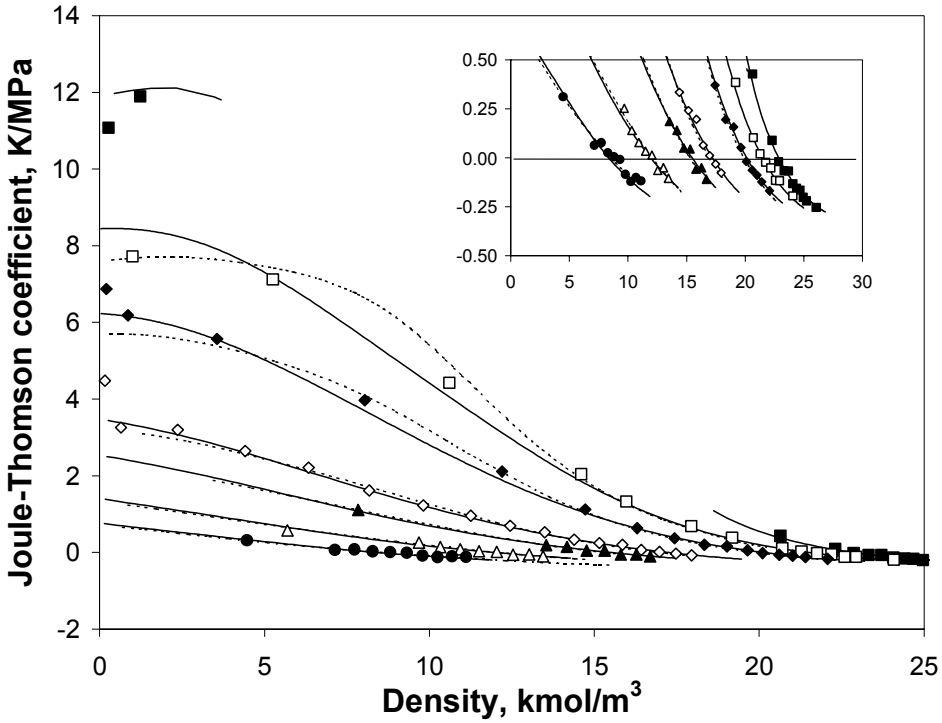

Figure 3.6. Joule-Thomson coefficient versus density diagram for carbon dioxide. Legend as in figure 3.2.

Finally, in figure 3.7 the speed of sound is plotted against density. The representation of speed of sound is regarded as a sensitive test since it involves not only the correct representation of heat capacities, but also of the first derivatives of the volume. The overall predictions can be considered excellent. The largest deviations are once more found for the lower temperature high-density region. These deviations are consistent with the deviations found in density. The largest error in the speed of sound is approximately 5%, which is considerably lower than the errors found in the properties involved in its definition, C_p and κ (see equation 3.11), in the extended critical region, possibly due to a compensation of errors

in the quotient of these two quantities. This suggests that speed of sound as a single property may provide a less sensitive test than heat capacity and isothermal compressibility, each by itself, particularly in the near-critical region. For instance, CO_2 at 330 K is sufficiently close to critical conditions that a clearly defined peak is observed in κ (figure 3.4) and C_p (figure 3.5), yet there is no equivalent minimum in u (figure 3.7), which requires a lower temperature to appear.

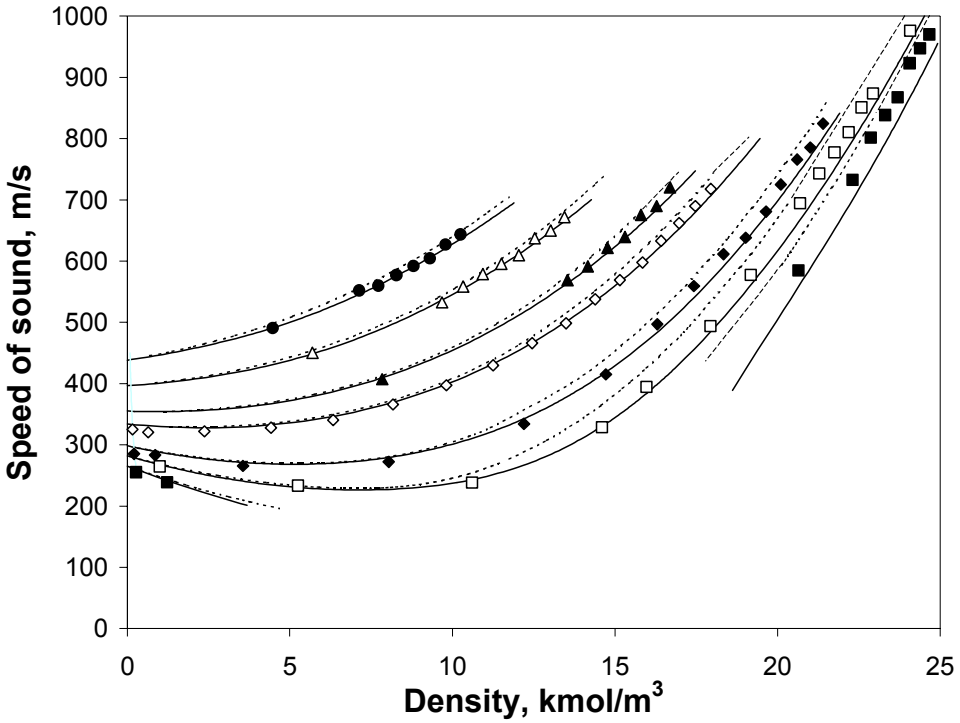

Figure 3.7. Speed of sound versus density diagram for carbon dioxide. Legend as in figure 3.2.

3.8 Conclusions

The parameters for the 2CLJQ model for carbon dioxide were obtained by Möller and Fischer [2] by fitting experimental saturation properties. It has been shown that these

parameters give good predictions of vapor-liquid equilibria properties [2]. In this work, the transferability of the parameters to the supercritical region has been studied through a comprehensive comparison between calculated values of several thermodynamic properties for CO_2 and their experimental values (represented by the Span-Wagner EOS) as well as against the 2CLJQ EOS. We have presented simulation results for the isobaric heat capacity, volume expansivity, isothermal compressibility and combinations of these quantities such as the speed of sound and the Joule-Thomson coefficient for which experimental data are available.

It has been shown that these parameters can be used with confidence for the prediction of thermodynamic properties, including those of industrial interest such as the speed of sound or Joule-Thomson coefficient, for CO_2 in the supercritical region, except in the extended critical region. This region is larger than usual due to the differences between the critical point predicted for the 2CLJQ model for carbon dioxide and the experimental critical point. Unfortunately, this region is extremely important for the so-called CO_2-driven process where the tunability of CO_2 plays a key role. Therefore, care must be taken when using this potential to model CO_2 in this extended critical region.

We also show that the agreement of calculated and experimental values for speed of sound does not necessarily guarantee good agreement in the isobaric heat capacity and the first derivatives of the volume.

Deviations between the 2CLJQ EOS and simulations, which can be quite large in the two-phase region [21], appear to become less important at higher supercritical temperatures and pressures. The present results, however, are limited to CO_2 only. More extensive testing with a wider range of fluids will be required before the predictive capabilities of the 2CLJQ model can be fully assessed in the supercritical region.

Acknowledgments

This work was supported in part by the STC Program of the National Science Foundation under Agreement No. CHE 9876674, and by the Grant Agency of the Czech Republic under Grant No. 203/02/0805.

3.9 References

[1] G. Kronome, T. Kristóf, J. Liszi and I. Szalai, "Heat capacities of two-centre Lennard-Jones fluid from NpT ensemble Monte Carlo simulations", Fluid Phase Equilib. **155**, 157 (1999).

[2] D. Möller and J. Fischer, "Determination of an effective intermolecular potential for carbon-dioxide using vapor liquid-phase equilibria from NPT plus test particle simulations", Fluid Phase Equilib. **100**, 35 (1994).

[3] M. Mecke, A. Müller, J. Winkelmann and J. Fischer, "An equation of state for two-center Lennard-Jones fluids", Int. J. Thermophys. **18**, 3, 683 (1997). Erratum 2. Int. J. Thermophys. **19**, 5, 1495 (1998).

[4] B. Saager and J. Fischer, "Construction and application of physically based equations of state. Part II. The dipolar and quadrupolar contributions to the Helmholtz energy", Fluid Phase Equilib. **72**, 67(1992).

[5] R. Span and W. Wagner. "A new equation of state for carbon dioxide covering the fluid region from the triple-point temperature to 1100 K at pressures up to 800 MPa", J. Phys. Chem. Ref. Data **25**, 1509 (1996).

[6] J.G. Harris and K.H. Yung, "Carbon dioxide's liquid-vapor coexistence curve and critical properties as predicted by a simple molecular model", J. Phys Chem. **99**, 12021 (1995).

[7] J.J. Potoff, J.R. Errington and A.Z. Panagiotopoulos, "Molecular simulations of phase equilibria for mixtures of polar and non-polar components", Mol. Phys. **97**, 1073 (1999).

[8] J. Vrabec, J. Stoll, and H. Hasse, "A set of molecular models for symmetric quadrupolar fluids", J. Phys. Chem. B ***105,*** 12126 (2001).

[9] K. Singer, A. Taylor and J.V.L Singer, "Thermodynamic and structural properties of liquids modeled by 2-Lennard-Jones centers pair potentials", Mol. Phys. **33**, 1757 (1977).

[10] C.S. Murthy, S.F. O'Shea, and I.R. McDonald, "Electrostatic interactions in molecular crystals. Lattice dynamics of solid nitrogen and carbon dioxide", Mol. Phys. **50**, 531 (1983).

[11] J. Yang, Y. Ren, A. and T.H. Sun, "COMPASS force field for 14 inorganic molecules, He, Ne, Ar, Kr, Xe, H2,O2,N2, NO, CO, CO2, NO2,CS2, and SO2, in liquid phases", J. Phys. Chem. B **104**, 4951 (2000).

[12] J.J. Potoff and J.I. Siepmann, "Vapor-liquid equilibria of mixtures containing alkanes, carbon dioxide, and nitrogen", AICHE J.**47**, 7, 1676(2000).

[13] K. Fotouh and K. Shukla, "Effect of quadrupole moment on excess properties of binary 2CLJQ mixtures from molecular dynamics simulation: model and real mixtures", Fluid Phase Equilib. **135** , 35(1997).

[14] J. Vrabec and J. Fischer, "Vapor-liquid equilibria of the ternary mixture CH4+C2H6+CO2 from molecular simulation", AIChE J. **43**, 212 (1997).

[15] J. Vrabec and J. Fischer, "Vapor-liquid equilibria of binary mixtures containing methane, ethane, and carbon dioxide from molecular simulation", Int. J. of Thermophysics **17**, 889 (1996).

[16] A. De Santis, R. Frattini, D. Gazzillo and M. Sampoli, "The potential model dependence of the neutron radial and partial distribution functions for liquid CO_2 ", Mol. Phys. **60**, 21 (1987).

[17] B. Chen, J.I. Siepmann and M.L. Klein, "Direct Gibbs ensemble Monte Carlo simulations for solid-vapor phase equilibria: Applications to Lennard-Jonesium and carbon dioxide", J. Phys. Chem. B **105**, 9840 (2001).

[18] C.M. Colina, M. Lísal, F. R. Siperstein and K.E. Gubbins, "Accurate CO_2 Joule-Thomson inversion curve by molecular simulations", Fluid Phase Equilib. **202**, 253 (2002).

[19] D.A. McQuarrie, "Statistical Mechanics", HarperCollins, New York, 1976.

[20] M. Lagache, P. Ungerer, A. Boutin and A. H. Fuchs, "Prediction of thermodynamic derivative properties of fluids by Monte Carlo simulation", PCCP **3**, 4333 (2001).

[21] G. Kronome, J. Liszi and I. Szalai, "Monte Carlo simulation of some thermophysical properties of two-centre Lennard-Jones fluids along the vapour-liquid equilibrium curve", Mol. Phys. **93**, 279 (1998).

[22] J. Stoll, J. Vrabec, H. Hasse, J. Fischer, "Comprehensive study of the vapour-liquid equilibria of the pure two-centre Lennard-Jones plus pointquadrupole fluid", Fluid Phase Equilib. **179**, 339 (2001).

Chapter 4

Predictions of the Joule-Thomson inversion curve for the n-alkane series and carbon dioxide from the Soft-SAFT Equation of State*

Coray M. Colina[1,2], Luis F. Turrens[3] , Keith E. Gubbins[1], Claudio Olivera-Fuentes[2] and Lourdes F. Vega[3]

[1]Department of Chemical Engineering, North Carolina State University
Raleigh, NC27695, USA
[2]TADiP Group, Thermodynamics and Transport Phenomena Department
Simón Bolívar University, AP 89000, Caracas 1080, Venezuela
[3]Departament d'Enginyeria Química, ETSEQ, Universitat Rovira i Virgili
Carretera de Salou s/n, 43006 Tarragona (Spain)

4.1 Abstract

In this work we use a molecular based equation of state, the Soft-SAFT equation, to predict complete Joule-Thomson inversion curves for carbon dioxide and the n-alkanes, including heavy *n*-alkanes up to octatetracontane (*n* -$C_{48}H_{98}$). Comparisons with available experimental and correlation data, for carbon dioxide and the lighter n-alkanes, show good quantitative agreement. We observe a strong dependence of the inversion curve on the set of molecular parameters used in the calculations, especially near the inversion point and in the high temperature region. The equation is able to predict the general trend of inversion curves even for extreme conditions, with reduced pressure, $P_r=P/P_c$, values up to 40, and reduced temperatures, $T_r=T/T_c$, of almost 5.

* *Ind. Eng. Chem. Res.* **41**, 1069-1075 (2002)

4.2 Introduction

Joule-Thomson expansion [1], or throttling, is a process in which the enthalpy of a fluid remains constant. As the pressure drops, temperatures can either increase or decrease, depending on the initial pressure and temperature, final pressure, and composition of the fluid. The regions where cooling and heating take place are separated by the Joule-Thomson inversion curve (JTIC), which is the locus of states in which the Joule-Thomson coefficient, μ, is zero:

$$\mu \equiv \left(\frac{\partial T}{\partial P}\right)_h = 0 \tag{4.1}$$

where *T*, *P* and *h* are the fluid's temperature, pressure and enthalpy, respectively. The JTIC is usually represented in pressure-temperature coordinates, where it extends from a minimum in temperature corresponding to a saturated state on the vapor pressure line, to a maximum in temperature corresponding to the ideal-gas limit at zero density and pressure. It passes through a pressure maximum at an intermediate temperature, and should have no other extrema or inflection points [2].

Although knowledge of the inversion curve is obviously essential for the design and operation of throttling processes, direct measurement of inversion points is difficult and unreliable. At near-inversion conditions, the vanishing Joule-Thomson coefficients imply that even large pressure changes will produce very small temperature differences, detectable only by extremely accurate measurements. Hence, it is generally preferable to make use of thermodynamics relations such as:

$$\mu = \frac{1}{C_P}\left[T\left(\frac{\partial v}{\partial T}\right)_P - v\right] = \frac{RT^2}{C_P P}\left(\frac{\partial Z}{\partial T}\right)_P \tag{4.2}$$

to derive Joule-Thomson coefficients and inversion points from experimental P-*v*-T data either by direct numerical treatment of the raw data, or by first fitting the data by an equation of state (EOS). Even then, the inversion curves of the heavier fluids cannot be completely determined, because they extend into regions of high temperature and pressure not attainable experimentally.

In fact, the computation of the JTIC is one of the most demanding tests that can be performed on a set of experimental (or simulation) data or on analytical equations of state. For volume-explicit EOSs, an equivalent formulation of the thermodynamic inversion criterion of eqns 4.1 and 4.2 is given by:

$$T\left(\frac{\partial P}{\partial T}\right)_v + v\left(\frac{\partial P}{\partial v}\right)_T = 0 \tag{4.3}$$

where v is the specific or molar volume. This equation shows that the EOS must accurately predict not only the P(T, v) function but also its first partial derivatives with respect to temperature and volume, over wide temperature and pressure ranges which in many cases exceed reduced values $T_r = 5$ and $P_r = 12$. Even the most carefully developed EOSs may fail to generate physically correct inversion curves when extrapolated to such extreme conditions. In fact, several authors [3, 4, 5, 6] have used the prediction of JTICs as a criterion to assess and rank the predictive capabilities of available EOS, by comparing computed inversion curves against experimental data and empirical correlations available for simple fluids.[3, 7] More recently, generalized correlations have also been developed for non-simple fluids [8,9] based on the Lee-Kesler [10] (LK) and Boublík-Alder-Chen-Kreglewski [11] (BACK) EOSs.

It is often claimed that a main advantage of molecular-based models is the fact that the molecular parameters are *independent* of the thermodynamic conditions. Hence, once the molecular model is tested against available experimental data, the same model can be used to predict, with confidence, the thermodynamic properties of the same system at other conditions. It would be of great interest to check the validity of this assertion by calculating

JTICs from a molecular-based EOS. Although several authors have mentioned this need, the only published work for on real fluids we are aware of is the calculation of the JTIC of carbon dioxide by molecular simulation.[12]

In this work, we concentrate on calculating the JTICs of the n-alkanes series and of carbon dioxide from one of these molecular-based equations, the SAFT (Statistical Associating Fluid Theory) EOS. In particular, we present predicted inversion curves for heavy n-alkanes, up to octatetracontane ($C_{48}H_{98}$). The phase behavior of pure alkanes and their mixtures has been calculated using SAFT by several authors.[13,14,15,16,17,18,19] There are different versions of this equation, depending, mainly, on the reference fluid used; for details on its implementation and application to several mixtures see the reviews of Müller and Gubbins [20, 21] and references therein.

Recently, Pàmies and Vega [16] have published predictions for the phase equilibria of pure and binary mixtures of heavy *n* -alkanes, using the so-called Soft-SAFT EOS, a modified version of the original SAFT equation. They proposed a new set of transferable molecular parameters that provide a significant improvement over previous calculations [13], especially for the heavy members of the series. A correlation for the critical properties of heavy *n* -alkanes was also proposed. Comparisons of the Soft-SAFT EOS predictions with available experimental and simulation data of pure and selected binary mixtures showed that the equation is able to capture the main features of the phase envelope in all cases, giving the same degree of accuracy as molecular simulation models [22,23,24]. An excellent quantitative agreement with experimental data for these mixtures was obtained when two fitted binary interaction parameters, independent of the thermodynamic conditions, were used. The main conclusion of their work, related to the work presented here, is that the molecular parameters must be finely tuned in order to obtain accurate predictions well apart from the data used in the fitting procedure.

Since a correlation of molecular parameters for any member of the series is available, the accuracy of this and other correlations will be checked by comparing the Soft-SAFT

predicted JTICs with available experimental data and with inversion curves obtained from the BACK and the LK models. The accuracy and reliability of these two EOSs as sources of pseudo-experimental inversion data has been the subject of more detailed analysis and verification elsewhere.[8, 9] Neither model is however applicable to heavy *n* -alkanes. The LK EOS is a three-parameter corresponding states EOS that extends beyond n-octane only as an extrapolation. The BACK EOS is a repulsion/attraction model with up to five fluid-specific parameters, available in the TRC Tables [25] for a number of substances, but not for *n* -alkanes above *n* -decane.

It should be emphasized that the Soft-SAFT parameters used here were obtained by fitting vapor-liquid equilibria data for the light members of the series. Hence, by performing this test, a double check is done: (1) the accuracy of the equation in predicting first partial derivatives is tested, and (2) the accuracy of the molecular parameters correlation itself when used to predict other thermodynamic properties, is investigated.

4.3 The Soft-SAFT EOS

The Soft-SAFT EOS [26] is a modification of the original SAFT equation proposed by Chapman et al.[27] and Huang and Radosz.[28, 29] in which the reference term is a Lennard-Jones fluid. As in the rest of the SAFT equations, the chain contribution is obtained based on Wertheim's first order perturbation theory [30, 31, 32]. As mentioned earlier, the reviews of Müller and Gubbins [20,21] present details on the SAFT approach as well as the differences among several modifications and extensions, and the reader is referred to them for further details. Here we will explain just the features concerning its implementation in this work.

The equation is written in terms of the Helmholtz free energy. The residual Helmholtz free energy for a fluid of chain molecules can be expressed as a sum of two terms: a reference term, $A^{ref,}$ including the repulsive and attractive energies, and a chain term, A^{chain}:

$$\frac{A}{N_m k_B T} - \frac{A^{ideal}}{N_m k_B T} = \frac{A^{ref}}{N_m k_B T} + \frac{A^{chain}}{N_m k_B T} \tag{4.4}$$

where N_m is the number of chain molecules in the system and k_B the Boltzmann constant. The form of A^{ideal} in eqn 4.4 is:

$$\frac{A^{ideal}}{N_m k_B T} = ln\,\rho_m \Lambda^3 - 1 \tag{4.5}$$

where $\rho_m = N_m / V$ is the molecular density, N_m the number of molecules, V the volume of the system and Λ the thermal de Broglie wavelength. ρ_m, the total number of chains per unit volume, can be related to the total monomer density by $\rho = m\rho_m$, m being the chain length.

The reference term accounts for the repulsive and attractive interactions of the Lennard-Jones segments forming the chains. As in previous works, we have used the equation of Johnson et al. [33]

The chain contribution for a fluid of chains with bond length equal to σ, the diameter of a Lennard-Jones segment, is written as:

$$\frac{A^{chain}}{N_m k_B T} = 1 - m\,ln\,y_R(\sigma) \tag{4.6}$$

where $y_R(\sigma)$ is the contact value of the cavity correlation function for spherical segments of the Lennard-Jones reference fluid. $y_R(\sigma)$ is given by

$y_R(\sigma) = g_R(\sigma) exp(\phi_{LJ}(\sigma_i)/k_B T)$, with $g_R(\sigma)$ the pair radial distribution function of the Lennard-Jones fluid and $\phi_{LJ}(\sigma)$ the Lennard-Jones potential energy.

4.4 Molecular Model

Following previous work, *n* -alkanes are described as homonuclear chain-like molecules, modeled as *m* Lennard-Jones segments of equal diameter σ and the same dispersive energy ε, bonded tangentially to form the chain. We must emphasize that although the molecular parameters have physical meaning (chain length, segment diameter and dispersive energy per segment) they are *effective* parameters, hence care must be taken when using them for other applications, as will be discussed later. Although the model is simple compared to more realistic models, such as those used in recent simulations, [22,23,24] it conserves the relevant features of the real system, and it has proved to predict with high accuracy the phase equilibria of *n* -alkane multicomponent mixtures [13, 16,17,18] as well as the critical properties of *n* -alkane binary mixtures.[14,15]

In a similar manner, carbon dioxide is modeled as a chain of *m* Lennard-Jones segments, with size parameter σ and dispersive energy $\tilde{\varepsilon}$. The quadrupolar moment is not included explicitly, however, the fitted values of *m*, σ and ε effectively account for it.

According to this model, three molecular parameters, *m*, σ and ε are required to describe all thermodynamic properties of each compound. The molecular parameters for carbon dioxide used in this work have been obtained by fitting the experimental liquid density and equating the chemical potential in both phases. The resulting values are: m = 2.6815, σ= 2.532 and ε/κ_B =153.16.

As mentioned above, several correlations of the molecular parameters for the n-alkanes series have been proposed in the literature. Among them, the one recently proposed by Pàmies and Vega [16] (the PV correlation) seems to be the most accurate for predicting the vapor-liquid

equilibria of heavy n-alkanes and their mixtures, as well as their critical properties. This correlation is given by the following equations:

$$m = 0.0255\, M_w + 0.628 \tag{4.7}$$

$$m\,\sigma^3 = 1.73\, M_w + 22.8 \tag{4.8}$$

$$m\,\varepsilon / k_B = 7.89\, M_w + 38.0 \tag{4.9}$$

Units of σ^3 and ε / k_B are $Å^3$ and K, respectively. M_w is the *n* -alkane molecular weight, in g/mol.

4.5 Results and Discussion

We have followed a standard procedure [5, 6, 34] to compute each inversion curve by solving eqns 4.3 and 4.4 simultaneously as follows: we first choose a temperature value and solve eqn 4.3 for the volume; with these temperature and volume values, the corresponding value of the pressure is obtained through eqn 4.4. By repeatedly increasing *T* and calculating *v* and *P*, the complete inversion curve is obtained.

Among the main advantages of molecular-based equations over macroscopic models is the fact that they have fewer parameters, and these parameters have physical meaning. However, since a non-linear optimization procedure is used when fitting *molecular* parameters to an experiment, one could find different sets of parameters compatible with the desired accuracy of the fitting. Hence, the predictive capability of one particular set of parameters would be demonstrated if accurate predictions are obtained at conditions well apart from those used in the fitting procedure and, especially, if they can be used to predict, with confidence, other thermodynamic properties than the ones used in the fitting. We have

performed this test here for different sets of molecular parameters available for *n* -alkanes with the Soft-SAFT EOS.

4.5.1 The inversion curve of carbon dioxide

Predicted JTICs for carbon dioxide from the LK, BACK (with parameters taken from the TRC compilation [25]) and Soft-SAFT (with the parameters given in the previous section) equations are shown in Figure 4.1, together with values generated from the multiparameter equation by Span-Wagner [35] and the Ely et al. equation implemented in the ALLPROPS computer package (Lemmon et al. [36]). Also shown are the experimental values interpolated from Vukalovich and Altunin's interpolation of data of Price, given in Perry's Handbook.[37] The JTIC obtained from the Pitzer-Sterner [38] EOS and the molecular simulation points of Chacín et al.[12] are not shown, because it has been recently demonstrated [39] that, at high temperatures, the former is incorrect due to physically erroneous prediction of third virial coefficients, and the latter are subject to uncertainty.

It can be seen that both multiparameter EOSs give similar results, and are in reasonable agreement with the experimental data. The largest deviations from the predicted (LK, BACK, Soft-SAFT) curves occur around the maximum inversion pressure and in the upper temperature branch of the JTIC. Although the BACK equation gives better agreement with the experimental data available, the agreement obtained with Soft-SAFT EOS can be considered good, given the crude molecular model used. An improvement should be expected if the quadrupolar moment is explicitly considered.

4.5.2 Inversion curves for the *n*-alkanes series

Regarding the n-alkane series, we begin our calculations with methane, a simple fluid for which there is abundant experimental and theoretical data available. Figure 4.2 shows the calculated JTIC for methane as obtained with the Soft-SAFT EOS with the BV parameters [13]. Results are compared with predictions from the BACK EOS, the LK correlation, and

the multiparameter equations of Ely et al., taken from the ALLPROPS package [36], and of Sychev et al.[40] It is observed that the molecular equation gives quantitative agreement with the multiparameter models, matching the maximum pressure slightly better than the LK and BACK EOSs, and it otherwise follows the same trend as these two equations. The experimental critical point of methane has been used to reduce the pressure and temperature in all cases.

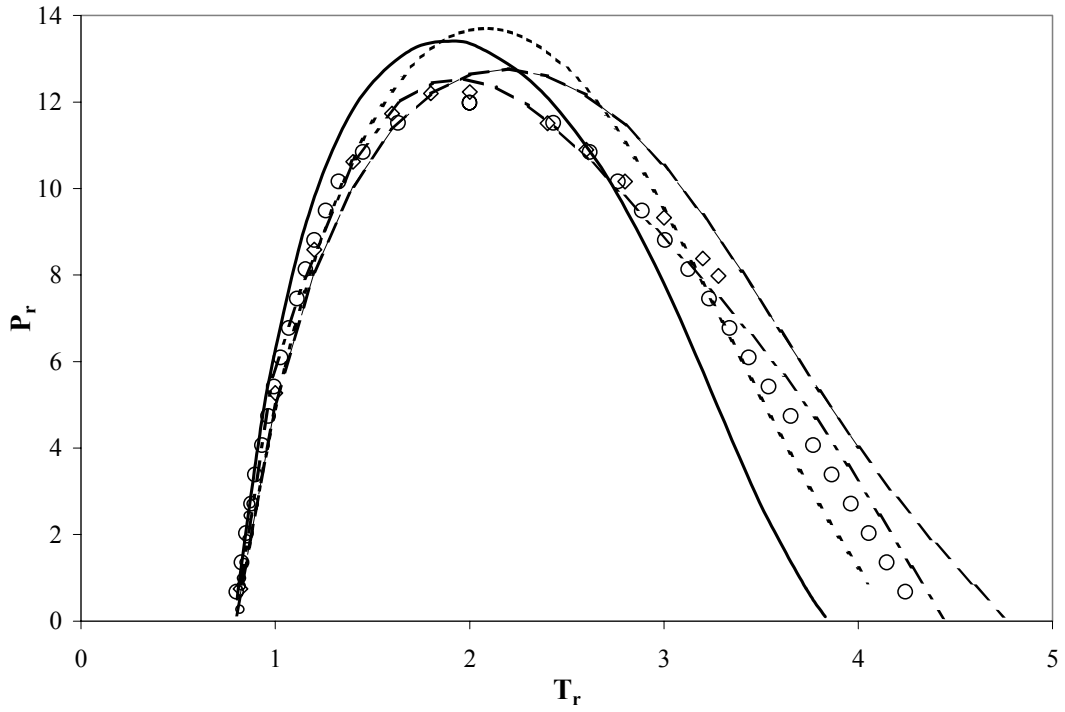

Figure 4.1 The Joule-Thomson inversion curve for carbon dioxide. (o) Experimental values interpolated from Vukalovich and Altunin's interpolation of data of Price presented in Perry's Handbook [37]; (◊) Ely et al. equation implemented in the ALLPROPS computer package (Lemmon [36] et al.); dotted-dashed line Span-Wagner [35] EOS; dotted line LK EOS; dashed line BACK EOS; continuous line Soft-SAFT EOS.

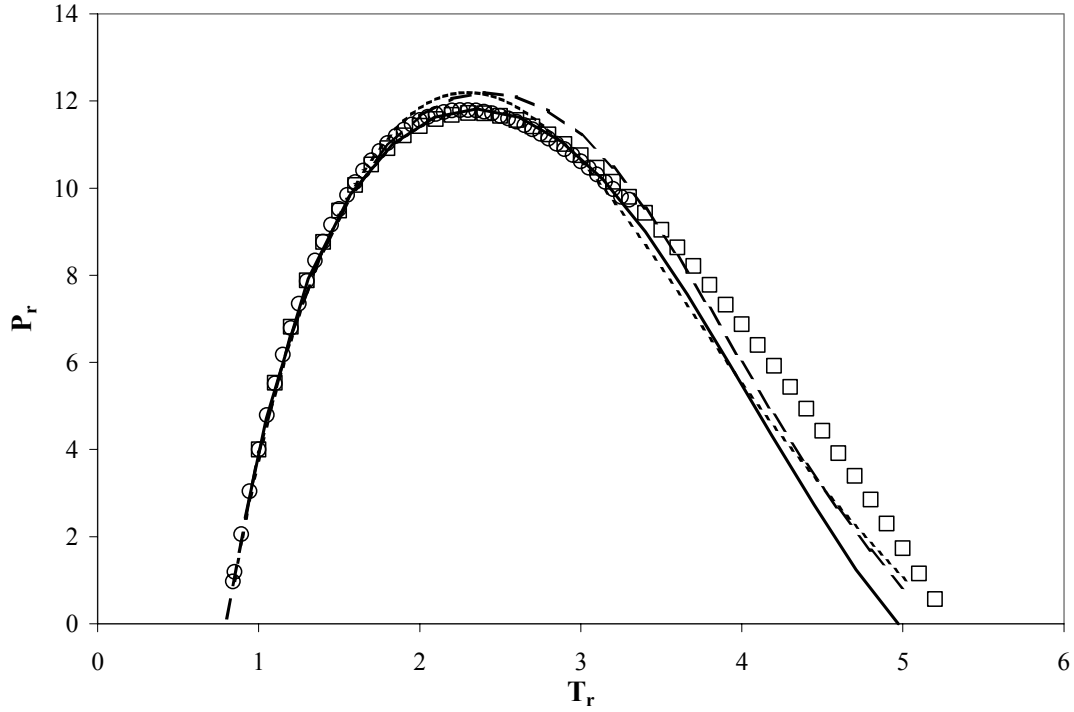

Figure 4.2. The Joule-Thomson inversion curve for methane: (o) Ely et al. equation implemented in the ALLPROPS computer package (Lemmon et al. [36]); (□) Sychev et al.[40] EOS; dotted line LK EOS; dashed line BACK EOS; continuous line Soft-SAFT EOS.

To check the influence of the molecular parameters used on the inversion results, we have obtained the JTIC of light *n* -alkanes with the same Soft-SAFT equation, but using three different sets of molecular parameters: the BV and PV correlations, two sets of parameters obtained by fitting the experimental liquid densities and equating chemical potentials, but choosing different solutions in the optimization procedure, and the PVr correlation, obtained from the PV correlation by re-scaling to the critical point (see reference 16 for details). Pàmies and Vega [16] observed that the PV correlation gives much better predictions of the vapor-liquid equilibria of heavy *n* -alkanes than the BV correlation, the performance of both being similar for the light members of the series. The PVr correlation was developed only to predict the critical properties of heavy *n* -alkanes, for which experimental data is impossible to obtain due to their thermal instability. The accuracy of the PVr correlation is expected to deteriorate away from the critical point, since it is impossible to simultaneously describe the

vapor-liquid equilibrium region and the critical region by an analytical equation of state, unless a crossover treatment is included.[41]

Figure 4.3 displays the JTICs for butane with the three different sets of parameters, as compared to the BACK and LK equations. It is observed that the Soft-SAFT EOS with the PV correlation gives predictions in almost quantitative agreement with LK, while the BV correlation, quite accurate for methane, begins to deviate for n-butane. As expected, the performance of the PVr correlation is not as good as the others, for the reasons given above.

The JTIC for *n*-octane is shown in figure 4.4. Here, differences between predictions from different sets of parameters become obvious for both the BACK and the Soft-SAFT EOSs. It must first be recalled that the LK corresponding states model uses n-octane as a reference fluid, incorporating an EOS developed specifically for it. LK predictions for n-octane are thus expected to be quite reliable. It is striking to see the influence of the tuned parameters in predicting properties. Predictions from the Soft-SAFT EOS with the PV parameters are excellent compared to the LK correlation, while the BV strongly deviates for this system. Similar behavior is seen from the BACK equation, for which two sets of parameters have been reported in the literature.[25, 42] It is interesting to observe that the BACK JTICs extend to considerably higher temperatures than the LK correlation, while the BV and PV Soft-SAFT curves span a narrower temperature range, the latter in particular matching extremely well the maximum inversion temperature given by the LK EOS.

Since the preceding comparisons show that the best predictions from the Soft-SAFT EOS are obtained by using the PV correlation, we have employed only this particular version of the EOS for the rest of our calculations. Figure 4.5 displays the JTICs obtained for the light members of the n-alkane series, from methane to *n*-octane. Figure 4.6 similarly depicts JTICs predicted for selected heavier *n*-alkanes, from *n*-decane to *n*-octatetracontane ($C_{48}H_{98}$). For all *n* -alkanes from propane onwards, the computed inversion temperatures and pressures were reduced using critical properties obtained from a correlation [43] that gives quantitative agreement with experimental data [44, 45].

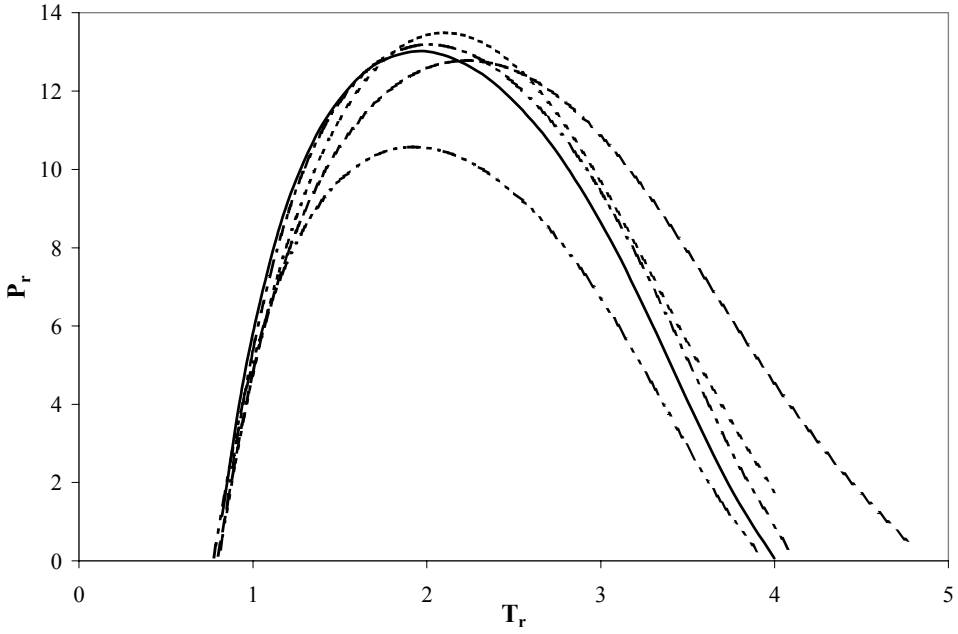

Figure 4.3. Influence of different sets of Soft-SAFT molecular parameters on the Joule-Thomson inversion curve for *n*-butane: continuous line BV parameters; dotted-dashed line PV parameters; double-dotted-dashed line PVr parameters; dotted line LK; dashed line BACK EOS.

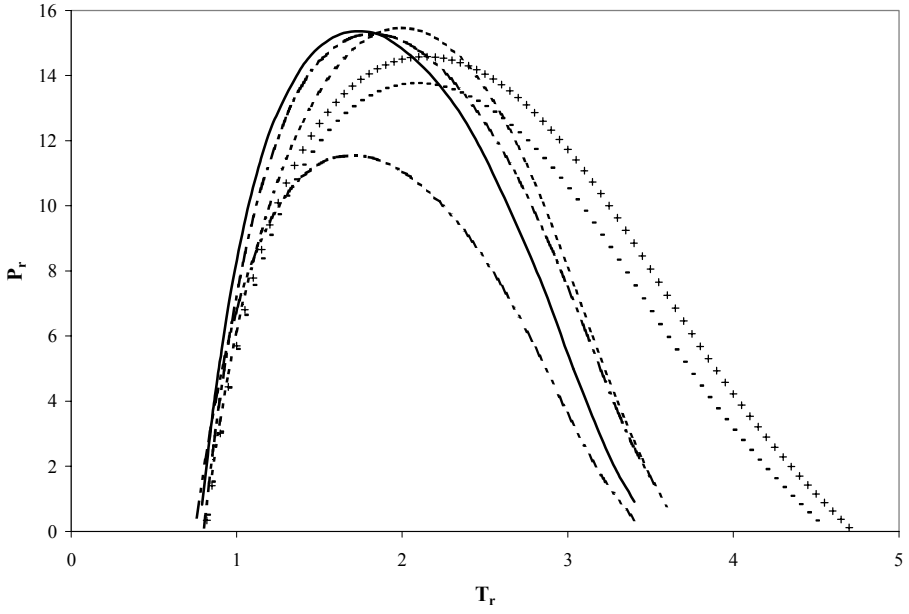

Figure 4.4. Comparison of predicted inversion curves for *n* -octane. Continuous line BV parameters; dotted-dashed line PV parameters; double-dotted-dashed line PVr parameters; dotted line LK EOS. (-) BACK EOS with TRC [25] parameters. (+) BACK EOS with parameters from Simnick et al.[42]

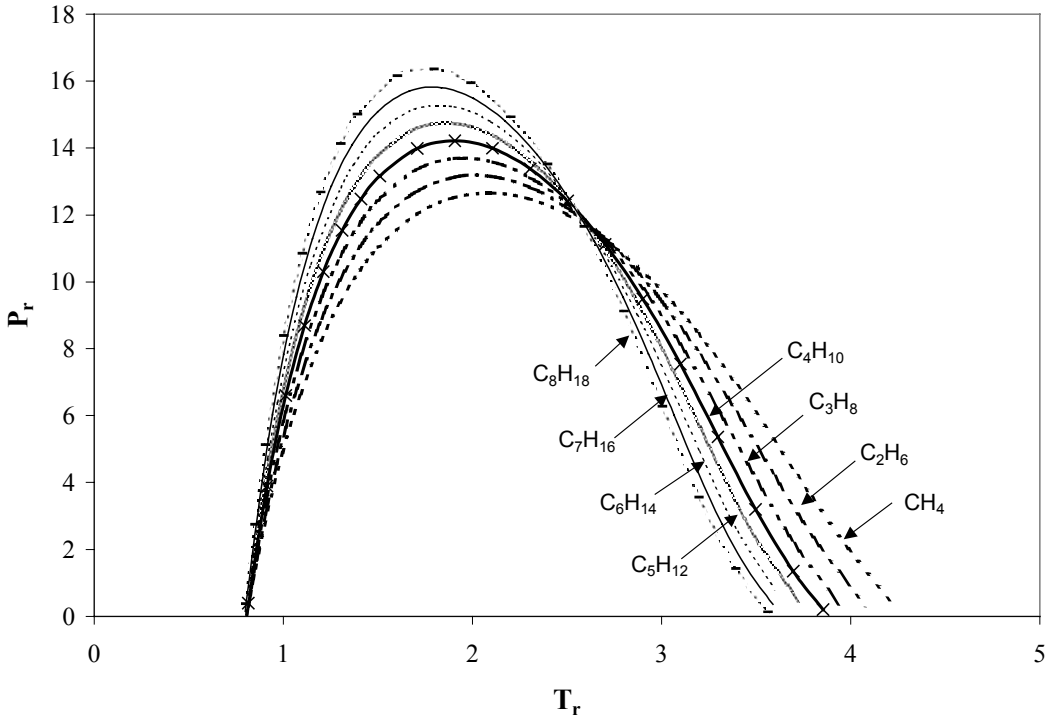

Figure 4.5. Predicted inversion curves for the light members of the *n* -alkane series, from methane to n-octane as obtained from the Soft-SAFT EOS with PV parameters (see figure for details).

Several comments may be made regarding the curves in Figures 4.5 and 4.6. We first note that there is a clear dependence of the JTIC on molecular weight for this homologous series of compounds, with maximum inversion pressures increasing and maximum inversion temperatures decreasing as the carbon number increases. This correlation is consistent with previous findings by Colazo et al.,[6] who demonstrated that the displacement of the JTIC towards higher pressures and lower temperatures is in fact related to a decreasing value of the critical compressibility factor. Most traditional equations of state break down when attempting to predict the complete JTIC of many compounds, because of the extrapolation involved either in temperature (for lighter fluids) or in pressure (for heavier fluids). The Soft-SAFT model, with its inbuilt molecular formulation for chainlike molecules, encounters no difficulties in extending to these extreme conditions, and is able to generate (at least) qualitatively correct inversion curves for compounds of very high molecular weight. Included in this consideration is the problem of the critical coordinates themselves; since *n* -

alkanes are thermally unstable for temperatures above 650 K, the experimental determination of critical points of *n* -alkanes heavier than *n* -decane becomes extremely difficult. The PVr correlation proposed by Pàmies and Vega [16,43] allows predicting the critical point of any *n*- alkane compound, with the Soft-SAFT EOS. Results from the equation with this set of parameters are in quantitative agreement with available experimental data [44,45]. Hence, we have a powerful tool, which in fact allows us to also calculate the JTIC of these heavy compounds, otherwise impossible to obtain.

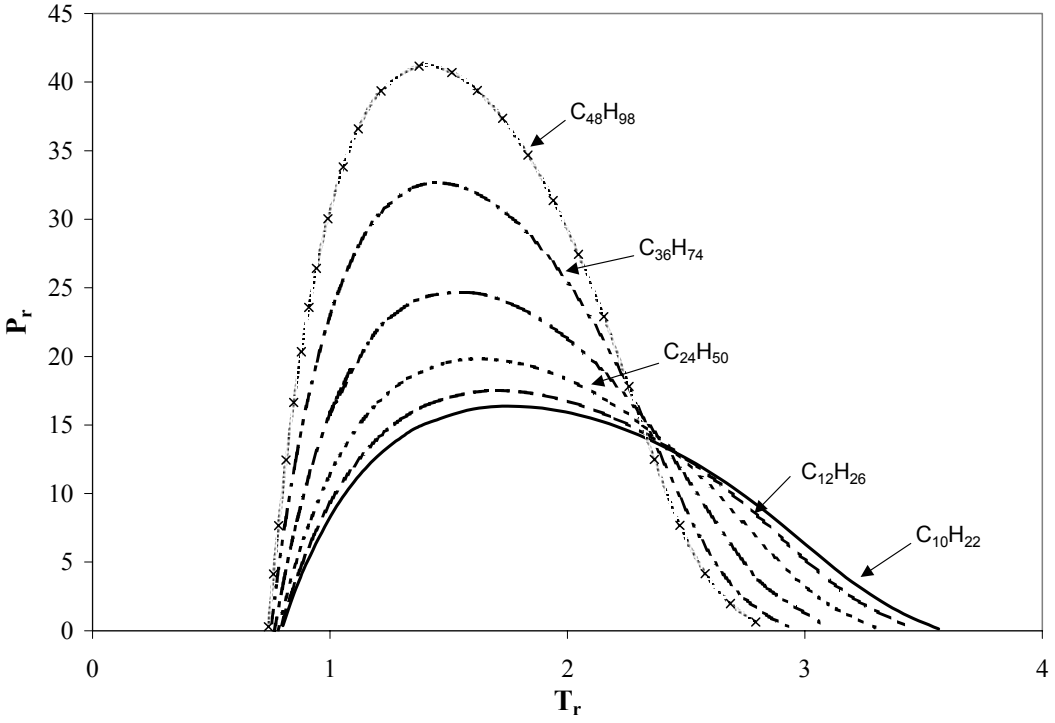

Figure 4.6. Predictions of the inversion curves for selected heavy *n*-alkanes. See figure for details.

It may of course be validly argued that the determination of the complete JTIC of very heavy n-alkanes is mostly an academic exercise, because the experimental conditions at which this inversion behavior takes place are unlikely to be met in practice. However, it seems to us of central importance that the EOS has the capability to represent and predict this behavior correctly. Otherwise, any future attempts at extending the same model to the prediction of the inversion properties of complex mixtures of hydrocarbons, e.g. reservoir fluids, would be put

in doubt by the possible inability of the EOS to deal with Joule-Thomson processes for the individual components. The practical importance of the Joule-Thomson effect in the temperature changes observed during production of petroleum fluids has been underlined in the previously cited work by Kortekaas et al. [1]

Finally, we remark on the crossing of the inversion curves in the diagrams of Figures 4.5 and 4.6. The Lee-Kesler EOS, which is an analytical representation of Pitzer's linear three-parameter corresponding states principle $Z(T_r, P_r; \omega) = Z^{(0)}(T_r, P_r) + \omega Z^{(1)}(T_r, P_r)$, necessarily predicts, as a mathematical consequence of eqn 4.2, that all inversion curves of normal fluids intersect at a common point in reduced coordinates, located at T_r = 2.72, P_r = 11.59. [9] Inspection of Figures 4.5 and 4.6 reveals that the Soft-SAFT EOS does not support this conclusion, although all the JTICs plotted in these diagrams do tend to come together in a narrow region at somewhat lower temperatures and higher pressures than predicted by the LK model. Strict compliance with the linear Pitzer principle is of course not an a priori expectation; it is not satisfied, for instance, by cubic EOSs in common use.[46] More detailed experimental evidence would be required to determine the correct nature of this particular feature of inversion curves.

4.6 Conclusions

We have been able to obtain complete inversion curves for carbon dioxide and the *n* -alkanes series using a molecular-based equation of state. The molecular parameters of carbon dioxide were obtained by fitting the vapor-liquid equilibrium data with the Soft-SAFT EOS, while we have used a correlation for the molecular parameters of the *n* -alkanes series available in the literature for the same equation.

Predicted inversion curves for carbon dioxide were compared with available experimental and theoretical results. Although the model used for carbon dioxide was too crude, it was able to reproduce the correct trend of the inversion curve.

Inversion curves for light hydrocarbons were obtained with the same Soft-SAFT equation but using different sets of molecular parameters. We have observed that the predicted curves strongly depend on the set of parameters used in the calculations, proving, once more, the importance of finely tuning the molecular parameters in the fitting procedure. Calculated curves for these compounds are in agreement with LK calculations.

Finally, the molecular nature of the parameters used in the Soft-SAFT equation, and the availability of a correlation for estimating critical points have allowed us to predict inversion curves for the first time for heavy *n* -alkanes, up to octatetracontane. In fact, there is in principle no limitation on chain length with this approach, provided the critical properties needed to reduce the temperature and the pressure are known or can be estimated.

Acknowledgments

Discussions with J.C. Pàmies are gratefully acknowledged. We are thankful to O. Garcia for fitting the molecular parameters of the carbon dioxide. CMC and KEG acknowledge the support received for this work by the STC Program of the National Science Foundation under Agreement No. CHE-9876674.

4.7 References

[1] Kortekaas W.G.; Peters C.J.; de Swaan Arons J. Joule-Thomson Expansion of High-Pressure-High-Temperature Gas Condensates. *Fluid Phase Equilibria* **1997**, *139*, 205.

[2] Deiters U. K.; De Reuck K. M. Guidelines for Publication of Equations of State – I. Pure Fluids. Pure Appl. Chem. 1997, 69 (6), 1237.

[3] Miller D. G. Joule-Thomson Inversion Curve, Corresponding States and Simpler Equations of State. *Ind. Eng. Chem. Fundam*. **1970**, *9*, 585.

[4] Juris K.; Wenzel L. A. A study of inversion curves. *AIChE J*. **1972**, *18*, 684.

[5] Dilay G. W.; Heidemann R. A. Calculation of Joule-Thomson Inversion Curves from Equations of State. *Ind. Eng. Chem. Fundam.* **1970**, *25*,152.

[6] Colazo A. V.; Da Silva F. A.; Müller E. A.; Olivera-Fuentes C. Joule-Thomson Inversion Curves and the Supercritical Cohesion Parameters of Cubic Equation of State. *Lat. Am. Appl. Res.* **1992**, *22*, 135.

[7] Gunn R. D.; Chueh P. L.; Prausnitz J. M. Inversion Temperatures and Pressures for Cryogenic Gases and their Mixtures. *Cryogenics,* **1966**, *6*, 324.

[8] Castillo M. G.; Colina C. M.; Dubuc J. E.; Olivera-Fuentes C. G. Three-Parameter Corresponding-States Correlations for Joule-Thomson Inversion Curves. *Int. J. Thermophysics*, **1999**, *20*, 6, 1737.

[9] Colina C. M.; Olivera-Fuentes C. An Improved Three-Parameter Corresponding States Correlation of Inversion Curves for Non-Simple Fluids, *in preparation*.

[10] Lee B. I.; Kesler M. G. A Generalized Thermodynamic Correlation Based on Three-Parameter Corresponding States. *AIChE J.* **1975**, *21*, 510.

[11] Chen S. S.; Kreglewski A. Applications of the Augmented van der Waals Theory of Fluids. I. Pure Fluids, *Ber. Bunsen-Ges. Phys. Chem*. **1977**, *81*, 1048.

[12] Chacín A.; Vásquez J.M.; Müller E.A. Molecular Simulation of the Joule-Thomson Inversion Curve of Carbon Dioxide. *Fluid Phase Equilibria* **1999**, *165*, 147.

[13] Blas F. J.; Vega L. F. Prediction of Binary and Ternary Diagrams using the Statistical Associating Fluid Theory (SAFT) Equation of State. *Ind. Eng. Chem. Res.* **1998**, *37*, 660.

[14] Blas F. J.; Vega L. F. Critical Behavior and Partial Miscibility Phenomena in Binary Mixtures of Hydrocarbons by the Statistical Associating Fluid Theory. *J. Chem. Phys*. **1998**, *109*, 7405.

[15] Vega L. F.; Blas F. J. Tricritical Phenomena in Chain-Like Mixtures from a Molecular-Based Equation of State. *Fluid Phase Equilibria* **2000**, *171*, 91.

[16] Pàmies, J.C.; Vega, L.F. The Vapor-Liquid Equilibria and Critical Behavior of Heavy n-Alkanes using Transferable Parameters from the Soft-SAFT Equation of State. *Ind. Eng. Chem. Res*. **2001**, in press

[17] Kraska, T.; Gubbins, K. E. Phase Equilibria Calculations with a Modified SAFT Equation of State .1. Pure Alkanes, Alkanols, and Water. *Ind. Eng. Chem. Res.* **1996**, 35, 4727.

[18] Kraska, T.; Gubbins, K. E. Phase Equilibria Calculations with a Modified SAFT Equation of State .2. Binary Mixtures of n-Alkanes, 1-Alkanols, and Water. *Ind. Eng. Chem. Res.* **1996**, 35, 4738.

[19] McCabe, C.; Jackson, G. SAFT-VR Modelling of the Phase Equilibrium of Long-Chain n-Alkanes. *Phys. Chem. Chem. Phys.* **1999**, *1*, 2057.

[20] Müller E. A.; Gubbins K. E. Associating Fluids and Fluids Mixtures, in J. V. Sengers, R. F. Kayser, C. J. Peters and H. J. White, Jr. (Eds), *Equations of State for Fluids and Fluid Mixtures. Experimental Thermodynamics*, Volume 5, Elsevier, Amsterdam, 2000, pp 435-478.

[21] Müller E. A.; Gubbins K. E. Molecular-Based Equations of State for Associating Fluids: A Review of SAFT and Related Approaches. *Ind. Eng. Chem. Res*. **2001**, in press.

[22] Martin M. G.; Siepmann J. I. Transferable Potentials for Phase Equilibria. 1. United-Atom Description of n-Alkanes. *J. Phys. Chem. B* **1998**, *102*, 2569.

[23] Errington J. R.; Panagiotopoulos A. Z. A New Intermolecular Potential Model for the n-Alkane Homologous Series. *J. Phys. Chem. B* **1999**, *103*, 6314

[24] Nath S. K.; Escobedo F. A.; de Pablo J. J. On the Simulation of Vapor-Liquid Equilibria for Alkanes. *J. Chem. Phys.* **1998**, *108*, 9905. Nath S. K.; Escobedo F. A.; de Pablo J. J.; Patramai I. Simulation of Vapor-Liquid Equilibria for Alkane Mixtures. *Ind. Eng. Chem. Res.* **1998**, *37*, 3195.

[25] Thermodynamics Research Center, *TRC Thermodynamic Tables*, The Texas A & M University System, College Station, TX, 1986.

[26] Blas F. J.; Vega L. F. Thermodynamic Behaviour of Homonuclear and Heteronuclear Lennard-Jones Chains with Association Sites from Simulation and Theory. *Mol. Phys.* **1997**, *92*, 135.

[27] Chapman W.G.; Gubbins K.E.; Jackson G.; Radosz M. New Reference Equation of State for Associating Liquids. *Ind. Eng. Chem. Res*. **1990**, *29*, 1709.

[28] Huang S. H.; Radosz M. Equation of State for Small, Large, Polydisperse, and Associating Molecules. *Ind. Eng. Chem. Res.* **1990**, *29*, 2284.

[29] Huang S.H.; Radosz M. Equation of State for Small, Large, Polydisperse, and Associating Molecules - Extension to Fluid Mixtures. *Ind. Eng. Chem. Res.* **1991**, *30*, 1994.

[30] Wertheim M. S. Fluids with Highly Directional Attractive Forces .1. Statistical Thermodynamics. *J. Stat. Phys.* **1984**, *35*, 19.

[31] Wertheim M. S. Fluids with Highly Directional Attractive Forces .2. Thermodynamic Perturbation-Theory and Integral-Equations. *J. Stat. Phys.* **1984**, *35*, 35.

[32] Wertheim M. S. Fluids with Highly Directional Attractive Forces .4. Equilibrium Polymerization. *J. Stat. Phys.* **1986**, *42*, 477.

[33] Johnson, J. K.; Zollweg, J. A.; Gubbins, K. E. The Lennard-Jones Equation of State Revisited. *Mol. Phys.* **1993**, *78*, 591.

[34] Colina C. M.; Olivera-Fuentes C. Prediction of the Joule-Thomson Inversion Curve of Air from Cubic Equations of State. *Cryogenics* **1998**, *38*, 721.

[35] Span R.; Wagner W. A New Equation of State for Carbon Dioxide Covering the Fluid Region from the Triple-Point Temperature to 1100 K at Pressures up to 800 MPa. *J. Phys. Ref. Data* **1996**, 25 (6), 1509.

[36] Lemmon E. W.; Jacobsen R. T.; Penoncello S. G.; Beyerlein S. W. *Computer Programs for Calculating Thermodynamic Properties of Fluids of Engineering Interest*, Report 97-1, Center for Applied Thermodynamic Studies, University of Idaho: Moscow, ID 1997.

[37] Perry R.H., Green D. *Perry's Chemical Engineer's Handbook*, 6th Edn., McGraw Hill: New York, 1984.

[38] Pitzer K. S.; Sterner S. M. Equations of State Valid Continuously from Zero to Extreme Pressures for H_2O and CO_2. *J. Chem. Phys.* **1994**, 101 (4), 3111.

[39] Colina C.M. ; Olivera-Fuentes C. On the Predicted Inversion Curve and Third Virial Coefficients of Carbon Dioxide at High Temperatures. *Ind. Eng. Chem. Res.* **2001**, submitted.

[40] Sychev, V. V.; Vasserman, A. A.; Zagoruchenko, V. A.; Kozlov, A. D.; Spiridonov, G. A.; Tsymarny, V. A.. Thermodynamic Properties of Methane. Hemisphere Publ., New York, **1987**.

[41] Kiselev S.B.; Ely J.F. Crossover SAFT Equation of State: Application for Normal Alkanes. *Ind. Eng. Chem. Res*. **1999**, *38*, 4993.

[42] Simnick J. J.; Lin H. M.; Chao K. C. The BACK Equation of State and Phase Equilibria in Pure Fluids and Mixtures, Adv. Chem. Series 1979, 182, 209.

[43] Pàmies, J. C.; Vega, L. F. Critical Properties of Heavy n-Alkanes from the Soft-SAFT Equation of State. Proceedings of the *Second Conference on Engineering Thermodynamics*, Tarragona, June 2001.

[44] Anselme M. J.; Gude M.; Teja A. S. The Critical Temperatures and Densities of the n-Alkanes from Pentane to Octadecane. *Fluid Phase Equilibria* **1990**, *57*, 317.

[45] Nikitin E. D. The Critical Properties of Thermally Unstable Substances: Measurement Methods, Some Results and Correlations. *High Temp.* **1998**, *2*, 305.

[46] Ledanois J.-M.; Müller E. A.; Colina C. M.; González-Mendizabal D.; Santos J. W.; Olivera-Fuentes C. Correlations for direct calculation of vapor pressures from cubic equations of state, *Ind. Eng. Chem. Res*. **1998**, *37* (5), 1673.

Chapter 5

Phase Behavior of Carbon Dioxide Mixtures with *n*-Alkanes and *n*-Perfluoroalkanes*

C. M. Colina[1], A. Galindo[2], F. J. Blas[3] and K.E.Gubbins[1]

[1]Chemical Engineering Department, North Carolina State University
Raleigh, NC 27695, USA
[2]Department of Chemical Engineering and Chemical Technology
Imperial College London, South Kensington Campus, London SW7 2AZ, UK
[3]Departamento de Física Aplicada, Facultad de Ciencias Experimentales
Universidad de Huelva, 21071 Huelva, Spain

5.1 Abstract

The phase behavior of mixtures containing carbon dioxide, *n*-alkanes and *n*-perfluoroalkanes is studied using the statistical associating fluid theory for potentials of variable attractive range (SAFT-VR). The molecules are modeled as fully flexible chains of tangentially bonded attractive spherical segments of hard-core diameter σ. The attractive interactions are treated via square-well potentials of depth ε and range λ. The pure component intermolecular parameters for carbon dioxide and the n-alkane molecules were determined in previous works by fitting to vapor pressures and saturated liquid densities; the same procedure is followed in this work to determine the parameters for the *n*-perfluoroalkane molecules. The optimized conformal parameters (σ and ε) are rescaled with the experimental critical point of each of the pure components. A set of transferable mixture parameters is presented, which provide a good description of the mixtures phase behavior, and additionally offer an insight into the higher solubility of *n*-perfluoroalkanes in carbon dioxide as compared to the solubility of *n*-alkanes.

* *Fluid Phase Equilb*. In press (2004)

5.2 Introduction

The development of amphiphilic molecules for use as surfactants in supercritical carbon dioxide (CO_2) and other supercritical fluids has led to the study of micellar and microemulsion phases in supercritical fluid media (see for example reference [1] and references therein). Diblock copolymers are often used for this purpose since they can self-assemble into micelles when placed in supercritical carbon dioxide. To date, the most successful surfactants for use in supercritical carbon dioxide have contained perfluorinated chains as the CO_2-philic part [2]. Unfortunately, highly fluorinated compounds are expensive, and thus there is great incentive to design new, inexpensive CO_2-philic groups.

In order to design surfactants with tailored solubility in CO_2, knowledge of the intermolecular amphiphile-solvent interactions is essential. There is considerable controversy over the origin of the solvation power of CO_2, in particular in relation to the origin of the exceptional solubility of fluorinated polymeric compounds. It is known than fluorinated compounds are more soluble in CO_2 than their hydrocarbon counterparts [3, 4]. Iezzi et al. [3] carried out experimental measurements of the phase behavior of CO_2 + *n*-hexane and CO_2 + *n*-perfluorohexane and showed that the differences in phase behavior between CO_2- *n*-hexane and CO_2- *n*-perfluorohexane are consistent with the differences in pure-component critical parameters. Using dielectric constant measurements, Yee et al. [4] found no evidence of special attractive interactions between CO_2 and perfluoroethane. Moreover, they suggested that CO_2 is more repulsive to perfluoroethane than to ethane on the basis of observed frequency shifts of the ν_2 bending mode of CO_2 in perfluoroethane and ethane, and concluded that the enhanced solubility of perfluorocarbons in CO_2 is due to the highly repulsive nature of fluorocarbon-fluorocarbon interactions, which make the solute-solute interactions less favorable than the solute-solvent interactions. Dardin *et al*. [5] studied the proton and fluorine chemical shifts of *n*-hexane, *n*-perfluorohexane, and 1,1-dihydroperfluorooctylpropionate dissolved in supercritical carbon dioxide using high-pressure, high-resolution nuclear magnetic resonance. They attribute the excess magnetic

shielding to van der Waals interactions between the fluorinated sites in the solute and carbon dioxide.

Additionally, various theoretical approaches, including *ab initio* calculations, have also been applied to this problem. Based on Hartree-Fock calculations Cece *et al*. [6] credited the enhanced binding in the CO_2-C_2F_6 to the electrostatic interaction between the positively charged carbon atom of CO_2 and the negatively charged fluorine atoms in the fluorocarbon. These findings agree with the experimental results of Darlin *et al*. [5]. However, Diep *et al*. [7], in contrast to the study by Cece *et al*. [6], do not find any enhanced attraction between CO_2 and perfluorocarbons relative to the analogous hydrocarbons, and concluded that it is not possible to discern the reason for the greater solubility of perfluorocarbons than of hydrocarbons in CO_2 from calculations on the small clusters used in their study. Cui *et al*. [8] have studied the vapor-liquid behavior of *n*-alkane and carbon dioxide + *n*-perfluoroalkane and carbon dioxide binary mixtures using the Gibbs ensemble Monte Carlo simulation technique. They employed molecular simulation with simple interaction-site models to explore the effects of van der Waals interactions between *n*-hexane and CO_2 and between *n*-perfluorohexane and CO_2. Their results suggest that the dispersion interaction and the geometric packing may have a predominant role in accounting for the solubility difference between *n*-alkane and *n*-perfluoroalkane in CO_2. Recent molecular dynamics calculations [9] suggest that larger cavities are found in perfluorinated liquids than in alkane liquids. Although this fact is likely to contribute to the larger solubility of gases in perfluorinated compounds, it cannot explain the larger solubility of CO_2 as compared to that of other gases. In summary, a complete understanding of the mixing of perfluoroalkanes with CO_2 is still lacking. Together with this understanding, it is important to be able to predict the phase behavior of mixtures containing the three components (CO_2, alkane and perfluoroalkane). Molecular equations of state can provide a means to understand better the interactions in these mixtures, and to consider different mixture scenarios which may lead to better processes.

In this work we use the statistical associating fluid theory for potentials of variable range (SAFT-VR) [10,11] to study the phase behavior of CO_2 + *n*-alkane and CO_2 + *n*-perfluoroalkane mixtures. The SAFT approach is based on the thermodynamic perturbation theory of Wertheim for associating [12, 13, 14, 15] and chain molecules [16, 17, 18, 19]. It takes into account repulsive (spherical and chain-like), dispersion, and association (hydrogen bonding) interactions explicitely. The work undertaken over the past decade has amply demonstrated that the SAFT framework provides a state-of-the-art thermodynamic description of complex multicomponent mixtures (several recent review articles collect the many applications and modifications of the approach [20, 21, 22, 23]). In the SAFT-VR approach a non-conformal intermolecular potential parameter describes the range of the segment-segment interactions, and the approach can be used to model the phase behavior of mixtures containing small strongly associating molecules, such as water [24], polar compounds, such as hydrofluorinated refrigerants [25], as well as long-chain molecules such as alkanes [26] and polyethylene [27]. In addition to this, the SAFT-VR equation has recently been used to study the global phase behavior of CO_2 + *n*-alkane binary mixtures [28, 29]. One of the goals of those previous works [28, 29] was to provide model parameters that could be used in a transferable way; in this work we continue in the same spirit and use the same pure component and mixture parameters. The phase behavior of binary mixtures of *n*-alkanes (from methane to *n*-heptane) and *n*-perfluroalkanes (from perfluoromethane to *n*-perfluorobutane) has also been studied previously using transferable parameters [30]. In this work we consider the application of transferable parameters to predict the phase behavior of mixtures containing CO_2, *n*-alkanes (C_6H_{14}, C_7H_{16}, C_8H_{18}) or *n*-perfluoroalkanes (C_6F_{14}, C_7F_{16}), as well as attempting to provide a link between the effective intermolecular parameters of the equation of state, and the differences in phase behavior (in solubility) between *n*-alkanes and *n*-perfluoroalkanes in CO_2.

5.3 Models and Theory

In the SAFT-VR approach [10,11] the molecules are modeled as chains of tangentially bonded spherical segments of hard-core diameter σ. The attractive interactions are described

by square-well potentials of variable range λ and depth ε, and the contribution to the free energy due to the dispersion interactions is obtained following the framework of the perturbation theory of Barker and Henderson [32, 33, 34]. As in other SAFT approaches, association interactions can also be considered through embedded short-range attractive interaction sites, but in this work we treat non-associating molecules, and so this contribution is not necessary. The Helmholtz free energy A for an n-component mixture of CO_2, *n*-alkane and *n*-perfluoroalkane molecules can thus be written as,

$$\frac{A}{NkT} = \frac{A^{IDEAL}}{NkT} + \frac{A^{MONO}}{NkT} + \frac{A^{CHAIN}}{NkT}, \tag{5.1}$$

where N is the number of molecules, k the Boltzmann constant, and T the temperature. The ideal gas contribution to the free energy is given by a sum over all species i in the mixture [31]

$$\frac{A^{IDEAL}}{NKT} = \sum_{i=1}^{n} x_i \, ln(\rho_i \Lambda_i^{\,3}) - 1 \ , \tag{5.2}$$

where $x_i = N_i/N$ is the mole fraction, $\rho_i = N_i/V$ the number density, N_i the number of molecules, V the volume of the system, and Λ_i the thermal de Broglie wavelength of species i. The monomer Helmholtz free energy can be written in terms of the free energy per monomer a^M as

$$\frac{A^{MONO}}{NKT} = \left(\sum_{i=1} x_i m_i \right) a^M \ , \tag{5.3}$$

where m_i is the number of spherical segments of chain. Using the Barker and Henderson [32, 33, 34] perturbation theory for mixtures with a hard-sphere reference system, the monomer free energy per segment can be obtained from the expansion

$$a^M = a^{HS} + \frac{1}{kT} a_1 + \left(\frac{1}{kT}\right)^2 a_2 . \tag{5.4}$$

The expression of Boublík [35] and Mansoori *et al*. [36] for a multicomponent mixture of hard spheres is used for the reference hard-sphere term,

$$a^{HS} = \frac{6}{\pi\rho_s}\left[\left(\frac{\zeta_2^3}{\zeta_3^2} - \zeta_0\right) ln(1-\zeta_3) + \frac{3\zeta_1\zeta_2}{(1-\zeta_3)} + \frac{\zeta_2^3}{\zeta_3(1-\zeta_3)^2}\right], \tag{5.5}$$

where $\rho_s = N_s/V$ is the total number density of spherical segments and ζ_i are reduced densities. The mean attractive energy a_1, is obtained from the sum of the partial terms corresponding to each type of pair interaction

$$a_1 = \sum_{i=1}^{n}\sum_{j=1}^{n} x_{s,i} x_{s,j} a_1^{ij} , \tag{5.6}$$

where, using the mean value theorem, and the van der Waals (vdW) one-fluid approximation (see [10, 11] for more details) each of the monomer-monomer free energy contributions can be written as

$$a_1^{ij} = -\rho_s \alpha_{ij}^{vdw} g_0^{HS}(\sigma_\chi ; \zeta_\chi^{eff}) . \tag{5.7}$$

In the case of a square-well potential the van der Waals attractive constant α_{ij}^{vdw} is given by

$$\alpha_{ij}^{vdw} = \frac{2}{3}\pi\, \varepsilon_{ij}\sigma_{ij}^3(\lambda_{ij}^3 - 1), \tag{5.8}$$

and $g_0^{HS}(\sigma_x;\zeta_x^{eff})$ is the contact radial distribution function of a hypothetical pure fluid of average diameter σ_x, and is obtained from the Carnahan and Starling equation of state [37].

The effective packing fraction ζ_x^{eff} is obtained from the corresponding packing fraction of the fluid ζ_x using,

$$\zeta_x^{eff}(\zeta_x, \lambda_{ij}) = c_1(\lambda_{ij})\zeta_x + c_2(\lambda_{ij})\zeta_x^2 + c_3(\lambda_{ij})\zeta_x^3 \tag{5.9}$$

Coefficients c_1, c_2, and c_3 are given in reference [10]. It should be noted that this corresponds to the MX1b mixing rule of reference [11].

The first fluctuation term a_2 is written in terms of a_1 within the local compressibility approximation [10, 11] as

$$a_2 = \sum_{i=1}^{n}\sum_{j=1}^{n} x_{s,i}x_{s,j}\frac{1}{2}\varepsilon_{ij}K^{HS}\rho_s\frac{\partial a_1^{ij}}{\partial \rho_s}, \tag{5.10}$$

where K^{HS} is the hard-sphere isothermal compressibility of Percus-Yevick [38].

The contribution to the free energy due to chain formation is expressed in terms of the contact value of the monomer background correlation function, y_{ii}^{MONO} as

$$\frac{A^{CHAIN}}{NkT} = -\sum_{i=1}^{n} x_i(m_i - 1)\ln y_{ii}^{MONO}(\sigma_{ii}) \tag{5.11}$$

where, for square-well chains $y_{ii}^{MONO}(\sigma_{ii}) = y_{ii}^{SW}(\sigma_{ii})$, and $y_{ii}^{SW}(\sigma_{ii}) = g_{ii}^{SW}(\sigma_{ii})\exp(\varepsilon_{ii}/kT)$ [10, 11]. In the SAFT-VR approach the radial distribution function of the system of unbonded monomers is obtained from a high-temperature expansion

$$g_{ii}^{SW}(\sigma_{ii}) = g_{ii}^{HS}(\sigma_{ii}) + \frac{\varepsilon_{ii}}{kT}g_1(\sigma_{ii}), \tag{5.12}$$

where the reference term is evaluated using the expression of Boublík [35], and $g_1(\sigma_{ii})$ from a self-consistent method for the pressure P from the Clausius virial theorem and from the density derivative of the Helmholtz free energy (see reference [10] for more details). Once the free energy is known, standard thermodynamic relations can be used to determine the pressure and chemical potentials, and the phase equilibrium conditions (equality of temperature, pressure and chemical potentials of each component in all phases) are solved using a numerical algorithm [39].

5.4 Results and Discussion

Following previous work [28, 29] carbon dioxide is modeled as a non-associating and non-spherical molecule. The attractive dispersion interactions and the quadrupole are treated in an effective way via a square-well potential of depth ε_{11} and adjustable range λ_{11}. The linear non-spherical nature of the molecule is treated in an explicit way modeling the molecule with 2 tangentially bonded square-well segments; i.e., $m_1 = 2$. The values of the parameters were obtained in previous work by fitting to experimental vapor pressures and saturated densities; the resulting values are presented in table 5.1 here for completeness. The *n*-alkane molecules have also been studied using the SAFT-VR approach in previous works [26, 28, 29, 30]. These molecules are modeled as chains of m_2 tangentially bonded segments of hard-sphere diameter σ_{22}, interacting through square-well potentials of depth ε_{22} and range λ_{22}. The number of segments m_2 forming the model chain can be obtained as a function of the number of carbon atoms C of the *n*-alkane molecule by $m_2 = (C-1)/3+1$ [26]. Using this value for m_2 McCabe and Jackson [26] have carried out the optimization of the monomer intermolecular parameters for a large number of *n*-alkanes (from methane to *n*-hexatriacontane) using experimental vapor pressures and saturated liquid densities. We use their optimized intermolecular parameters in this work (see table 5.1). The number of segments m_3 forming a model *n*-perfluoroalkane chain is related to the number of carbons of the *n*-perfluoroalkane molecule by $m_3 = (C-1)\times 0.37+1$ as in previous works [30]. Using

these values for m_3, parameters for perfluoromethane to *n*-perfluorobutane have been presented previously [30], but are not available for longer molecules. In the case of *n*-perfluorohexane a large amount of pure component experimental data is available [40, 41, 42, 43]. Although more limited, some experimental data are also available in the literature for *n*-perfluoroheptane [41, 44, 45, 46]. Hence, we follow the same procedure as in previous works and determine the parameters by comparison to experimental vapor pressures and saturated liquid densities. The optimized intermolecular parameters for the *n*-perfluoroalkane molecules used in this work are presented in table 5.1.

Table 5.1. Optimized SAFT-VR square-well intermolecular potential parameters. The subscript c indicates that the parameters have been rescaled to the experimental critical point. Parameters in italics were obtained in this work.

	m	σ/Å	ε/k (K)	λ	T_c^*	$p_c^* 10^3$	σ_c/Å	ε_c/k (K)
CO_2	2.0	2.7864	179.27	1.5157	0.18146	5.1528	3.1364	168.89
C_6H_{14}	2.667	3.920	250.4	1.552	0.1957	3.995	4.479	236.6
C_7H_{16}	3.0	3.933	251.3	1.563	0.2021	3.607	4.529	237.3
C_8H_{18}	3.333	3.945	250.3	1.574	0.2076	3.275	4.564	236.5
C_6F_{14}	*2.85*	*4.529*	*277.33*	*1.4390*	*0.21448*	*4.3652*	*5.0315*	*264.24*
C_7F_{16}	*3.22*	*4.464*	*285.34*	*1.4365*	*0.22179*	*3.9102*	*5.1233*	*272.63*

In order to provide a better description of the critical region we rescale the pure-component conformal parameters σ and ε for all of the substances considered; the critical parameters, and the theoretical critical temperatures and pressures, which are used to obtain the scaled parameters are also given in table 5.1. We should note here that, although the critical region is more accurately represented with the scaled parameters, this is always at the expense of accuracy at lower temperatures. In particular the saturated liquid densities are underpredicted with these parameters, while the vapor pressures of the pure components far from the critical region are overpredicted. Recently, a cross-over approach has been presented which

overcomes this difficulty [47,48]; unfortunately it cannot be straightforwardly applied to mixtures.

Once the intermolecular pure component parameters are determined, the calculation of mixture phase behavior requires determining a number of unlike intermolecular parameters. In the case of the SAFT-VR approach for non-associating chain molecules these are: σ_{ij}, ε_{ij} and λ_{ij}. Traditionally, the modified Lorentz-Berthelot combining rules are used [49],

$$\sigma_{ij} = \frac{\sigma_{ii} + \sigma_{jj}}{2},\ \varepsilon_{ij} = \xi_{ij}\sqrt{\varepsilon_{ii}\varepsilon_{jj}}\ \text{, and} \quad \lambda_{ij} = \gamma_{ij}\frac{\lambda_{ii}\sigma_{ii} + \lambda_{jj}\sigma_{jj}}{\sigma_{ii} + \sigma_{jj}} \tag{5.13}$$

In the case of hard core potentials, σ_{ij} is given exactly by the expression shown in equation (5.13), but the parameters describing the unlike square-well energy ε_{ij} and range λ_{ij} are only approximate, so that two adjustable parameters ξ_{ij} and γ_{ij} often need to be introduced in order to improve the agreement with the experimental mixture phase behavior. The adjustable parameters used in this work are presented in table 5.2.

Table 5.2. SAFT-VR square-well intermolecular potential parameters for the binary mixtures.

System	ξ_{12}	γ_{12}
$CO_2 + C_6H_{14}$	0.88	0.989
$CO_2 + C_6F_{14}$	0.88	0.989
$C_6F_{14} + C_7F_{16}$	0.929	1

Values of ξ_{12} = 0. 88 and γ_{12} = 0.989 were determined in previous works [28, 29] for mixtures of CO_2 + *n*-alkanes. These parameters ensure that the mixture of CO_2 + *n*-$C_{13}H_{28}$ exhibits type IV phase behavior in the classification of Scott and van Konynenburg [50], and it was shown that they can be transferred to study the global phase behavior, and the transitions between types of phase diagram of a large number of mixtures of the CO_2 + *n*-

alkane mixtures. Here we show that the same parameters provide a prediction of the vapor-liquid equilibria of the CO_2 + *n*-C_6H_{14} mixture (see figure 5.1), at constant temperatures of 353 K and 313 K in very good agreement with experimental data [3, 51, 52]. Although it can be seen in figure 5.1b that the slope of the liquid composition at the lowest temperature (the closest to the critical point of CO_2) is somewhat different than suggested by the experimental data, considering that the calculations are totally predictive, we still find the results very encouraging. Moreover, the set of parameters used is not temperature dependent, so that it can be used to describe the phase behavior of the mixture for the entire fluid range, and can be transferred to other CO_2 + *n*-alkane mixtures [28, 29] (see also the results in figure 5.3).

In figure 5.1, the phase behavior of the CO_2 + *n*-C_6H_{14} is also compared with that of CO_2 + *n*-C_6F_{14} [3] and with SAFT-VR calculations. In the case of the mixture CO_2 + *n*-C_6F_{14}, we find that the same unlike adjustable intermolecular parameters can be used. The choice of parameters may, at first, seem surprising (perfluroalkane molecules are known to be more soluble in CO_2 than alkane molecules). In our SAFT-VR model we have treated the quadrupolar interactions characteristic of carbon dioxide in an effective way through square-well potentials, and the parameters ξ_{ij} and γ_{ij} mainly provide a correction of this approximation. In this context, it makes sense to obtain similar correction parameters for both mixtures studied. To support this idea we refer to the work of Cui *et al*. [8], who have obtained the phase behavior of a mixture of CO_2 + *n*-C_6H_{14} and of CO_2 + *n*-C_6F_{14} using computer simulations. In their work charge-charge interactions are incorporated to model carbon dioxide, and they find that the usual Lorentz-Berthelot combining rule can be used to determine the depth in the Lennard –Jones potential both between CO_2 and the *n*-alkane and between CO_2 and the *n*-perfluoroalkane; i.e., the same combining rule can be used for both systems. In our approach it is more useful to compare the unlike van der Waals integrated energy parameters as a measure of the amount of dispersion interaction between components. Using the unlike transferable parameters proposed it is straightforward to calculate the values of α_{ij}^{vdW} from the optimized pure component parameters. The results for the molecules considered are shown in figure 5.2. It can be seen that the unlike energy parameters of our model are larger for the mixtures of CO_2 with the *n*-perfluorocarbons than with the *n*-alkanes.

This could result in the larger solubility seen for the perfluorinated molecules. It is also noticeable that the difference in the unlike dispersion energy decreases for increasing number of carbons in the molecules. This could suggest that the differences in solubility would also decrease with increasing chain lengths.

Taking advantage of the transferability of parameters, the vapor-liquid phase equilibria for a mixture of CO_2 + *n*-C_7H_{16}, and for a mixture of CO_2 + *n*-C_7F_{16} have been studied at 310.65 K and 353.15 K. A comparison with the experimental data available for the CO_2 + *n*- C_7H_{16} mixture [53] is presented in figure 5.3, where the agreement is excellent. Unfortunately, no experimental data was found for the CO_2 + *n*-C_7F_{16} mixture at these conditions. Our predictions indicate that the mixtures of *n*-C_7H_{16} and *n*-C_7F_{16} with CO_2 present a similar phase behavior as seen in the CO_2 + *n*-C_6H_{14} and CO_2 + *n*- C_6F_{14} mixtures, at least at the conditions studied in figure 5.3. It is worth noting here that for high CO_2 concentrations, the model predicts very similar solubilities for *n*-heptane and *n*-perfluoroheptane, especially at the lower temperature. Unfortunately, no experimental or molecular simulation data are available to corroborate our predictions for the CO_2 + C_7F_{16} system at these conditions. A small set of experimental data is however available for this mixture at constant atmospheric pressure [54]; a comparison with the SAFT-VR prediction is provided in figure 5.4. Our theoretical predictions are in excellent agreement (of the order of 1%) with the experimental data. At the lowest temperatures in this phase diagram solid phases will become stable, and so calculations were not continued below 220K.

Thus far we have presented a transferable approach to study the phase behavior of binary mixtures of CO_2 with *n*-alkanes or *n*-perfluoroalkanes. Studying the integrated unlike energy parameters for the mixtures, we find that these are larger in the mixtures of the perfluorinated molecules with CO_2; this would also suggest larger dispersion interactions. Our future plan is to use these models to study the ternary phase behavior of mixtures of CO_2 + n-alkanes + n-perfluoroalkanes. In order to carry this out the alkane-perfluoroalkane unlike intermolecular parameters must also be determined. We now turn our attention to these systems.

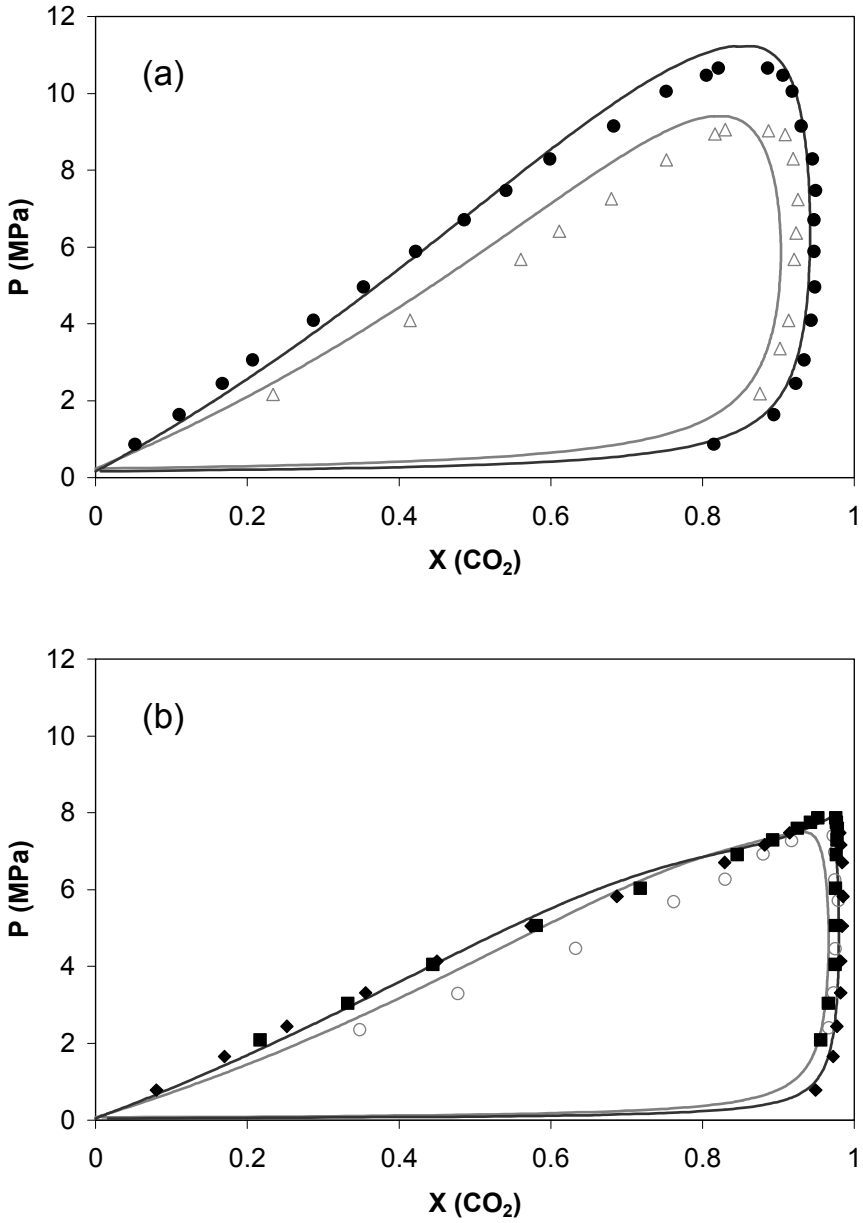

Figure 5.1. Constant temperature pressure-composition *Px* phase diagrams for CO_2 + *n*-hexane and CO_2 + *n*-perfluorohexane compared with the SAFT-VR predictions. Symbols represent experimental data and lines are the SAFT-VR predictions. (a) T = 353 K for CO_2 + *n*-hexane (●, –) [51], and CO_2 + *n*-perfluorohexane (Δ,–); (b) T = 313 K for CO_2 + *n*-hexane (♦ [51], ■ [52], –) and CO_2 + *n*-perfluorohexane (O [3], –).

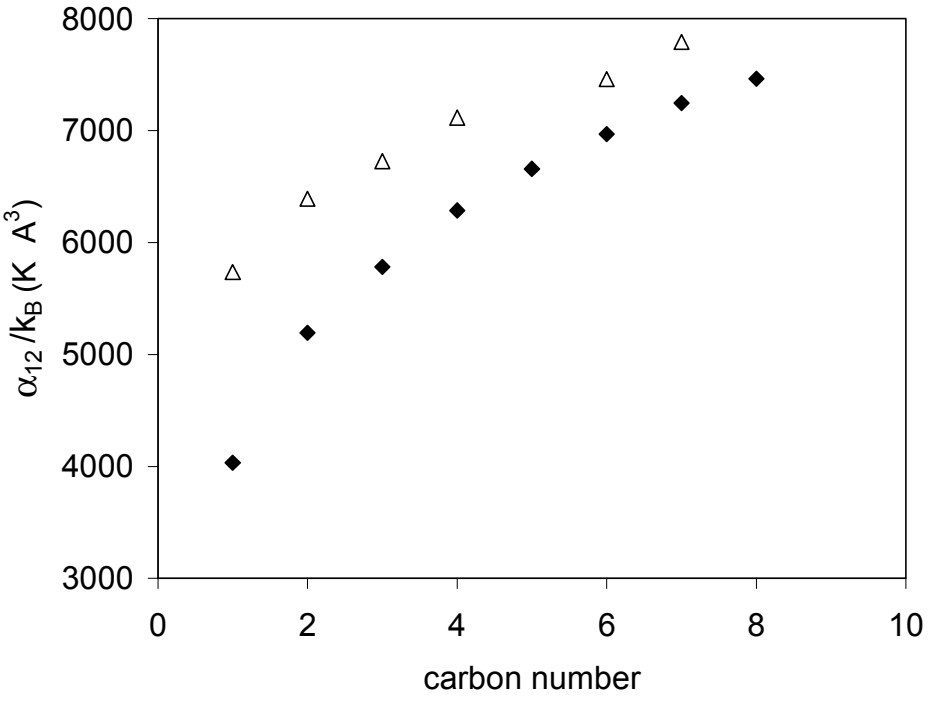

Figure 5.2. Unlike van der Waals integrated energy parameter, α_{ij}/k_B, as a function of the carbon number for *n*-alkanes (♦) and *n*-perfluoroalkanes (Δ).

Binary *n*-alkane + *n*-perfluoroalkane mixtures exhibit type II phase behavior in the classification of Scott and van Konynenburg [50] when the difference in chain length between the two components is not very large (symmetric or close-to symmetric systems). This type of behavior is characterized by the presence of liquid-liquid phase separation and continuous vapor-liquid critical curves. The mixtures considered in this work exhibit this type of phase diagram. McCabe *et al*. [30] studied the high-pressure phase behavior of a number of *n*-perfluroalkane (C_1-C_4) + *n*-alkane (C_1-C_7) binary mixtures, and suggested a value $\xi_{23} = 0.9234$ (with $\gamma_{23} = 1$, as could be expected since both molecules are non-polar). However, in the previous work [30] little liquid-liquid coexistence data were used to determine the unlike ξ_{23} parameter. We find that the slightly different value of $\xi_{23} = 0.929$ (with $\gamma_{23} = 1$) provides a better fit to the upper critical solution temperature (UCST) of the C_6H_{14} +C_6F_{14} [55] system (see figure 5.5). It is worth noting that, as can be expected for a classical equation of state, while our choice of parameters provides the best agreement of the

critical point of the mixture, this is in detriment of the prediction of the compositions of the liquid phases. As before the unlike parameters can be used in a transferable way; in figure 5.5 the liquid-liquid envelope for a mixture of *n*-C_7H_{16} + *n*-C_6F_{14} is also shown. We have also calculated the vapor-liquid phase behavior of the *n*-C_6H_{14} + *n*-C_6F_{14} mixture, and compare our results with the available experimental data [56] in figure 5.6. The mixture presents azeotropic behavior, which is well described by the theoretical approach with the set of transferable parameters chosen for this family of systems, although a small overprediction in the equilibrium pressure is seen as compared to the experimental data. This overprediction of the pressure comes as a result of the overprediction in the pure component vapor pressures due to the rescaling the parameters to the critical point. We have also considered the vapor-liquid coexistence compositions of the *n*-C_6H_{14} + *n*-C_7F_{16} system using the same transferable parameters; good agreement is found with the available experimental data [57] (see figure 5.7a)). In figure 5.7b) the *Pxy* behavior of the system *n*-C_6H_{14} + *n*-C_6F_{14} is compared with the one of *n*-C_6H_{14} + *n*-C_7F_{16}. Even though the azeotropic point is the only data available for the system *n*-C_6H_{14} + *n*-C_7F_{16}, the SAFT-VR predictions are in good agreement with the experiments. Calculations for a mixture of *n*-C_8H_{18} + *n*-C_6F_{14} are presented in figure 5.8. The vapor-liquid coexistence mole fractions and the liquid-liquid phase behavior are considered, and as before good agreement with the experimental data available is obtained used the transferable parameters. As expected the predicted phase envelope is narrower than the experimental, however the UCST predicted by the equation is 331.35 K, which is very close to 335.4 K as reported from experiments [58]; note that the unlike parameters were not optimized to reproduced this critical point. Summing up this part of the work, we have shown that it is possible to predict the overall phase behavior of different binary mixtures involving carbon dioxide, *n*-alkanes and *n*-perfluoroalkane using unique sets of unlike intermolecular parameters characteristic of each homologous series.

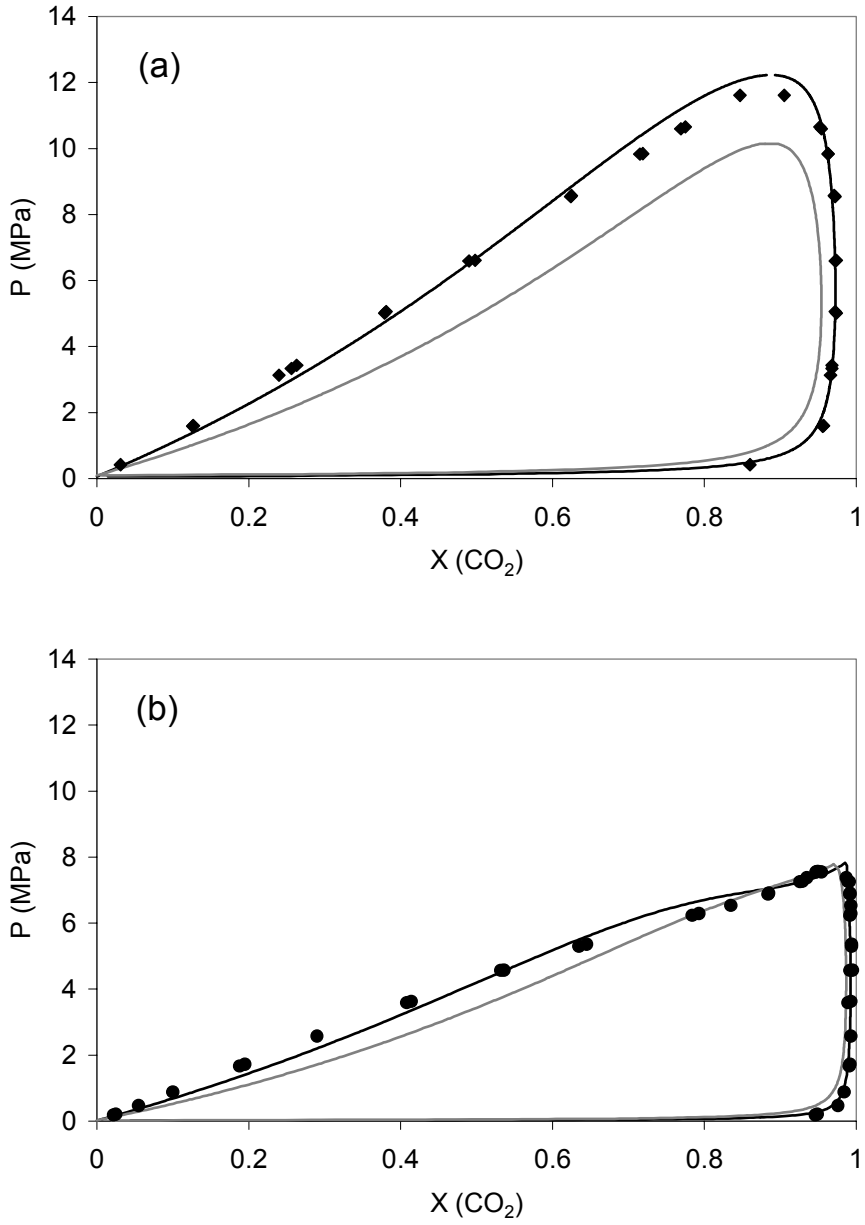

Figure 5.3. Vapor-liquid equilibrium for the CO_2 + *n*-heptane, and CO_2 + *n*-perfluoroheptane binary mixtures compared with the SAFT-VR predictions. Symbols represent the experimental data [53] at (a) 353.15 K and (b) 310.65 K for CO_2 + *n*-heptane. The theoretical predictions are shown by the continuous curves. Black line: CO_2 + *n*-heptane, grey line: CO_2 + *n*-perfluoroheptane.

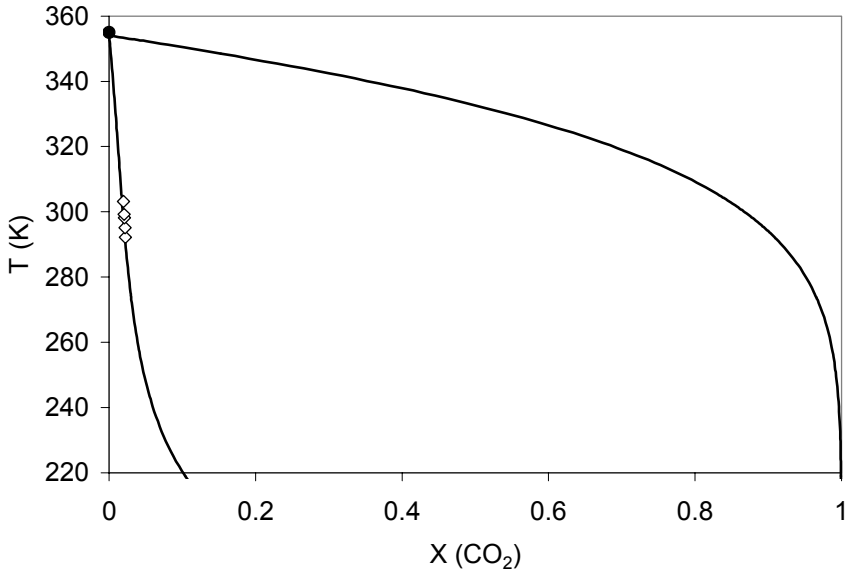

Figure 5.4. Vapor-liquid equilibrium for the CO_2 + *n*-perfluoroheptane binary mixture compared with the SAFT-VR predictions. Symbols represent the experimental data (◊ [54], ● [59]) at 101.325 kPa. The theoretical predictions are shown by the continuous curves.

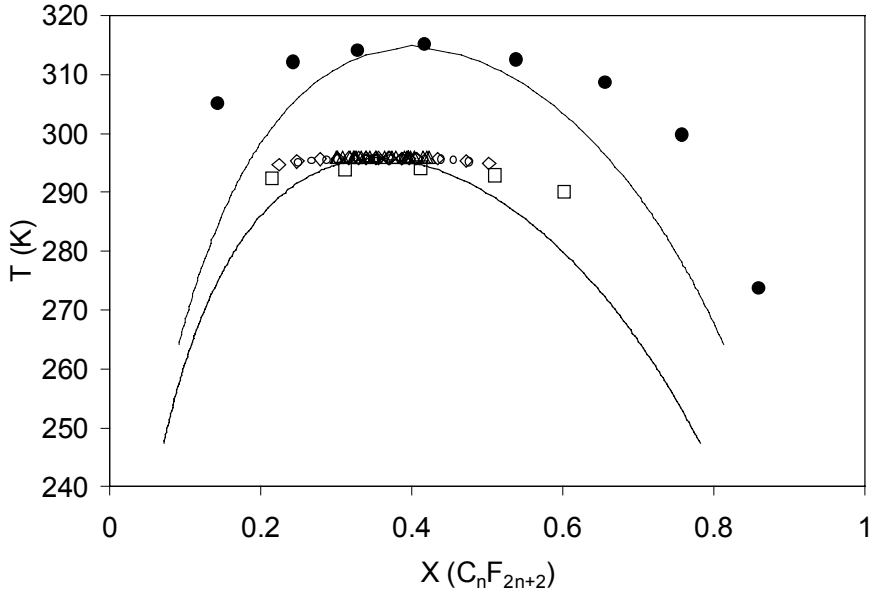

Figure 5.5. Liquid-liquid equilibrium for (a) the *n*-hexane + *n*-perfluorohexane and (b) *n*-hexane + *n*-perfluoroheptane binary mixtures compared with the SAFT-VR predictions. Symbols represent the experimental data for: C_6H_{14} + C_7F_{16} (●) [56], and C_6H_{14} + C_6F_{14} (Δ [60], ◊ [61], □ [56]). The theoretical predictions are shown by the continuous curves.

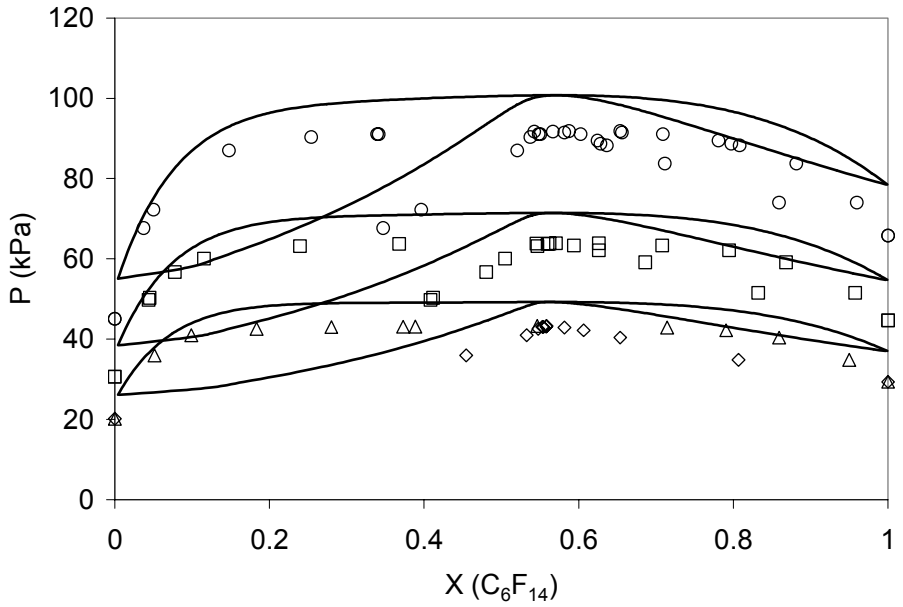

Figure 5.6. Vapor-liquid equilibrium for the *n*-hexane + *n*-perfluorohexane binary mixture compared with the SAFT-VR predictions. Symbols represent the experimental data of Dunlap *et al.* [56]: (O) 318 K, (□) 308 K and (Δ) 298 K. The theoretical predictions are shown by the continuous curves.

5.5 Conclusions

The phase behavior of a number of carbon dioxide (CO_2), *n*-alkane (C_6H_{14}, C_7H_{16}, C_8H_{18}) and *n*-perfluoroalkane (C_6F_{14}, C_7F_{16}) binary mixtures has been studied using the statistical associating fluid theory for potentials of variable attractive range (SAFT-VR). The molecules are modeled as chains of tangentially bonded attractive spherical segments, with the attractive interactions treated as square-well potentials of variable range. Even though the characteristic quadrupole of carbon dioxide is not taken into account explicitly, the approach can be used to predict the phase behavior of the homologous series studied. Our proposed framework supports the proposition that the increased solubility of perfluoroalkanes in CO_2 may be closely related to larger attractive dispersion interactions. Cui et al. [8] have already suggested that packing and dispersion interaction play a major role. In addition to this, the SAFT-VR approach has the advantage of being entirely predictive, so that the phase behavior of a large number of binary mixtures can be studied by fitting only the pure component

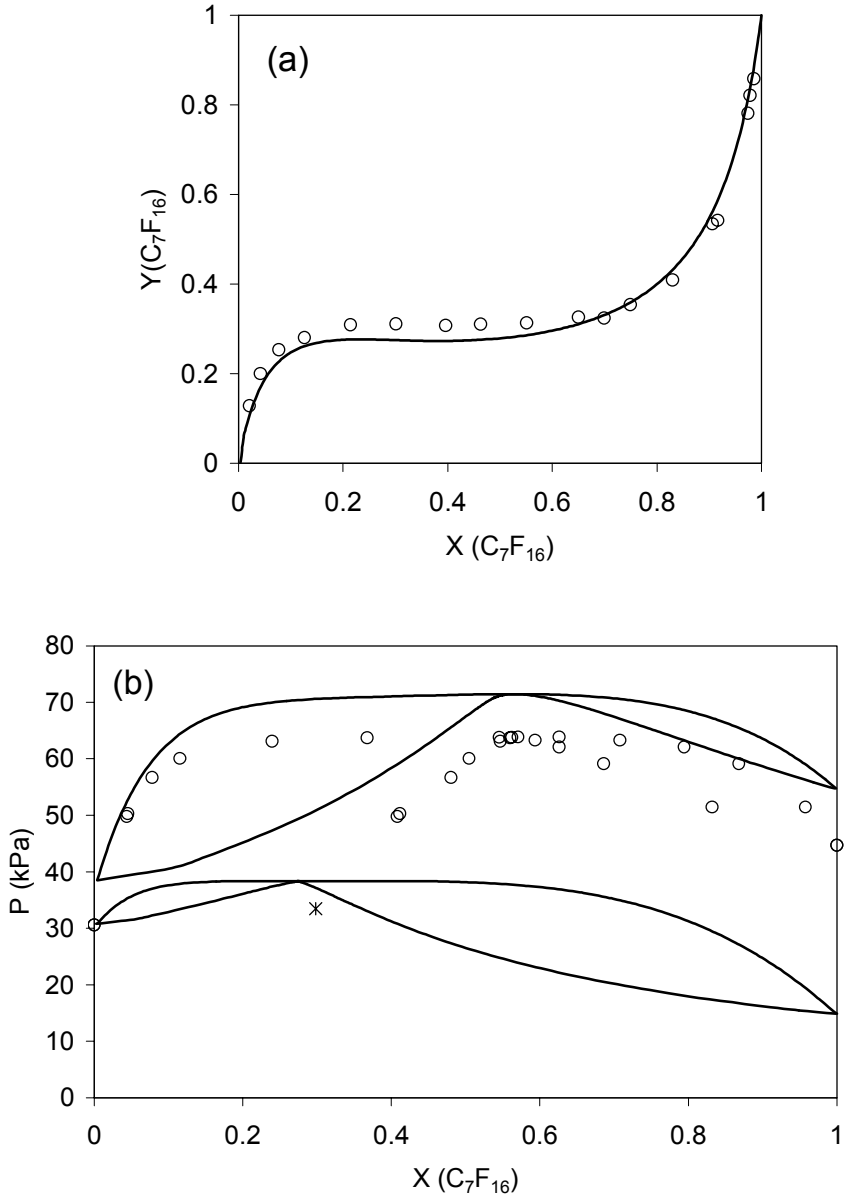

Figure 5.7. a) Vapor phase mole fraction *vs.* liquid phase mole fraction for *n*-hexane + *n*-perfluoroheptane at 303.15 K. Symbols represent the experimental data of Duce *et al*. [57]. The theoretical predictions are shown by the continuous curves. b) Vapor-liquid equilibrium for the *n*-hexane + *n*-perfluorohexane and *n*-hexane + *n*-perfluoroheptane binary mixtures compared with the SAFT-VR predictions. Symbols represent the experimental data of: Dunlap *et al.* [51] at 298.15 K (O) for C_6H_{14} + C_6 F_{14} and Duce *et al*. [57] at 303.15 K (*) for C_6H_{14} + C_7F_{16}.

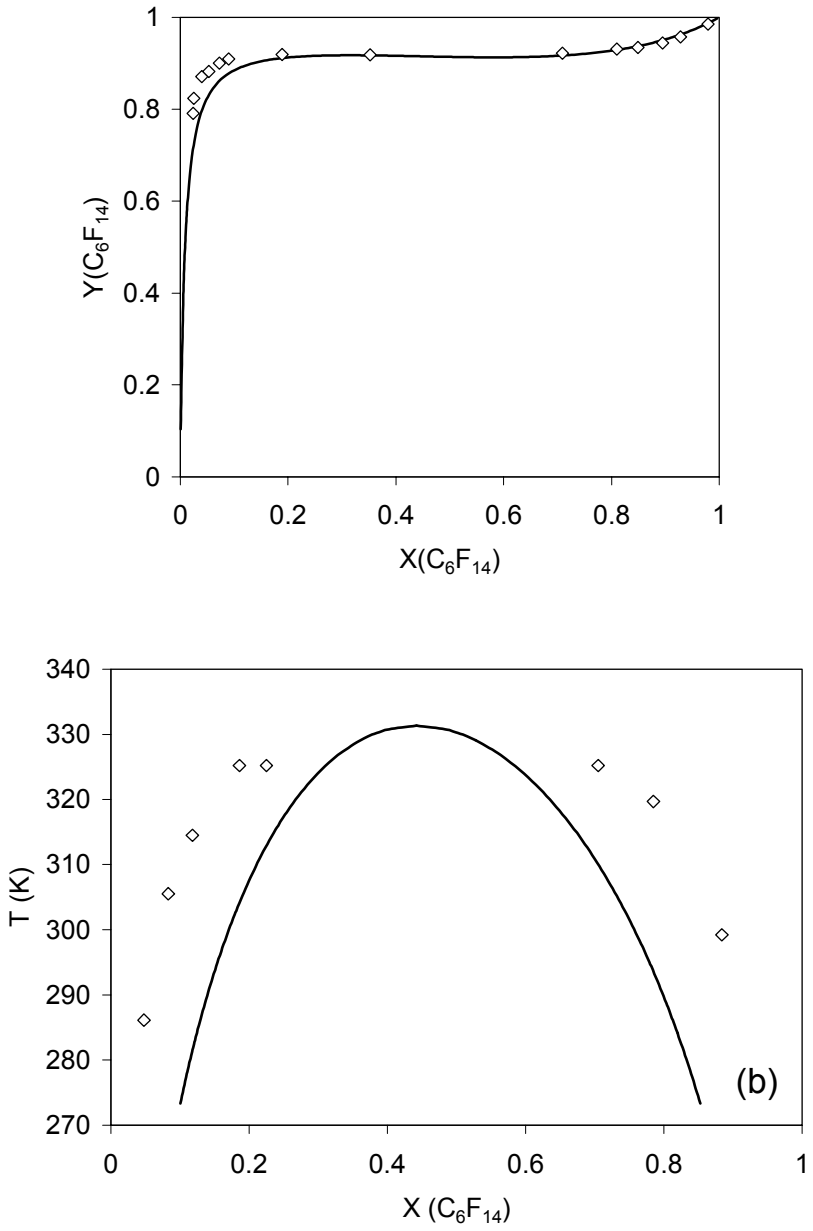

Figure 5.8. a) Vapor phase mole fraction *vs.* liquid phase mole fraction for *n*-octane + *n*-perfluorohexane at 313.15 K. Symbols represent the experimental data of Duce *et al.* [57]. The theoretical predictions are shown by the continuous curves. b) Liquid-liquid equilibrium for the *n*-octane + *n*-perfluorohexane binary mixture compared with the SAFT-VR predictions.

parameters of the *n*-perfluoroalkane molecules. In future it would be desirable to obtain a parametrization similar to that available for *n*-alkane molecules [26], so that the method could be used in the context of mixture design. The nature of the SAFT approach, and indeed, of most equations of state, is such that only binary interaction parameters are required, so that once the adjustable parameters for a set of binary mixtures are known, multicomponent phase behavior can be studied. In future we plan to assess the validity of the predictions in the context of ternary phase behavior. A predictive approach such as the one proposed could be helpful in identifying possible new CO_2-philic groups as well as co-solvents for CO_2.

Acknowledgements

The authors thank Keith Johnston and Valery Bondar for helpful discussions. This work was partly supported by the STC Program of the National Science Foundation under Agreement No. CHE 9876674. AG would like to thank the Engineering and Physical Sciences Research Council of the UK for the award of an Advanced Research Fellowship. FJB would like to thank financial support from project number BFM-2001-1420-C02-02 of the Spanish DGICYT (Dirección General de Investigación Científica y Técnica). Additional support from Universidad de Huelva and Junta de Andalucía is also acknowledged.

5.6 References

[1] Salaniwal, S., Cui, S. T., Cochran, H. D. and P. T. Cummings, *Langmuir*, 17 (2001) 1773-1783.

[2] Buhler, E., Dobrynin, A. V., DeSimone, J. M. and M. Rubinstein, *Macromolecules,* 31 (1998) 7347-7355.

[3] Iezzi, A., Bendale, P., Enick, R. M Turberg and J. Brandy, *Fluid Phase Equilib*. 52 (1989) 307-317.

[4] Yee, G. G., Fulton, J. L. and R. D. Smith, *J. Phys. Chem.* 96 (1992) 6172-6181.

[5] Dardin, A., DeSimone, J. M. and E. T. Samulski, *J. Phys. Chem. B,* 102 (1998) 1775 - 1780.

[6] Cece, A., Jureller, S. H., Kerschner, J. L. and K. F. Moschner, *J. Phys. Chem.* 100 (1996) 7435-7439.

[7] Diep, P., Jordan, K. D., Johnson, J. K. and E. J. Beckman, *J. Phys. Chem. A*, 102 (1998) 2231 - 2236.

[8] Cui, S. T., Cochran, H. D. and P. T. Cummings, *J. Phys. Chem. B*. 103 (1999) 4485-4491.

[9] Costa-Gomes, M. F. and A. H. Padua, *J. Phys. Chem. B*, 107 (2003) 14020-14024.

[10] Gil-Villegas, A., Galindo, A., Whitehead, P. J., Mills, S. L., Jackson, G. and A. N. Burgess, *J. Chem. Phys.* 106 (1997) 4168-4186.

[11] Galindo, A., Davies, L.A., Gil-Villegas, A. and G. Jackson, *Molec. Phys.* 93 (1998) 241-252.

[12] Wertheim, M. S., *J. Stat. Phys*. 35 (1984) 19-34.

[13] Wertheim, M. S., *J. Stat. Phys*. 35 (1984) 35-47.

[14] Wertheim, M. S., *J. Stat. Phys*. 42 (1986) 459-476.

[15] Wertheim, M. S., *J. Stat. Phys*. 42 (1986) 477-492.

[16] Jackson, G., Chapman, W. G. and K. E. Gubbins, *Mol. Phys*. 65 (1988) 1 – 31.

[17] Chapman, W. G., Jackson, G. and K. E. Gubbins, *Mol. Phys.* 65 (1988) 1057 – 1079.

[18] Wertheim, M. S., *J. Chem. Phys.* 85 (1986) 2929-2936.

[19] Wertheim, M. S., *J. Chem. Phys.* 87 (1987) 7323-7331.

[20] Müller, E. A. and K.E. Gubbins, in J.V.Sengers, R.F. Kayser, C.J. Peters and H. J. White, Jr. (Eds), Equations of State for Fluids and Fluid Mixtures. Experimental Thermodynamics, Volume 5, Elsevier, Amsterdam, 2000, pp 435-478.

[21] Müller, E. A. and K. E. Gubbins. *Ind. Eng. Chem. Res.* 40 (2001) 2193-2211.

[22] Wei, Y.S. and R. Sadus, *AIChE J.*, 46 (2000) 169 –196.

[23] Economou, I. G. *Ind. Eng. Chem. Res.,* 41 (2002) 953- 962.

[24] Galindo, A., Gil-Villegas, A., Jackson, G. and A.N. Burgess. *J. Phys. Chem*. B 103 (1999) 10272-10281.

[25] Galindo, A., Gil-Villegas, A., Whitehead, P. J., Jackson, G. and A.N. Burgess. *J. Phys. Chem. B* 102 (1998) 7632-7639.

[26] McCabe, C. and G. Jackson. *Phys. Chem. Chem. Phys*. 1 (1999) 2057-2064.

[27] McCabe, C., Galindo, A., Garcia-Lisbona, M. N. and G. Jackson. *Ind. Eng. Chem. Res*. 40 (2001) 3835-3842.

[28] Blas, F. J. and A. Galindo, *Fluid Phase Equilb.* 194-197 (2002) 501-509.

[29] Galindo, A. and F. J. Blas, *J. Phys. Chem. B.*, 106 (2002) 4503-4515.

[30] McCabe, C., Galindo, A., Gil-Villegas, A. and G. Jackson, *J. Phys. Chem. B* 102 (1998) 8060-8069.

[31] J. S. Rowlinson and F. L. Swinton, *Liquids and Liquid Mixtures*, 3rd ed., Butterworth Scientific: London 1982.

[32] Barker, J. A. and D. J. Henderson, *J. Chem. Phys.* 47 (1967) 2856- 2861.

[33] Barker, J. A. and D. J. Henderson, *J. Chem. Phys.* 47 (1967) 4714- 4721.

[34] Barker, J. A. and D. J. Henderson, *Rev. Mod. Phys*. 48 (1976) 587-671.

[35] Boublik, T., *J. Chem. Phys.* 53 (1970) 471-472.

[36] Mansoori, G. A., Carnahan, N. F., Starling, K. E. and T. W. Leland, *J. Chem. Phys.* 54 (1971) 1523-1525.

[37] Carnahan, N. F. and K. E. Starling, *J. Chem. Phys*. 51 (1969) 635-636.

[38] Percus, J. K. and G. J.Yevick, *Phys Rev.* 110 (1958)1-13.

[39] Press, W. H., Teukolsky, S.A., Vetterling, W.T. and B. P. Flannery, *Numerical Recipes in Fortran*, 1st ed., Cambridge University Press: Cambridge, U. K. 1986.

[40] Crowder, G.A., Taylor, Z. L., Reed, T. M. and J. A. Young*, J. Chem. Eng. Data*, 12 (1967) 481-485.

[41] Ermakov, H. V. and V. P. Skripov, *Teplofiziki*, 1 (1971) 44-49.

[42] Dunlap, R. D., Murphy, C. J. Jr. and R. G. Bedford, *J. Am. Chem. Soc.,* 80 (1958) 83-85.

[43] Mousa, A. H. N., *J. Chem. Eng. Data,* 23 (1978) 133-134.

[44] Oliver, G. D. and J. W. Grisard, *J. Am. Chem. Soc.*, 73 (1951) 1688-1690.

[45] Milton, H. T. and G. D. Oliver, *J. Am. Chem. Soc.***,** 74 (1952) 3951-3952.

[46] Oliver, G. D., Blumkin, S. and C. W. Cunningham, *J. Am. Chem. Soc.*, 73 (1951) 5722-5725.

[47] McCabe, C. and S. B. Kiselev, *Fluid Phase Equilib*, 219 (2004) 3-9.

[48] McCabe, C. and S. B. Kiselev, *Ind. Eng. Chem. Res*., 43 (2004) 2839-2851.

[49] J.M. Prausnitz, R.N. Lichtenthaler and E. Gomez de Azevedo. Molecular Thermodynamics of Fluid-Phase Equilibria. Third Edition. Prentice Hall, New Jersey, 1999.

[50] Scott, R. L. and P. H. van Konynenburg, *Discuss. Faraday Soc*. 49 (1970) 87-97.

[51] Li, Y-H., Dillard, K. H. and R.L. Robinson, Jr., *J. Chem. Eng. Data* 26 (1981) 53-55.

[52] Wagner, Z. and I. Witchterle, *Fluid Phase Equilib.* 33 (1987) 109-123.

[53] Kalra, H., Kubota, H., Robinson, D. B. and H-J Ng, *J. Chem. Eng. Data,* 23 (1978) 317-321.

[54] Kobatake, Y, and J. H. Hildebrand, *J. Phys. Chem.* 65 (1961) 331-335.

[55] Hicks, C. P. and C. L. Young, *Chem. Rev.* 75 (1975) 119-175.

[56] Dunlap, R. D., Bedford, R. G., Woodbrey, J. C. and S. D. Furrow, *J. Am. Chem. Soc.*, 81 (1959) 2927-2930.

[57] Duce, C.,Tine, M. R., Lepori, L. and E. Matteoli, *Fluid Phase Equilib.* 199(1-2) (2002) 197-212.

[58] Waterson, D. S., Semmens, J. and C. L. Young, *Aust. J. Chem*. 33 (1980) 1987-1992.

[59] Linstrom, P. J. and W.G. Mallard, Eds., NIST Chemistry WebBook, NIST Standard Reference Database Number 69, March 2003, National Institute of Standards and Technology, Gaithersburg MD, 20899 (http://webbook.nist.gov).

[60] Block, T. E., Judd, N. F., McLure, I. A., Knobler, C. M. and R. L. Scott, *J. Phys. Chem.,* 85 (1981) 3282-3290.

[61] Gaw, W. J. and R. L. Scott, *J. Chem. Thermod*. 3 (1971) 335-345.

Chapter 6

Vapor-Liquid and Vapor-Liquid-Liquid Equilibria of Carbon Dioxide / *n*-Perfluoroalkane / *n*-Alkane Ternary Mixtures*

Coray M. Colina and Keith E. Gubbins

Department of Chemical Engineering, North Carolina State University
Raleigh, NC 27695, USA

6.1 Abstract

Perfluoroalkanes have numerous applications (e.g. in the medical field and the chemical industry), and their high affinity with carbon dioxide make them attractive as surfactants and co-solvents. Although research in this area has grown in the last few years, very little phase equilibrium data is available in the open literature for these systems. In this work we present, for the first time, predictions of vapor-liquid and vapor-liquid-liquid equilibria of binary and ternary systems of carbon dioxide/*n*-perfluoroalkane/*n*-alkane. Our results are based on the SAFT-VR EOS (Statistical Associating Fluid Theory of Variable Range, equation of state), and we study the influence of temperature, pressure, composition and chain length on the phase diagram. The predicted phase diagrams are based on temperature-independent binary interaction parameters, and no ternary parameters are introduced. Comparisons against the available experimental and molecular simulation data show that the predicted diagrams should provide a good representation of the phase equilibria.

* Submitted to *J. Phys. Chem.* (2004)

6.2 Introduction

Perfluoroalkanes have been used in the medical field and the chemical industry in numerous applications. Liquid ventilation is a novel life support technique in which the lungs are partially or totally filled with a neat liquid perfluorocarbon that acts as the oxygen and carbon dioxide carrier [1,2]. Perfluorooctylbromide ($C_8F_{17}Br$) is undergoing Food and Drug Administration Phase II and III clinical evaluation, and several other (liquid) perfluorocarbons, including perfluorooctane (*n*-C_8F_{18}), are currently under investigation [2]. Moreover, these fluids have been suggested as a vehicle for drug delivery [2], based on their higher solubilities for oxygen and carbon dioxide and lower surface tension than water. Additionally, their resemblance to inhaled anesthetic agents suggests the possibility of application in vaporization [1], a new medical technique that has significantly improved oxygenation and pulmonary function in oleic acid-induced lung injury. Perfluorohexane (*n*-C_6F_{14}) has been used to investigate [1] its effects on gas exchange and lung function in an ovine model of oleic acid-induced lung injury.

Perfluoroalkanes are also widely used in the chemical industry. For example, the linear perfluoroalkyl unit is present in most ZONYL intermediates surfactants as a mixture of chain lengths [3]. The distribution of these chains has concentrations up to 50% in *n*-C_6F_{14} and *n*-C_8F_{18} and up to 30% in *n*-$C_{10}F_{22}$, with average distribution of 7, 8, and 9 carbons. Moreover, short chain perfluoroalkanes (*n*-C_6F_{14}-*n*-$C_{10}F_{22}$) can be added to colloids or nanoparticles to act as stabilizers in the presence of CO_2, and provide unique tools not only in process application but also in biomedical research [4].

It is then surprising that very little data (experimental or theoretical) is available in the open literature for these systems, limiting to a great extent their use for present and future applications. It is the objective of the present work to present for the first time phase equilibria diagrams for ternary, and in several cases binary, mixtures of CO_2/ *n*-perfluoroalkanes/*n*-alkanes. We use for this purpose the Statistical Associating Fluid Theory of Variable Range (SAFT-VR). We study the influence that temperature, pressure,

composition and chain length have on the phase diagram, showing that the predicted diagrams should represent the expected phase equilibria behavior with good accuracy.

6.3 Model Description

The Statistical Associating Fluid Theory [5,6] (SAFT) is based on a resummed perturbation series due to Wertheim [7,8], and accounts in a realistic way for association between molecules, in addition to dispersion plus repulsive interactions. Moreover, SAFT can account for chain effects, including polymer molecules.

The SAFT equation has proved to be a significant improvement over more empirical equation of state (EOS), because it has a firm basis in statistical mechanics. In SAFT [5,6], molecules are modeled as chains of covalently bonded spheres. Homologous series, such as *n*-alkanes, n-perfluoroalkanes and polymers, can be modeled as chains of identical spheres, where the number of spheres in the chain is proportional to the molecular weight. In SAFT, the residual Helmholtz energy, A^{res}, is of the form

$$\frac{A^{res}}{NkT} = \frac{A^{seg}}{NkT} + \frac{A^{chain}}{NkT} + \frac{A^{assoc}}{NkT} \tag{6.1}$$

where A^{seg} is the part of the Helmholtz energy due to segment-segment interactions (interactions between monomer units in different molecules, usually modeled as hard sphere, Lennard-Jones (LJ) or square-well interactions), A^{chain} is the additional Helmholtz energy due to chain formation, and A^{assoc} is that due to association, e.g. hydrogen bonding, between different molecules. N is the number of molecules, k the Boltzmann constant, and T the temperature.

The most widely used version of SAFT is the implementation of Huang and Radosz [9] (SAFT-HR), who fitted the potential parameters to the experimental vapor pressure and saturated liquid density data for more than a hundred real fluids. For the segment term, they used the sum of a hard-sphere part, given by the Carnahan-Starling equation [10], and a

dispersion part, given by the BACK equation of Chen and Kreglewski [11]. Some recent papers [12,13,14,15] compare SAFT EOS and extensions of it against other existing methods. In general, SAFT, with its more rigorous foundation, is found to be more reliable both for fitting data and for prediction; this is particularly the case for associating fluids and chain molecules.

Among several modifications we would like to highlight the so-called Soft-SAFT, PC-SAFT and SAFT-VR. The Soft-SAFT EOS [16,17] is a modification of the original SAFT equation proposed by Chapman *et al.*[6] in which the reference term is a Lennard-Jones fluid. Chapman [*18*] was the first to extend the equation to a reference fluid of Lennard-Jones spheres. In the Soft-SAFT version the equation of Johnson *et al.* [19] is used for modeling the Lennard-Jones fluid. As in the rest of the SAFT equations, the chain contribution is obtained based on Wertheim's first order perturbation theory [7,8]. Blas and Vega have shown in a series of papers [16,17] that this version is very accurate in predicting the thermodynamic properties and phase equilibria behavior of model and real hydrocarbon mixtures. Recently Dias *et al.* [20] studied binary mixtures of xenon or oxygen in *n*-perfluoroalkanes (*n*-C_1F_4 to *n*-C_8F_{18}) within this approach.

The model development of the PC-SAFT (Perturbed-Chain SAFT) equation-of-state is described in detail by Gross and Sadowski [21]. In contrast to the SAFT equation of state (EOS), the PC-SAFT model accounts for the non-spherical shape of the molecules also in the dispersion term. The perturbation theory of Barker and Henderson [22] was applied using a hard chain fluid as the reference system, whereas a hard sphere reference was considered in earlier SAFT models. The theory was tested for square-well chains versus computer simulations [23] leading to a satisfactory prediction of the simulated behavior. Readjusting of model constants for real substances led to the PC-SAFT EOS [21].

Gil-Villegas *et al.*[24,25] proposed a version of SAFT with an attractive potential of variable range (SAFT-VR). In the framework of perturbation theory, they deduced analytical perturbation expressions for the contribution of the Helmholtz free energy for several potentials, such as square well, Sutherland, Yukawa and Mie m-n potentials. The

incorporation of an additional non-conformal range parameter allows for an accurate description of the bulk thermodynamics of systems ranging from small strongly associating or polar molecules such as water [26] and replacement refrigerants [27], to long-chain alkanes [28] and polyethylene [29]. Moreover, linear perfluoroalkanes have been studied within the SAFT-VR approach, by McCabe *et. al.*[30] and Colina *et al*.[31] with the so-called SAFT-VR EOS. Galindo and Blas [32,33] studied the global phase behavior of carbon dioxide/*n*-alkanes binary mixtures, and compared the predictions of the SAFT-VR EOS with the extensive experimental data available for these mixtures. Recently [31], we studied the phase behavior of binary mixtures containing carbon dioxide, *n*-alkanes (*n*-C_6H_{14}, *n*-C_7H_{16} and *n*-C_8H_{18}) and *n*-perfluoroalkanes (*n*-C_6F_{14}, *n*-C_7F_{16}) with the same theory, and very good agreement was found with available experimental data. These previous works provide a solid base from which to proceed, and we elected then to use in this work the SAFT-VR EOS for the prediction of ternary phase diagrams among carbon dioxide, *n*-perfluoroalkanes and *n*-alkanes.

In the SAFT-VR approach [24,25] the molecules are modeled as chains of tangentially bonded hard spherical segments of diameter σ. The attractive interactions are described by a square-well potential of variable range λ_{ij} and depth ε_{ij}, and the contribution to the free energy due to the dispersion interactions is obtained following the framework of perturbation theory. Association interactions can also be considered through embedded short-range attractive interaction sites. In this work we treat non-associating molecules, so that this contribution is not necessary. The Helmholtz free energy A for an n-component mixture of CO_2, *n*-perfluoroalkane and *n*-alkane molecules can be written as,

$$\frac{A}{NkT} = \frac{A^{IDEAL}}{NkT} + \frac{A^{MONO}}{NkT} + \frac{A^{CHAIN}}{NkT}, \tag{6.2}$$

The ideal contribution to the free energy is given by a sum over all species i in the mixture[24]

$$\frac{A^{IDEAL}}{NKT} = \sum_{i=1}^{n} x_i \, ln(\rho_i \Lambda_i^{\,3}) - 1 \tag{6.3}$$

where $x_i = N_i/N$ is the mole fraction, $\rho_i = N_i/V$ the number density, N_i the number of

molecules, V the volume of the system, and Λ_i the thermal de Broglie wavelength of species i. The monomer Helmholtz free energy can be written as

$$\frac{A^{MONO}}{NKT} = \left(\sum_{i=1} x_i m_i\right)\left(a^{HS} + \frac{1}{kT}a_1 + \left(\frac{1}{kT}\right)^2 a_2\right) \tag{6.4}$$

where

$$a^{HS} = \frac{6}{\pi\rho_s}\left[\left(\frac{\zeta_2^3}{\zeta_3^2} - \zeta_0\right)ln(1-\zeta_3) + \frac{3\zeta_1\zeta_2}{(1-\zeta_3)} + \frac{\zeta_2^3}{\zeta_3(1-\zeta_3)^2}\right] \tag{6.5}$$

$$a_1 = \sum_{i=1}^{n}\sum_{j=1}^{n} x_{s,i}x_{s,j}\left(-\frac{2}{3}\pi\,\varepsilon_{ij}\sigma_{ij}^3(\lambda_{ij}^3 - 1)\rho_s g_0^{HS}(\sigma_\chi;\zeta_\chi^{eff})\right) \tag{6.6}$$

$$a_2 = \sum_{i=1}^{n}\sum_{j=1}^{n} x_{s,i}x_{s,j}\,\frac{1}{2}\varepsilon_{ij}K^{HS}\rho_s\,\frac{\partial a_1^{ij}}{\partial\rho_s} \tag{6.7}$$

where m_i is the number of spherical segments of chain i, $\rho_s = N_s/V$ is the total number density of spherical segments and ζ_i are reduced densities. The mean attractive energy a_1, is obtained from the sum of the partial terms corresponding to each type of pair interaction; $g_0^{HS}(\sigma_x;\zeta_x^{eff})$ is the contact radial distribution function of a hypothetical pure fluid of average diameter σ_x. The effective packing fraction ζ_x^{eff} is obtained from the corresponding packing fraction of the fluid ζ_x, using $\zeta_x^{eff}(\zeta_x,\lambda_{ij}) = c_1(\lambda_{ij})\zeta_x + c_2(\lambda_{ij})\zeta_x^2 + c_3(\lambda_{ij})\zeta_x^3$, where c_1, c_2, and c_3 are coefficients given in reference 24. Finally, K^{HS} is the hard-sphere isothermal compressibility of Percus-Yevick theory [34].

The contribution to the free energy due to chain formation is expressed in terms of the contact value of the monomer background correlation function as

$$\frac{A^{CHAIN}}{NkT} = -\sum_{i=1}^{n} x_i(m_i - 1)ln\,y_{ii}^{MONO}(\sigma_{ii}) \tag{6.8}$$

where, for square-well chains $y_{ii}^{MONO}(\sigma_{ii}) = y_{ii}^{SW}(\sigma_{ii})$, and $y_{ii}^{SW}(\sigma_{ii}) = g_{ii}^{SW}(\sigma_{ii})\exp(\varepsilon_{ii}/kT)$. In the SAFT-VR approach the radial distribution function of the system of unbonded monomers is obtained from a high-temperature expansion $g_{ii}^{SW}(\sigma_{ii}) = g_{ii}^{HS}(\sigma_{ii}) + \varepsilon_{ii}/kT \cdot g_1(\sigma_{ii})$, where the reference term is evaluated using the expression of Boublík [35]. Once the free energy is known, standard thermodynamic relations can be used to determine the pressure and chemical potentials, and the phase equilibrium conditions (equality of temperature, pressure and chemical potentials of each component in all phases) can be solved using a numerical algorithm [36].

6.3.1 Pure component parameters

The first step in the application of the SAFT-VR to multicomponent mixtures, and in general any EOS, is to determine the intermolecular pure component parameters. As was mentioned before, for a nonassociating component there are four component parameters. m_i is the number of spherical segments in a chain, and this is treated as an adjustable parameter. The diameter of hard spherical segments tangentially bonded together is σ. The attractive interactions are described by a square-well potential of variable range λ_{ij} and depth ε_{ij}.

Blas and Galindo [32,33] obtained carbon dioxide (CO_2) parameters by fitting to experimental vapor pressures and saturated densities. CO_2 is modeled as a non-associating and non-spherical molecule, where the non-spherical, i.e. linear, nature of the molecule is treated in an explicit way by modeling the molecule with 2 tangentially bonded square-well segments. The attractive dispersion interactions and the quadrupole are treated in an effective way via a square-well potential of depth ε_{ii} and adjustable range λ_{ii}. The *n*-alkane molecules have also been studied in a number of previous works with the SAFT-VR approach [24,28,32]. The number of segments m_i forming the model chain can be obtained as a function of the number of carbon atoms C of the *n*-alkane molecule by $m_i = (C-1)/3+1$. Using this value for m_i, McCabe and Jackson [28] have carried out the optimization of the monomer intermolecular parameters for a large number of *n*-alkanes (from methane to *n*-hexatriacontane) using experimental vapor pressures and saturated liquid densities; these

values are used in this work. Carbon dioxide and *n*-alkanes parameters are presented in table 1 here for completeness.

Table 6.1. Optimized SAFT-VR square-well intermolecular potential parameters. The subscript c indicates that the parameters have been rescaled to the experimental critical point.

	m	λ	σ_c/Å	ε_c/k (K)
CO_2	2.0	1.5157	3.1364	168.89
C_6H_{14}	2.667	1.552	4.479	236.6
C_7H_{16}	3.0	1.563	4.529	237.3
C_8H_{18}	3.333	1.574	4.564	236.5
C_9H_{20}	3.667	1.602	4.545	227.4
$C_{10}H_{22}$	4.0	1.621	4.561	220.4
C_6F_{14}	2.85	1.4390	5.0315	264.24
C_7F_{16}	3.22	1.4365	5.1233	272.63
C_8F_{18}	3.59	1.4554	5.0694	270.51

Following previous works [30], the number of segments m_i forming a model *n*-perfluoroalkane chain is related to the number of carbons, C, of the *n*-perfluoroalkane molecule by $m_i = (C-1)*0.37+1$. Using these values for m_i, parameters for perfluoromethane to *n*-perfluorobutane have been presented previously by McCabe *et al*.[30] Recently we presented [31] the parameters for *n*-perfluorohexane and *n*-perfluoroheptane. In the case of *n*-perfluorooctane some experimental data [37] is available in the literature for experimental vapor pressures and saturated liquid densities. The optimized intermolecular parameters for the *n*-perfluoroalkane molecules used in this work are also presented in table 1.

6.3.2 Mixture parameters

The extension to multicomponent mixtures is straightforward with the SAFT EOS since the reference terms can be extended to mixtures based on rigorous statistical mechanics. In the case of the SAFT-VR approach, for non-associating chain molecules the calculation of mixture phase behavior requires determining a number of unlike intermolecular parameters.

These are: σ_{ij}, ε_{ij} and λ_{ij}. Traditionally, the modified Lorentz-Berthelot combining rules are used [38],

$$\sigma_{ij} = \frac{\sigma_{ii} + \sigma_{jj}}{2},\ \varepsilon_{ij} = \xi_{ij}\sqrt{\varepsilon_{ii}\varepsilon_{jj}},\ and\ \lambda_{ij} = \gamma_{ij}\frac{\lambda_{ii}\sigma_{ii} + \lambda_{jj}\sigma_{jj}}{\sigma_{ii} + \sigma_{jj}} \tag{6.9}$$

In the case of hard core potentials, σ_{ij} is given exactly by the expression shown in equation (9), but the parameters describing the unlike square-well energy ε_{ij} and range λ_{ij} are only approximate, so that two adjustable parameters ξ_{ij} and γ_{ij} often need to be introduced in order to improve the agreement with the experimental mixture phase behavior. The adjustable parameters used in this work are presented in table 2.

Table 6.2. SAFT-VR square-well intermolecular potential parameters for the binary mixtures.

System	ξ_{ij}	γ_{ij}
CO_2/*n*-C_nH_{2n+2}	0.88	0.989
CO_2/*n*-C_nF_{2n+2}	0.88	0.989
C_6F_{14} /*n*-C_nH_{2n+2}	0.929	1
C_7F_{16} /*n*-C_nH_{2n+2}	0.932	1
C_8F_{18} /*n*-C_nH_{2n+2}	0.932	1

n: 6 -10

Values of $\xi_{alkane\text{-}CO2}$ = 0.88 and $\gamma_{alkane\text{-}CO2}$ = 0.989 were determined by Blas and Galindo [32,33] to ensure that the mixture of CO_2/*n*-$C_{13}H_{28}$ exhibits type IV phase behavior in the classification of Scott and van Konynenburg [39]. The set of parameters used is not temperature dependent, so that it can be used to describe the phase behavior of the mixture for the entire fluid range, and can be transferred to other CO_2/*n*-alkane mixtures [32]. This transferability was confirmed in our previous work [31] for mixtures of CO_2/*n*-hexane and CO_2/*n*-heptane. Here we show that the same parameters provide a good description of the vapor-liquid and vapor-liquid-liquid equilibria in binary and ternary mixtures.

In the case of the mixtures of CO_2/*n*-perfluorohexane and CO_2/*n*-perfluoroheptane we found [31] the same unlike adjustable intermolecular parameters can be used; i.e., $\xi_{\text{perfluoroalkane-CO2}} = 0.88$, and $\gamma_{\text{perfluoroalkane-CO2}} = 0.989$. The similarity with the *n*-alkane parameters was explained based on the use of square-well potentials to treat the quadrupolar interactions characteristic of carbon dioxide in an effective way, and the parameters ξ_{ij} and γ_{ij} mainly provide a correction for this approximation. Moreover, this previous work supports the proposition that the increased solubility of *n*-perfluoroalkanes in CO_2 may be closely related to larger attractive dispersion interactions. For a complete discussion on this topic the reader is referred to our previous work [31].

Binary *n*-alkane/*n*-perfluoroalkane mixtures are known to exhibit type II phase behavior in the classification of Scott and van Konynenburg [39], when the difference in chain length between the two components is not very large ("symmetric" (same carbon number) or close-to symmetric systems). Mixtures of the components considered in this work exhibit this type of phase diagram. McCabe *et al*.[29] studied the high-pressure phase behavior of a number of *n*-perfluroalkanes (*n*-C_1F_4- *n*-C_4F_{10}) and *n*-alkane (*n*-C_1H_4- *n*-C_7H_{16}) systems, and suggested a value $\xi_{\text{alkane-perfluoroalkane}} = 0.9234$ (with $\gamma_{\text{alkane-perfluoroalkane}} = 1$, as could be expected since both molecules are non-polar), for the "symmetric" case and $\xi_{\text{alkane-perfluoroalkane}} = 0.9206$ or $\xi_{\text{alkane-perfluoroalkane}} = 0.8948$ for unsymmetrical cases. We found that the slightly different value of $\xi_{\text{alkane-perfluoroalkane}} = 0.929$ (with $\gamma_{\text{alkane-perfluoroalkane}} = 1$) provides a better fit to the upper critical solution temperatures [40] (UCST) of *n*-C_6H_{14}/ *n*-C_6F_{14} and *n*-C_6H_{14}/ *n*-C_7F_{16}. The influence of the value of the $\xi_{\text{alkane-perfluoroalkane}}$ parameter on the equilibrium conditions will be discussed in the next section.

It is important to mention that all the values mentioned above for binary interaction parameters are within the expected range for a binary interaction parameter (i.e. between 0.85 and 1.15 or -0.15 to 0.15 depending of the definition used). It is essential to keep in mind that binary interaction parameters are used to "correct" a theory, in a way that real systems can be represented with higher accuracy. Bigger values of these parameters would indicate that the model (or combining rule) employed is not the most adequate to represent the system under investigation and modifications or different models should be utilized. For example, a binary

interaction parameter of 0.5 (-0.5 or 1.5) would indicate that the predictions of the model are off by 50 %, and thus, modifications or different models should be used. We would like to stress that the present rule of thumb is valid for interaction parameters in any model, combining or mixing rule.

In the next section, we show that the SAFT-VR EOS predicts, in very good agreement with the available experimental and molecular simulation data, the vapor-liquid equilibria (VLE), liquid-liquid equilibria (LLE) and vapor-liquid-liquid equilibria (VLLE) of binary and ternary mixtures of *n*-alkanes, *n*-perfluoralkanes and CO_2.

6.4 Results and Discussion

One-, two- and three-phase regions can exist simultaneously in ternary systems at particular temperatures and pressures, yet only one or two of each one/two-phase region are present in the majority of the systems that have been investigated to date [41]. The shapes of such regions may differ markedly from system to system or with the range of conditions. The reader is referred to Wallas' book [41] for an introductory, but comprehensive, discussion on ternary phase diagrams.

Fifty years ago Francis [42] presented a set of 464 qualitative ternary diagrams with (liquid) carbon dioxide as one of the components, displaying a great variety of behavior at or near room temperature, and around 6.6 MPa. Even though the triangular graphs presented are qualitative they represented a vast amount of information for the 261 substances studied. Unfortunately perfluoroalkanes were not included in that study, and neither were the effect of temperature or pressure.

6.4.1 CO_2/n-perfluorohexane/ n-alkane phase equilibria

In a recent work [31], we found excellent agreement for the vapor-liquid equilibria (VLE) of the CO_2/*n*-C_6H_{14} mixture when comparing against the available experimental data at 313 K and 353 K. Additionally, very good predictions were found for the VLE of CO_2/*n*-C_6F_{14} at

the same temperatures, and for VLE and liquid-liquid equilibria (LLE) of n-C_6H_{14}/n-C_6F_{14}. In this section, we present ternary diagrams obtained for the mixture CO_2/n-C_6F_{14}/n-C_6H_{14} as a function of temperature and pressure. For the sake of completeness we also present some binary diagrams.

In figure 6.1 the VLE predictions of the CO_2/n-C_6H_{14} mixture at different temperatures (298 K, 303 K, 323 K and 393 K) are compared with the available experimental data [43,44,45]. In general, good agreement is found. It can be seen in this figure that the theory predicts coexisting liquid compositions that are somewhat too small at low temperatures, and pressures that are too high at the highest temperature studied. Similarly, in figure 6.2 we present the VLE predictions of CO_2/n-C_6F_{14} at different temperatures (298 K, 314.65 K and 353 K) and compare with the available experimental data. An underprediction is found for the liquid compositions at 298 K; this is less pronounced at the other temperatures. However, it is important to keep in mind that these calculations are totally predictive, i.e. they were obtained from pure component parameters and a set of binary interaction parameters that are neither fluid nor temperature dependence [31,32,33].

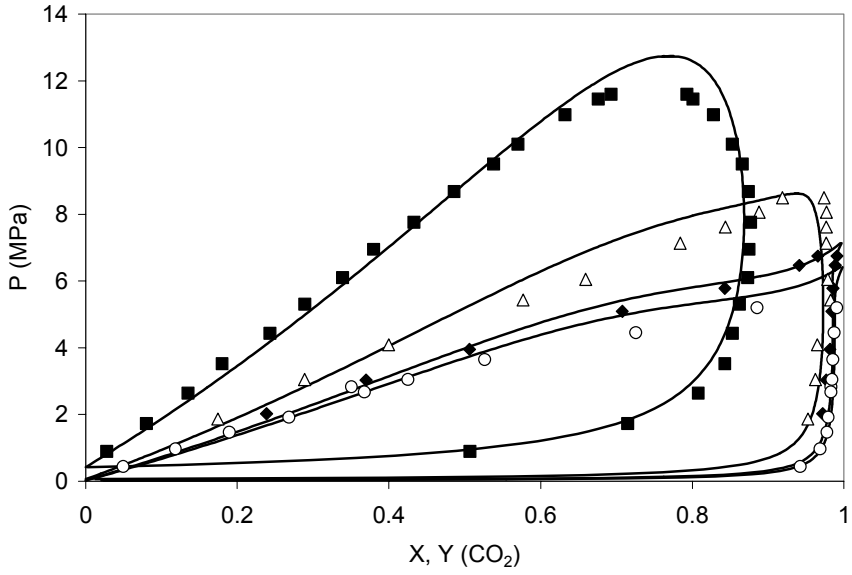

Figure 6.1. Vapor-liquid equilibrium for the CO_2/n-hexane binary mixture compared with the SAFT-VR predictions. Symbols represent the experimental data at: (o) 298 K [43]; (♦) 303 K [44]; (Δ) 323 K [44] and (■) 393 K [45]. The theoretical predictions are shown by the continuous curves.

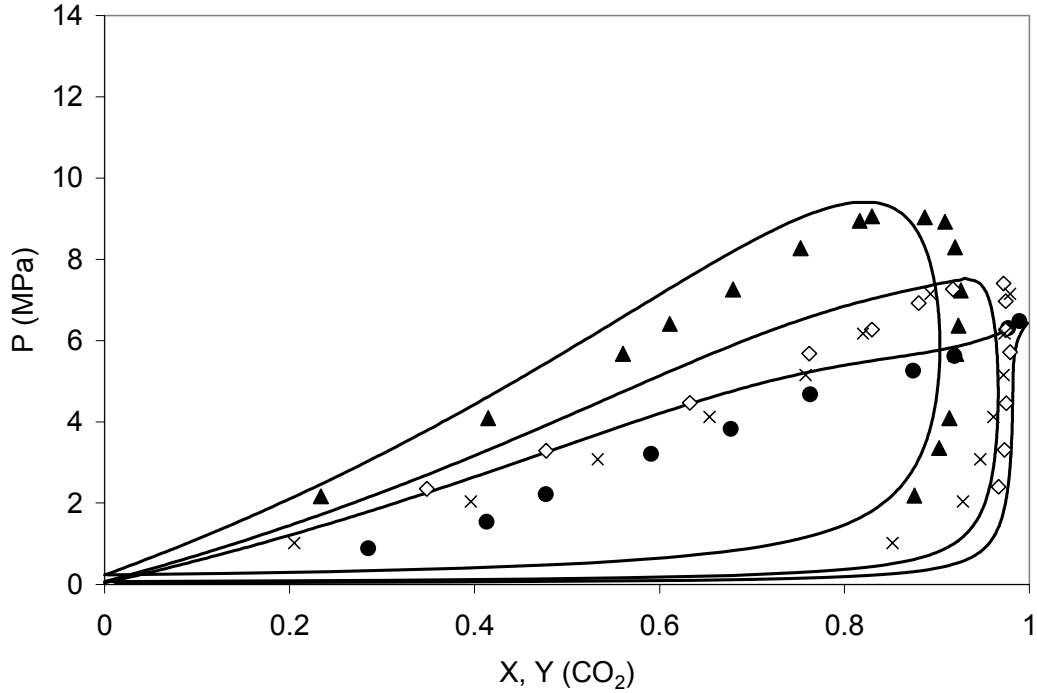

Figure 6.2. Vapor-liquid equilibrium for the CO_2/*n*-perfluorohexane binary mixture compared with the SAFT-VR predictions. Symbols represent the experimental data at: (●) 298 K [46]; (◊) 314.65 K[47] and (▲) 353 K [48]; crosses correspond to the molecular simulations of Zhang and Siepmann [53] at 315 K. The theoretical predictions are shown by the continuous curves.

It is well known that choosing parameters to provide the best agreement for the critical point (UCST) of a mixture is to the detriment of the prediction of the compositions of the liquid phases [31]. In figure 6.3a the LLE of *n*-C_6F_{14}/*n*-C_6H_{14} is presented for two different unlike intermolecular parameters and compared with the available experimental data. The bold line represent the predictions obtained from a fit (ξ= 0.929) of the UCST of the *n*-C_6F_{14}/ *n*-C_6H_{14} system in our previous work [31]. The gray line corresponds to the value suggested by Mc Cabe *et al.*[30] for "symmetric" systems (ξ= 0.9234). This value was obtained from a fit of the UCST of the *n*-C_4F_{10}/*n*-C_4H_{10} mixture), and used here as a transferable parameter. The predictions with both parameters are shown in this figure to demonstrate the high impact that the selection of this parameter has on the LLE. However, the VLE do *not* strongly depend on the value of this parameter, as can be seen in figure 6.3b.

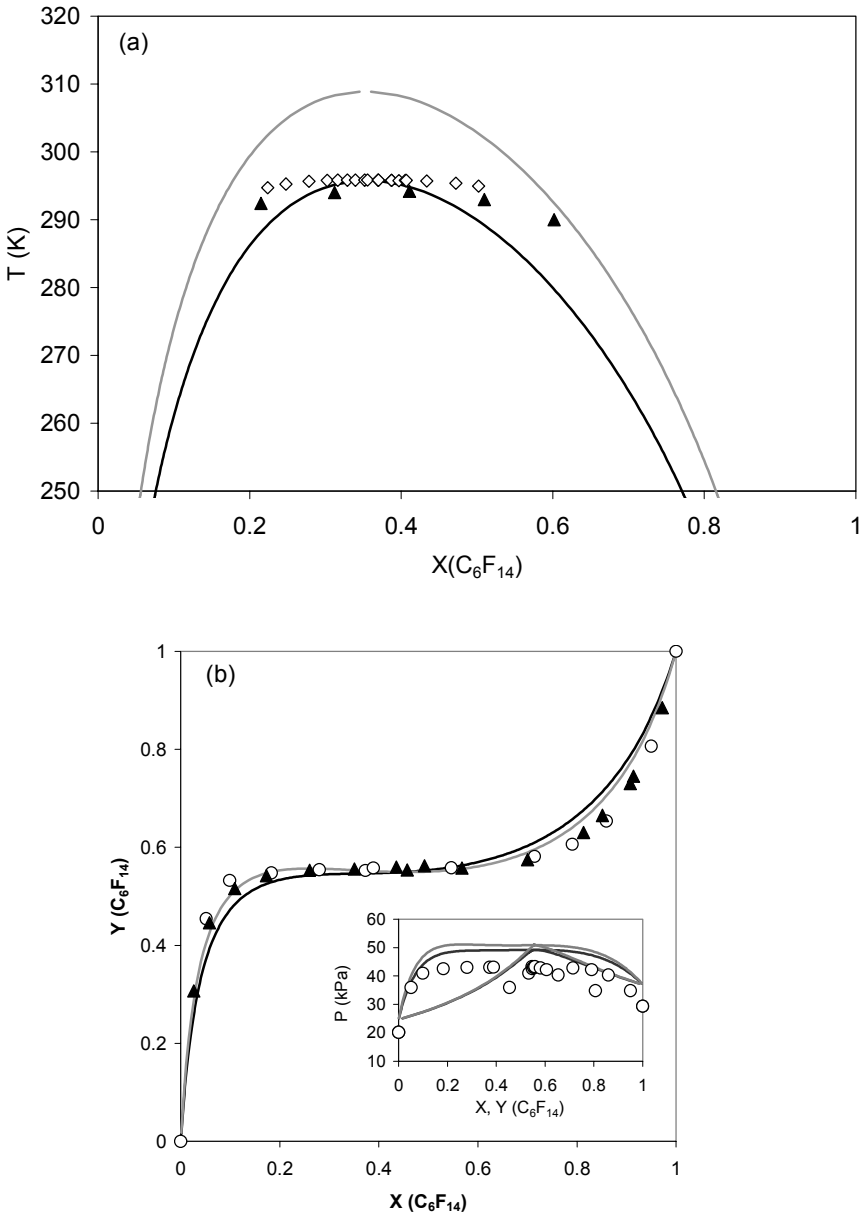

Figure 6.3. (a) Liquid-liquid and (b) Vapor-liquid equilibrium for the *n*-hexane /*n*-perfluorohexane binary mixture compared with the SAFT-VR predictions for two different unlike parameters. Symbols represent the experimental data of (▲)Duce *et al*.[48]; (◊) Gaw *et al*. [49] and (o) of Dunlap *et at*. [50]. The theoretical predictions are shown by the continuous lines. Bold line corresponds to ξ= 0.929, and the gray line corresponds to ξ= 0.9234.

The UCST of *n*-C_6F_{14}/*n*-C_6H_{14} mixtures has been reported [51] to be 295.9 K. At temperatures above this value, and in the presence of CO_2, only two phases (vapor-liquid) are present. In figure 6.4 we present the vapor-liquid equilibria (VLE) for the system CO_2/ *n*-

C_6F_{14}/*n*-C_6H_{14} at 298.15 K. Different isobars are presented. Vapor compositions are in the upper corner of the figure, in the region shown by the arrow, and liquid compositions lie along the isobars shown. Only a few tie lines, at 1.57 MPa, are shown for clarity. Pressure increases from 1.57 MPa to 5.33 MPa, and as the pressure increases the liquid phase region increases, as should be expected.

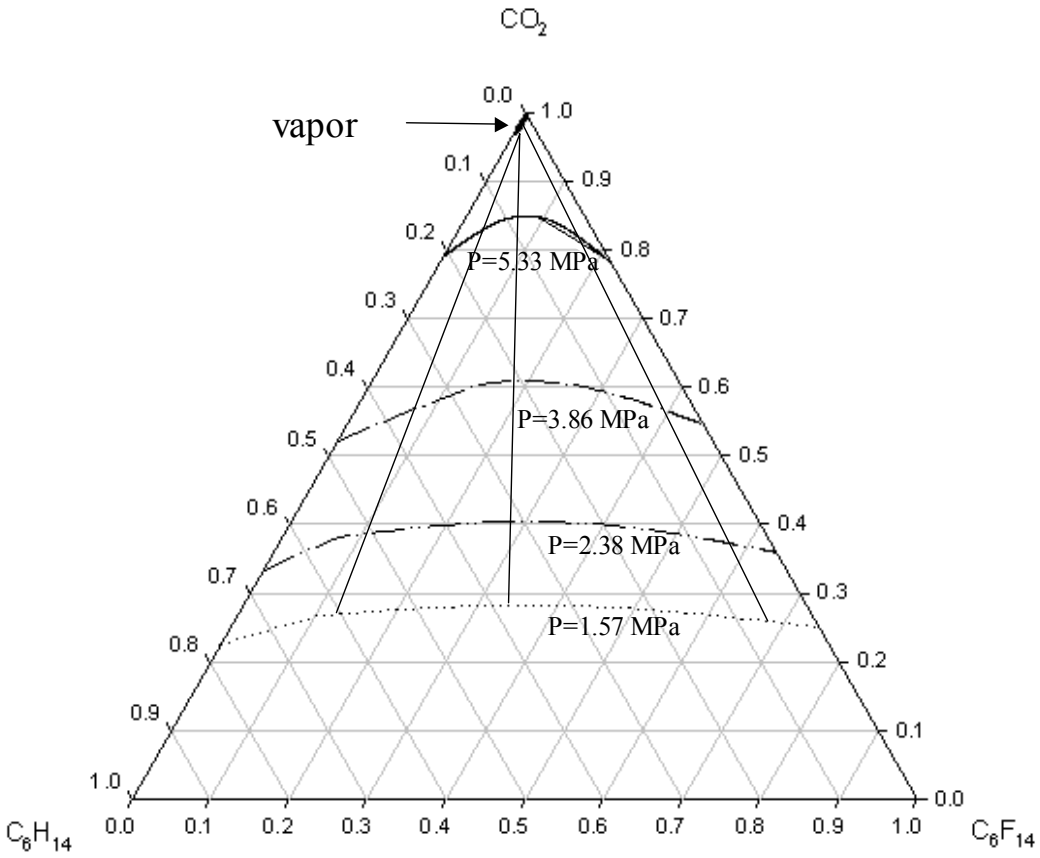

Figure 6.4. SAFT-VR predictions for the vapor-liquid equilibrium (VLE) for the system CO_2/*n*-perfluorohexane/*n*-hexane at 298.15 K. Dotted line: 1.57 MPa, double-dotted dashed line: 2.38 MPa, dotted dashed line: 3.86 MPa, continuous line: 5.33 MPa.

The vapor-liquid-liquid equilibrium (VLLE) for the system CO_2/*n*-C_6F_{14}/*n*-C_6H_{14} at 278.15 K is presented in figure 6.5. In this figure the filled circles represent the liquid phases in equilibrium with the vapor phase (represented by the bold line). Selected points in equilibrium are shown with different symbols, and one VLL equilibrium state is highlighted as light dotted lines. It is important to note that the equilibrium pressure changes over the set of conditions in this graph: the pressure increases as the amount of CO_2 in the liquid phases

increases, or in other words the immiscibility gap among the *n*-perfluoroalkane-rich liquid phase and the *n*-alkane-rich liquid phase decreases with increasing pressure (and carbon dioxide content) at constant temperature.

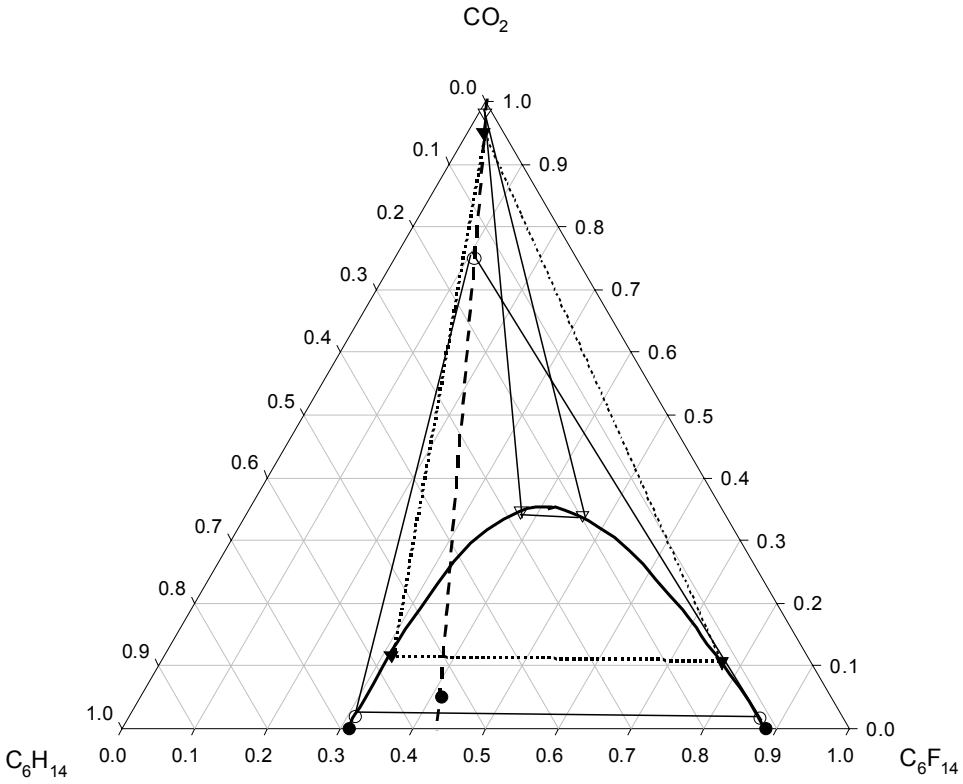

Figure 6.5. SAFT-VR predictions for the vapor-liquid-liquid equilibrium (VLLE) for the system CO_2/*n*-perfluorohexane/*n*-hexane at 278.15 K. (●) liquid-liquid equilibria, continuous bold line: vapor phase in equilibrium with liquid-liquid phases. Dotted lines represent the tie lines. Symbols correspond to points in equilibrium at constant pressure: (o) 90.51 kPa, (∇) 471.88 kPa and (□) 986.14 kPa.

For clarity the pressure is shown as a function of *n*-perfluorohexane composition in the liquid phases in figure 6.6a, (and in figure 6.6b as a function of *n*-perfluorohexane composition in the same phases but on a solvent free basis (without CO_2). It can be seen from these figures that *n*-C_6F_{14} and *n*-C_6H_{14} become completely miscible at approximately 986 kPa, in the presence of carbon dioxide. It is important to note however, that as a consequence of the adjustment of the $\xi_{\text{alkane-perfluoroalkane}}$ parameter to the UCST of the *n*-alkane/*n*-perfluoroalkane system, very good predictions are obtained in pressure, but the compositions of the two liquid phases in coexistence should be under-predicted (see figure 6.3), i.e. the predicted liquid-liquid immiscibility gap is somewhat narrower than the one that would be obtained if

experiments (or molecular simulations) were performed, as will become evident for the system CO_2/*n*-C_6F_{14}/*n*-$C_{10}H_{22}$, where molecular simulation data is available.

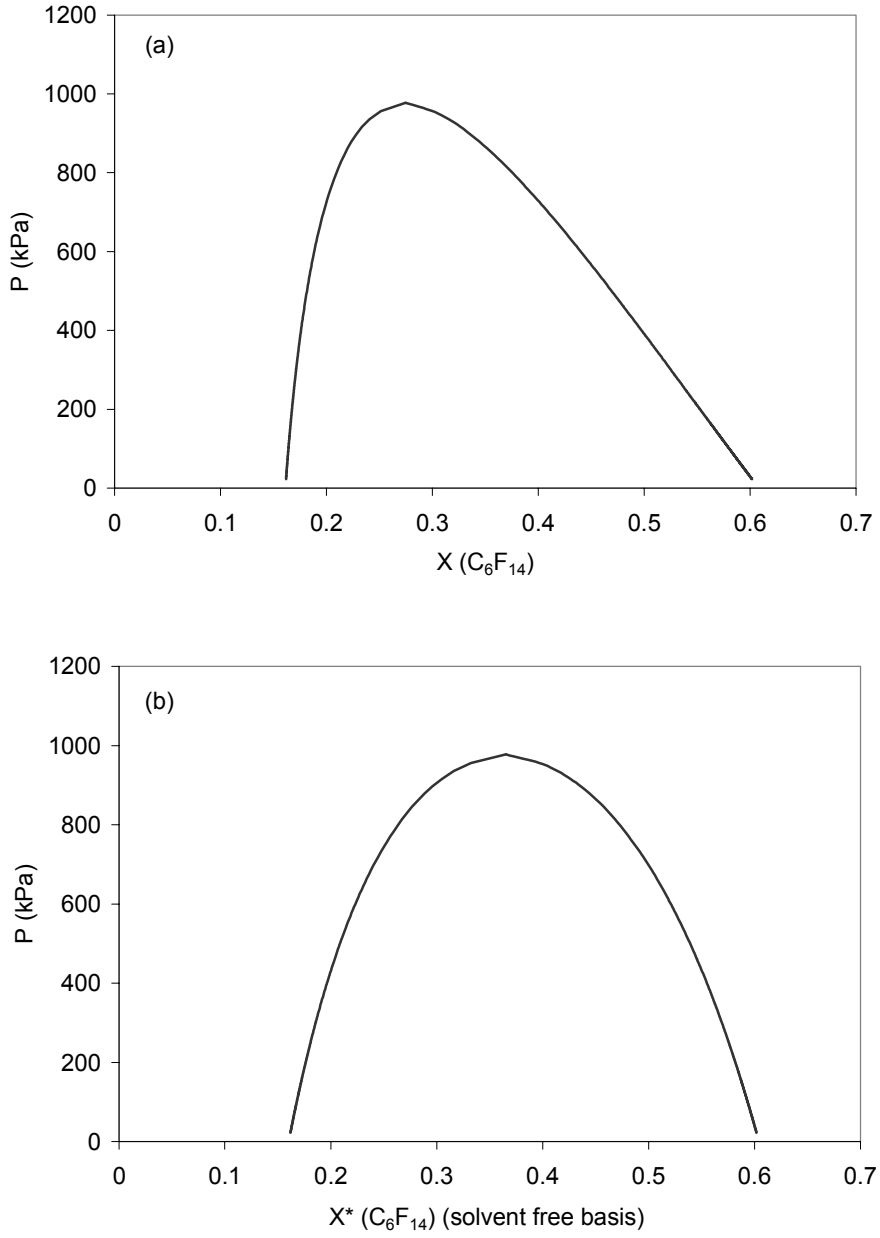

Figure 6.6. Pressure (a) as a function of the composition of *n*-perfluorohexane in the liquid phases and, (b) as a function of *n*-perfluorohexane in the liquid phases on a solvent free basis (without CO_2). The theoretical predictions, with $\xi = 0.929$, are shown by the continuous line. The pressure-composition diagrams show the pressure along the liquid-liquid coexistence curve.

The influence of temperature for CO_2/*n*-perfluoralkane/*n*-alkane mixtures is shown in figure 6.7 for CO_2/*n*-C_6F_{14}/*n*-C_7H_{16} as an example. It can be seen that the liquid-liquid immiscibility region decreases with an increase of temperature, as expected. However, the influence of temperature on the vapor phase is less marked. It is also important to keep in mind that in the ternary plots presented in this work the pressure of the system increases as the amount of CO_2 increases. Table 6.A1 (additional information section) contains some selected PTx equilibria points for the system CO_2/*n*-C_6F_{14}/*n*-C_7H_{16} at different conditions, as well as for the system CO_2/*n*-C_6F_{14}/*n*-C_6H_{14} at 278.15 K. Compositions of CO_2 in each phase can be obtained from the sum condition ($X(CO_2)$ = 1-$X(C_6F_{14})$-$X(C_nH_{2n+2})$). Free-solvent compositions (X*) can easily be calculated: $X(C_6F_{14})^* = X(C_6F_{14})/(1- X(C_nH_{2n+2}))$.

In figure 6.8 ternary diagrams are shown for the systems CO_2/*n*-C_6F_{14}/*n*-C_nH_{2n+2}, n = 7-10, at 298.15 K, where LLVE is present for all systems at these conditions. The system CO_2/*n*-C_6F_{14}/*n*-C_6H_{14} is not included here because it does not present LLV equilibria at 298.15 K (see figure 6.4). A single set of tie lines for an equilibrium condition (at 101. 325 kPa) is shown. As expected the theory predicts that the liquid-liquid immiscibility region increases with the carbon number of the *n*-alkane chain. It can also be observed that the partition of the *n*-alkane and *n*-perfluorohexane decreases in the vapor phase (while the *n*-alkane carbon number increases), until almost pure carbon dioxide is only present. This plot can be very useful, since it specifies not only the amount of material required to obtain homogenous (or heterogenous as desired) liquid phase, but also indicates the partition coefficients of the components in different phases. This information could be used to guide experiments. For the system CO_2/*n*-C_6F_{14}/*n*-C_7H_{14} it was found experimentally [52] that at room temperature the minimum pressure needed to obtain LVE was 1.5 MPa. This result agrees with our predictions shown in figure 8, where LLVE is predicted for pressures of 1.22 MPa or below. Moreover, Zhang and Siepmann [53] have recently reported LLVE predictions obtained from Monte Carlo simulations, for the system CO_2/*n*-C_6F_{14}/*n*-$C_{10}H_{22}$ at 298 K. The comparison between our results and their predictions are shown in figure 6.9. The agreement between both methods is encouraging, because very similar results were obtained from two independent studies. For this system the SAFT-VR EOS predicts an upper critical miscibility

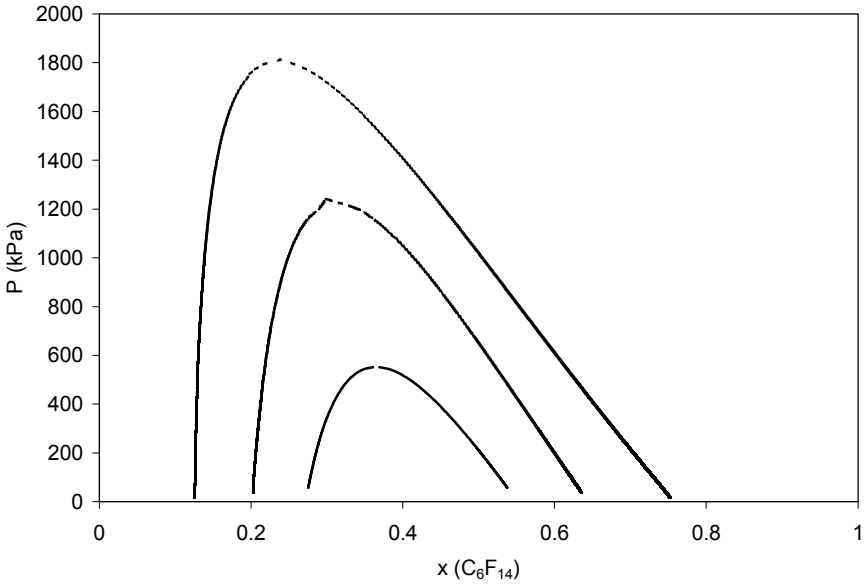

Figure 6.7. SAFT-VR predictions for the vapor-liquid-liquid equilibrium (VLLE) for the system CO_2/*n*-heptane/*n*-perfluorohexane at 278.15 K (dotted line), 298.15 K (dotted-dashed line) and 308.15 K (continuous line).

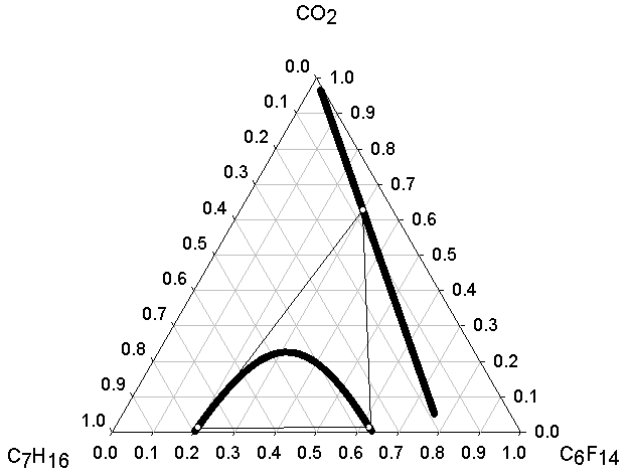

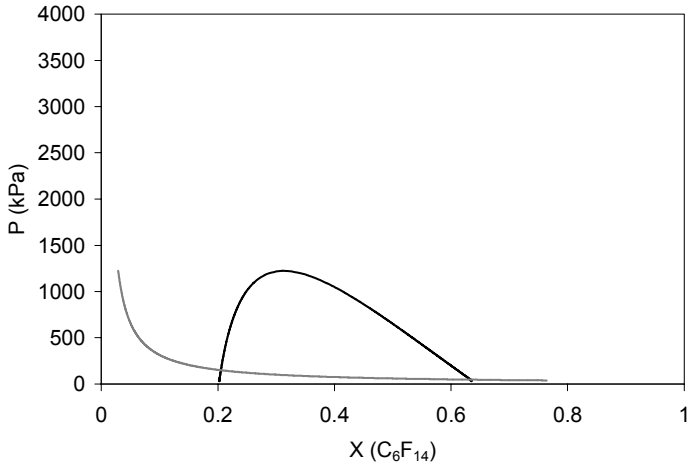

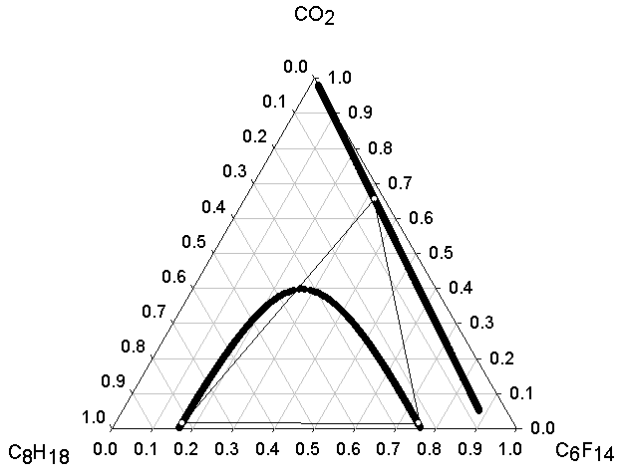

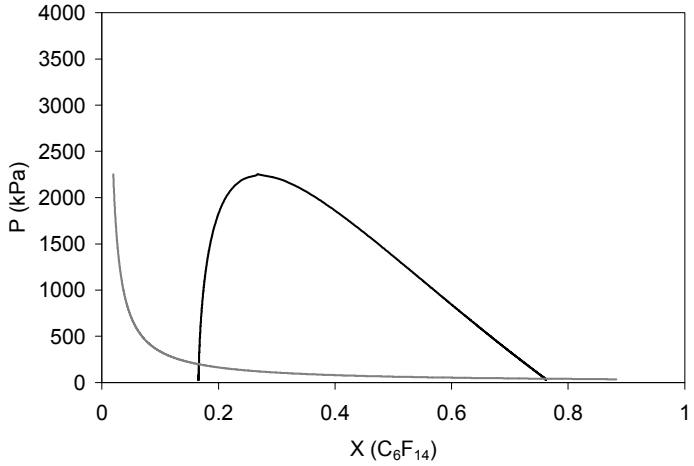

Figure 6.8. SAFT-VR predictions for the vapor-liquid-liquid equilibrium (VLLE) for the system CO_2/*n*-perfluorohexane/C_nH_{2n+2} at 298.15 K, for n = 7 – 10. The pressure-composition diagrams show: (a) as a black line the pressure along the liquid-liquid coexistence curve; (b) as a gray line the pressure along the vapor phase curve.

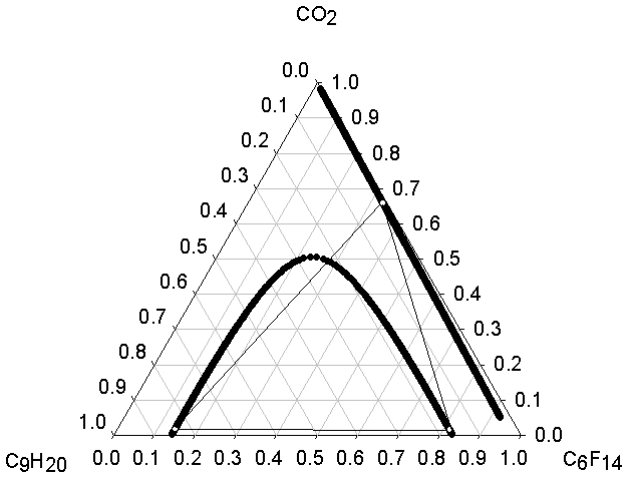

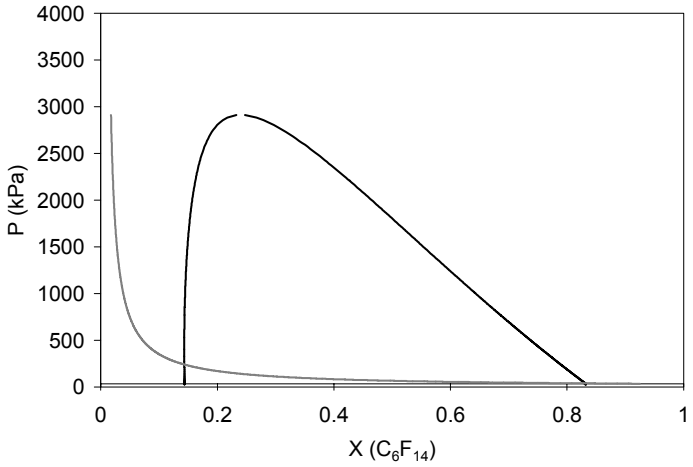

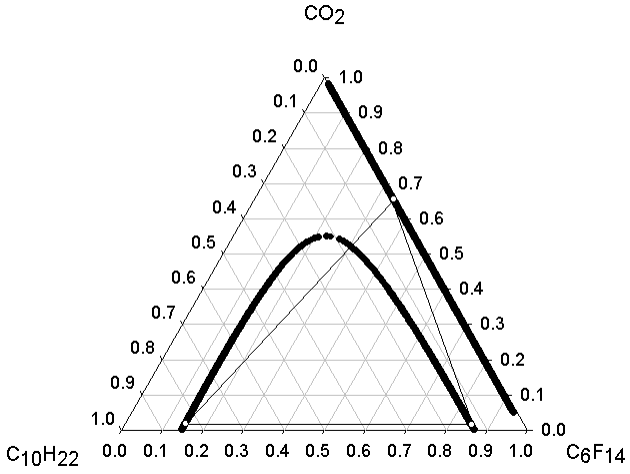

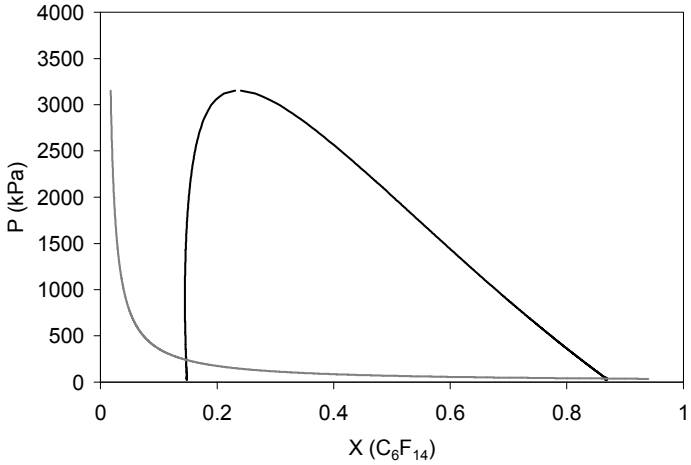

Figure 6.8 (Continued). SAFT-VR predictions for the vapor-liquid-liquid equilibrium (VLLE) for the system CO_2/*n*-perfluorohexane/C_nH_{2n+2} at 298.15 K, for n = 7 – 10. The pressure-composition diagrams show: (a) as a black line the pressure along the liquid-liquid coexistence curve; (b) as a gray line the pressure along the vapor phase curve.

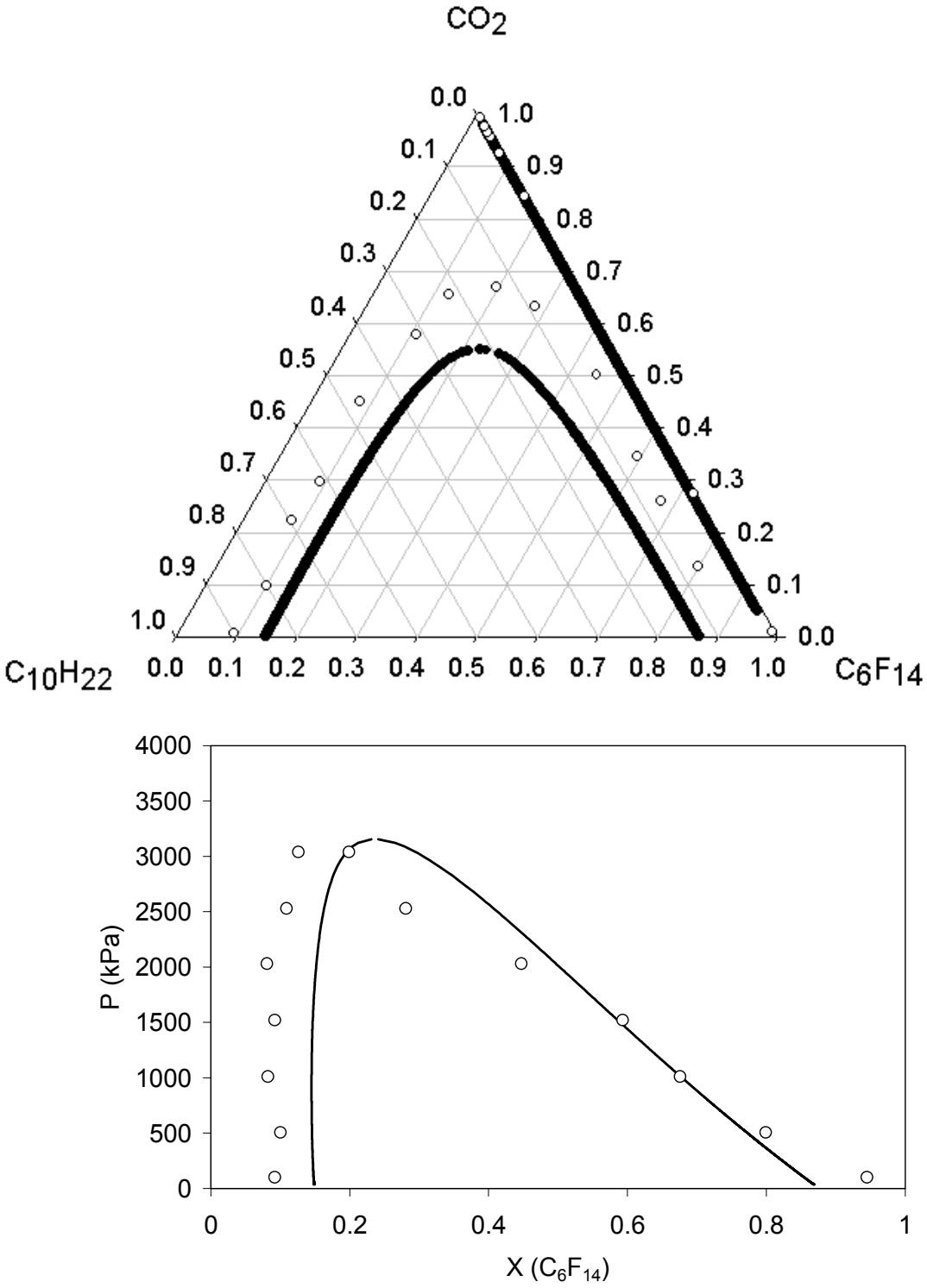

Figure 6.9. SAFT-VR predictions for the vapor-liquid-liquid equilibrium (VLLE) for the system CO_2/*n*-perfluorohexane/*n*-decane at 298 K. Symbols correspond to the molecular simulations of Zhang and Siepmann [53]. The theoretical predictions of this work are shown by the continuous lines.

pressure of 3.15 MPa, while Zhang and Siepmann predicts 3.3 MPa from Monte Carlo simulations. The good agreement in pressures (figure 6.9b) from our predictions and the Monte Carlo simulations is gratifying; however the compositions are under-predicted by the theory. While molecular simulations can provide a deeper understanding, since molecular structures can be observed, results from a molecular-based equation of state, such as SAFT-VR, can provide rapid and accurate predictions, and the calculations are at least 3 orders of magnitude faster. This feature permits systematic studies for different sets of conditions, as shown in this work. Moreover, these results can be used to guide experiments, and at the same time provide insight into the underlying thermodynamics. In this respect on table 6.A2 selected equilibrium points for the systems CO_2/*n*-C_6F_{14}/*n*-C_nH_{2n+2}, for n = 7-10 are given.

6.4.2 CO_2/n-perfluoroheptane /n-alkane or CO_2/n-perfluorooctane/n-alkane phase equilibria

For the rest of the triangular diagrams shown in this paper we also elected to use a binary interaction parameter for the *n*-alkane/*n*-perfluoralkane interaction that provides a good prediction of the UCST of the liquid phases. This results in liquid-liquid subcritical compositions that are underpredicted. We found that this binary interaction parameter is dependent on the perfluoroalkane under study. For example, figures 6.3 to 6.9 were generated with a constant value $\xi_{\text{alkane-perfluorohexane}} = 0.929$. This unique value was obtained from a fit of the UCST for the system *n*-C_6F_{14}/*n*-C_6H_{14} and used (giving excellent predictions, as shown in figures 6.3-6.9) for all the mixtures among *n*-perfluorohexane and the *n*-alkanes (C6-C10), in a transferable fashion.

In figure 6.10a we show the LLE among perfluoroheptane and *n*-alkanes and in figure 6.10b among perfluorooctane and *n*-alkanes, predicted with $\xi_{\text{alkane-perfluoroheptane}} = \xi_{\text{alkane-perfluorooctane}} = 0.932$ adjusted to the UCST of *n*-C_8F_{18}/*n*-C_6H_{14}. Also shown, as dotted lines in the figures, are the experimental UCST values. The agreement is in general excellent, especially taking into account that the binary interaction parameter, used here in a transferable fashion, was adjusted to only one UCST, that for *n*-C_8F_{18}/*n*-C_6H_{14} mixtures. Moreover, in figure 6.10b is

also shown the prediction for the system *n*-C_8F_{18}/*n*-$C_{13}H_{28}$, which is in excellent agreement with the experimental UCST for this system.

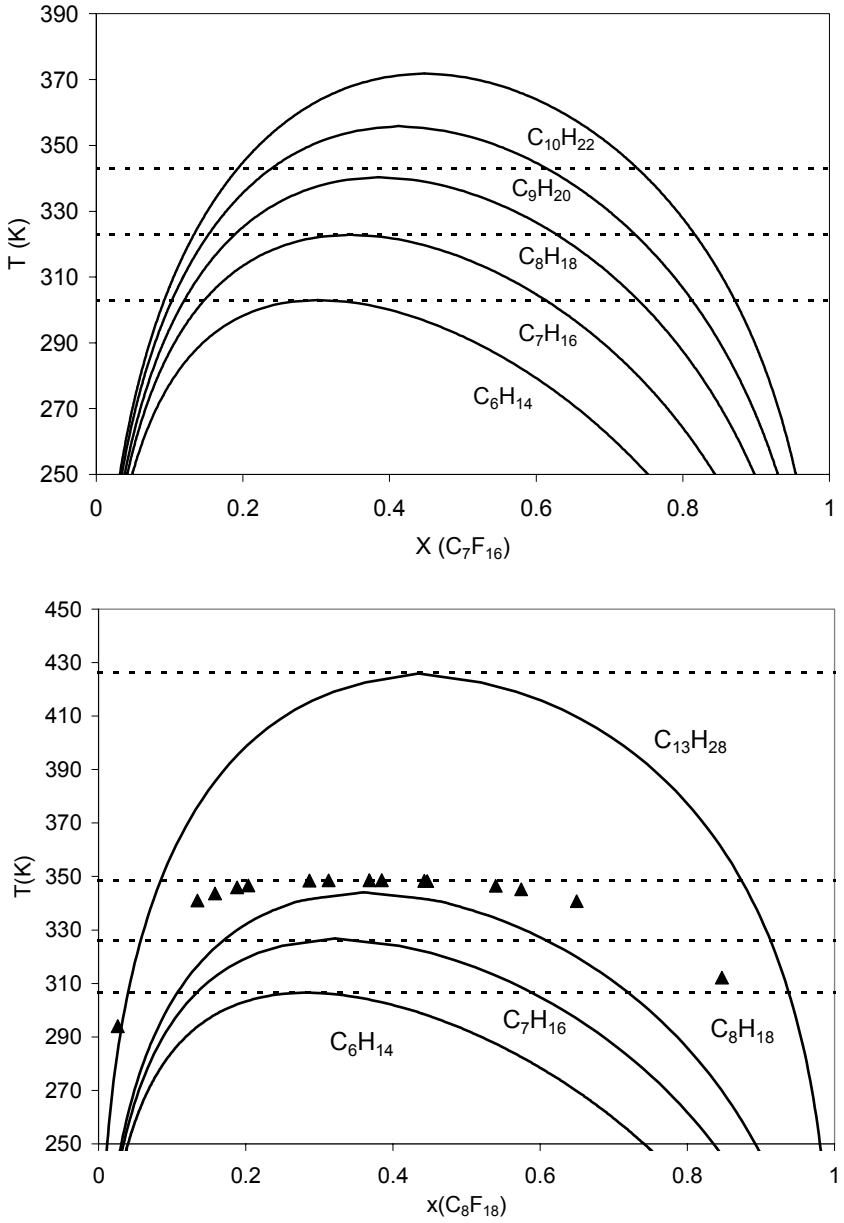

Figure 6.10. Liquid-liquid equilibrium for the (a) *n*-perfluoroheptane/*n*-C_nH_{2n+2} and (b) *n*-perfluorooctane/*n*-C_nH_{2n+2} binary mixtures compared with the SAFT-VR predictions, for n = 7 –13. Symbols represent the experimental data of (▲)Duce *et al*. [48] and dotted lines represent the upper critical solution temperature reported by Christou et al.[54] The theoretical predictions, obtained with ξ= 0.932 for all the cases, are shown by the continuous lines.

It is important to note, however, that different interaction parameters were obtained for $\xi_{alkane\text{-}perfluorohexane}$ and $\xi_{alkane\text{-}perfluoroheptane.}$ This is in contrast with our previous work [31]. In our previous work we reported a unique binary interaction parameter of 0.929 for both *n*-perfluoroalkanes. However, in the previous work [31] we only evaluated *n*-perfluoroheptane/*n*-alkane systems for VLE. As was shown in figure 3, this parameter has practically no influence on the VLE, but a strong influence on the LLE, and therefore the LLVE for ternary systems. It appears that to provide good predictions for the LLE and VLLE, for both binary and ternary systems, the predicted UCST for each *n*-perfluoroalkane with a given *n*-alkane (in the range studied in this work) should be adjusted. Thus, only one experimental mixture point (the UCST of a binary *n*-alkane/*n*-perfluoroalkane mixture) is needed to adjust the binary interaction parameter for each *n*-perfluoroalkane, and then it can be used in a transferable fashion. In table 2 are shown the binary interaction parameters used in this work.

In figures 6.11 and 6.12 ternary diagrams are shown for the systems CO_2/*n*-C_7F_{16}/*n*-C_nH_{2n+2} and CO_2/*n*-C_8F_{18}/*n*-$C_nH_{2n+2,}$ with n = 7-10 at 298.15 K, respectively. Selected equilibrium points are presented in tables 6.A3 and 6.A4 for the same systems. LLVE is present for all systems at these conditions. Similarly to figure 6.8, the theory predicts, as expected, that the liquid-liquid immiscibility region increases as the carbon number of the *n*-alkane chain increases. It can also be observed that the partition of the *n*-alkanes and *n*-perfluoroheptane or *n*-perfluorooctane decreases in the vapor phase as the *n*-alkane carbon number increases, until the vapor is almost pure carbon dioxide. Comparing figures 6.8, 6.11 and 6.12 it is clear that at constant temperature (298.15 K), and constant *n*-alkane (e.g. *n*-C_7H_{16}) the vapor composition shifts to the alkane-rich side of the triangular diagram, as the molecular weight of the *n*-perfluoroalkane increases. This is due to the fact that the *n*-perfluoroalkane chain is longer and then less soluble in the vapor phase. Similarly, it can be observed that the pressure necessary to achieve miscibility of the liquid phases almost doubles from *n*-C_6F_{14} to *n*-C_8F_{18} (when the alkane is *n*-C_7H_{16}).

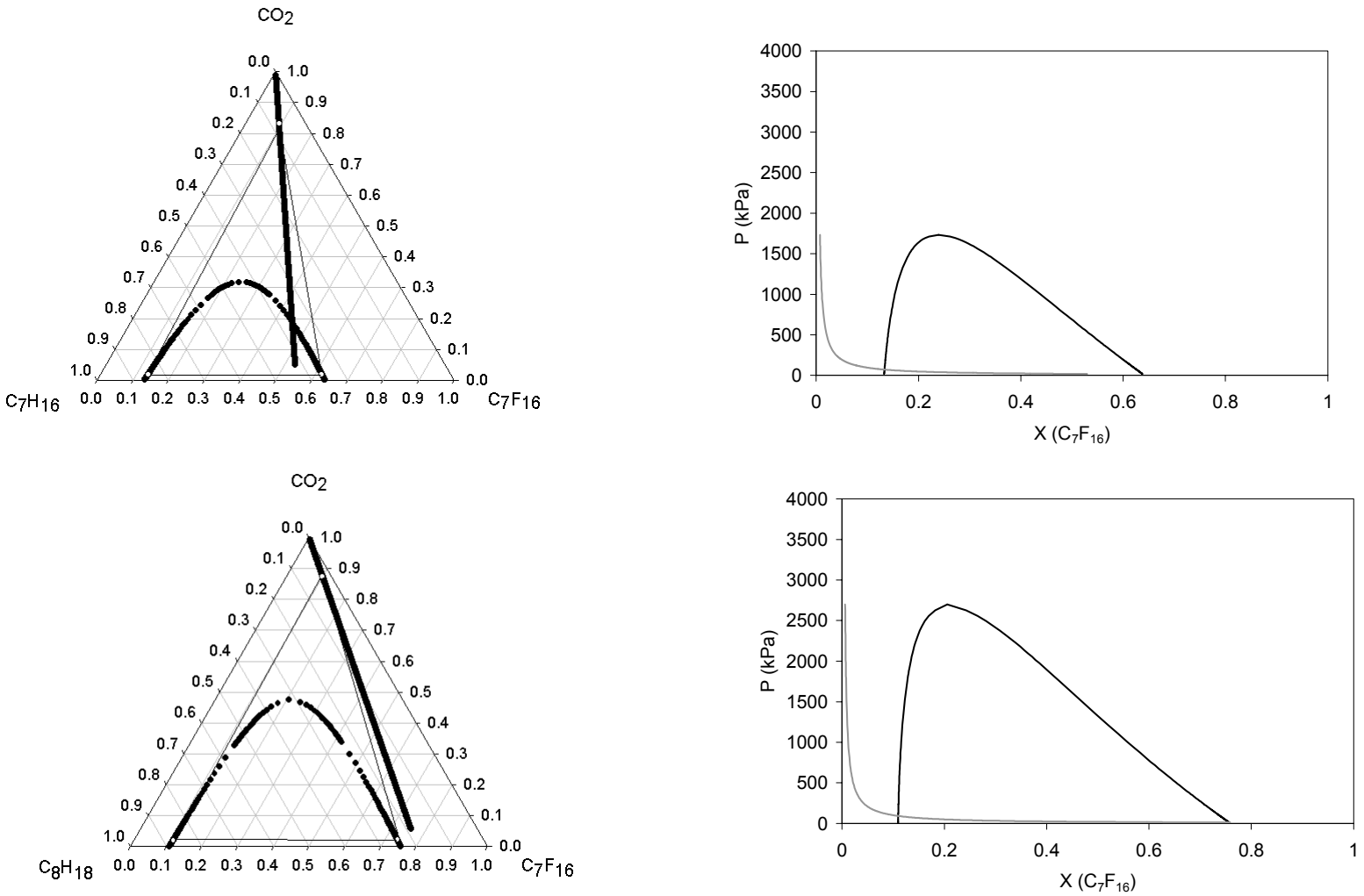

Figure 6.11. SAFT-VR predictions for the vapor-liquid-liquid equilibria (VLLE) for the system CO_2/*n*-perfluoroheptane/*n*-C_nH_{2n+2} at 298 K, for n = 7 – 10.

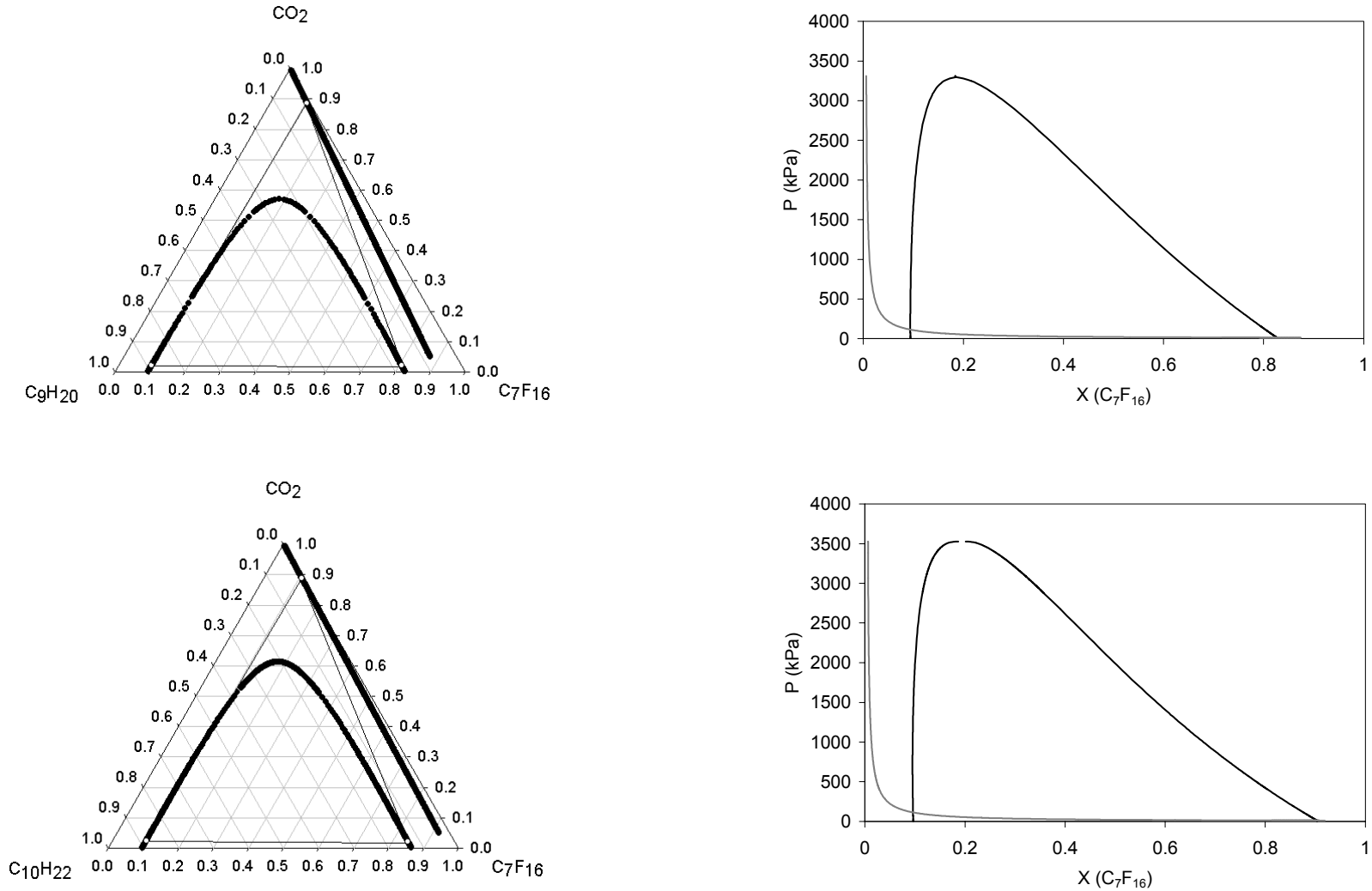

Figure 6.11 (Continued) SAFT-VR predictions for the vapor-liquid-liquid equilibria (VLLE) for the system CO_2/*n*-perfluoroheptane/*n*-C_nH_{2n+2} at 298 K, for n = 7 – 10.

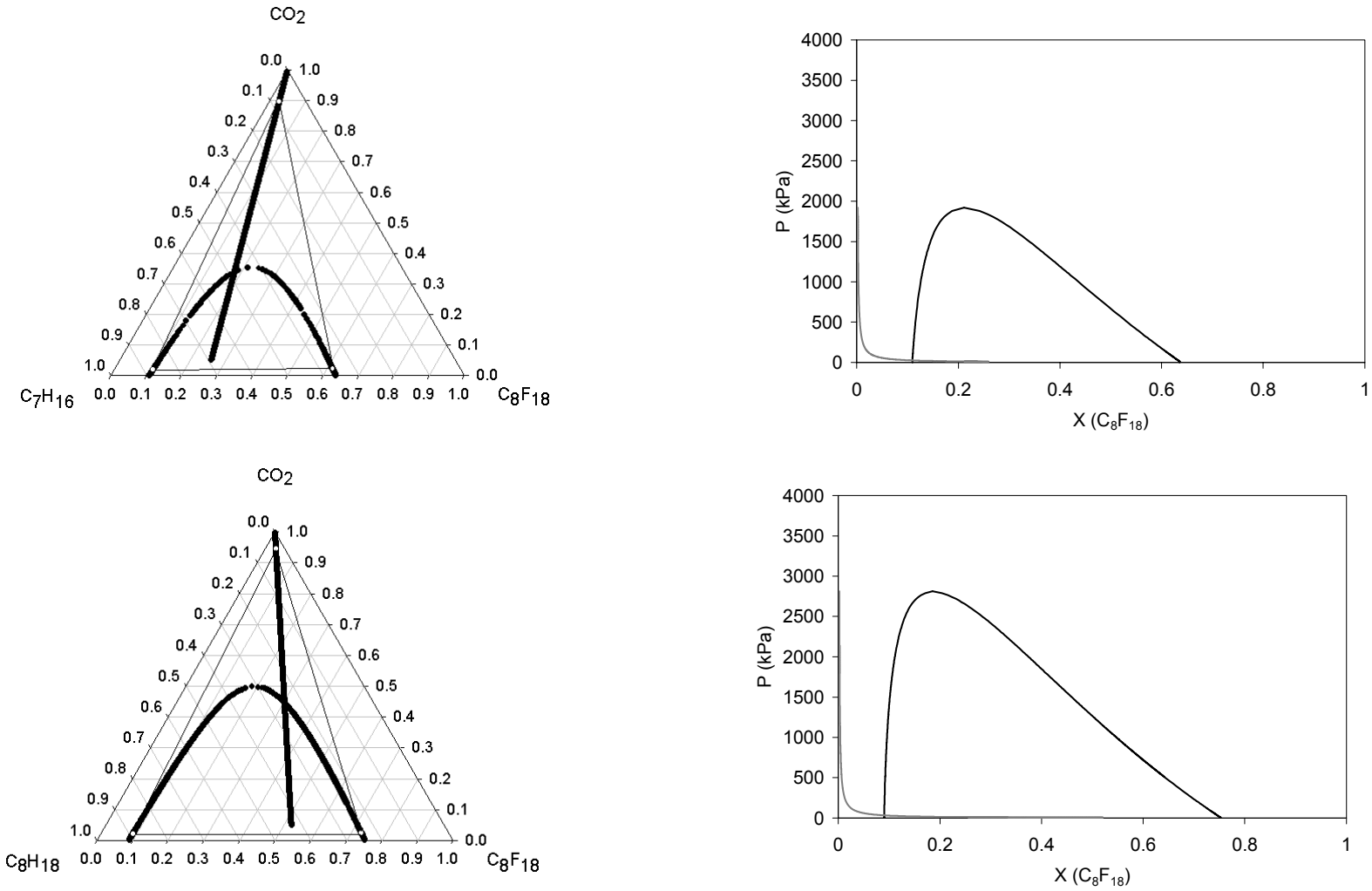

Figure 6.12. SAFT-VR predictions for the vapor-liquid-liquid equilibria (VLLE) for the system CO_2/*n*-perfluorooctane/*n*-C_nH_{2n+2} at 298 K, for n = 7 – 10.

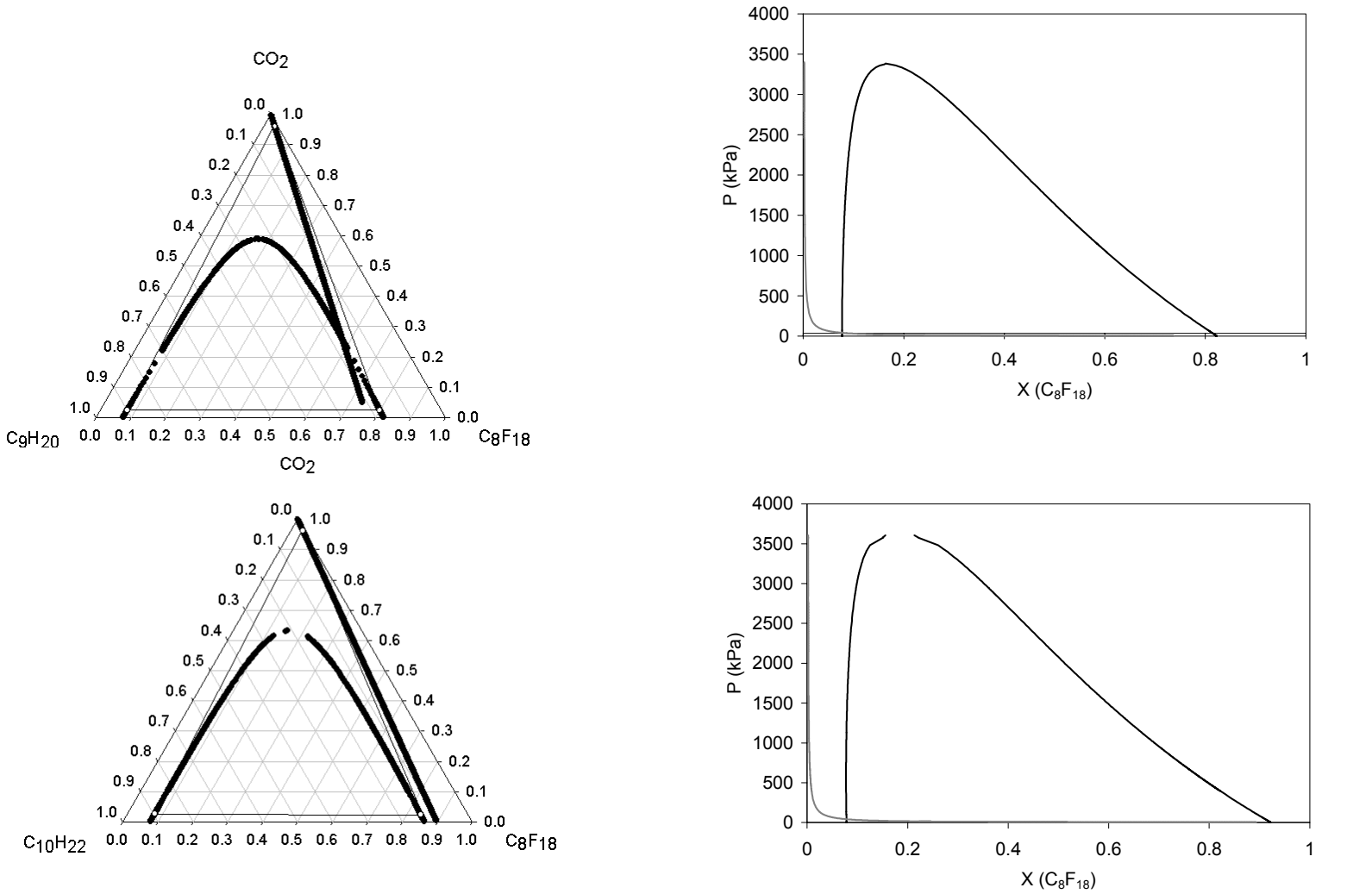

Figure 6.12 (Continued). SAFT-VR predictions for the vapor-liquid-liquid equilibria (VLLE) for the system CO_2/*n*-perfluorooctane/*n*-C_nH_{2n+2} at 298 K, for n = 7 – 10.

These ternary plots represent, to the best of our knowledge, the first available data for the *n*-perfluoroalkanes (*n*-C_6F_{14}, *n*-C_7F_{16}, *n*-C_8F_{18}), *n*-alkanes (*n*-C_6F_{14} to *n*-$C_{10}F_{22}$) and CO_2 systems. This information could be used to guide experiments.

6.5 Conclusions

In this work we presented vapor-liquid and vapor-liquid-liquid equilibria for ternary and several binary systems involving CO_2, *n*-alkanes, and *n*-perfluoroalkanes. We used for this purpose the SAFT-VR EOS, and studied the influence of temperature, pressure, composition and chain length on the phase diagram, and showed that when compared with the available experimental and molecular simulation data, the predicted phase diagrams should represent the expected phase equilibria behavior with good accuracy.

Our results show that it is possible to predict the overall phase behavior of different binary and ternary mixtures involving carbon dioxide, *n*-perfluoroalkanes and *n*-alkanes using transferable binary interaction parameters. Upper critical solution pressures for several *n*-alkane/*n*-perfluoroalkane systems are also provided. Moreover, the ternary diagrams presented in this work represent, to the best of our knowledge, the first available data for CO_2/*n*-perfluoroalkane/*n*-alkanes systems. The data provide in this work could be helpful in identifying possible new CO_2-philic groups as well as co-solvents for CO_2.

Acknowledgements

We would like to thank Amparo Galindo, J. Ilja Siepmann and Ling Zhang for helpful discussions. We also thank A. G. for providing the main routine of the SAFT-VR EOS. CMC thanks Valery Bondar, Francisco Hung and Erik Santiso for helpful comments. This work was supported by the STC Program of the National Science Foundation under Agreement No. CHE 9876674.

6.6 References

[1] Bleyl, J. U.; Ragaller, M.; Tscho, U.; Regner, M.; Hubler, M.; Kanzow, M.;. Vincent O; Albrecht, M. *Crit Care Med.,* 2002, 30, 1340.

[2] Riess, J.G. *Chemical Reviews*, 2001, 101, 2797.

[3] DuPont Zonyl. Fluorochemical Intermediates, 2001.

[4] Krafft, M. P. *Current Opinion in Colloid and Interface Science,* 2003, 8, 213.

[5] Jackson, G.; Chapman, W. G; Gubbins, K. E. *Mol. Phys*. 1988, 65, 1.

[6] Chapman, W. G.; Jackson, G; Gubbins, K. E. *Mol. Phys*. 1988, *65*, 1057.

[7] Wertheim, M. S., *J. Chem. Phys.* 1986, *85*, 2929.

[8] Wertheim, M. S., *J. Chem. Phys.* 1987, *87*, 7323.

[9] Huang, S.H. ; Radosz, M. *Ind. Eng. Chem. Res.* 1990, *29*, 2284.

[10] Carnahan, N. F.; Starling, K. E. *J. Chem. Phys*. 1969, *51*, 635.

[11] Chen, S. S.; Kreglewski, A. *Ber. Bunsen-Ges. Phys. Che*m. 1977, *81*, 1048.

[12] Müller, E. A. and K.E. Gubbins, in J.V.Sengers, R.F. Kayser, C.J. Peters and H. J. White, Jr. (Eds), Equations of State for Fluids and Fluid Mixtures. Experimental Thermodynamics, Volume 5, Elsevier, Amsterdam, 2000, pp 435-478.

[13] Müller, E. A.; Gubbins, K. E. *Ind. Eng. Chem. Res.* 2001, *40*, 2193.

[14] Wei, Y.S.; Sadus, R. *AIChE J.* 2000, *46*, 169.

[15] Economou, I. G. *Ind. Eng. Chem. Res.* 2002, *41*, 953.

[16] Blas, F. J.; Vega, L. F. *Ind. Eng. Chem. Res.* 1998, *3*7, 660.

[17] Blas, F. J.; Vega, L. F. *J. Chem. Phy*s. 1998, *10*9, 7405.

[18] Chapman, W. G. *J. Chem. Phys*, 93, 1990, 4299.

[19] Johnson, J. K.; Zollweg, J. A.; Gubbins, K. E., *Mol. Phys.* 1993, *7*8, 591.

[20] Dias, A. M. A.; Pamies, J. C.; Coutinho, J. A. P.; Marrucho, I. M; Vega, L.F. *J. Phys. Chem. B*, 2004, 108, 1450.

[21] Gross, J.; Sadoswki, G. *Ind. Eng. Chem. Res*. 2001, *40*, 1244.

[22] Barker, . J.A.; Henderson,D. *J. Chem. Phys*. 1967, *47*, 2856.

[23] Gross, J.; Sadoswki, G. *Fluid Phase Equilb.* 2002, *168*, 183.

[24] Gil-Villegas, A.; Galindo, A.; Whitehead, P. J.; Mills, S. L.; Jackson, G.; Burgess, A. N. *J. Chem. Phys.* 1997, 106, 4168.

[25] Galindo, A.; Davies, L.A.; Gil-Villegas, A; Jackson, G. *Molec. Phys.* 1998, 93, 241.

[26] Galindo, A.; Gil-Villegas, A.; Jackson, G.; Burgess, A.N. *J. Phys. Chem. B* 1999, 103, 10272.

[27] Galindo, A.; Gil-Villegas, A.; Whitehead, P. J.; Jackson, G.; Burgess., A.N. *J. Phys. Chem. B* 1998, 102, 7639.

[28] McCabe, C.; Jackson, G. *Phys. Chem. Chem. Phys*. 1999, 1, 2057.

[29] McCabe, C.; Galindo, A.; Garcia-Lisbona, M. N.; Jackson, *G. Ind. Eng. Chem. Res*. 2001, 40, 3835.

[30] McCabe, C.; Galindo, A.; Gil-Villegas, A; Jackson, G. *J. Phys. Chem. B* 1998, 102, 8060.

[31] Colina, C. M.; Galindo, A.; Blas, F. J.; Gubbins, K. E. *Fluid Phase Equilb.* 2004, in press.

[32] Galindo, A.; Blas, F. J. *J. Phys. Chem. B*. 2002, 106, 4503.

[33] Blas, F. J.; Galindo, A. *Fluid Phase Equilb* 2002, 194-197, 501.

[34] Percus, J. K.; Yevick, G. J. *Phys Rev.* 1958, 110, 1.

[35] Boublik, T. *J. Chem. Phys.* 1970, 53, 471.

[36] Press, W. H., Teukolsky, S.A., Vetterling, W.T. and B. P. Flannery, *Numerical Recipes in Fortran*, 1st ed., Cambridge University Press: Cambridge, U. K. 1986.

[37] Kreglewski, A. Bull.Acad. Pol. Sci., 1962, 10, 629.

[38] J.M. Prausnitz, R.N. Lichtenthaler and E. Gomez de Azevedo. Molecular Thermodynamics of Fluid-Phase Equilibria. Third Edition. Prentice Hall, New Jersey, 1999.

[39] Scott, R. L. and P. H. van Konynenburg, *Discuss. Faraday Soc*. 1970, 49, 87.

[40] Hicks, C. P. and C. L. Young, *Chem. Rev.* 75 (1975) 119-175.

[41] Wallas, S. "Phase Equilibria in Chemical Engineering", Butterworth Publishers, 1985.

[42] Francis, A. W. *J. Phys. Chem.* 1954, 58, 1099.

[43] Ohgaki K; Katayama, T. *J. Chem. Eng. Data* 1976, 21, 5355.

[44] Wagner, Z.; Witchterle, I. *Fluid Phase Equilib.* 1987, 33, 109.

[45] Li, Y-H ; Dillard, K.H.; Robinson, R.L. Jr. *J.Chem.Eng.Data* 1981, 26, 53.

[46] Kho, Y. W.; Conrad D. C.; Knutson, B. L. *Fluid Phase Equilib*. 2003, 206, 179.

[47] Iezzi, A.; Bendale, P.; Enick, R.; Turberg, M.; Brandy, J. *Fluid Phase Equilib*. 1989, 52, 307.

[48] Duce, C.;Tine, M. R.; Lepori, L.; Matteoli, E. *Fluid Phase Equilib.* 2002, 199, 197.

[49] Gaw, W. J.; Scott, R. L. *J. Chem. Thermod*. 1971, 3, 335.

[50] Dunlap, R. D.; Bedford, R. G.; Woodbrey, J. C.; Furrow, S. D. *J. Ame. Chem. Soc.* 1959, 81, 2927.

[51] Hicks, C. P.; Hurle, R. L.; Toczylkin, L. S.; Young, C. L. *Aust. J. Chem*. 1978, 31, 19.

[52] Bondar, V. Personal Communication, (2003).

[53] Zhang, L.; Siepmann, J. I. *J. Phys .Chem. B.* 2004, submitted for publication.

[54] Christou, G.; Morrow, T.; Sadus, R. J.; Young, C. L. *Fluid Phase Equilb*. 1986, 25, 263.

Table 6.A1. PTx equilibria points for the system CO_2/*n* C_6F_{14}/*n*-C_6H_{14} at 278.15 K as well as for the system CO_2/*n*-C_6F_{14}/*n*-C_7H_{16} at 278.15 K, 298.15 K and 308.15 K.

T = 278.15 K

$y(C_6F_{14})$	$y(C_6H_{14})$	$x^I(C_6F_{14})$	$x^I(C_6H_{14})$	$x^{II}(C_6F_{14})$	$x^{II}(C_6H_{14})$	P(kPa)
0.5305	0.4195	0.1614	0.8383	0.6032	0.3965	22.76
0.2434	0.1926	0.1622	0.8307	0.5957	0.3965	50.07
0.1630	0.1290	0.1630	0.8238	0.5889	0.3966	75.13
0.1217	0.0963	0.1639	0.8166	0.5819	0.3967	101.05
0.0821	0.0649	0.1656	0.8028	0.5684	0.3970	150.92
0.0620	0.0490	0.1674	0.7888	0.5548	0.3975	201.21
0.0419	0.0331	0.1716	0.7606	0.5275	0.3991	301.71
0.0318	0.0252	0.1764	0.7321	0.5002	0.4015	402.08
0.0257	0.0203	0.1822	0.7023	0.4716	0.4051	504.75
0.0218	0.0172	0.1890	0.6727	0.4436	0.4099	602.75
0.0190	0.0150	0.1974	0.6417	0.4144	0.4167	699.86
0.0167	0.0133	0.2096	0.6055	0.3804	0.4273	803.48
0.0150	0.0120	0.2279	0.5634	0.3411	0.4447	903.93
0.0139	0.0111	0.2710	0.4994	0.2810	0.4888	986.14

T = 278.15 K

$y(C_6F_{14})$	$y(C_7H_{16})$	$x^I(C_6F_{14})$	$x^I(C_7H_{16})$	$x^{II}(C_6F_{14})$	$x^{II}(C_7H_{16})$	P(kPa)
0.7874	0.1626	0.1257	0.8740	0.7530	0.2468	16.63
0.2648	0.0547	0.1260	0.8647	0.7440	0.2464	50.03
0.1321	0.0274	0.1264	0.8506	0.7304	0.2460	101.12
0.0675	0.0140	0.1273	0.8235	0.7043	0.2453	200.87
0.0455	0.0095	0.1283	0.7965	0.6783	0.2448	302.06
0.0281	0.0059	0.1309	0.7443	0.6280	0.2445	502.98
0.0206	0.0044	0.1343	0.6931	0.5787	0.2453	704.22
0.0165	0.0035	0.1389	0.6423	0.5297	0.2474	906.36
0.0136	0.0029	0.1459	0.5841	0.4735	0.2520	1135.41
0.0127	0.0028	0.1494	0.5610	0.4513	0.2547	1224.04
0.0119	0.0026	0.1543	0.5333	0.4245	0.2587	1327.84
0.0107	0.0023	0.1672	0.4779	0.3710	0.2701	1521.59
0.0102	0.0023	0.1748	0.4532	0.3471	0.2771	1599.34
0.0094	0.0021	0.2112	0.3758	0.2722	0.3132	1780.77

T = 298.15 K

$y(C_6F_{14})$	$y(C_7H_{16})$	$x^I(C_6F_{14})$	$x^I(C_7H_{16})$	$x^{II}(C_6F_{14})$	$x^{II}(C_7H_{16})$	P(kPa)
0.7640	0.1860	0.2025	0.7971	0.6353	0.3643	39.05
0.6000	0.1462	0.2027	0.7946	0.6329	0.3644	50.00
0.3004	0.0733	0.2039	0.7829	0.6215	0.3647	101.32
0.1547	0.0379	0.2064	0.7605	0.5998	0.3657	200.05
0.1046	0.0257	0.2092	0.7377	0.5779	0.3671	300.22
0.0795	0.0197	0.2125	0.7151	0.5560	0.3689	400.08
0.0645	0.0160	0.2162	0.6922	0.5339	0.3714	500.13
0.0544	0.0136	0.2205	0.6689	0.5115	0.3745	600.55
0.0473	0.0118	0.2256	0.6452	0.4886	0.3784	700.87
0.0420	0.0105	0.2316	0.6210	0.4653	0.3834	800.12
0.0378	0.0095	0.2391	0.5953	0.4406	0.3899	900.80
0.0345	0.0087	0.2487	0.5678	0.4141	0.3988	1000.22
0.0317	0.0081	0.2625	0.5358	0.3834	0.4120	1101.24
0.0290	0.0074	0.3113	0.4641	0.3113	0.4641	1225.33

T = 308.15 K

$y(C_6F_{14})$	$y(C_7H_{16})$	$x^I(C_6F_{14})$	$x^I(C_7H_{16})$	$x^{II}(C_6F_{14})$	$x^{II}(C_7H_{16})$	P(kPa)
0.7518	0.1982	0.2754	0.7240	0.5379	0.4615	56.80
0.5736	0.1514	0.2766	0.7195	0.5336	0.4624	75.06
0.4287	0.1133	0.2783	0.7130	0.5273	0.4637	101.26
0.2926	0.0774	0.2817	0.7006	0.5153	0.4664	150.01
0.2213	0.0587	0.2856	0.6876	0.5028	0.4696	200.04
0.1785	0.0475	0.2899	0.6742	0.4899	0.4733	249.86
0.1500	0.0400	0.2949	0.6603	0.4765	0.4776	299.46
0.1287	0.0343	0.3010	0.6449	0.4616	0.4831	351.77
0.1136	0.0304	0.3079	0.6292	0.4465	0.4895	401.01
0.1017	0.0273	0.3167	0.6116	0.4294	0.4978	450.81
0.0922	0.0248	0.3291	0.5904	0.4089	0.5097	500.52
0.0883	0.0237	0.3381	0.5771	0.3960	0.5186	524.62
0.0859	0.0231	0.3470	0.5654	0.3846	0.5274	540.22
0.0843	0.0227	0.3607	0.5497	0.3691	0.5412	551.15

Table 6.A2. PTx equilibria points for the system CO_2/*n*-C_6F_{14}/*n*-C_nH_{2n+2} at 298.15 K.

$y(C_6F_{14})$	$y(C_7H_{16})$	$x^I(C_6F_{14})$	$x^I(C_7H_{16})$	$x^{II}(C_6F_{14})$	$x^{II}(C_7H_{16})$	P(kPa)
0.7640	0.1860	0.2025	0.7971	0.6353	0.3643	39.05
0.3004	0.0733	0.2039	0.7829	0.6215	0.3647	101.32
0.1046	0.0257	0.2092	0.7377	0.5779	0.3671	300.22
0.0544	0.0136	0.2205	0.6689	0.5115	0.3745	600.55
0.0378	0.0095	0.2391	0.5953	0.4406	0.3899	900.80
0.0345	0.0087	0.2487	0.5678	0.4141	0.3988	1000.22
0.0317	0.0081	0.2625	0.5358	0.3834	0.4120	1101.24
0.0290	0.0074	0.3113	0.4641	0.3113	0.4641	1225.33

$y(C_6F_{14})$	$y(C_8H_{18})$	$x^I(C_6F_{14})$	$x^I(C_8H_{18})$	$x^{II}(C_6F_{14})$	$x^{II}(C_8H_{18})$	P(kPa)
0.8826	0.0674	0.1658	0.8338	0.7621	0.2375	36.03
0.3205	0.0246	0.1660	0.8190	0.7482	0.2373	101.32
0.1117	0.0087	0.1669	0.7755	0.7070	0.2368	300.13
0.0583	0.0046	0.1692	0.7127	0.6470	0.2372	600.66
0.0405	0.0033	0.1727	0.6525	0.5888	0.2391	901.67
0.0317	0.0027	0.1780	0.5945	0.5319	0.2428	1199.74
0.0264	0.0023	0.1860	0.5351	0.4731	0.2495	1504.48
0.0230	0.0020	0.1988	0.4734	0.4117	0.2612	1806.20
0.0205	0.0019	0.2247	0.4001	0.3383	0.2863	2107.66
0.0196	0.0018	0.2675	0.3345	0.2675	0.3345	2253.98

$y(C_6F_{14})$	$y(C_9H_{20})$	$x^I(C_6F_{14})$	$x^I(C_9H_{20})$	$x^{II}(C_6F_{14})$	$x^{II}(C_9H_{20})$	P(kPa)
0.9249	0.0251	0.1438	0.8558	0.8320	0.1676	35.76
0.3336	0.0091	0.1436	0.8401	0.8181	0.1674	101.31
0.1163	0.0033	0.1433	0.7944	0.7771	0.1668	300.10
0.0607	0.0018	0.1433	0.7298	0.7179	0.1665	600.88
0.0423	0.0013	0.1442	0.6697	0.6615	0.1670	900.93
0.0332	0.0010	0.1460	0.6128	0.6067	0.1682	1201.84
0.0277	0.0009	0.1488	0.5580	0.5528	0.1705	1504.81
0.0242	0.0008	0.1530	0.5059	0.5004	0.1741	1801.14
0.0216	0.0008	0.1594	0.4524	0.4455	0.1799	2106.20
0.0198	0.0007	0.1696	0.3970	0.3878	0.1894	2410.90
0.0184	0.0007	0.1881	0.3363	0.3239	0.2069	2705.28
0.0176	0.0007	0.2327	0.2635	0.2472	0.2497	2911.36

$y(C_6F_{14})$	$y(C_{10}H_{22})$	$x^I(C_6F_{14})$	$x^I(C_{10}H_{22})$	$x^{II}(C_6F_{14})$	$x^{II}(C_{10}H_{22})$	P(kPa)
0.9399	0.0101	0.1483	0.8512	0.8681	0.1315	36.04
0.6824	0.0073	0.1481	0.8476	0.8651	0.1315	50.00
0.3416	0.0037	0.1478	0.8343	0.8541	0.1314	101.32
0.1761	0.0019	0.1471	0.8094	0.8334	0.1312	200.10
0.1193	0.0013	0.1465	0.7850	0.8128	0.1311	300.05
0.0908	0.0010	0.1460	0.7614	0.7926	0.1310	400.27
0.0738	0.0008	0.1456	0.7387	0.7728	0.1310	500.07
0.0624	0.0007	0.1453	0.7165	0.7533	0.1310	600.22
0.0543	0.0006	0.1450	0.6951	0.7342	0.1311	700.40
0.0481	0.0006	0.1449	0.6739	0.7151	0.1312	801.76
0.0435	0.0005	0.1448	0.6538	0.6966	0.1314	900.85
0.0397	0.0005	0.1449	0.6339	0.6782	0.1317	1001.17
0.0366	0.0005	0.1450	0.6145	0.6600	0.1320	1101.58
0.0341	0.0004	0.1453	0.5953	0.6417	0.1325	1203.16
0.0320	0.0004	0.1456	0.5773	0.6244	0.1329	1300.42
0.0301	0.0004	0.1460	0.5586	0.6062	0.1335	1403.53
0.0285	0.0004	0.1466	0.5406	0.5885	0.1342	1504.51
0.0271	0.0004	0.1473	0.5228	0.5708	0.1350	1606.19
0.0259	0.0004	0.1481	0.5056	0.5535	0.1358	1705.56
0.0249	0.0003	0.1491	0.4880	0.5355	0.1369	1808.82
0.0240	0.0003	0.1502	0.4719	0.5190	0.1379	1903.76
0.0231	0.0003	0.1516	0.4541	0.5005	0.1393	2010.02
0.0224	0.0003	0.1531	0.4388	0.4844	0.1407	2101.94
0.0217	0.0003	0.1549	0.4219	0.4664	0.1424	2203.51
0.0211	0.0003	0.1568	0.4059	0.4493	0.1442	2299.52
0.0205	0.0003	0.1594	0.3881	0.4301	0.1466	2405.22
0.0200	0.0003	0.1622	0.3717	0.4122	0.1491	2501.91
0.0195	0.0003	0.1658	0.3534	0.3921	0.1524	2607.65
0.0191	0.0003	0.1696	0.3370	0.3739	0.1558	2699.72
0.0187	0.0003	0.1746	0.3186	0.3533	0.1604	2799.34
0.0183	0.0003	0.1819	0.2971	0.3291	0.1669	2907.49
0.0179	0.0003	0.1937	0.2703	0.2988	0.1774	3025.26
0.0176	0.0003	0.2119	0.2410	0.2655	0.1936	3120.59
0.0175	0.0003	0.2309	0.2196	0.2412	0.2105	3153.80

Table 6.A3. PTx equilibria points for the system CO_2/*n*-C_7F_{16}/*n*-C_nH_{2n+2} at 298.15 K.

$y(C_7F_{16})$	$y(C_7H_{16})$	$x^I(C_7F_{16})$	$x^I(C_7H_{16})$	$x^{II}(C_7F_{16})$	$x^{II}(C_7H_{16})$	P(kPa)
0.5295	0.4205	0.1329	0.8669	0.6376	0.3622	17.56
0.1879	0.1491	0.1333	0.8598	0.6305	0.3617	50.12
0.0937	0.0743	0.1340	0.8486	0.6195	0.3609	101.61
0.0329	0.0261	0.1369	0.8062	0.5779	0.3587	299.77
0.0173	0.0137	0.1426	0.7429	0.5169	0.3575	601.64
0.0117	0.0093	0.1519	0.6716	0.4493	0.3603	943.88
0.0095	0.0075	0.1634	0.6103	0.3923	0.3675	1226.90
0.0089	0.0071	0.1690	0.5872	0.3710	0.3719	1327.57
0.0078	0.0061	0.1949	0.5122	0.3025	0.3960	1608.29
0.0074	0.0058	0.2392	0.4434	0.2392	0.4434	1732.48

$y(C_7F_{16})$	$y(C_8H_{18})$	$x^I(C_7F_{16})$	$x^I(C_8H_{18})$	$x^{II}(C_7F_{16})$	$x^{II}(C_8H_{18})$	P(kPa)
0.7582	0.1868	0.1097	0.8901	0.7565	0.2433	13.14
0.1010	0.0250	0.1100	0.8703	0.7370	0.2420	101.02
0.0352	0.0088	0.1107	0.8267	0.6943	0.2395	300.55
0.0184	0.0046	0.1124	0.7628	0.6321	0.2367	609.92
0.0128	0.0032	0.1150	0.6996	0.5708	0.2352	933.51
0.0104	0.0026	0.1181	0.6470	0.5200	0.2352	1214.14
0.0087	0.0023	0.1229	0.5896	0.4648	0.2369	1527.32
0.0078	0.0020	0.1291	0.5365	0.4138	0.2408	1817.73
0.0070	0.0019	0.1393	0.4764	0.3563	0.2490	2135.08
0.0065	0.0018	0.1563	0.4128	0.2959	0.2651	2433.70
0.0064	0.0017	0.1694	0.3799	0.2649	0.2785	2558.22
0.0062	0.0017	0.2055	0.3200	0.2055	0.3200	2700.33

$y(C_7F_{16})$	$y(C_9H_{20})$	$x^I(C_7F_{16})$	$x^I(C_9H_{20})$	$x^{II}(C_7F_{16})$	$x^{II}(C_9H_{20})$	P(kPa)
0.8740	0.0760	0.0941	0.9058	0.8267	0.1732	11.91
0.1048	0.0092	0.0940	0.8840	0.8062	0.1722	101.77
0.0368	0.0032	0.0940	0.8377	0.7626	0.1704	301.52
0.0193	0.0017	0.0944	0.7711	0.6996	0.1682	609.83
0.0137	0.0013	0.0953	0.7120	0.6433	0.1668	905.10
0.0110	0.0010	0.0966	0.6564	0.5899	0.1661	1200.59
0.0093	0.0009	0.0987	0.6026	0.5378	0.1662	1502.09
0.0082	0.0008	0.1016	0.5485	0.4851	0.1674	1817.07
0.0075	0.0007	0.1057	0.4962	0.4337	0.1699	2129.29
0.0070	0.0007	0.1107	0.4505	0.3884	0.1736	2402.77
0.0066	0.0007	0.1188	0.3992	0.3373	0.1805	2700.52
0.0063	0.0007	0.1330	0.3410	0.2792	0.1938	3006.38
0.0062	0.0007	0.1525	0.2927	0.2310	0.2132	3204.12
0.0061	0.0007	0.1837	0.2458	0.1837	0.2458	3311.17

$y(C_7F_{16})$	$y(C_{10}H_{22})$	$x^I(C_7F_{16})$	$x^I(C_{10}H_{22})$	$x^{II}(C_7F_{16})$	$x^{II}(C_{10}H_{22})$	P(kPa)
0.9186	0.0314	0.0964	0.9034	0.8651	0.1347	11.64
0.4303	0.0147	0.0964	0.8998	0.8620	0.1346	25.03
0.2166	0.0074	0.0963	0.8931	0.8561	0.1344	50.07
0.1083	0.0037	0.0961	0.8795	0.8443	0.1341	101.24
0.0561	0.0019	0.0958	0.8543	0.8222	0.1334	199.30
0.0377	0.0013	0.0955	0.8287	0.7996	0.1328	302.39
0.0290	0.0010	0.0953	0.8052	0.7786	0.1322	400.71
0.0237	0.0008	0.0952	0.7821	0.7579	0.1317	500.30
0.0201	0.0007	0.0951	0.7595	0.7374	0.1313	601.11
0.0176	0.0006	0.0951	0.7378	0.7177	0.1309	700.63
0.0156	0.0006	0.0951	0.7162	0.6978	0.1306	803.38
0.0142	0.0005	0.0952	0.6957	0.6789	0.1304	903.23
0.0130	0.0005	0.0953	0.6756	0.6602	0.1302	1003.58
0.0120	0.0005	0.0955	0.6555	0.6414	0.1300	1106.73
0.0113	0.0004	0.0958	0.6365	0.6235	0.1300	1206.71
0.0106	0.0004	0.0961	0.6171	0.6051	0.1300	1311.26
0.0100	0.0004	0.0965	0.5978	0.5867	0.1300	1417.59
0.0095	0.0004	0.0970	0.5794	0.5689	0.1302	1521.59
0.0091	0.0004	0.0975	0.5626	0.5527	0.1304	1617.66
0.0088	0.0004	0.0980	0.5487	0.5391	0.1306	1699.06
0.0085	0.0003	0.0988	0.5277	0.5185	0.1311	1823.19
0.0082	0.0003	0.0997	0.5098	0.5008	0.1316	1930.98
0.0080	0.0003	0.1004	0.4966	0.4876	0.1320	2011.59
0.0078	0.0003	0.1013	0.4821	0.4731	0.1326	2100.72
0.0076	0.0003	0.1024	0.4661	0.4570	0.1334	2200.13
0.0074	0.0003	0.1038	0.4481	0.4388	0.1344	2312.19
0.0072	0.0003	0.1056	0.4277	0.4180	0.1358	2440.26
0.0071	0.0003	0.1068	0.4163	0.4063	0.1367	2511.75
0.0069	0.0003	0.1099	0.3904	0.3795	0.1392	2673.94
0.0068	0.0003	0.1120	0.3754	0.3639	0.1410	2767.15
0.0067	0.0003	0.1148	0.3584	0.3461	0.1433	2870.81
0.0067	0.0003	0.1157	0.3535	0.3408	0.1441	2900.90
0.0066	0.0003	0.1189	0.3368	0.3232	0.1469	3000.11
0.0065	0.0003	0.1230	0.3191	0.3044	0.1505	3101.36
0.0064	0.0003	0.1280	0.3008	0.2850	0.1550	3200.89
0.0064	0.0003	0.1346	0.2811	0.2639	0.1609	3300.12
0.0063	0.0003	0.1443	0.2581	0.2392	0.1699	3401.36
0.0063	0.0003	0.1512	0.2451	0.2252	0.1762	3449.12
0.0063	0.0003	0.1636	0.2262	0.2049	0.1878	3501.48
0.0063	0.0003	0.1865	0.2013	0.1865	0.2013	3527.73

Table 6.A4. PTx equilibria points for the system CO_2/*n*-C_8F_{18}/*n*-C_nH_{2n+2} at 298.15 K

$y(C_8F_{18})$	$y(C_7H_{16})$	$x^I(C_8F_{18})$	$x^I(C_7H_{16})$	$x^{II}(C_8F_{18})$	$x^{II}(C_7H_{16})$	P(kPa)
0.2593	0.6907	0.1094	0.8905	0.6358	0.3641	10.76
0.0563	0.1497	0.1098	0.8819	0.6270	0.3631	50.22
0.0282	0.0748	0.1104	0.8709	0.6157	0.3618	101.44
0.0099	0.0261	0.1127	0.8287	0.5733	0.3577	301.06
0.0053	0.0137	0.1173	0.7665	0.5124	0.3537	603.18
0.0037	0.0093	0.1243	0.6984	0.4479	0.3528	939.11
0.0030	0.0077	0.1319	0.6450	0.3987	0.3555	1199.24
0.0026	0.0064	0.1460	0.5759	0.3365	0.3652	1516.47
0.0023	0.0057	0.1722	0.4984	0.2682	0.3904	1806.36
0.0022	0.0055	0.2114	0.4354	0.2114	0.4354	1919.34

$y(C_8F_{18})$	$y(C_8H_{18})$	$x^I(C_8F_{18})$	$x^I(C_8H_{18})$	$x^{II}(C_8F_{18})$	$x^{II}(C_8H_{18})$	P(kPa)
0.0302	0.0248	0.0905	0.8879	0.7299	0.2455	101.82
0.0104	0.0086	0.0913	0.8428	0.6840	0.2418	308.17
0.0057	0.0047	0.0927	0.7825	0.6236	0.2377	600.11
0.0041	0.0033	0.0948	0.7237	0.5657	0.2348	900.70
0.0033	0.0027	0.0977	0.6674	0.5112	0.2334	1201.07
0.0028	0.0023	0.1015	0.6126	0.4588	0.2335	1502.82
0.0025	0.0020	0.1068	0.5581	0.4075	0.2358	1805.08
0.0023	0.0019	0.1143	0.5028	0.3559	0.2410	2107.02
0.0022	0.0018	0.1265	0.4425	0.3004	0.2519	2414.24
0.0021	0.0017	0.1533	0.3662	0.2311	0.2798	2719.55
0.0021	0.0017	0.1574	0.3583	0.2240	0.2843	2741.77
0.0021	0.0017	0.1857	0.3160	0.1857	0.3160	2812.48

$y(C_8F_{18})$	$y(C_9H_{20})$	$x^I(C_8F_{18})$	$x^I(C_9H_{20})$	$x^{II}(C_8F_{18})$	$x^{II}(C_9H_{20})$	P(kPa)
0.7368	0.2132	0.0772	0.9228	0.8223	0.1777	4.25
0.0318	0.0092	0.0772	0.8991	0.7987	0.1762	101.15
0.0108	0.0032	0.0773	0.8503	0.7505	0.1734	310.77
0.0046	0.0014	0.0784	0.7436	0.6459	0.1686	816.45
0.0035	0.0010	0.0801	0.6706	0.5751	0.1665	1199.68
0.0030	0.0009	0.0820	0.6170	0.5233	0.1659	1499.67
0.0027	0.0008	0.0845	0.5656	0.4737	0.1663	1799.03
0.0025	0.0007	0.0880	0.5149	0.4249	0.1678	2102.13
0.0023	0.0007	0.0931	0.4622	0.3743	0.1712	2419.49
0.0022	0.0007	0.1001	0.4117	0.3258	0.1770	2716.05
0.0022	0.0007	0.1111	0.3587	0.2749	0.1873	3004.45
0.0021	0.0007	0.1370	0.2883	0.2076	0.2138	3301.52
0.0021	0.0007	0.1614	0.2518	0.1730	0.2396	3373.04
0.0021	0.0007	0.1683	0.2408	0.1683	0.2408	3402.57

$y(C_8F_{18})$	$y(C_{10}H_{22})$	$x^I(C_8F_{18})$	$x^I(C_{10}H_{22})$	$x^{II}(C_8F_{18})$	$x^{II}(C_{10}H_{22})$	P(kPa)
0.8937	0.1013	0.0782	0.9218	0.8632	0.1368	3.60
0.1293	0.0147	0.0782	0.9159	0.8577	0.1366	25.16
0.0647	0.0073	0.0781	0.9090	0.8513	0.1363	50.62
0.0440	0.0050	0.0781	0.9025	0.8453	0.1361	74.79
0.0323	0.0037	0.0780	0.8952	0.8385	0.1358	102.47
0.0162	0.0018	0.0778	0.8673	0.8127	0.1347	210.10
0.0108	0.0012	0.0776	0.8391	0.7864	0.1337	323.60
0.0089	0.0010	0.0775	0.8207	0.7693	0.1331	400.17
0.0072	0.0008	0.0775	0.7974	0.7474	0.1323	500.42
0.0062	0.0007	0.0775	0.7746	0.7261	0.1316	600.94
0.0054	0.0006	0.0775	0.7528	0.7056	0.1310	700.83
0.0049	0.0006	0.0776	0.7314	0.6855	0.1305	801.38
0.0044	0.0005	0.0777	0.7109	0.6662	0.1300	900.55
0.0041	0.0005	0.0779	0.6904	0.6469	0.1296	1002.25
0.0038	0.0005	0.0781	0.6709	0.6283	0.1292	1102.22
0.0036	0.0004	0.0784	0.6514	0.6098	0.1290	1204.18
0.0034	0.0004	0.0787	0.6329	0.5923	0.1288	1302.85
0.0032	0.0004	0.0791	0.6147	0.5748	0.1286	1402.93
0.0031	0.0004	0.0796	0.5972	0.5580	0.1286	1500.66
0.0030	0.0004	0.0801	0.5799	0.5414	0.1286	1599.09
0.0028	0.0004	0.0807	0.5617	0.5239	0.1287	1704.69
0.0028	0.0003	0.0813	0.5444	0.5071	0.1289	1806.77
0.0027	0.0003	0.0820	0.5287	0.4920	0.1291	1900.37
0.0026	0.0003	0.0829	0.5111	0.4748	0.1295	2007.80
0.0026	0.0003	0.0837	0.4960	0.4601	0.1299	2100.10
0.0025	0.0003	0.0847	0.4790	0.4434	0.1305	2205.67
0.0025	0.0003	0.0859	0.4628	0.4275	0.1312	2307.04
0.0024	0.0003	0.0870	0.4480	0.4129	0.1320	2399.90
0.0024	0.0003	0.0885	0.4311	0.3961	0.1331	2507.01
0.0024	0.0003	0.0900	0.4163	0.3814	0.1342	2600.22
0.0023	0.0003	0.0920	0.3990	0.3641	0.1357	2709.34
0.0023	0.0003	0.0948	0.3775	0.3426	0.1380	2842.97
0.0023	0.0003	0.0962	0.3680	0.3330	0.1392	2901.43
0.0023	0.0003	0.0990	0.3516	0.3165	0.1416	3000.94
0.0023	0.0003	0.1023	0.3345	0.2991	0.1445	3102.03
0.0022	0.0003	0.1063	0.3167	0.2810	0.1481	3203.22
0.0022	0.0003	0.1111	0.2987	0.2626	0.1525	3300.28
0.0022	0.0003	0.1181	0.2773	0.2406	0.1591	3406.18
0.0022	0.0003	0.1508	0.2215	0.1509	0.2214	3575.02
0.0022	0.0003	0.1556	0.2132	0.1557	0.2132	3603.40

Chapter 7

Phase Behavior of PVAC-PTAN Block Copolymer in Supercritical Carbon Dioxide using SAFT*

Coray M. Colina, Carol K. Hall and Keith E. Gubbins

Department of Chemical Engineering
North Carolina State University, Raleigh, NC 27695

7.1 Abstract

Statistical Associating Fluid Theory (SAFT) is an equation of state that can be used to calculate the phase behavior of mixtures comprised of components that exhibit wide disparities in molecular size, such as solvent-polymer mixtures. In this paper we model the phase behavior of a PVAC-PTAN block copolymer composed of a CO_2-phobic polyvinyl acetate (PVAC) and a CO_2-philic poly(1,1,2,2-tetrahydroperfluorooctyl acrylate) (PTAN) in supercritical carbon dioxide ($scCO_2$) using SAFT. SAFT is a molecular-based equation that is designed to account for effects of molecular association, chain flexibility, repulsive and dispersion interactions. The group contribution approach of Lora et al. was used to obtain the physical SAFT parameters for PVAC and PTAN polymers. PTAN was modeled as a non-associating polymer while PVAC was modeled with two association sites per molecule. Cloud curves of PVAC-CO_2, PTAN-CO_2 and of the PVAC-b-PTAN/CO_2 system were predicted, and good agreement was obtained with the experimental data available. Additionally, critical micellar densities (CMD) appear to be successfully predicted for the PVAC-b-PTAN/CO_2 system using a criteria based in the variation of osmotic pressure with surfactant concentration. This was made possible by the ability of SAFT to handle long chain and association interactions.

* *Fluid Phase Equilb.* **194-197**, 553-565 (2002)

7.2 Introduction

The development of amphiphilic molecules for use as surfactants in supercritical CO_2 and other supercritical fluids has led to the study of micellar and microemulsion phases in supercritical fluid media. Diblock copolymers are often used for this purpose since they can self-assemble into micelles when placed in supercritical carbon dioxide [1]. If one of the two blocks is highly CO_2-philic and the other less so, at high pressure the entire copolymer should be soluble. By decreasing the pressure, and hence the CO_2 concentration, the copolymer should then show a tendency to aggregate, forming structures similar to aqueous micelles with the CO_2-phobic segments in the core. In short, it is expected that as the pressure is lowered the copolymer will aggregate, so that a monomer-aggregate equilibrium will exist below a certain pressure determined by the polymer structure [2]. This monomer-aggregate transition occurs at the *critical micellar density* (CMD), i.e., the density of the solvent at which a sharp, reversible monomer-aggregate transition occurs [3].

The study of copolymer-solvent systems would be greatly facilitated if it were possible to simulate different process scenarios with an accurate equation of state. Models or correlations developed for this purpose should be able to predict the changes in phase behavior observed as a function of solvent quality or as a function of polymer architecture with a minimum number of fitted parameters [4]. An appealing approach to take is to use the SAFT [5] equation based on a resumed perturbation series due to Wertheim, which accounts for association between molecules in addition to dispersion and repulsive interactions. Furthermore, SAFT can account for chain effects and is applicable to polymer molecules. The SAFT equation has proved to be a significant improvement over more empirical equations of state because it has a firm basis in statistical mechanics. In particular, chain and association effects are explicitly accounted for, which means that associating and chain-molecule fluids can be modeled successfully. Such calculations are typically eight or nine orders of magnitude cheaper, and about six orders of magnitude faster, than an experimental phase-equilibrium measurement for a binary mixture [6]. Recently Müller and Gubbins [7,8] presented reviews of the SAFT EOS and related approaches. Despite many theoretical

improvements, one of the most successful modifications remains the Huang-Radosz [9] version of the SAFT equation (SAFT-HR).

In this paper we model the phase behavior of a PVAC-PTAN block copolymer composed of a CO_2-phobic polyvinyl acetate (PVAC) and a CO_2-philic poly(1,1,2,2-tetrahydroperfluorooctyl acrylate) (PTAN) section in $scCO_2$ with the Statistical Associating Fluid Theory. We used the widely applied original version of SAFT due to Huang and Radosz. Although several modifications of this model are available [10,11,12] for copolymers, we have used the "original" (and simpler) HR version because our purpose is to determine if SAFT is capable of predicting the phase behavior and the critical micellar density of a co-polymer/supercritical fluid mixture.

7.3 Model

In SAFT, molecules are modeled as chains of covalently bonded spheres. Homologous series, such as *n*-alkanes and polymers, can be modeled as chains of identical spheres, where the number of spheres in the chain is proportional to the molecular weight. In SAFT, the residual Helmholtz energy, a^{res}, is of the form

$$a^{res} = a^{seg} + a^{chain} + a^{assoc} \tag{7.1}$$

where a^{seg} is the part of the Helmholtz energy due to segment-segment interaction (interactions between monomer units in different molecules, usually modeled as hard sphere, LJ or square-well interactions), a^{chain} is the additional Helmholtz energy due to chain formation, and a^{assoc} is that due to association, e.g. hydrogen bonding, between different molecules.

A detailed discussion of the mathematical form of the SAFT equation can be found elsewhere [9] and is not reproduced here. For mixtures, the dispersion part of the segment

Helmholtz energy is the only place requiring the use of mixing rules; the composition dependence is built into the chain and association terms by statistical thermodynamics.

7.3.1 Parameters for pure components

The first step in the application of the SAFT equation of state to multicomponent mixtures is to determine the pure component parameters. There are five pure-component parameters in the equation. The first parameter is the number of hard spheres *m* that forms a molecule, and this is treated as an adjustable parameter. The second parameter is the volume of a mole of these spheres when closely packed, v^{00}; this sets their size. The third pure-component parameter is the segment energy u^0, which determines segment-segment interactions. In addition to these three parameters for nonassociating molecules, the equation has two association parameters, ε^{AA} and κ^{AA}. The parameter ε^{AA} characterizes the association energy and the parameter κ^{AA} characterizes the association volume for association site A.

Supercritical Carbon Dioxide

Due to its structural symmetry, CO_2 does not have a dipole moment, but it does have a substantial quadrupole moment that operates over a much shorter distance than dipolar interactions. Despite this, it is normally assumed that CO_2 exhibits dispersive attractions only, which means that just three parameters (m, v^{00}, u^0) need to be determined with the SAFT-HR EOS. These parameters were first determined by fitting experimental data for vapor pressure and liquid molar volume data [9], but it is now known that the resulting prediction around the critical point is not good. Because solubility data on the polymers at temperatures close to the critical temperature of CO_2 has been measured, the model used must give a good representation of the critical point of CO_2, as is discussed elsewhere [13,14].

Takishima *et al*. [13] re-determined pure CO_2 parameters by regressing saturated vapor pressures, saturated liquid densities and the critical properties. With these parameters the

resulting SAFT prediction for critical properties were T_c=306.3 K, P_c = 7.88 MPa and ρ_c=10.7 mol/l (471.014 kg/m^3). These are close to the experimental values [15] (T_c = 304.128 ± 0.015 K, P_c= 7.3773 ± 0.0030 MPa, ρ_c=467.6 ± 0.6 kg/m^3). This set of parameters was used in this work.

Polymer parameters

Since high molecular weight polymers have no detectable vapor pressure and since they thermally degrade before exhibiting a critical point, EOS parameters for polymers are generally determined using measured pure liquid molar volume data. Unfortunately with SAFT-HR, it is known that a regression of polymer parameters from this type of data generally leads to incorrect phase equilibrium calculations [4,13]; when parameters are determined from such restricted data, a variety of pure component parameter sets will fit the data.

Huang and Radosz in their original work [9] proposed v^{00} = 12 ml/mol and u^0/k = 210 K for polymers, and estimated the segment number parameter from the n-alkane corollary:

$$\boldsymbol{m} = 0.05096\, \boldsymbol{M_n} \tag{7.2}$$

where M_n stands for the number average polymer molecular weight*. This number average molecular weight is the sum of all the molecular weights of the individual molecules present in a sample divided by their total number, that is $\boldsymbol{M_n} = \sum \boldsymbol{N_i M_i} / \sum \boldsymbol{N_i}$. This approach should be reasonable for predicting polyolefin-supercritical solvents phase behavior because it is based on the values of an infinite molecular weight alkane [4].

* Although in the original publication and some later works, Radosz and co-workers used the weight average molecular weight ($\boldsymbol{M_w} = \sum \boldsymbol{N_i M_i^2} / \sum \boldsymbol{N_i M_i}$),they were working with nearly monodisperse polymers in those cases.

An alternative approach to obtaining the polymer parameters is to regress a pure component parameter for the polymer from the binary phase equilibria data [4,13,16,17]. The polymer-SCF solvent cloud-point curve could be used to obtain a value for u^o/k. A third alternative based on a combination of these two approaches, was proposed by Lora et al. [16]. They extended the group contribution approach of Huang and Radosz for calculating m and v^{00} for acrylate polymers as a function of the values for a repeat unit, with m being corrected for the size of the polymer according to the number average molecular weight.

Even though the polymers are polydisperse in all of these approaches, the calculations are performed taking a "monodisperse" molecular weight equal to M_n. However, it is possible to model the polymer as a mixture of pseudo-components if the data for the molecular weight fractions of the polymer are available (see for example ref. [18]).

7.3.2 Binary Mixtures

The extension to multicomponent mixtures is straightforward with the SAFT EOS since the three reference terms can be extended to mixtures based on rigorous statistical mechanics. Mixing rules are only required for the dispersion term in the SAFT EOS.

Mixing Rules

One of the more useful mixing rules is based on the van der Waals one-fluid theory (vdW1); this is often referred to as the vdW1 mixing rule. There are only two parameters in the dispersion term that require mixing rules [19], u/k and m,

$$\frac{u}{kT} = \frac{\sum_i \sum_j x_i x_j m_i m_j \left[\frac{u_{ij}}{kT}\right] \left(v^o\right)_{ij}}{\sum_i \sum_j x_i x_j m_i m_j \left(v^o\right)_{ij}} \tag{7.3}$$

where

$$\left(v^o\right)_{ij} = \left[\frac{1}{2}\left[\left(v^o\right)_i^{1/3} + \left(v^o\right)_j^{1/3}\right]\right]^3 \tag{7.4}$$

$$u_{ij} = \left(1 - k_{ij}\right)\left(u_{ii}u_{jj}\right)^{1/2} \tag{7.5}$$

and

$$m = \sum_i \sum_j x_i x_j \left(\frac{1}{2}\left(m_i + m_j\right)\right) \tag{7.6}$$

An alternative mixing rule is the so-called "volume-fraction" mixing rule,

$$\frac{u}{kT} = \sum_i \sum_j f_i f_j \left[\frac{u_{ij}}{kT}\right] \tag{7.7}$$

where f_i is the volume fraction of component i

$$f_i = \frac{x_i m_i v_i^0}{\sum_j x_i m_i v_i^0} \tag{7.8}$$

This volume-fraction mixing rule, while not perfect, represents experimental data near critical conditions better than vdW1 mixing rules [13,20,19], and so is to be preferred if the system under study has one of the components near its critical point. This mixing rule was used in this work.

Binary interaction parameter

The binary interaction parameter k_{ij} is a fitted, binary mixture parameter that corrects the mean-field energy contribution to SAFT. This parameter is usually determined by fitting SAFT to experimental phase equilibrium data, and is expected to lie between ± 0.10. A second mixture parameter could also be used, but the fit of the cloud curves is not expected

to be significantly improved by this because the two parameters have similar effects on the calculated fit. Therefore, only a single mixture parameter was used in this work.

7.3.3 Copolymer Parameters

In many copolymer-solvent studies, the copolymer properties are determined with mixing rules that combine parameters for the two homopolymers that comprise the copolymer. In one approach, the mixing rules used for these calculations are similar to the vdW1 mixing rule, except that they are applied to the two homopolymers that comprise the copolymer rather than to two components in the mixture.

Another approach was suggested by Takishima et al. [13] in which simple averaging rules, dependent only upon the molecular weights of blocks, were used to estimate the parameters. These rules are physically realistic since they are based on the volume fractions of the various blocks,

$$v_{A-B}^{00} = \frac{\sum_i v_i^{00} m_i}{\sum_i m_i} \tag{7.9}$$

$$\left(u_{A-B}^{0}\right)^{1/2} = \sum_i f_i^0 \left(u_i^0\right)^{1/2} \tag{7.10}$$

$$f_i^0 = \frac{m_i v_i^{00}}{\sum_i v_i^{00} m_i} \tag{7.11}$$

$$\left(1 - k_{12(A-B)}\right)\left(u_{A-B}^{0}\right)^{1/2} = \sum_i f_i^0 \left(1 - k_{12(i)}\right)\left(u_i^0\right)^{1/2} \tag{7.12}$$

where the subscript A-B represents the copolymer formed by the polymer A and the polymer B. This approach was used in this work.

7.4 Results and Discussions

In this section we first describe the ability of SAFT-HR to calculate cloud-point (liquid-liquid transition) curves for PVAC-CO_2 and PTAN-CO_2. We then describe the prediction of the cloud curve and aggregate formation for the copolymer PVAC-b-PTAN/CO_2 system.

7.4.1 Cloud curves

Mawson *et al*.[21] reported experimental cloud curves for PTAN (M_n = 60.4 kg/mol) in CO_2 at concentrations ranging from 0.087 to 7.32 wt%. The PTAN-CO_2 cloud point curve represents a phase separation of the lower critical solution temperature (LCST) type. This type of phase separation is typical for polymers in supercritical fluids.

A pseudogroup-contribution method for acrylate polymers suggested by Lora *et al*. [16] is used in this work to obtain the polymer parameters, m and v^{00} for PVAC and PTAN. The number of segments, m, for a particular acrylate is determined by first calculating m for the base ester group, CH_3-CH_2COO-, from the values given for a series of propanoates [9] and then substracting the contribution of the -CH_2- and -CH_3 groups that constitute the alkyl tail on the propanoate. The value for the product of mv^{00} for the poly(acrylate) is calculated with the same group contribution approach used to obtained m. The resulting parameters for the PVAC (M_n = 10.3 kg/mol) are m = 572.235 and v^{00} = 8.597 cm^3/mol.

For PTAN we used the same pseudo-group approach, but here it was necessary to estimate the contribution of the -CF_2- group. PTAN has a similar structure to PFOA as can be seen in figure 7.1. In previous work Luna-Barcenas et al.[17] studied cloud curve behavior for a PFOA-CO_2 system. They obtained the SAFT *m* parameter for PFOA (m_{PFOA} = 22182.1) by

adjusting it to experimental data. Due to the similar structure between PFOA and PTAN the value of m_{CF2}, can be estimated as follows:

$$m_{FOA} = m_{PFOA} \frac{M_{FOA}}{M_n(PFOA)} = m_{PFOA} \frac{M_{FOA}}{I\, M_W(PFOA)} = 20.26015$$

where *I* represents the polydispersity index, and was reported equal to 2 for PFOA by Triolo et al.[22]. Then, following the pseudo-group approach, the *m* parameter for the $(CF_2)_6$-CF_3 group can be determined as $m_{(CF2)6\text{-}CF3}$ = 15.7442. Finally approximating $m_{CF_2} \sim m_{(CF2)6-CF3}/7$ the m_{CF2} obtained is 2.2492. Using this value, the PTAN parameters obtained are: m = 24.758 and ν^{00} = 15.198 cm^3/mol.

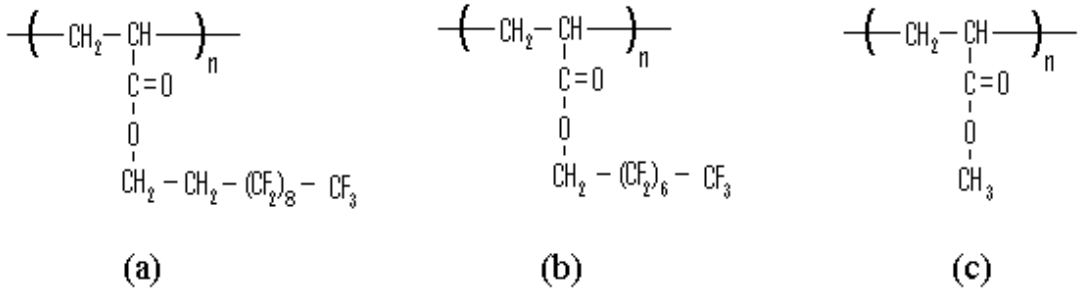

Figure 7.1. Chemical structures of (a) PTAN, (b) PFOA, (c) PVAC.

Unfortunately, the attractive energy of a segment u^0/k cannot be obtained with the pseudogroup-contribution approach; therefore this energy parameter is usually fitted to one cloud point curve. For PTAN u^0/k was fitted to the 40 ^oC cloud-curve experimental data [23], and a value of 200 K was obtained. FTIR spectroscopy [23] does not appear to provide evidence of any specific forces, and so the interactions between CO_2 and the fluorocarbon brushes of PTAN are believe to be due to van der Waals forces. Therefore, the association parameters were taken to be zero. PVAC, in contrast, is expected to have self-association and polar interactions with CO_2. Lora et al. [16] ignored any complex formation due to these

forces thus avoiding the introduction of two new parameters for the association part of the SAFT EOS. They instead introduced a higher value of u^0/k, that accounts for this association. In this study, we prefer to explicitly account for this complex formation using the total capabilities of SAFT, and obtain these parameters by fitting to cloud curve experimental data at 40 ^oC. Two associating sites per molecule were used and the values obtained are summarized in table 7.1 along with the parameters for PTAN and CO_2. Additionally the parameters for the co-polymer PVAC-b-PTAN obtained from equations (9)-(12) are shown in table 7.1.

Comparison of predicted and experimental cloud point isotherms for PTAN in CO_2 at concentrations ranging from 0.1 to 8 wt % are shown in figure 7.2. For a given temperature, one phase is present at a pressure above the cloud point pressure. The maximum pressure is the liquid-fluid upper critical solution pressure corresponding to the LCST; at this point, the composition of the two phases becomes the same. Qualitatively the results are in reasonably good agreement with the experimental data [21]. The comparison of experimental and predicted cloud point isotherms for the PVAC-CO_2 are satisfactory, but are not shown due to space limitations.

Table 7.1. SAFT parameter values

	M_n *(g/mol)*	v^{oo} (cm^3/mol)	*m* (-)	u^o/k (K)	*e/k* (K)	ε/k (K)	κ	$k_{CO2\text{-}polymer}$*
CO_2	44.02	21.310	1	246.43	72.642	0	0	
PVAC	10,300	8.597	572.235	225	10	500	0.01	-0.05
PTAN	60,400	15.198	2686.303	200	10	0	0	-0.05
PVAC-b-PTAN	70,700	14.039	3258.538	202.62	10	500	0.01	-0.05

*obtained from one cloud-curve experimental data at 40 C.

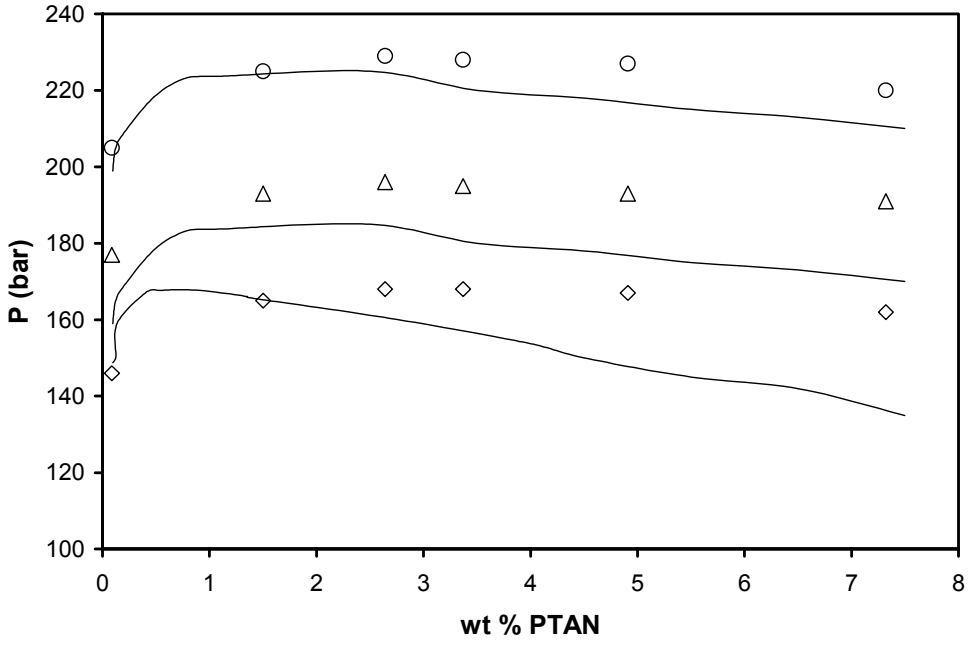

Figure 7.2. Predicted (lines) and experimental (symbols) cloud curves for the PTAN-CO_2 mixture. (◊) 40 C, (Δ) 50 C, (O) 60 C.

7.4.2 Critical micellar density

The critical micelle concentration (CMC) can be measured by methods sensitive either to the monomer or counterion concentration or to the micelle concentration. Methods sensitive to the concentration of the monomers or the counterions are, for example, measurements of electric conductivity, surface tension, and colligative properties such as vapor pressure depression, freezing point or osmotic pressure.

Figure 7.3 shows schematically the concentration dependence of the osmotic pressure for surfactant solutions. A more detailed explanation can be found elsewhere [24]. The CMC can readily be recognized as a break in the curve. From the osmotic pressure measurements it can be seen that the monomer concentration increases only up to the CMC and remains approximately constant; this behavior has been related with the formation of micelles. Careful measurements of the osmotic pressure (and in general any property) in the CMC

region show that the CMC is not represented by a break in the curve but by a transition region. This is schematically represented in figure 7.3 by the filled points.

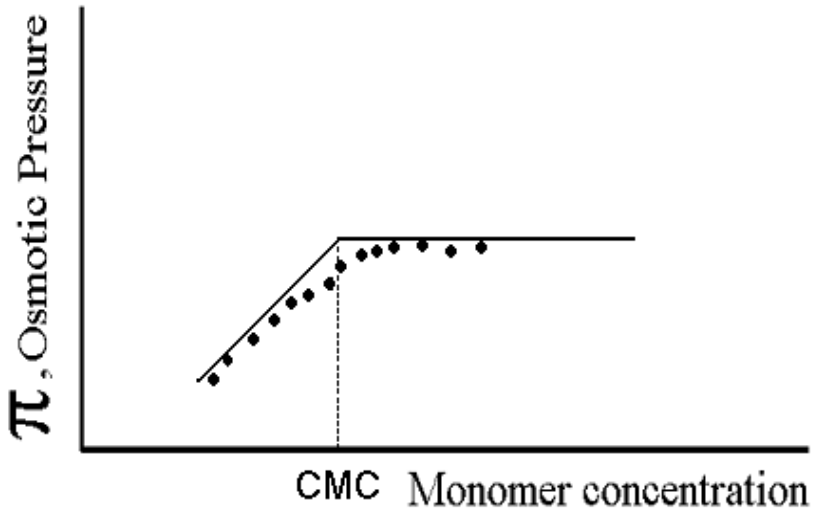

Figure 7.3. Schematic plot of osmotic pressure, π, as a function of surfactant concentration.

The critical micellar density (CMD) is analogous to the CMC observed in many surfactant systems in conventional solvents. The CMD is a monomer to micelle transition that is dependent on the density of the medium. Below a critical CO_2 density, block copolymer surfactants will exist as micellar aggregates in solution, as CO_2 will be a good solvent for one of the blocks (PTAN) but a relatively poor solvent for the other (PVAC). With increasing CO_2 density, the micelles will decrease in size and aggregation number due to the greater solubilization of the surfactant. At a critical density, CO_2 will become a good solvent for both blocks of the block copolymer and the micelles will break up into monomers.

The chemical potentials and hence the osmotic pressure can be obtained from an equation of state. This suggests that the CMD (or CMC) could be located by searching for a break in a plot of osmotic pressure versus monomer concentration associated with a given equation of state. This break might be expected to occur if the equation is capable of predicting association between molecules, and association is responsible for the aggregate formation

that occurs during micellization. SAFT is a molecular based EOS that accounts in a realistic way for association between molecules in addition to accounting for dispersion and repulsive interactions. For this reason it is a natural choice to evaluate this possibility.

The osmotic pressure, π, is related to the chemical potential of mixing of the solvent by [25]

$$\pi = -\frac{\mu_1 - \mu_1^0}{V_1} \tag{7.13}$$

where μ_1^0 is the chemical potential of pure CO_2, μ_1 is the chemical potential of CO_2 in the CO_2-copolymer mixture, and V_1 is the molar volume of the solvent.

In figure 7.4 we show the predicted chemical potential of CO_2 in the CO_2-copolymer mixture at 45 C and 135 bar, using the parameters obtained as described in the last section. Additionally we present in figure 7.5 the fraction of free unimers predicted with the SAFT equation at the same conditions of figure 7.4. This figure shows that the fraction of free unimers decreases (meaning that the fraction of associated sites increases) with copolymer concentration (or CO_2 density) until a certain point at which it becomes practically constant, indicating that all the "new" surfactant that is added goes to form aggregates. This indicates that SAFT is able to reproduce the behavior characteristic of aggregate formation. Of course with SAFT it is not possible to predict that these aggregates are spherical micelles, but by comparing with experiments [1] this tendency can be related with the formation of reverse spherical micelles.

The chemical potential of carbon dioxide in the CO_2-copolymer mixture predicted by SAFT at 45 ^oC and 440 bar for the copolymer-CO_2 system studied here is shown in figure 7.6. In this case, the curve does not present a break in its shape, possibly due to the absence of aggregates. This could be because the higher CO_2 density causes the aggregates to break up into monomers in solution.

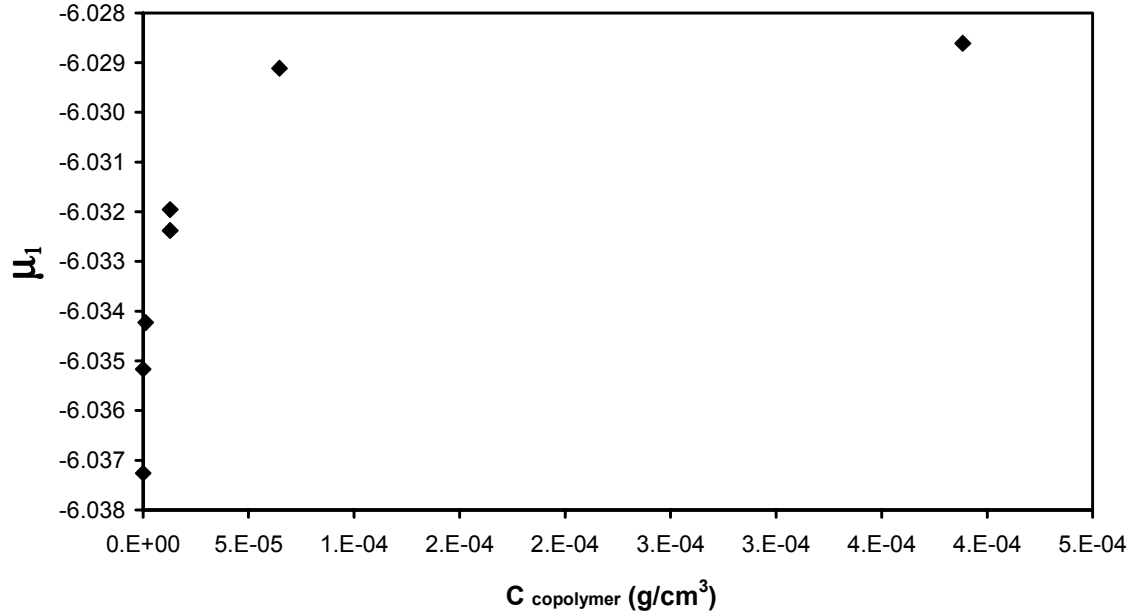

Figure 7.4. Chemical potential of CO_2 in the CO_2-copolymer mixture versus copolymer concentration for the PTAN-b-PVAC/CO_2 system at 45 C and 135 bar.

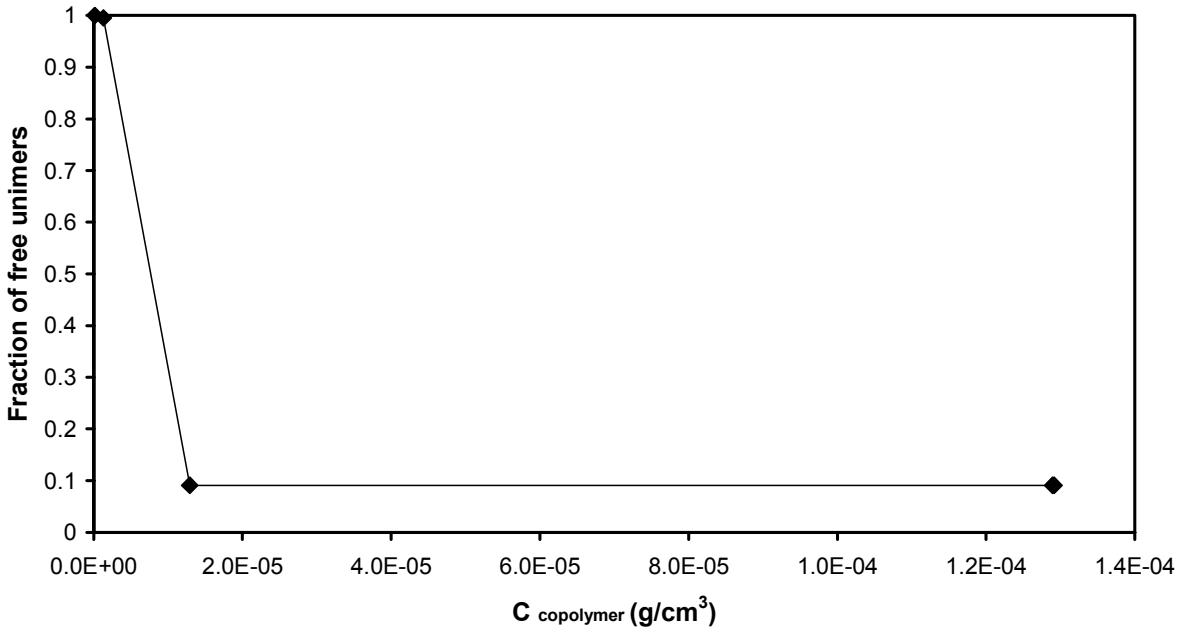

Figure 7.5. Fraction of free unimers as a function of copolymer concentration at 45 C and 135 bar.

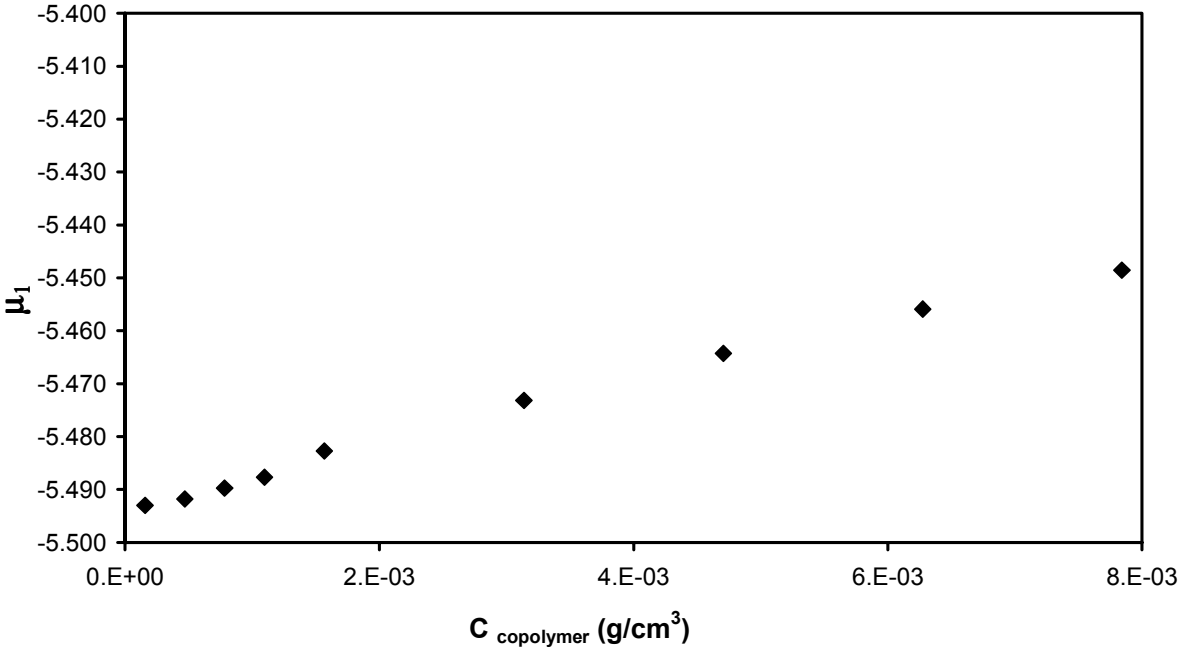

Figure 7.6. Chemical potential of CO_2 in the CO_2-copolymer mixture versus copolymer concentration for PTAN-b- PVAC/CO_2 system at 45 C and 440 bar, as predicted by SAFT.

Finally, in figure 7.7 we present the predicted phase diagram for this system together with the experimental [1] results. Although the agreement is qualitative, the results indicate that the SAFT EOS seems to be able to predict the formation of aggregates.

7.5 Conclusions

A previously proposed method based on a group contribution approach was used to obtain the physical parameters for SAFT-HR EOS for PVAC and PTAN polymers. Following the approach by Lora et al.[16] the contribution of a CF_2 group was obtained. PTAN was modeled as a non-associating polymer while PVAC was modeled with two association sites per molecule. Cloud curves of PVAC-CO_2, PTAN-CO_2 and PVAC-b-PTAN/CO_2 system were predicted and good agreement with the experimental data available was obtained.

Critical micellar densities appear to be successfully predicted for the PVAC-b-PTAN/CO_2 system using a criteria based in the variation of osmotic pressure (or chemical potential) with

surfactant concentration. Such capability would be valuable to many researchers, since the calculations would be much faster (by 3-4 orders of magnitude) and simpler than a full-scale molecular simulation. A large number of systems of interest could be quickly screened using such an equation to determine the onset of aggregation formation.

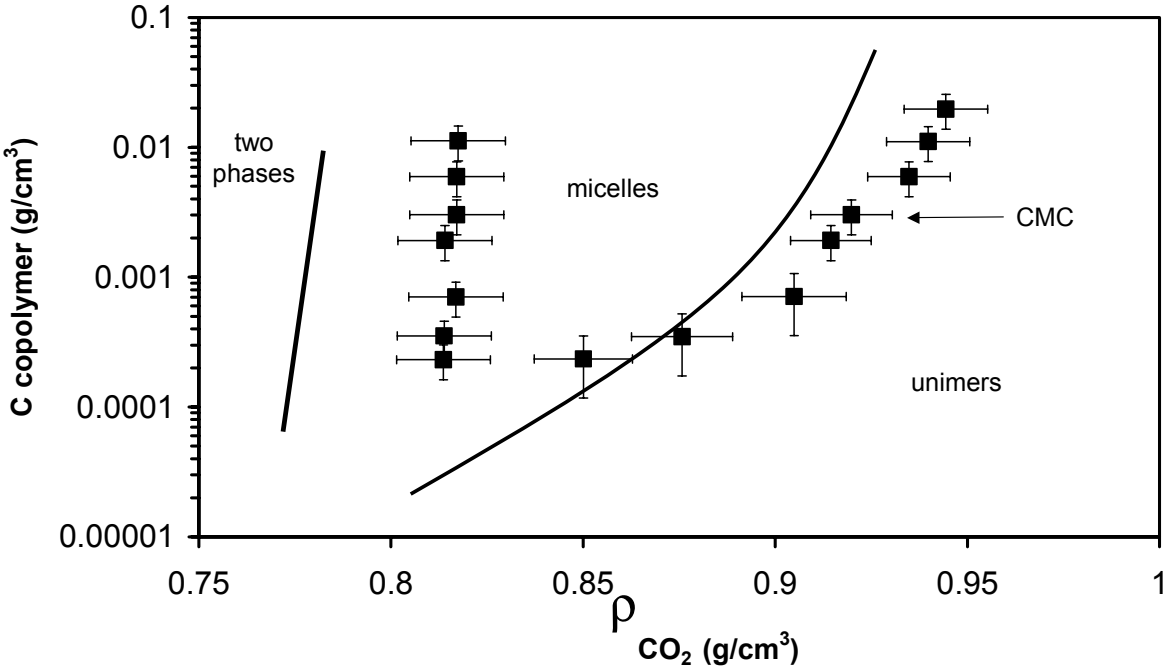

Figure 7.7. Phase diagram for PTAN-b-PVAC in CO_2 (M_n (PTAN) = 60.4 kg/mol, M_n (PVAC) = 10.3 kg/mol) at 45 C. Symbols are experimental points [1]. Lines this work.

Efforts are now under way to compare molecular simulation with SAFT calculations using the same intermolecular potential models, in order to better ascertain SAFT's ability to predict micellization.

Acknowledgments

The material is based upon work supported by the STC Program of the National Science Foundation under Agreement No. CHE-9876674. CMC thanks Flor Siperstein and Martin Lísal for many helpful discussions.

7.6 References

[1] E. Buhler, A.V. Dobrynin, J.M. DeSimone and M. Rubinstein, *Macromolecules,* 31 (1998) 7347-7355.

[2] R. Triolo, A. Triolo, F. Triolo, D.C. Steytler, C.A. Lewis, R.K. Heenan, G.D. Wignall and J.M. DeSimone, *Physical Review E,* 61 4 (2000) 4640-4643.

[3] A. Triolo, F. Triolo, D.E. Betts, J.B. McClain, J.M. DeSimone, G.D. Wignall and R. Triolo. *Physical Review E,* 62 4 (2000) 5839-5842.

[4] C.F. Kirby and M.A. McHugh. *Chem. Rev.,* 99 (1999) 565-602.

[5] W.G. Chapman, K.E. Gubbins, G. Jackson and M. Radosz, *Ind. Eng. Chem. Res., 29* (1990) 1709-1721.

[6] K.E. Gubbins, *Fluid Phase Equilib.*, 83 (1993) 1-14.

[7] E.A. Müller and K.E. Gubbins. Associating Fluids and Fluids Mixtures, in J.V.Sengers, R.F. Kayser, C.J. Peters and H.J. White, Jr. (Eds), Equations of State for fluids and fluid Mixtures.Experimental Thermodynamics, Volume 5, Elsevier, Amsterdam, 2000, pp 435-478.

[8] E.A. Müller and K.E. Gubbins. *Ind. Eng. Chem. Res.* In press. (2001)

[9] S.H. Huang and M. Radosz, *Ind. Eng. Chem. Res.,* 29 (1990) 2284-2294.

[10] K.P. Shukla and W.G. Chapman, *Molecular Physics*, 91 6 (1997) 1075-1081.

[11] K.P. Shukla and W.G. Chapman, *Molecular Physics*, 98 24 (2000) 2045-2052.

[12] H. Adidharma and M. Radosz, *Ind. Eng. Chem. Res.*, 37 (1998) 4453-4462.

[13] S. Takishima, M.L. O'Neil and K.P. Johnston, *Ind. Eng. Chem. Res.*, 36 (1997) 2821-2833.

[14] J,P. Passarello, S. Benzaghou, S. and P. Tobaly, *Ind. Eng. Chem. Res.*, 39 7 (2000) 2578-2585.

[15] R. Spang and W. Wagner, *J. Phys. Chem. Ref. Data*, 25 6 (1996) 1509-1596.

[16] M. Lora, F. Rindfleisch and M.A. McHugh, *J. Appl. Polym. Sci.,* 73 (1999) 1979-1991.

[17] G. Luna-Bárcenas, S. Mawson, S. Takishima, J.M. DeSimone, I.C. Sanchez, and K.P. Johnston, *Fluid Phase Equilib*. 146 (1998) 325-337.

[18] S. Behme, G. Sadowski, and W. Arlt, *Fluid Phase Equilib.*, 158-160 (1999) 869-877.

[19] S.T. Huang and M. Radosz., *Ind.Eng.Chem.Res.*, 32 (1993) 762.

[20] J.M. Prausnitz, R.N. Lichtenthaler and E. Gomez de Azevedo. Molecular Thermodynamics of Fluid-Phase Equilibria. Third Edition. Prentice Hall, New Jersey, 1999.

[21] S. Mawson, K.P. Johnston, J.R. Combes and J.M. DeSimone, *Macromolecules,* 28 (1995) 3182-3191.

[22] F. Triolo, R. Triolo, J.D. Londono, G.D. Wignall, J.B. McClain, D.E. Betts, S. Wells, E.T. Samulski and J.M. DeSimone, *Lagmuir*, 16 (2000) 416-421.

[23] S. Mawson, K.P. Johnston, J.R. Combes and J.M. DeSimone, *Macromolecules*, 28 (1995) 3182-3191.

[24] H. Hoffmann and W. Ulbricht, in Hans-Jürgen Hinz (Eds.) The formation of micelles, in Thermodynamics data for biochemistry and biotechnology. Springer-Verlag, 1986, pp. 297-348.

[25] H. Tompa, Polymer Solutions. Butterworths Scientific Publications. 1956.

Chapter 8

The Influence of High-Pressure Carbon Dioxide on the Phase Behavior of PDMS/PEMS Blends: An Experimental and Theoretical Investigation*

Coray M. Colina, Teri A. Walker, Richard J. Spontak and Keith E. Gubbins
Chemical Engineering Department, North Carolina State University, Raleigh, NC 27695

8.1 Abstract

In this work the effect of high-pressure CO_2 on the miscibility of low-polydispersity poly(dimethylsiloxane)/poly(ethylmethylsiloxane) (PDMS/PEMS) blends in which $M_{w,PDMS}$ = 44.5 kg/mol and $M_{w,PEMS}$ = 14.6 kg/mol is investigated by complementary experimental and theoretical methods. Experimental measurements of phase equilibria in ternary PDMS/PEMS/ CO_2 systems are obtained as functions of blend composition and CO_2 pressure by high-pressure spectrophotometry. Results indicate that the cloud point of the blend (T_{cp}) increases with increasing CO_2 pressure. This observation reveals that CO_2 serves to reduce blend miscibility by translating the entire phase envelope of our PDMS/PEMS blend to higher temperatures, in marked contrast to previous studies of PDMS/PEMS blends subjected to hydrostatic pressure (which enhances blend miscibility by depressing T_{cp}). We have modeled the phase behavior of these PDMS/PEMS/CO_2 systems using the SAFT equation of state, which is a molecular-based formalism that is designed to account for the effects of molecular association and chain flexibility, as well as repulsive and dispersion interactions. The SAFT parameters for PDMS are obtained from binary cloud curves previously reported in the literature for PDMS/CO_2 mixtures, whereas PEMS parameters are obtained from an extended group contribution approach established for PDMS systems. The ability of the model to predict the phase behavior of the ternary PDMS/PEMS/CO_2 system is corroborated by comparing theoretical predictions with the experimental data reported herein.

*6th International Symposium on Supercritical Fluids, CD-ROM Document MP2.pdf, Versailles, France, (2003)

8.2 Introduction

Most commercially relevant polymer blends exhibit upper critical solution temperature (UCST) behavior in which increasing temperature (or decreasing hydrostatic pressure) promotes an increase in miscibility. Horiuchi et al. [1] have demonstrated that the PDMS/ PEMS system is partially miscible, with an experimentally accessible UCST that may (depending on the molecular weights of the constituent polymers) reside near ambient temperature. These characteristics, along with the ability to design the shape of the phase boundary and position of the UCST through judicious choice of polymer molecular weights, make this blend attractive for the present study. Moreover, this system is also interesting for another reason: due presumably to its negative excess volume change upon mixing [2], it becomes more miscible when exposed to an increase in hydrostatic pressure. This is contrary to the conventional UCST behavior of most polymer pairs and provides us with an opportunity to explore the effect of high-pressure condensable gas on blend phase behavior.

In this work we seek to elucidate the response of the PDMS/PEMS blend to high-pressure CO_2, which has been shown [3] to significantly swell PDMS. Recent efforts have demonstrated that high-pressure CO_2 can enhance the miscibility [4] of blends exhibiting UCST behavior and reduce the miscibility of LCST blends [5]. For this study, we have selected model polymers with relatively low polydispersity indices (M_w/M_n) so that the effect of polydispersity on the phase diagram can be neglected.

8.3 Experimental Section

The PDMS (M_w = 44.5 kg/mol, M_w/M_n = 1.09) and PEMS (M_w = 14.6 kg/mol, M_w/M_n = 1.13) homopolymers were purchased from Polymer Source (Dorval, Quebec, Canada) and subjected individually to pretreatment in high-pressure CO_2 to remove any low-molecular-weight (CO_2-soluble) fraction. Cloud point temperatures for various PDMS/PEMS blend compositions were determined by cooling blends from the homogeneous state at constant CO_2 pressures and measuring the change in turbidity with a 632 nm laser source in

conjunction with a photometric power meter. The cloud points reported herein corresponded to the temperature at the inflection point of the power (intensity) *versus* temperature curve. The detailed experimental procedure for this measurement is described elsewhere [6].

8.4 Experimental Results

8.4.1 PDMS/PEMS blends

As a baseline for comparison with prior studies [1, 2, 7-10] of PDMS/PEMS blends, we have measured the cloud curve of our blend in the absence of CO_2. Figure 8.1 shows T_{cp} as a function of blend composition (w_{PDMS}) for three series of PDMS/PEMS blends, with the closed circles representing the results of this study. The coexistence curve measured by Kuwahara et al. [7] (open squares) for a mixture of PDMS (M_w = 19.1 kg/mol, M_w/M_n = 1.03) and PEMS (M_w = 14.0 kg/mol, M_w/M_n =1.02) is included for comparison. The critical temperature extracted from their high-precision data is located at 30.662°C and 55.04 wt% PEMS. Beiner et al. [2] have previously reported the critical points of three different blends. Only one of these, blend "C" composed of PDMS (M_w = 10.7 kg/mol) and PEMS (M_w = 12.4 kg/mol) with polydispersities between 1.04 and 1.12, is shown (as an open triangle) in Figure 8.1. In this case, the critical temperature lies below -50°C at 50 wt% PEMS. Note that $M_{w,PEMS}$ is approximately the same for the three blends displayed in Figure 8.1, whereas $M_{w,PDMS}$ nearly doubles in each series. This figure illustrates the dramatic effect that $M_{w,PDMS}$ can have on the cloud point temperatures of relatively low-molecular-weight PDMS/PEMS blends.

8.4.2 PDMS/PEMS blends in presence of supercritical CO_2

Pressure can serve to either compatibilize or demix polymer blends, depending on the specific characteristics of the constituent polymers and their mutual interaction. It has been shown that (hydrostatic) pressure enhances the miscibility of model PDMS/PEMS blends that exhibit UCST behavior. Beiner et al. [2] have suggested that this unusual behavior is

caused by a negative excess volume change upon mixing when pressure-induced mixing becomes significant ($\delta T_c/\delta P \approx$ -25 K/kbar). Our studies of this blend under reasonably high pressure include an additional complication, the presence of CO_2, which swells polysiloxanes.

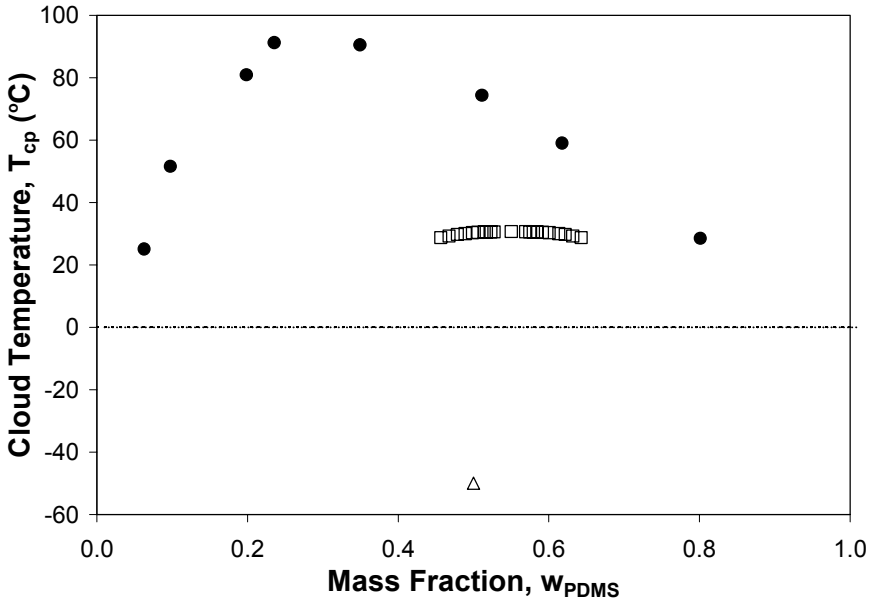

Figure 8.1. Cloud point temperatures of model PDMS/PEMS blends.

Figure 8.2 shows the experimental cloud point temperatures obtained in this study for the PDMS/PEMS blend as a function of PDMS mass fraction (solvent-free basis) and CO_2 pressure, as discerned by high-pressure spectrophotometry. At constant PDMS/PEMS mass fraction, an increase in CO_2 pressure increases the cloud temperature, thus reducing the miscibility of the UCST blend. It must be recognized, however, that an increase in CO_2 pressure implies an increase in the amount of CO_2 present in the system.

8.5 Modeling

According to the SAFT equation of state [11], molecules are modeled as chains of covalently bonded spheres, and different molecules of homologous series (such as *n*-alkanes or

polymers that only differ in molecular weight) are considered as chains of identical spheres. In this case the number of spheres in the chain is directly proportional to the molecular weight. Within the context of the SAFT framework, the residual Helmholtz energy, a^{res}, is of the form

$$a^{res} = a^{seg} + a^{chain} + a^{assoc} \tag{8.1}$$

where a^{seg} reflects segment-segment interactions (interactions between repeat units in different molecules) usually modeled in terms of hard-sphere, LJ or square-well potentials; a^{chain} is the additional Helmholtz energy due to chain formation; and a^{assoc} is the contribution due to association between different molecules due, for example, to H-bonding. Therefore, in this work we set the parameters comprising a^{assoc} to zero. A detailed discussion of the mathematical form of the SAFT equation can be found elsewhere [12,13] and is not reproduced here.

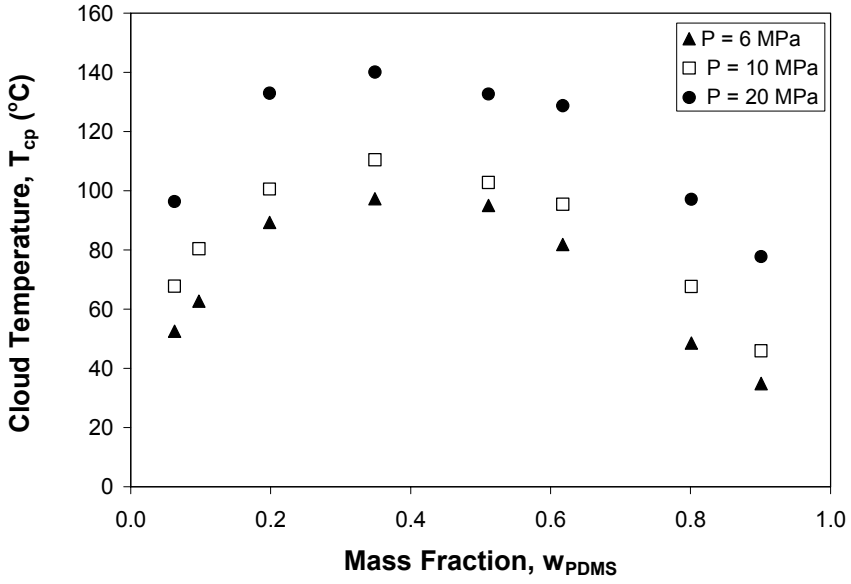

Figure 8.2. Cloud point temperatures of PDMS/PEMS blends as a function of blend composition (solvent-free) and CO_2 pressure.

8.5.1 Determination of parameters

Since high-molecular-weight polymers do not possess a detectable vapor pressure and since they commonly undergo thermal degradation before exhibiting a critical point, equation-of-state parameters for polymers are generally determined from experimental pure-liquid molar volume data. Unfortunately, regression of polymer parameters from this procedure generally results in poor predictions of phase equilibrium afforded by the SAFT equation [14,15]. When parameters are determined from such restricted data, a variety of pure-component parameter sets fit the data. Recent efforts [16] have demonstrated that this shortcoming remains in newer versions of the SAFT equation of state (such as PC-SAFT).

An alternative approach to obtain polymer parameters is to regress a pure-component parameter for the polymer from binary phase equilibria data [14,15]. In this work, the SAFT parameters for PDMS are obtained from binary cloud curves reported elsewhere [17-19] for PDMS/CO_2 mixtures, and the relevant CO_2 parameters have been extracted from the literature [20]. Regrettably, data corresponding to PEMS/CO_2 phase equilibria are not presently available, in which case the PEMS parameters have been estimated from an extended group contribution approach proposed by Lora et al. [21] for acrylate polymers. Colina et al. [22] have recently used a similar pseudo-group approach to determine the parameters for poly(1,1,2,2-tetrahydroperfluorooctyl acrylate) (PTAN), estimating the contribution of the -CF_2- group, from high molecular weight poly(1,1-dihydroperfluorooctyl acrylate) (PFOA).

Lora et al. [21] argue that the number of segments (m) for a given acrylate polymer is determined by first calculating m for the base ester group. The m for a particular alkyl tail is calculated by summing the m values of the appropriate number of -CH_2- and -CH_3 groups. The values of m for -CH_3 and -CH_2- are obtained from regressions of alkane and alkene parameters. The value for the product of mv^{00}, where v^{00} represents the segment volume, for the base is determined from the same group contribution approach used to obtained m. Using

a similar approach for PEMS, we estimate the contributions of the –Si-O- group: m_{SiO} = 5.742 and v^{00}_{SiO} = 15.597 cm^3/mol.

Since the attractive energy of a segment (u^0/k) cannot be obtained by this method, we have elected to determine this energy parameter from one experimental cloud point. For PEMS, regression of u^0/k fitted to the 60°C data obtained in this work yields a value of 204 K, which compares well with that of PDMS (u^0/k = 200 K).

The binary interaction parameter k_{ij} is a fitted, binary mixture parameter that corrects the mean-field energy contribution to SAFT. This parameter is usually determined by fitting SAFT to experimental phase equilibrium data, and is expected to lie between ±0.10. From a careful analysis of binary and ternary blends of low-polydispersity blends, Horiuchi et al. [1] conclude that the PDMS/PEMS pair exhibits no evidence of specific interactions. On the basis of this finding, we have elected to set $k_{PDMS/PEMS}$ = 0 in this work. Moreover, we assume $k_{PEMS/CO2} = k_{PDMS/CO2}$ = 0.017, which is obtained from PDMS/CO_2 experimental data [17-19].

A comparison of predicted and experimental cloud point isobars for PDMS/PEMS blends in CO_2, with PDMS concentrations varying from 5 to 90 wt%, is provided in Figure 8.3. At any pressure, the homogeneous region lies above the cloud point temperature. The maximum temperature in the cloud curve is the UCST, where the compositions of the two coexisting phases become equal. We apply a freehand closure to our predicted curves in the immediate vicinity of the UCST. As this figure attests, the predictions from SAFT are in reasonably good quantitative agreement with the experimental data.

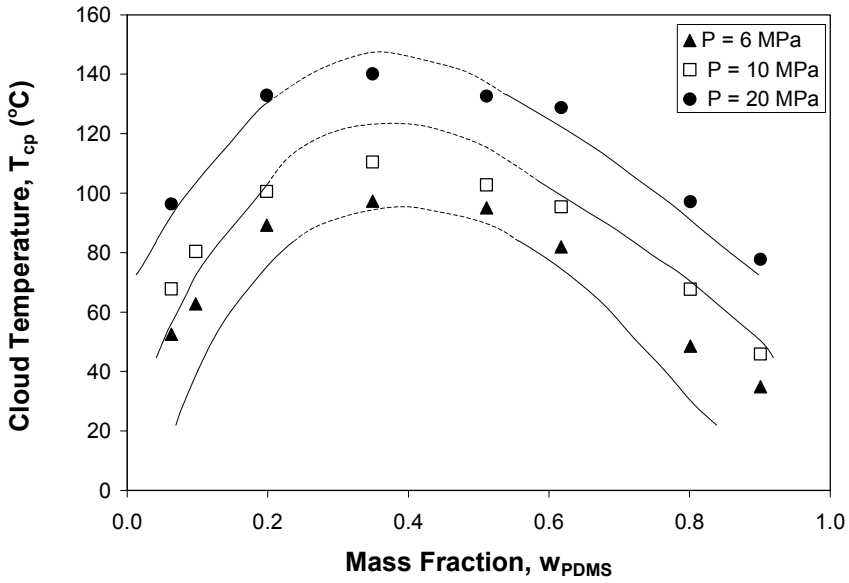

Figure 8.3. Cloud point temperatures of PDMS/PEMS blends in CO_2. Symbols denote experimental results; curves signify corresponding SAFT predictions.

8.6 Conclusions

We have measured cloud curves for the PDMS/PEMS/CO_2 system. Results indicate that the cloud point increases with increasing CO_2 pressure, which is contrary to the response of this blend to hydrostatic pressure. Predictions from the SAFT equation of state compare favorably with experimental results, confirming the versatility of this theoretical approach.

Acknowledgments

This work was supported, in part, by the STC Program of the National Science Foundation under Agreement No. CHE 9876674, and by the Kenan Center for the Utilization of CO_2 in Manufacturing.

8.7 References

[1] HORIUCHI, H., IRIE, S., NOSE, T., Polymer, Vol. 32, **1991**, p. 1970

[2] BEINER, M., FYTAS, G., MEIER, G., KUMAR, S., Phys. Rev. Lett., Vol. 81, **1998**, p. 554

[3] ROYER, J.R., DESIMONE, J.M., KHAN, S.A., Macromolecules, Vol. 32, **1999**, p. 8965

[4] WALKER, T.A., RAGHAVAN, S.S., ROYER, J.R., SMITH, S.D., WIGNALL, G.D., MELNICHENKO, Y., KHAN, S.A., SPONTAK, R.J., J. Phys. Chem. B, Vol. 103, **1999**, p. 5472

[5] RAMACHANDRARAO, V.S., WATKINS, J.J., Macromolecules, Vol. 33, **2000**, p. 5143

[6] WALKER, T.A.**,** COLINA, C.M., GUBBINS, K.E., SPONTAK, R.J., in preparation, **2003**

[7] KUWAHARA, N., SATO, H., KUBOTA, K., Phys. Rev. Lett., Vol. 75, **1995**, p. 1534

[8] SATO, H., KUWAHARA, H., KUBOTA, K., Phys. Rev. E, Vol. 53, **1996**, p. 3854

[9] ENDERS, S., STAMMER, A., WOLF, B.A., Macromol. Chem. Phys., Vol. 197, **1996**, p. 2961

[10] BEINER, M., FYTAS, G., MEIER, G., KUMAR, S., J. Chem. Phys., Vol. 116, **2002**, p. 1185

[11] CHAPMAN, W.G., GUBBINS, K.E., JACKSON, G. RADOSZ, M., Ind. Eng. Chem. Res., Vol. 29, **1990**, p. 1709

[12] HUANG, S.H, RADOSZ, M., Ind. Eng. Chem. Res., Vol. 29, **1990**, p. 2284

[13] MÜLLER, E.A., GUBBINS, K.E., Ind. Eng. Chem. Res., Vol. 40, **2001**, p. 2193

[14] KIRBY, C.F., McHUGH, M.A., Chem. Rev., Vol. 99, **1999**, p. 565

[15] TAKISHIMA, S., O'NEIL, M.L., JOHNSTON, K.P., Ind. Eng. Chem. Res., Vol. 36, **1997**, p. 2821

[16] GROSS, J., SADOWSKI, G., Ind. Eng. Chem. Res., Vol. 41, **2002**, p. 1084

[17] BAYRAKTAR, S., KIRAN, E., J. Appl. Polym. Sci., Vol. 75, **2002**, p. 1397

[18] O'NEILL, M.L., CAO, Q., JOHNSTON, K.P., WILKINSON, S.P., SMITH, C.D., KERSCHNER, J.L. JURELLER, S.H., Ind. Eng. Chem. Res., Vol. 37, **1998**, p. 3067

[19] GARG, A., GULARI, E., MANKE, W., Macromolecules, Vol. 27, **1994**, p. 5643

[20] LUNA-BARCENAS, G., MAWSON, S., TAKISHIMA, S., DESIMONE, J.M., SANCHEZ, I.C., JOHNSTON, K.P., Fluid Phase Equil., Vol. 146, **1998**, p. 325

[21] LORA, M., RINDFLEISCH, F., McHUGH, M.A., J. Appl. Polym. Sci., Vol. 73, **1999**, p. 1979

[22] COLINA, C.M., HALL, C.K., GUBBINS, K.E., Fluid Phase Equil., Vol. 194-197, **2002**, p. 553

Chapter 9

Conclusions and Future Directions

In this work, we presented a molecular modeling study of the phase behavior of small molecules and macromolecules in the presence of supercritical carbon dioxide. We chose to evaluate three of the several versions available of the SAFT[1-4] approach, based on their reference term: SAFT-HR[4] (hard sphere), Soft-SAFT[5,6] (Lennard-Jones) and SAFT-VR[7,8] (square-well). We showed the utility of the approach not only by predicting the phase behavior with the different models, but also by evaluating other general properties such as derivative properties and formation of aggregates.

We divided the project into three major areas: a) a fundamental investigation of the thermophysical properties of pure carbon dioxide, using predictions from both molecular simulations and equations of state; b) a detailed study of the phase equilibria of binary and ternary mixtures of CO_2, *n*-perfluoroalkanes and *n*-alkanes, as a representation of small CO_2-philic and partially CO_2-phobic compounds; and c) a study of phase equilbria of binary and ternary mixtures of CO_2, CO_2-philic and CO_2-phobic polymers.

We first studied[9] the predictive capabilities of the SAFT equation of state for the supercritical solvent through the Joule-Thomson inversion curves, which is considered one of the most demanding tests not only for equations of state, but also for molecular simulations and in fact experimental data. Very good agreement was obtained with both experimental data and molecular simulations, and the work has resolved an apparent anomaly in the Joule-Thomson inversion curve that had been reported in the literature. We continued studying the predictive capabilities of molecular simulations and molecular-based equations of state for the supercritical solvent, through derivative properties and the explicit inclusion of the CO_2 quadrupole. Very good agreement was obtained[10] with both experimental data available in the literature and the molecular simulations performed in this work. Moreover, this work has

shown that agreement between calculated and experimental values for speed of sound does not necessarily guarantee good agreement for the isobaric heat capacity and the first derivative of the volume, as is commonly assumed.

Specifically, we have presented simulation results for the Joule-Thomson inversion curve (JTIC), volume expansivity, isothermal compressibility, isobaric heat capacity, Joule-Thomson coefficient and speed of sound for carbon dioxide in the supercritical region, using two different approaches based on Monte Carlo simulations in the isothermal-isobaric ensemble. We modeled carbon dioxide as a quadrupolar two-center Lennard-Jones (2CLJQ) fluid using potential parameters reported in the literature and derived from vapor-liquid equilibria of CO_2. We showed that a precision of four significant figures in ensemble averages of thermodynamic quantities of interest is needed to obtain the JTIC accurately. This accuracy would not have been feasible for a molecular simulation ten to fifteen years ago, but with the current computational power it is now possible. The agreement between the experimental data, the Span-Wagner[11] equation of state (EOS) and our simulation results indicates that the 2CLJQ potential represents an excellent balance between simplicity and accuracy in modeling of carbon dioxide. Additionally, we calculated the JTIC using the BACKONE[12] EOS (that uses the same intermolecular potential as our simulations) and showed that the BACKONE EOS performs very well in predicting the JTIC for carbon dioxide. We also demonstrated that the anomalous behavior of the CO_2 JTIC obtained by Chacín *et al.*[13] is not due to the potential model used (2CLJQ potential), but arises from high uncertainty in the high-temperature branch of the JTIC.

It is concluded that the VLE-based parameters used to model CO_2 as a quadrupolar two-center Lennard-Jones fluid (for both simulations and equation of state) can be used with confidence for the prediction of thermodynamic properties for CO_2 in the supercritical region, except in the extended critical region. This region is larger than usual due to the differences between the critical point predicted for the 2CLJQ model for carbon dioxide and the experimental critical point. Unfortunately, this region is extremely important for CO_2-driven processes where the tunability of CO_2 plays a key role. Therefore, care must be taken

when using this potential to model CO_2 in this extended critical region. Deviations between the 2CLJQ EOS and simulations, which can be quite large in the two-phase region, appear to become less important at higher supercritical temperatures and pressures. The present results, however, are limited to CO_2 only. More extensive testing with a wider range of pure fluids (e.g. ethane, nitrogen, etc) will be required before the predictive capabilities of the 2CLJQ can be fully assessed in the supercritical region.

Our results illustrate the predictive capabilities of molecular simulations. We have found quantitative agreement for JTIC among experimental measurements and predictions from both the equation of state and simulations. The agreement is excellent even though all properties were not included in the optimization of the intermolecular potential. In light of this, further work can focus on predicting JTIC and derivative properties from molecular simulations for different fluids with well known intermolecular potentials with parameters obtained from vapor-liquid equilibrium conditions. In fact, the JTICs obtained in this way could be used in lieu of the scarce experimental data to permit a rigorous test of the various predictions from equations of state.

We then evaluated complete Joule-Thomson inversion curves for pure carbon dioxide and the *n*-alkane series, including heavy *n*-alkanes up to octatetracontane (*n*-$C_{48}H_{98}$), predicted within the SAFT approach. In this part of the project[14] we used the Soft-SAFT[5,6] equation, in which the reference term is a Lennard-Jones fluid. Comparisons with available experimental and correlation data for carbon dioxide and the lighter *n*-alkanes show good quantitative agreement. Although the model used for carbon dioxide was too crude, it was able to reproduce the correct trend of the inversion curve. Inversion curves for light hydrocarbons were obtained with the same Soft-SAFT equation but using different sets of molecular parameters. We observe a strong dependence of the inversion curve on these parameters, especially near the maximum inversion pressure and in the high temperature region. The molecular nature of the parameters used in the Soft-SAFT equation, and the availability of a correlation for estimating critical points, have allowed us to predict inversion curves for the first time for heavy *n*-alkanes, up to octatetracontane. In fact, there is in principle no

limitation on chain length with this approach, provided the critical properties needed to reduce the temperature and the pressure are known or can be estimated. The equation is able to predict the general trend of inversion curves even for extreme conditions, with values of reduced pressure $P_r=P/P_c$ up to 40, and reduced temperatures $T_r=T/T_c$ of almost 5.

Further tests of the SAFT models should include the study of other derived thermodynamic properties, such as residual properties (enthalpy, entropy and heat capacities), as well as first partial derivatives with respect to temperature and volume, especially at supercritical conditions. Particular attention should be given to properties obtained from a combination of others, such as the speed of sound, where cancellations of errors could lead to erroneous conclusions. It is natural to expect that an EOS that gives a good representation of Joule-Thomson inversion curves will also provide improved predictions of other derivative thermodynamic properties. Extended comparisons of the SAFT approach and cubic EOS would be worth attempting.

The phase behavior (vapor-liquid, liquid-liquid and vapor-liquid-liquid equilibria) of a number of carbon dioxide (CO_2), *n*-alkane (C_6H_{14} to $C_{13}H_{28}$) and *n*-perfluoroalkane (C_6F_{14}, C_7F_{16}, C_8F_{18}) binary[15] and ternary[16] mixtures has been studied using the statistical associating fluid theory for potentials of variable attractive range (SAFT-VR). The molecules were modeled as chains of tangentially bonded attractive spherical segments, with the attractive interactions treated as square-well potentials of variable range. Even though the characteristic quadrupole of carbon dioxide was not taken into account explicitly, the approach can be used to predict the phase behavior of the homologous series studied. The pure component intermolecular parameters for carbon dioxide and the *n*-alkane molecules were determined in previous works by fitting to vapor pressures and saturated liquid densities; the same procedure was followed in this work to determine the parameters for the *n*-perfluoroalkane molecules. The optimized conformal parameters (σ and ε) were rescaled with the experimental critical point of each of the pure components. A set of transferable mixture parameters was presented, which provides a good description of the mixture phase behavior,

and additionally offers insight into the higher solubility of *n*-perfluoroalkanes in carbon dioxide as compared to the solubility of *n*-alkanes.

The predicted phase diagrams are based on temperature-independent binary interaction parameters, and no ternary parameters are introduced. We studied the influence of temperature, pressure, composition and chain length on the phase diagram, and showed that when compared with the scarce experimental and molecular simulation data available, the predicted phase diagrams should represent the expected phase equilibrium behavior with good accuracy. Upper critical solution pressures for several *n*-alkane/*n*-perfluoroalkane systems were also obtained. Moreover, the ternary diagrams presented in this work represent, to the best of our knowledge, the first available data for CO_2/*n*-perfluoroalkane/*n*-alkane systems. Although research in this area has grown in the last few years, very little phase equilibrium data is available in the literature for these systems. The data provided in this work could be helpful in identifying possible new CO_2-philic groups as well as co-solvents for CO_2.

Our proposed framework supports the proposition that the increased solubility of perfluoroalkanes in CO_2 may be closely related to larger attractive dispersion interactions. Cui *et al.*[17] have already suggested that packing and dispersion interactions play a major role. In addition to this, the SAFT-VR approach has the advantage of being entirely predictive, so that the phase behavior of a large number of binary and ternary mixtures can be studied by fitting only the pure component parameters of the *n*-perfluoroalkane molecules. In the future it would be desirable to obtain a parameterization similar to that available for *n*-alkane molecules, so that the method could be used in the context of mixture design. The nature of the SAFT approach is such that *in general* only binary interaction parameters are required, and once the adjustable parameters for a set of binary mixtures are known, multicomponent phase behavior can be predicted.

Despite significant advances in the development and formulation of molecular-based equations of state such as SAFT, their practical use has been limited, at least in part, by the

unavailability of the fluid-specific constants. Traditionally, parameters for molecular based EOS are obtained by fitting experimental vapor pressures and liquid volumes. This technique presents as drawbacks that (a) a fairly extensive body of experimental data on the pure substance is needed to obtain reasonable parameters, (b) a sophisticated computer routine (e.g. a Marquardt or Nelder-Mead algorithm) is required to perform the multivariable search for the parameters that minimize the desired objective function, and (c) the critical region is overpredicted. The first two, (a) and (b), require more time and effort than the average user of the molecular-based EOS may be willing to expend. We believe that the unavailability of fluid-specific parameters is still a major obstacle in the application of molecular-based EOS. Therefore, future efforts in improving SAFT, and in fact any molecular based equation of state, should explore the possibility and consequences of parameterizing them. As a preliminary work in this line, we explored a simple way to estimate molecular based EOS parameters for a wide variety of fluids. We scaled critical and saturation properties from a molecular based EOS, and approximated them by polynomial expansions. We have studied a simple parameterization strategy which forces the molecular based EOS to match the experimental T_c, P_c and acentric factor (ω) of the target fluid, and shown that it gives good prediction of phase envelopes within the limitations of each particular EOS model. In this way it is *not* necessary to fit the EOS parameters to extensive experimental data, because the parameters obtained are fully equivalent to those generated from complex minimization techniques. We should note however, that although the critical region will be more accurately represented with these parameters, the saturated liquid densities at low temperatures would be underpredicted in different degrees depending on the model. In a second strategy, the experimental V_c and ω are matched, and a simple one-dimensional search is used to minimize the average absolute deviation of saturation pressures, which subsequently improves density predictions. This strategy also shows some success and deserves further investigation. By following these techniques, modifications of these and other strategies may be devised and studied at reduced computational cost.

The study of polymer-solvent systems, mixtures comprised of components that exhibit wide disparities in molecular size, would be greatly facilitated if it were possible to simulate

different process scenarios with an accurate equation of state. Our aim was to demonstrate the utility of the SAFT approach for polymeric systems, and to use it to understand the thermodynamics and phase equilibria of systems containing homopolymers and polymer blends in supercritical carbon dioxide. The ability of the SAFT approach to perform such predictions relies on its more rigorous foundation, since it is, practically, the only approach that has been able to migrate from "small molecules" to macromolecules.

We have shown the utility of the SAFT approach by predicting the phase behavior (vapor-liquid, liquid-liquid, vapor-liquid-liquid and fluid-liquid equilibria), for binary (homopolymer/CO_2) and ternary mixtures (binary polymer blends/CO_2). Special emphasis was made on the characteristics of binary interaction parameters (values, temperature dependence), range of applicability (temperature, pressure, compositions) and association. Good agreement was found between predictions of the SAFT equations and experimental data.

To evaluate the capabilities of the SAFT approach in polymer-solvent mixtures, we first[18] chose to model the phase behavior of CO_2-philic poly(1,1,2,2-tetrahydroperfluorooctyl acrylate) (PTAN) in supercritical carbon dioxide ($scCO_2$), using the SAFT equation proposed by Huang and Radosz where hard spheres are taken for the reference term. We also studied the phase behavior of a CO_2-phobic polyvinyl acetate (PVAC) and a PVAC-PTAN block copolymer. The group contribution approach of Lora *et al.* was used to obtain the physical SAFT parameters for PVAC and PTAN polymers. PTAN was modeled as a non-associating polymer, whereas PVAC was modeled with two association sites per molecule. Following the approach by Lora *et al.* the contribution of a CF_2 group was obtained. Cloud curves (liquid-fluid equilibrium) for PVAC-CO_2, PTAN-CO_2 and PVAC-b-PTAN/CO_2 systems were predicted, and good agreement was obtained with the experimental data available. Additionally, critical micellar densities (CMD) appear to be successfully predicted for the PVAC-b-PTAN/CO_2 system using a criterion based in the variation of osmotic pressure (or chemical potential) with surfactant concentration. This was made possible by the ability of SAFT to handle long chain and association interactions.

The effect of high-pressure CO_2 on the miscibility of low-polydispersity PDMS/PEMS blends (poly(dimethylsiloxane) / poly(ethylmethylsiloxane) blends), was investigated[19,20] by complementary experimental and theoretical methods. Experimental measurements of phase equilibria in ternary PDMS/PEMS/CO_2 systems were obtained by Teri Walker and Richard Spontak, for different blend compositions and CO_2 pressures by high-pressure spectrophotometry. Results indicated that the cloud point increases with increasing pressure (and CO_2 content), which is contrary to the response of the same blend (without CO_2) to hydrostatic pressure. This observation reveals that CO_2 serves to reduce blend miscibility by translating the entire phase envelope of the PDMS/PEMS blend to higher temperatures. We have modeled the phase behavior of these PDMS/PEMS/CO_2 systems using the Huang and Radosz version of the SAFT model. The SAFT parameters for PDMS were obtained from binary cloud curves previously reported in the literature for PDMS/CO_2 mixtures, whereas PEMS parameters were obtained from an extended group contribution approach established for PDMS systems. The ability of the model to predict the phase behavior of the ternary PDMS/PEMS/CO_2 system was corroborated by comparing theoretical predictions with the experimental data. In a complementary work[20], these experimental data was also analyzed by the Sanchez-Lacombe equation of state to ascertain the temperature dependence of an effective interaction parameter (χ) in terms of $A + B/T$, where A and B are both pressure-sensitive. The phase diagram of the ternary PDMS/PEMS/CO_2 system (expressed on a solvent-free basis) predicted with the Sanchez-Lacombe equation of state agrees well with the experimental results, however the use of temperature dependant binary interaction parameters was necessary.

In this part of the work we have been able to model two and three phases in equilibrium with two and three components, two of them being different polymers. Future efforts in improving the application of the SAFT equations to macromolecules should focus on three different areas: a) developing ways to obtain pure polymers parameters. Currently parameters are obtained from binary (or even ternary) experimental data of the polymer in a solvent. Using the same parameters it is not possible to provide good predictions of the phase equilibrium of

the pure polymer or polymer blends; b) study of derivative properties such as volumetric compressibilities. However, perhaps more significant for the polymeric scientific community would be the study of Flory-Huggins' parameters, or second osmotic virial coefficients, that are directly related with chemical potentials; c) a detailed study of copolymers, not only for the prediction of phase equilibria, but for studying the formation of aggregates. In this respect, the adequate modeling of associating polymers is essential.

Finally a detailed comparison among the different versions of the SAFT approach should be made in terms of phase equilibrium and derivative properties for both small molecules and macromolecules. The comparison should include a simultaneous evaluation of the SAFT equations with different reference terms (hard sphere, Lennard-Jones, square-well and chain of hard spheres).

References

[1] Chapman, W. G., Jackson, G. and K. E. Gubbins, *Mol. Phys.* **65**, 1057 – 1079 (1988).
[2] Jackson, G., Chapman, W. G. and K. E. Gubbins, *Mol. Phys.* **65**, 1 – 31 (1988).
[3] Chapman, W. G., Gubbins, K. E., Jackson, G. and M. Radosz, *Ind. Eng. Chem. Res.* **29**, 1709-172 (1990).
[4] Huang, S.H, and M. Radosz, *Ind. Eng. Chem. Res*., **29**, 2284-2294 (1990).
[5] Blas, F. J. and L. F. Vega, *Ind. Eng. Chem. Res.* **37**, 660-674 (1998)
[6] Blas, F. J. and L. F. Vega, *J. Chem. Phys.* **109**, 7405-7413 (1998).
[7] Gil-Villegas, A., Galindo, A., Whitehead, P.J., Mills, S.J., Jackson, G. and A. N. Burgess, *J. Chem. Phys.* **106**, 4168-4186 (1997).
[8] Galindo, A., Gil-Villegas, A., Jackson, G. and A.N. Burgess. *J. Phys. Chem*. B **103**, 10272-10281 (1999).
[9] Colina, C. M., Lísal, M., Siperstein, F. R. and K. E. Gubbins, *Fluid Phase Equilib*. **202**, 253-262 (2002).
[10] Colina, C. M., Olivera-Fuentes, C. G., Siperstein, F. R., Lísal, M. and K. E. Gubbins, *Molecular Simulation*, **29**, 405-412 (2003).
[11] Span, R. and W. Wagner, *J. Phys. Chem. Ref. Data*, **25** 1509-1596 (1996).
[12] Möller, D. and J. Fischer. *Fluid Phase Equilib.* **100**, 35-61(1994).
[13] Chacín, A., Vázquez, J.M. and E.A. Müller. *Fluid Phase Equilib.* **165**, 147-155 (1999).
[14] Colina, C. M., Turrens, L. F., Gubbins, K. E., Olivera-Fuentes, C. and L. F. Vega, *Ind. Eng. Chem. Res.* **41**, 1069-1075 (2002).

[15] Colina, C. M., Galindo, A., Blas, F. J. and K. E. Gubbins, in press, *Fluid Phase Equilib.* (2004).
[16] Colina, C. M. and K. E. Gubbins, submitted to *J. Phys. Chem. B.* (2004).
[17] Cui, S. T., Cochran, H. D. and P. T. Cummings, *J. Phys. Chem. B*. 103 (1999) 4485-4491.
[18] Colina, C. M., Hall, C. K. and K. E. Gubbins, *Fluid Phase Equilib.* **194-197**, 553-565 (2002).
[19] Colina, C. M., Walker, T. A., Spontak, R. J. and K. E. Gubbins, 6th International Symposium on Supercritical Fluids, CD-ROM, Document MP2.pdf, Versailles, France, (2003).
[20] Walker, T. A., Colina, C. M., Gubbins, K. E. and R. J. Spontak, Macromolecules, **37**, 2588-2595 (2004).